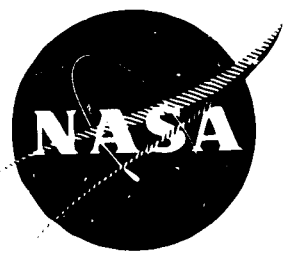


NASA CR-134538



ASSEMBLY AND ANALYSIS OF FRAGMENTATION DATA FOR LIQUID PROPELLANT VESSELS

By W. E. Baker, V. B. Parr, R. L. Bessey, and P. A. Cox
SOUTHWEST RESEARCH INSTITUTE
San Antonio, Texas 78284



prepared for
NATIONAL AERONAUTICS AND SPACE ADMINISTRATION
LEWIS RESEARCH CENTER
AEROSPACE SAFETY RESEARCH AND DATA INSTITUTE
CLEVELAND, OHIO 44135

C. David Miller, Project Manager
R. D. Siewert, Project Manager

Contract NAS 3-16009

(NASA-CR-134538) ASSEMBLY AND ANALYSIS
OF FRAGMENTATION DATA FOR LIQUID
PROPELLANT VESSELS (Southwest Research
Inst.) 236 p HC \$14.00 CSCL 20K

N74-15625
Unclas
G3/32 26767

FOREWORD

Many staff members at Southwest Research Institute contributed substantially to the multifaceted effort required during the work reported here. The authors gratefully acknowledge the special technical contributions of the following:

- Mr. A. B. Wenzel, for many of the initial visits and contacts to gather data, for review of Project PYRO films, and for assistance in project management.
- Mr. M. A. Sissung, for review of Project PYRO films, assistance in literature surveys, and report editing.
- Mr. R. Blackstone, for assistance in statistical studies.

In addition, these individuals helped the authors substantially in entering data into the ASRDI data bank by reviewing documents and filling out ASRDI Forms 102A for these documents.

The technical support of personnel at both NASA-Lewis Research Center and NASA-Kennedy Space Center contributed materially to the success of this work. In particular, Mr. C. David Miller at NASA-Lewis provided excellent technical guidance throughout the project, and Mr. James H. Deese at NASA-Kennedy gave us much insight into blast effects of liquid propellant explosions and provided us with the three most complete fragment maps from such explosions.

PRECEDING PAGE BLANK NOT FILMED

TABLE OF CONTENTS

	<u>Page</u>
LIST OF FIGURES	vii
LIST OF TABLES	xi
SUMMARY	xii
INTRODUCTION	1
Background	1
Related Work	3
Purpose of Present Work	6
Scope of Present Work	6
Significance	6
I. RETRIEVAL OF FRAGMENTATION DATA FOR LIQUID PROPELLANT VESSELS	9
II. DETERMINATION OF BLAST YIELD	13
A. General	13
B. Project PYRO and Related Experiments	15
C. Work of Farber and Deese	20
D. Estimation of Blast Wave Properties	26
III. DETERMINATION OF FRAGMENT VELOCITY DISTRIBUTION	49
A. General	49
B. Reduction of Film Data	49
C. Methods of Predicting Velocity	67
D. Correlation of Velocity Prediction Methods with Data	85
E. Frequency Distribution of Initial Velocity	97
IV. DETERMINATION OF FRAGMENT SIZE AND RANGE	104
A. Retrieval of Data from Accidents and Tests	104
B. Data Reduction	106
C. Statistical Studies	106
D. Methods of Prediction of Range Versus Fragment and Blast Yield Parameters	114
E. Correlation	129

Table of Contents (Cont'd) -		<u>Page</u>
V.	EFFECTS OF FRAGMENTS	135
	A. Introduction	135
	B. The Probability of Arrival of a Fragment of Specified Characteristics Versus Range	136
	C. Vulnerability Criteria	139
VI.	DISCUSSION OF RESULTS	142
VII.	CONCLUSIONS	146
VIII.	RECOMMENDATIONS	148
APPENDICES		
	APPENDIX A - Model Analysis for Mixing of Liquid Rocket Propellants	150
	APPENDIX B - Summary of Data Obtained From Films Read	165
	APPENDIX C - Model Analyses for Fragment Velocities, Range, Etc., for Bursting Liquid Pro- pellant Vessels	175
	APPENDIX D - Computer Program Entitled /W2/ In Fortran IV	186
	APPENDIX E - Computer Program Entitled /ROOT/ In Fortran IV	195
	APPENDIX F - Calculation of "W" Goodness of Fit Statistic from Reference 36	200
	APPENDIX G - Calculation of Approximate Probability for Obtaining the Calculated Value of "W"	207
	APPENDIX H - Computer Program Entitled /TEMP/ In Fortran IV	209
	APPENDIX I - List of Symbols	215
	REFERENCES	219

LIST OF FIGURES

<u>No.</u>	<u>Title</u>	<u>Page</u>
1	Normalized Pressure and Impulse Yields from Explosion of N_2O_4 /Aerozine 50	1
2	Representative Shock Impulses Showing Coalescence of Shock Waves from Dissimilar Sources (Stages (a) through (d))	16
3	Maximum Energy Release for a Three-Component Liquid Propellant Mixture (Ref. 27)	21
4	Mixing Function or Spill Function for Three-Component Liquid Propellant Spill Tests (Ref. 27)	23
5	Yield Potential as Time Function (Ref. 27)	24
6	Actual Yield for Random Ignition and Detonation (Ref. 27)	25
7	Estimated Explosive Yield as a Function of Propellant Weight (Ref. 27)	27
8	Terminal Yield vs. Impact Velocity for Hypergolic High-Velocity Impact (Ref. 16)	30
9	Pressure vs. Scaled Distance for Hypergolic Tests	31
10	Scaled Positive Impulse vs. Scaled Distance for Hypergolic Tests	32
11	Ignition Time vs. Yield LO_2 /RP-1 CBM	34
12	Pressure vs. Scaled Distance for LO_2 /RP-1 CBM Case	35
13	Scaled Positive Impulse vs. Scaled Distance for LO_2 /RP-1 CBM Case	36
14	Ignition Time vs. Normalized Yield LO_2 /RP-1 CBGS	37
15	Pressure vs. Scaled Distance for LO_2 /RP-1 CBGS-V Case	38
16	Scaled Positive Impulse vs. Scaled Distance for LO_2 /RP-1 CBGS-V Case	39
17	Terminal Yield vs. Impact Velocity for LO_2 /RP-1 (Ref. 16)	41

List of Figures (Cont'd) -

<u>No.</u>	<u>Title</u>	<u>Page</u>
18	Ignition Time vs. Yield LO_2/LH_2 CBM	42
19	Pressure vs. Scaled Distance for LO_2/LH_2 CBM Case	43
20	Scaled Positive Impulse vs. Scaled Distance for LO_2/LH_2 CBM Case	44
21	Ignition Time vs. Normalized Yield LO_2/LH_2 CBGS	45
22	Pressure vs. Scaled Distance for LO_2/LH_2 CBGS-V Case	46
23	Scaled Positive Impulse vs. Scaled Distance for LO_2/LH_2 CBGS-V Case	47
24	Terminal Yield vs. Impact Velocity for LO_2/LH_2 (Ref. 16)	48
25	Plan View of Camera Locations During PYRO Tests	50
26	Fireball and Fragment as Viewed by a Camera Located at Position A	54
27	Schematic Showing Actual and Calculated Fragment Vertical Displacements	56
28	Geometry for Fragment Position for Duplicate Views	59
29	Maximum Fragment Velocity as a Function of Number of Fragments	73
30	Maximum Fragment Velocity vs. Mass Ratio	74
31	Comparison of Taylor-Price to SwRI Solutions for Adiabatic Case	76
32	Schematic for Acceleration of Appurtenances by Propellant Blast	77
33	Interaction of Blast Wave with Irregular Object	79
34	Time History of Net Transverse Pressure on Object During Passage of a Blast Wave	80

List of Figures (Cont'd) -

<u>No.</u>	<u>Title</u>	<u>Page</u>
35	Blast Wave Time Constant b vs. Dimensionless Overpressure \bar{P}	81
36	Fragment Velocity: Correlation of Data from PYRO LH_2/LO_2 Tests with Theoretical Values, $W_t = 200$ lb	87
37	Fragment Velocity: Correlation of Data from PYRO Tests with Theoretical Values, $W_t = 1000$ lb	88
38	Fragment Velocity as a Function of Sound Speed in the Explosive Products	93
39	Initial Velocity Distribution, CBM, LO_2/LH_2 , Log Normal Plots	100
40	Initial Velocity Distribution, CBM, $\text{LO}_2/\text{RP-1}$, Log Normal Plots	100
41	Initial Velocity Distribution, CBGS, LO_2/LH_2 , Log Normal Plots	101
42	Initial Velocity Distribution, CBGS, $\text{LO}_2/\text{RP-1}$, Log Normal Plots	101
43	Event 3 Probability Distribution (Normal), Distance R	112
44	Event 3 Probability Distribution (Log Normal), Distance R	113
45	Event 4 Probability Distribution (Log Normal), Projected Area A	118
46	Event 4 Probability Distribution (Log Normal) Weight W	119
47	Event 1 Probability Distribution (Normal), Area/Weight (A/W)	120
48	Approximate Probability Percentage Points of "W" Test for Normality ($n = 9$)	121
49	Mean Distance vs. Yield	122
50	Mean Distance vs. Yield in lb TNT	123

List of Figures (Cont'd) -

<u>No.</u>	<u>Title</u>	<u>Page</u>
51	Mean Distance vs. Yield, with Estimated Range Containing 95% of the Fragments (\hat{R}_{05})	126
52	Standard Deviation S vs. Mean Distance R	130
53	Geometric Mean (A/W) vs. Geometric Mean Distance	131
54	Regression of Geometric Mean ($A/W^{2/3}$) vs. Geometric Mean Range \hat{R}	132

LIST OF TABLES

<u>No.</u>	<u>Title</u>	<u>Page</u>
I	Summary of Agencies Visited to Obtain Fragmentation Data or Documents	10
II	Detonation Energy Equivalents for Selected Liquid Propellants	14
III	Predicted Maximum Blast Yields (Ref. 24)	18
IV	Estimates of Terminal Yield (Ref. 16)	29
V	Summary of Fragment Velocity Measurements	62
VI	Comparison of Predicted Fragments with Pittman's Data (Ref. 33)	75
VII	Drag Coefficients C_D , of Various Shapes (Source: Ref. 35)	84
VIII	Fragment Velocity Predictions Compared with Measurements	86
IX	Grouping of Tests by Propellant and Configuration	99
X	Percentiles, Means and Standard Deviations for Grouped Velocity Data (fps)	102
XI	Chart of Events	105
XII	Calculated Statistics for Parameters of Eight Events	108
XIII	Percentiles for Plotting Parameters of Events 1 Through 8	110
XIV	Summary of Fragment Data	115
XV	Approximate Percentage Points of "W" Test for Normality (n = 9)	116
XVI	Summary of "W" Test for Normality for R, W, A, (A/W)	117
XVII	Confidence Limits on Mean, Standard Deviation and Distance Containing 95% of Fragments	125
XVIII	Predicted vs. Measured Fragment Ranges	133
XIX	Constants for Vulnerability Equations	140

SUMMARY

The objective of this work was to assemble and analyze fragmentation data for exploding liquid propellant vessels. These data were to be retrieved from reports of tests and accidents, including measurements or estimates of blast effects, fragment velocities, masses, shapes, and ranges. Correlations were to be made, if possible, of fragmentation effects with type of accident, type and quantity of propellant, blast yield, etc. A significant amount of data was retrieved from a series of tests conducted for measurement of blast and fireball effects of liquid propellant explosions (Project PYRO), a few well-documented accident reports, and a series of tests to determine autoignition properties of mixing liquid propellants. The data were reduced and fitted to various statistical functions. Comparisons were made with methods of prediction for blast yield, initial fragment velocities, and fragment range. Reasonably good correlation was achieved. Methods presented in the report allow prediction of fragment patterns, given type and quantity of propellant, type of accident, and time of propellant mixing. However, more work must be done before the results of this study can be easily applied to estimation of damaging effects of fragments from exploding liquid propellant vessels.

INTRODUCTION

Background

The primary hazard relating to large-scale explosions has in the past been assumed to be the blast wave generated by the explosion. Thermal effects have been considered next, and effects of damaging fragments last. This study attempts to partially rectify this situation by providing a comprehensive analysis of fragmentation effects of bursting liquid propellant vessels.

In storage or in a launch configuration within tankage in a rocket motor, liquid propellants are initially contained within vessels of various sizes, geometries, and strengths. Various modes of failure of these vessels are possible, from either internal or external stimuli. If the vessel is pressurized with static internal pressure, one possible mode of failure is simply fracture, instituted at a critical size flaw and propagated throughout the vessel. A similar kind of failure can occur if the vessel is accidentally immersed in a fire, and pressure increases internally because of vaporization of the internal propellant. Some launch vehicles have the liquid fuel and oxidizer separated by a common bulkhead. Accidental over-pressurization of one of these chambers can cause rupture of this bulkhead, and subsequent mixing and explosion of the propellant. External stimuli which can cause vessel failure include high-speed impact by foreign objects, accidental detonation of the warhead of a missile, dropping of a tank to the ground (as in toppling of a missile on the launch pad), as well as many other external sources. Vessel failure can result in an immediate release of energy or it can cause subsequent energy release because of mixing of propellant and oxidizer and the subsequent ignition. Other modes of failure which have resulted or could result in violent explosions are fall-back immediately after launch due to loss of thrust, or low-level failure of the guidance system after launch with subsequent impact into the ground at several hundred feet per second.

Failure of a vessel containing liquid propellants can result in various levels of energy release, ranging from negligible to the full heat value of the combined propellant and oxidizer. Toward the lower end of the scale of energy release might be the failure of a pressurized vessel due to crack propagation. Here, the stored pressure energy within the compressed propellant or gas in an ullage volume above the propellant could accelerate fragments of the vessel or generate a weak blast wave. In the intermediate range of energy releases could lie vessel failure by external stimulus and ignition, either very rapidly or at very late times, so that only small proportions of mixed propellant and oxidizer contribute to the energy release. At the upper end of the scale could be the explosion of a mixed propellant in a vessel wherein a pre-mixed propellant and oxidizer detonate in much the same fashion as a high explosive, and explosions resulting after violent impact with the ground. In

past studies of possible blast and fragmentation effects from vessel rupture, a critical problem has been to accurately assess the energy release as a result of the accident or incident. A common method of assessment of possible energy release or a correlation of the results of experiments has been to assess the energy release on the basis of equivalent pounds of TNT. This method is used because a large body of experimental data and theoretical analyses exist for blast waves generated by TNT or other solid explosives (refs. 1 and 2). Although the comparison with TNT is convenient, the correlation is far from exact. Specific energies which can be released, i. e., energy per unit volume or mass of reacting material, differ quite widely between TNT and various liquid propellants or mixtures of liquid propellants and oxidizers (ref. 3).

Dependent on the total energy release and the rate of this energy release, the sizes and shapes of fragments generated by liquid bursting propellant vessels and their appurtenances cover a very wide spectrum. At one extreme is the case of a vessel bursting because of seam failure or crack propagation from a flaw wherein only one "fragment" is generated, the vessel itself. This fragment, from a very slow reaction, can be propelled by releasing the contents of the vessel. At the other extreme is the conversion of the vessel and parts near it into a cloud of small fragments by an explosion of the contents of a vessel at a very rapid rate, similar to a TNT explosion (refs. 4 and 5). For most accidental vessel failures, the distribution of fragment masses and shapes undoubtedly lies between these two extremes. The modes of failure of the vessel may be dependent upon details of construction and the metallurgy of the vessel material. Some of the masses and shapes are dictated by the masses and shapes of attached or nearby appurtenances. In any event, assessment and prediction of these parameters undoubtedly is much more difficult than is true for the better understood phenomenon of shell casing fragmentation.

Once the masses, shapes, and initial velocities of fragments from liquid propellant vessels have been determined in some manner, then the trajectories of these fragments and their losses in velocity due to air drag or perforation or penetration of various materials must be computed. This problem is one of exterior ballistics. It differs from conventional exterior ballistic studies of trajectories of projectiles, bombs, or missiles in that the body in flight is invariably very irregular in shape and is usually tumbling violently. Exact trajectories cannot be determined then in the same sense that they can be for well-designed projectiles. Only approximate trajectories can be estimated, usually by assuming "equivalent spheres" or other geometric shapes for which exterior ballistics data and techniques exist. But, in some fashion, one can predict the ranges and impact velocities for fragments which were initially projected in specified directions from the bursting vessel with specified initial velocities. An example of results of such analysis is given by Ahlers (ref. 6).

This problem is not complete until one can assess the effect of fragments from the burst propellant vessels on various "targets". For a proper assessment of hazards, one should consider a wide variety of targets, including human beings, various classes of buildings, vehicles, and perhaps even aircraft. Problems of this nature are exceedingly complex, not only because of the inherent statistical nature of the characteristics of the impacting fragments but also because the terminal ballistic effects for large irregular objects impacting any of the targets described are not very well known. In most past studies of fragment damage from accidents, the investigators have been content to simply locate and approximate the size and mass of the fragments in impact areas and have ignored the important problem of the terminal ballistic effect of these fragments.

Related Work

Extensive studies have been carried out over many years regarding the potential failure of nuclear reactor vessels from a variety of causes. The source of energy causing a reactor vessel failure can be the stored compressive energy in a liquid or gas within the containment vessel, the chemical energy release, or the uncontrolled nuclear energy release. The latter source is, of course, not present in the failure of liquid propellant vessels, but the first two sources are present. Although many of the studies of nuclear reactor vessels have concentrated on the design of the pressure vessel and the attachments to it to obviate failure, many other studies also have been concerned with shock and fragmentation effects in the event that failure does occur. The literature in this field is far too voluminous to cite other than to give a few examples which are indicative of the parallels between these studies and those reported here. The specific references given all relate to production of or containment of fragments caused by vessel failure.

The first of these references cited is a review paper by Gwaltney (ref. 7) on missile generation and protection in one class of a nuclear power plant. Various types of vessel failure are considered and reviewed and formulas are given for estimations of velocities with which fragments will be ejected after failure. Effects of impact of the fragments are discussed, and a number of empirical penetration formulas for metal missiles penetrating and perforating steel and concrete are given. The paper also includes a simplified discussion of possible shock wave effects caused by the release of energy after vessel rupture. The second paper is reference 8. This is the final report of a multi-year experimental and analytical investigation by Stanford Research Institute of the problems of generation and containment of fragments generated by a runaway reactor. More details of various phases of the investigation are given in additional 6-month progress reports predating reference 8. Many of the aspects of the work reported in reference 8 are similar to the study reported here. Attempts were made to simulate the energy release rates in the event of reactor runaway by use of slow-detonating explosives and fuses.

These sources of energy release were used to apply pressure within model containment vessels and models of surrounding materials such as concrete. Failure of these model vessels was observed using high-speed cameras to determine velocities and initial trajectories of the fragments. In a parallel investigation, the Stanford Research Institute staff conducted a series of experiments simulating impacts by long, slender missiles such as reactor control rods. Penetration formulas for such rods striking steel plates were developed as part of the effort.

A good general listing of the classes of problems considered in nuclear reactor containment studies can be found in reference 9, which reports papers on reactor safety given at the Second International Conference on Peaceful Uses of Atomic Energy. In particular, reference 10, one of the papers in the Proceedings of the conference, discusses various sources of energy release and gives approximate limits to the magnitudes which can be expected, considers ways of attenuating blast energy and of stopping fragments, and gives in general a good overall review of the range of problems one must consider in reactor containment studies.

The explosive behavior of bombs, grenades, mines and warheads has always commended wide attention, and the most commonly used bombs are usually constructed from suitably corrugated steel casings, either fully or partially filled with explosives. Interest in the mechanics of fragmentation has largely been directed towards trying to predict the influence of casing material and wall thickness, the size of the explosive charge, and the type of explosive on the fragmentation velocity and the expanded radius of a casing at which fracture occurs.

In a series of papers (refs. 4, 5, 11 through 14), there has evolved a simple approximate treatment for the acceleration of fragments by high explosives. The basic assumption made was that the potential energy in the charge before detonation was equal to the kinetic energy of the charge and casing after detonation and expansion. It was also assumed that, after detonation, the gaseous detonation products were equally dense at all points and expanding uniformly. Formulas for fragment velocity at the radius for case breakup (essentially the maximum velocity) are presented in these references for various regular geometries of cased explosive charges. All are of the form

$$U = f(H_e, M/C) \quad (1)$$

where U is velocity and is a function of heat of explosion H_e , total casing mass M , and mass of the explosive charge C .

If the results of accidents involving explosions of liquid propellant vessels are well documented, they can provide useful data to assist in the

assessment of this problem. Some have indeed proven useful sources for our study, as we will document in later sections of this report. Although accident reports are useful in documenting the gross effects of vessel explosion, determining the maximum ranges to which fragments are projected, and indicating shapes and masses of fragments, they are often of less value in assessing this problem than are controlled experiments. Because they are accidents, usually there is no measure of blast yields, fragment trajectories, and other data that would be useful in analysis of vessel failure and subsequent effects.

Project PYRO involved many test explosions with liquid propellants. The purpose of Project PYRO (refs. 15 through 17), was "to develop a reliable philosophy for predicting the damage potential which may be experienced from the accidental explosions of liquid propellants during launch or test operations of military missiles or space vehicles". Three combinations of propellants and oxidizers were chosen for test and evaluation, and at least seven agencies were involved in the program. The primary objective was to estimate blast yield and its effects. The effects of fragmentation were secondary in the study. But, Jeffers (ref. 18) analyzed a small number of the photographic records to determine fragment velocity. As is apparent in later sections of this report, the films from Project PYRO, when studied carefully, provide the primary source of data for initial velocities for liquid propellant explosions.

There are a number of experimental studies and analyses of the effects of bursting pressure vessels which fail under the action of internal energy sources other than liquid propellants. A number of these can provide useful information for the problem at hand. Some specific examples follow.

Hunt, Walford, and Wood (ref. 19) have conducted an experimental study of the failure of a pressure vessel containing high temperature pressurized water. In this study, the authors observed the failure of a vessel with high-speed cameras and also located a number of blast transducers nearby to measure the resulting shock wave generated in the surrounding air. They also generated equations for calculation of velocities of the fragments resulting from burst of the vessel. In a somewhat similar study, Larson and Olson (ref. 20), measured the air blast effects from bursting pressure vessels containing high pressure gas. In this study, the authors also observed the flight of fragments from the bursting vessel and developed an empirical method for estimating fragment velocities based on an energy balance and knowledge of the strength of the shock wave generated by the bursting vessel. In a somewhat different category than the two previous studies are analyses and predictions of the effects of rupture of pressure vessels containing high pressure gases. An excellent example of such analyses is a compendium of gas autoclave engineering studies, edited by C. E. Muzzall (ref. 21). This compendium is an exhaustive study of the possible hazards associated with failure of a large, cylindrical vessel containing high pressure, high temper-

ature argon. Estimates are made of both the blast and fragmentation hazards in the event of failure of the vessel, of the effects of both fragments and blast on a test cell within which the vessel is operated, and recommendations for redesign of the test cell to withstand both blast and fragmentation effects. A second study of this same nature, but on a much more limited basis, is a report by Baker, et al., (ref. 22), on the possible effects of failure of a high pressure helium vessel while under test in a NASA vibration and acoustic test facility. Here, blast and fragmentation effects were estimated in the event of failure of the vessel, blast loading and response of the walls of the test facility were computed, as were possible penetration effects by fragments of the vessel. The report concluded with recommendations for modification of test procedures to obviate the very real hazards in the event the helium pressure vessel failed.

Purpose of Present Work

The purpose of the work reported here is to assemble fragmentation data for bursting liquid propellant vessels, analyze these data, and develop or modify methods of prediction of fragmentation effects of such explosions. An additional purpose is to enter all relevant reports, data, etc., into a data bank at the NASA Aerospace Safety Research and Data Institute (ASRDI).

Scope of Present Work

The primary purpose of this study and analysis is the retrieval, assembly and recording of available data regarding fragments from exploded vessels that contained liquid propellants or substances that have similar chemical properties. These data cover both test and accidental explosions and include blast yield, fragment sizes, fragment trajectories, fragment velocities, and a description of damage caused by the fragments.

The second part of the study and analysis shall be that of reducing the available data to a form most readily usable by aerospace engineers, for estimation of the integrated shrapnel hazard to which neighboring structures will be subjected. This reduction of the data shall be in the form of equations that will relate the blast yield to the nature and quantities of fuel and oxidants and to various parameters describing the type of explosion, and in the form of equations that will relate the blast yield to distributions of fragment size, initial fragment velocity, and initial direction of fragment motion.

Significance

It is believed that this report contains the first comprehensive study of fragmentation effects of bursting liquid propellant vessels. The results of this work should provide a better understanding of such fragment characteristics as initial velocity, mass, shape, and range as they relate to

estimated blast yield of exploding liquid propellant tanks. These characteristics used with munition fragment equations could predict the terminal or impact velocities of these fragments. Thus, it is possible to derive criteria that allow for the prediction of fragment hazards to people or the risk of damage to nearby facilities from the impact of these fragments. These criteria could be used to arrive at safe distances between populated areas at launch or test stands for fragments and overpressure hazards that are caused by exploding liquid propellant tanks. Moreover, intra-line separation distances can be established that would decrease the risk of damage to nearby facilities or systems from fragment impact; or, with a prediction of impact energy of fragments, barriers could be properly designed to protect these facilities at intra-line separation distances.

Statistical fitting to data on fragment range R versus measured terminal blast yield Y gave the following equation:

$$\hat{R} = 314.74 Y^{0.2775}$$

where \hat{R} is the mean range in feet, and Y is the terminal blast yield in percent TNT equivalent. Fitting to data on fragment weight W and mean presented area A gave the equation

$$\hat{R} = 9.864 (A/W^{2/3})^{0.78}$$

where W is fragment weight in pounds and A is mean fragment presented area in square inches. These two equations can be used for prediction, subject to restrictions and limits noted in the body of the report. Also included in Part IV are distribution functions for fragment initial velocities for various types of accident, which can be used to predict distributions of fragment sizes and masses for other postulated accidents.

Estimates of the distributions of the initial velocities for four specific combinations of configurations and propellants were derived. In all four cases, the initial velocity (U_i) in ft/sec. followed a log normal distribution function. The distribution functions for the four cases are given below, where \hat{u} and $\hat{\sigma}$ are estimates of means and standard deviations of $\ln U_i$ respectively:

1. Confined by Missile (CBM), LO_2/LH_2 propellant

$$f(U_i; \hat{u}, \hat{\sigma}) = (1/2.4753 U_i) \exp \left[- (\ln U_i - 6.464)^2 / 1.9503 \right]$$

2. CBM, $LO_2/ RP-1$ propellant

$$f(U_i; \hat{u}, \hat{\sigma}) = (1/1.5824 U_i) \exp \left[- (\ln U_i - 6.713)^2 / 0.7071 \right]$$

3. Confined-by-Ground-Surface (CBGS), LO_2/LH_2 propellant

$$f(U_i; \hat{\mu}, \hat{\sigma}) = (1/1.9339 U_i) \exp \left[- (\ln U_i - 6.129)^2 / 1.1904 \right]$$

4. CBGS, $\text{LO}_2/\text{RP-1}$ propellant

$$f(U_i; \hat{\mu}, \hat{\sigma}) = (1/1.6010 U_i) \exp \left[- (\ln U_i - 5.962)^2 / 0.8159 \right]$$

I. RETRIEVAL OF FRAGMENTATION DATA FOR LIQUID PROPELLANT VESSELS

The first task in this contract consisted of a series of contacts and visits with various government agencies and contractors to ascertain the extent of data available on fragmentation from liquid propellant explosions, either accidental or from planned tests, and to obtain pertinent data and reports for entry into the data bank at the Aerospace Safety Research and Data Institute (ASRDI) of NASA. The contacts and visits were supplemented by a conventional literature search of the open literature and the Defense Documentation Center (DDC).

The work commenced with an initial visit to ASRDI, and temporary transfer to SwRI of pertinent documents already acquired by the ASRDI staff. Potential sources of data and individuals to contact at various agencies, in addition to those already known to SwRI staff, were also identified during this visit. We then made a series of telephone contacts to determine whether specific agencies or firms had applicable data and could send such data to us, and if a visit was desirable. All major NASA centers, several AEC laboratories, the military service ordnance laboratories, Air Force Eastern and Western Test Ranges, the Department of Defense Explosive Safety Board, and a number of commercial and other contractors were contacted during this initial telephone survey. More than thirty such contacts were made. A number of the calls led to blind alleys, with no data available, or individuals who might have had data or known of it being no longer present. But, other calls unearthed potential sources of data and allowed appointments for visits to review these data.

Following the initial phone contacts, several SwRI staff members visited those agencies which were potential sources of data. As much as possible, trips were combined to agencies in the same general geographical area. When the visits yielded applicable or potentially applicable documents, reports or data, we tried to obtain them for permanent retention or loan, or tried to arrange for them to be transmitted to SwRI. The results of these visits are summarized in Table I, which lists the agencies visited, individuals contacted at each agency, and the type of applicable data found to be available to us at each agency. Several agencies had sufficient data or information to warrant a follow-up visit to further discuss the data or to attempt to obtain it for use on this contract. These agencies are indicated by an asterisk in Table I. Of particular importance to this contract is the library of motion pictures of the Project PYRO tests available at Air Force Rocket Propulsion Laboratory. We obtained these films, and they form the primary data base for determination of initial fragment velocities from bursting propellant vessels. Individuals visited at the various agencies were for the most part very cooperative and helpful in obtaining or transmitting applicable data and documents. In at least one instance, however, we have not been able to obtain

TABLE I - SUMMARY OF AGENCIES VISITED TO OBTAIN
FRAGMENTATION DATA OR DOCUMENTS

Agency	Individuals Contacted	Data Available			
		Docu- ments	Accident Reports	Films	Other
Aerospace Safety Re- search and Data In- stitute, NASA-Lewis	I. I. Pinkel C. D. Miller P. M. Ordin D. Forney	X	X		X
NASA-Kennedy*	J. H. Deese A. H. Moore F. X. Hartman A. J. Carraway	X	X		X
Air Force Eastern Test Range*	L. J. Ullian CPT R. P. Welborn T. Fewell Maj. K. Cailer	X	X		
Dept. of Mech. Eng., Univ. of Florida*	Prof. E. A. Farber Prof. E. Watts Prof. J. Smith	X		X	X
Air Force Rocket Propulsion Lab. Edwards AF Base*	J. G. Wancheck R. Thomas	X		X	
Aerospace Corp., El Segundo	R. Wolfe J. Smith R. Vega	X		X	
Air Force Space and Missile Systems Org.	CPT K. C. Tallman	X			
Gen. Elec. Co., Bay St. Louis, Miss.	P. V. King	X			

This agency was visited twice to obtain data identified during the first visit.

TABLE I. (Continued)

Agency	Individuals Contacted	Data Available			
		Documents	Accident Reports	Films	Other
NASA-Marshall	W. A. Riehl	X			
Central Propulsion Info Agency (CPLA), Johns Hopkins Univ., Applied Physics Lab	E. A. Cadwallader	X			X
Dept. of Defense Explosive Safety Board (DDESB)	Dr. T. A. Zaker R. Perkins	X	X		
URS Research Co., San Mateo, California	C. Wilton	X		X	X
U. S. Army Ballistic Research Labs.	D. Dunn C. Kingery A. J. Hoffman	X			

copies of accident reports which would provide useful fragmentation data, and have not been able to include these data in our review and further analysis.

As documents and data were received at SwRI as a result of our initial visit to ASRDI, our subsequent visits to other agencies, and our library and DDC literature searches, we reviewed each document, completed ASRDI form 102A for the documents and forwarded these forms to ASRDI. A total of 168 documents were reviewed in this manner, with various SwRI staff members completing the Forms 102A for documents which fell within their technical specialties.

We believe that we have discovered and reviewed most of the pertinent literature, data, and accident reports pertaining to fragmentation of liquid propellant rockets and vessels. There is, however, one possible exception. There may be a body of fragmentation data in accident reports in the Air Force Inspection and Safety Center at Norton Air Force Base, California, which we could not review or obtain for legal reasons. These reports were reviewed by staff members of the Center, and we have been notified that they contain no data which could be used in our study. Because we were not allowed to review the reports ourselves, we have no way of comparing them with other accident reports which have provided useful data, nor do we know the criteria applied by Norton personnel in assessing the potential value of specific reports to this project.

II. DETERMINATION OF BLAST YIELD

A. General

A prerequisite to estimation of fragmentation effects for liquid propellant explosions is the estimation of energy released during the explosion, which is synonymous with explosive yield. Furthermore, to properly estimate fragment velocities of appurtenances which can be accelerated by the blast wave from propellant explosions, one must know the time histories of various physical parameters describing the blast wave as a function of distance from the explosion. We must therefore consider blast effects in some detail, even though this is a study of fragmentation.

Accidents with liquid propellant rockets, both during static firing on a test stand and during launch, have shown that liquid propellants can generate violent explosions. These explosions "drive" air blast waves, which can cause direct damage and can accelerate fragments or nearby objects. The launch pads at the Air Force Eastern Test Range (ETR) have for a number of years been instrumented with air blast recorders to measure the overpressures generated during launch pad explosions, so some data are available on the intensities of the blast waves generated. Such measurements, and the common practice in safety circles of comparing explosive effects on the basis of blast waves generated by TNT, have led to expression of blast yields of propellant explosions in equivalent "pounds of TNT". (Although a direct conversion of pounds of TNT to energy can easily be made - 1 lb_m of TNT equals 1.4×10^6 ft-lb - this is seldom done.)

Liquid propellant explosions differ from TNT explosions in a number of ways, so that the concept of "TNT equivalence" quoted in pounds of TNT is far from exact. Some of the differences are described below.

- (1) The specific energies of liquid propellants, in stoichiometric mixtures, are significantly greater than for TNT (specific energy is energy per unit mass). Table II, taken from ref. 3, gives specific energies for a number of liquid-propellant/oxidizer mixtures, as ratios to TNT specific energy. Note that all of the energy ratios in Table II are greater than 1, and range as high as 5.3.
- (2) Although the potential explosive yield is very high for liquid propellants, the actual yield is much lower, because propellant and oxidizer are never intimately mixed in the proper proportions before ignition.

TABLE II - DETONATION ENERGY EQUIVALENTS FOR
SELECTED LIQUID PROPELLANTS (REF. 3)

			Oxygen/Fuel Ratio	Density (gm/cm ³)	Specific Energy (Relative to TNT)
Fuel	Aluminum Triethyl	Al (C ₂ H ₅) ₃			
Oxidizer	Oxygen	O ₂	1.5	1.019	2.61
Fuel	Aluminum Trimethyl	Al (C H ₃) ₃			
Oxidizer	Oxygen	O ₂	2.0	1.012	2.80
Fuel	Pentaborane	B ₅ H ₉			
Oxidizer	Oxygen	O ₂	2.35	1.075	2.29
	Nitrogen Tetroxide	N ₂ O ₄	3.35	1.220	3.36
	IRFNA*	H ⁺ N _{1.14} O _{3.24}	3.35	1.352	1.92
Fuel	Monomethylhydrazine	CH ₃ , NH NH ₂			
Oxidizer	Oxygen	O ₂	1.00	1.007	2.11
	Nitrogen Tetroxide	N ₂ O ₄	2.17	1.253	2.38
	IRFNA	H ⁺ N _{1.14} O _{3.24}	2.45	1.460	3.14
	Chlorine Trifluoride	Cl F ₃	3.13	1.578	2.37
Fuel	UDMH	(CH ₃) ₂ N ₂ H ₂			
Oxidizer	Oxygen	O ₂	1.70	1.009	2.85
	Nitrogen Tetroxide	N ₂ O ₄	2.55	1.246	2.33
	IRFNA	H ⁺ N _{1.14} O _{3.24}	2.85	1.365	3.16
Fuel	Hydrogen	H ₂			
Oxidizer	Oxygen	O ₂	5.00	.968	5.30
	Nitrogen Tetroxide	N ₂ O ₄	5.25	1.211	3.87
Fuel	Ammonia	NH ₃			
Oxidizer	Oxygen	O ₂	2.0	.964	3.19
	Nitrogen Tetroxide	N ₂ O ₄	6.0	1.312	1.57
Fuel	Hydrazine	N ₂ H ₄			
Oxidizer	Oxygen	O ₂	1.00	1.070	2.78
	Nitrogen Tetroxide	N ₂ O ₄	1.30	1.245	2.36
	IRFNA	H ⁺ N _{1.14} O _{3.24}	1.50	1.342	3.17
Fuel	50% N ₂ H ₄ - 50% UDMH	1.875 N ₂ H ₄ + (CH ₃) ₂ N ₂ H ₂			
Oxidizer	Oxygen	O ₂	1.52	1.043	2.77
	Nitrogen Tetroxide	N ₂ O ₄	2.0	1.262	2.40

* Inhibited Red Fuming Nitric Acid

- (3) Confinement of propellant and oxidizer, and subsequent effect on explosive yield, are very different for liquid propellants and TNT. Degree of confinement can seriously affect explosive yield of liquid propellants, but has only a secondary effect on detonation of TNT or any other solid explosive.
- (4) The geometry of the liquid propellant mixture at time of ignition can be quite different than that of the spherical or hemispherical geometry of TNT usually used for generation of controlled blast waves. The sources of compiled data for blast waves from TNT or Pentolite such as references 2 and 3, invariably rely on measurements of blasts from spheres or hemispheres of explosive. The liquid propellant mixture can, however, be a shallow pool of large lateral extent at time of detonation.
- (5) The blast waves from liquid propellant explosions show different characteristics as a function of distance from the explosion than do waves from TNT explosions. This is undoubtedly simply a manifestation of some of the differences discussed previously, but it does change the "TNT equivalence" of a "liquid-propellant explosion with distance from the explosion. Fletcher (ref. 37) discusses these differences and shows them graphically in Figs. 1 and 2. These differences are very evident in the results of the many blast experiments reported in Project PYRO (refs. 15-17). They have caused the coinage of the phrase "terminal yield", meaning the yield based on blast data taken at great enough distance from the explosion for the blast waves to be similar to those produced by TNT explosions. At closer distances, two different yields are usually reported: an overpressure yield based on equivalence of side-on peak overpressures, and an impulse yield based on equivalence of side-on positive impulses.

There exist at present at least three methods for estimating yield from liquid propellant explosions, which do not necessarily give the same predictions. One method is based on Project PYRO results (refs. 15-17), and the other two are the "Seven Chart Approach" and the "Mathematical Model" of Farber and Deese (ref. 23). We next discuss each method and some background information.

B. Project PYRO and Related Experiments

Project PYRO was a joint NASA/USAF project conducted during the period 1965-1967 with the purpose of determining the blast and thermal characteristics of three liquid propellant combinations in most common use in

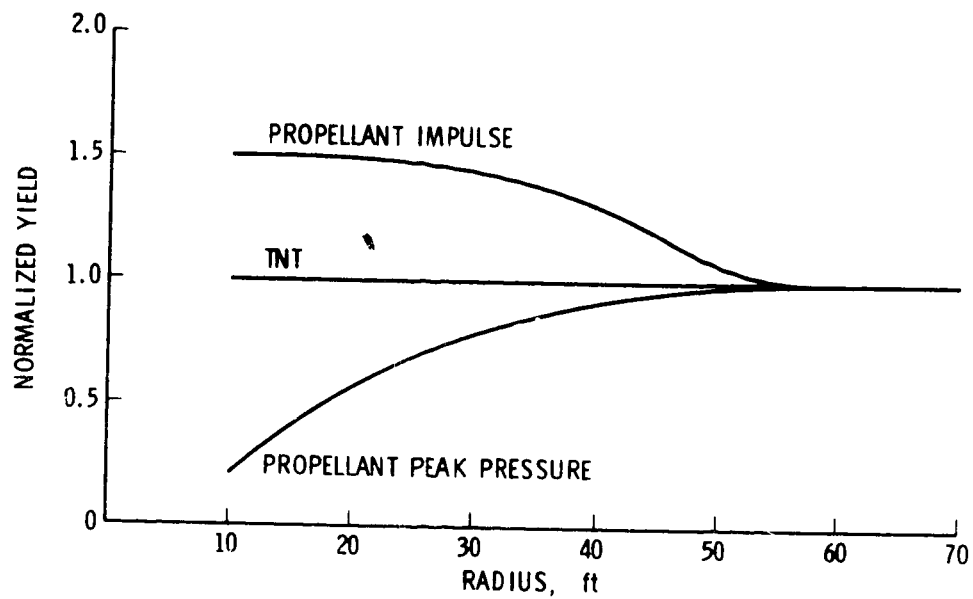


FIGURE 1 . NORMALIZED PRESSURE AND IMPULSE YIELDS FROM EXPLOSION OF N_2O_4 /AEROZINE 50

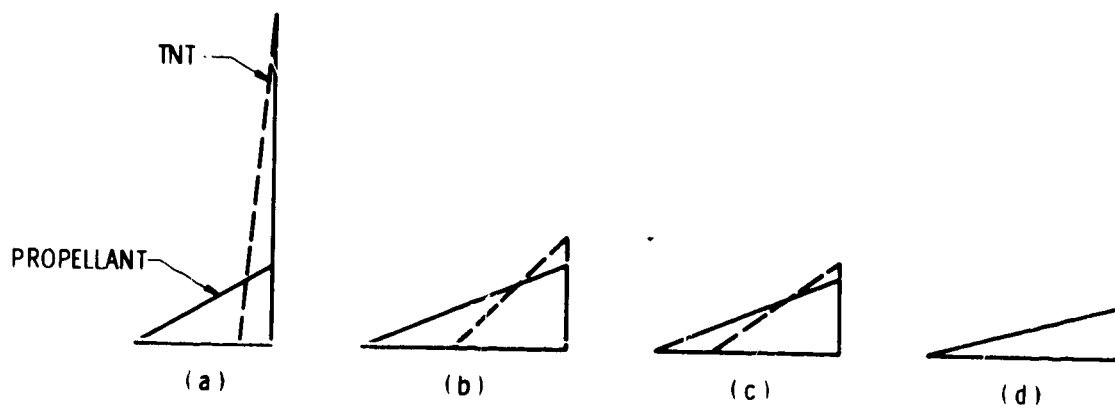


FIGURE 2 . REPRESENTATIVE SHOCK IMPULSES SHOWING COALESCENCE OF SHOCK WAVES FROM DISSIMILAR SOURCES [STAGES a) THROUGH d)]

military missiles and space vehicles. It included 270 tests with total weights of propellants ranging from 200 lb_m to 100,000 lb_m. Most of the tests were conducted at the Air Force Rocket Propulsion Laboratory (AFRPL) at Edwards AFB, California. Prime contractor for much of the effort was URS Systems Corp., Burlingame, California. The project was supervised by a Steering Committee of representatives from several NASA centers, the Air Force Eastern Test Range, and the Sandia Corp.

The emphasis in Project PYRO was almost exclusively experimental. Tests were designed to simulate various types of accidents which could cause mixing and ignition of the propellants. The primary blast instrumentation was an array of blast pressure transducers whose outputs as functions of time were recorded on magnetic tape. (Although fragmentation effects were incidental to the program objectives, high-speed motion picture cameras photographed most of the tests, and our data on fragment velocities are all obtained from these films.) The results of the program were reported in a three-volume final report, with Vol. I (ref. 15) describing the program and giving overall results, Vol. II (ref. 16) giving detailed test data, and Vol. III (ref. 17) giving prediction methods based on the program results. In the PYRO effort, three basic types of accidents were simulated. The first type consisted of failure of an interior bulkhead separating fuel and oxidizer in a missile stage. This was termed Confinement by the Missile (CBM). The second type of accident included impacts at various velocities of the missile on the ground, with all tankage ruptured, and subsequent ignition. This was termed Confinement by the Ground Surface (CBGS). The third type was High Velocity Impact (HVI) after launch.

Although Project PYRO generated much more data on explosive yields of liquid propellant explosions than all previous studies combined, several earlier experimental programs did give useful data and should be mentioned here. Arthur D. Little, Inc., (ref. 24) conducted a series of blast tests simulating spills and ignition on the ground of various combinations of propellants in the Saturn vehicles. The tests were designed to produce the maximum possible blast yield for this type of accident, with thorough mixing of fuels and oxidizer and delays of ignition until such mixing was complete. These anonymous investigators reported blast wave characteristics identical to those from TNT explosions in the overpressure range of their measurements (≤ 100 psi), and blast yields ranging from 0.23 to 1.98 lb TNT/lb propellant. They also estimated maximum potential yields (even including effects of afterburning of unburned fuel with oxygen in the air) of considerably less than in Table II. Their predicted maxima are given in Table III.

TABLE III

PREDICTED MAXIMUM BLAST YIELDS (REF. 24)

Propellant	Ratio of Blast Energies, lb TNT/lb Propellant
RP-1/LO ₂	1.25
LH ₂ /LO ₂	3.70
RP-1/LO ₂ /LH ₂	2.75

Another experimental effort prior to PYRO is reported by Pesante and Nishitazashi (ref. 25). These investigators measured the blast waves generated by fuels and oxidizers which were violently mixed by explosively shattering dewars containing one component, while the dewars were immersed in a bath of the other component. Blast yields ranging from 0.23 - 0.80 lb TNT/lb propellant were obtained in these experiments. (These tests also included attempts to measure velocities of objects placed near the blast wave, but no useful data were obtained.)

The final set of tests prior to PYRO is apparently a series reported by Gayle, et al. (ref. 26). Fuels and oxidizers were mixed by several different methods (anticipating the two primary simulation methods in PYRO), and blast wave properties measured as a function of distance. These investigators showed a much greater spread in blast yields for other methods of mixing than spill tests, with much smaller yields being observed in most tests for simulated bulkhead rupture, etc. Yields for LH₂/LO₂ combinations were most affected by the change in methods of mixing, being no greater than 0.014 lb TNT/lb propellant for any of the tests.

From the test results reported in references 15 and 24 through 26, a number of observations can be made regarding blast yields from liquid propellant explosions.

- (1) The yield is very dependent on the mode of mixing of fuel and oxidizer, i. e., on the type of accident which is simulated. Maximum yields are experienced when intimate mixing is accomplished before ignition.

- (2) Blast yield per unit mass of propellant decreases as total propellant mass increases.
- (3) The character of the blast wave as a function of distance differs between propellant explosions and TNT explosions, as noted before. There is some evidence that these differences are greatest for low percentage yield explosions. (They were not observed in tests of ref. 24, for example.)
- (4) On many of the LH_2/LO_2 tests (regardless of investigators), spontaneous ignition occurred very early in the mixing process, resulting in very low percentage yields.
- (5) Yield is very dependent on time of ignition, even ignoring the possibility of spontaneous ignition.
- (6) Yield is quite dependent on the particular fuel and oxidizer being mixed.
- (7) Variability in yields for supposedly identical tests was great, compared to variability in blast measurements of conventional explosives.

The PYRO blast yield prediction methods given in reference 17 are a set of "cook-book procedures" for estimating blast pressures and impulses for specific types of liquid propellant accidents and specified geometric and initial conditions. Inherent in the prediction method is scaling of ignition time according to $t/W^{1/3}$. Types of accidents considered are confinement by missile (CBM), confinement by the ground surface (CBGS), and high velocity impact (HVI). Equivalent TNT yields are determined and estimates of overpressure and impulse made based on compiled blast data for TNT (ref. 2), with a correction factor for impulse to account for the difference between TNT and liquid propellant explosions. Unfortunately, we feel that the prediction methods given in reference 17 are oversimplified (for example, they use discrete and different correction factors for impulse for different ranges of scaled distances, whereas the data in references 15 and 16 show a continuous variation in impulse with scaled distance), and they are based on a scaling of ignition time which is dubious, i. e., not proven by experiment (see Appendix A). The methods of reference 17 also are designed to give upper-bound estimates of blast effects, rather than most probable estimates. The possibility of limitation of blast yield by early autoignition when large masses of propellants are mixed is ignored in the PYRO prediction schemes. Considering the careful and well-documented experimental work reported in references 15 and 16, the prediction methods of reference 17 are quite disappointing.

C. Work of Farber and Deese

More or less concurrent with the PYRO work, but continuing to the present, Farber at the University of Florida and Deese at NASA-Kennedy have conducted a combined theoretical and experimental program of the study of the physical and chemical processes involved in mixing, ignition, and explosion of liquid rocket propellants. The results of this work are reported in a number of papers, with the efforts through October 1968 being best summarized and reported in reference 27. Later work is reported in references 28 through 30.

In the work reported in references 28-30, the problem of mixing, ignition and explosion of liquid rocket propellants is subdivided into a number of sub-problems, and each sub-problem studied more or less independently. The results of the subsequent analyses and experiments are then combined in several prediction schemes for explosive yield, of which the most detailed is the "Seven Chart Approach" of reference 23.

The sub-problems into which the overall problem was divided by Farber and Deese were:

- (1) Determination of the potential maximum explosive yield obtainable if the liquid propellants present were mixed in an optimum manner (yield potential function)
- (2) Determination of amounts of propellant which would be mixed as a function of time after "spill" (mixing function)
- (3) Determination of most probable times of delay of ignition and detonation (delay and detonation times)

Farber and Deese (ref. 23) also evolved a method of empirically fitting to experimental data a four-parameter probability function which would predict the probability of explosive yield to various levels of confidence, and have more recently evolved an hypothesis of a critical mass of mixing propellants for which autoignition is certain.

The yield potential function is calculated by Farber, et al (ref. 27) on the basis of chemical kinetics considering boiling and freezing of fuel-oxidizer components as a function of time after an assumed instantaneous mixing. Heat values for the various chemical reactions which could occur at various times, considering states and amounts of reactants present, are then calculated. Some details of the manner in which these calculations are made are given in reference 27, and a typical result for an initial mixture of $\text{LO}_2/\text{LH}_2/\text{RP-1}$ is shown in Figure 3. There are no experimental data which directly confirm such theoretical calculations of the yield function.

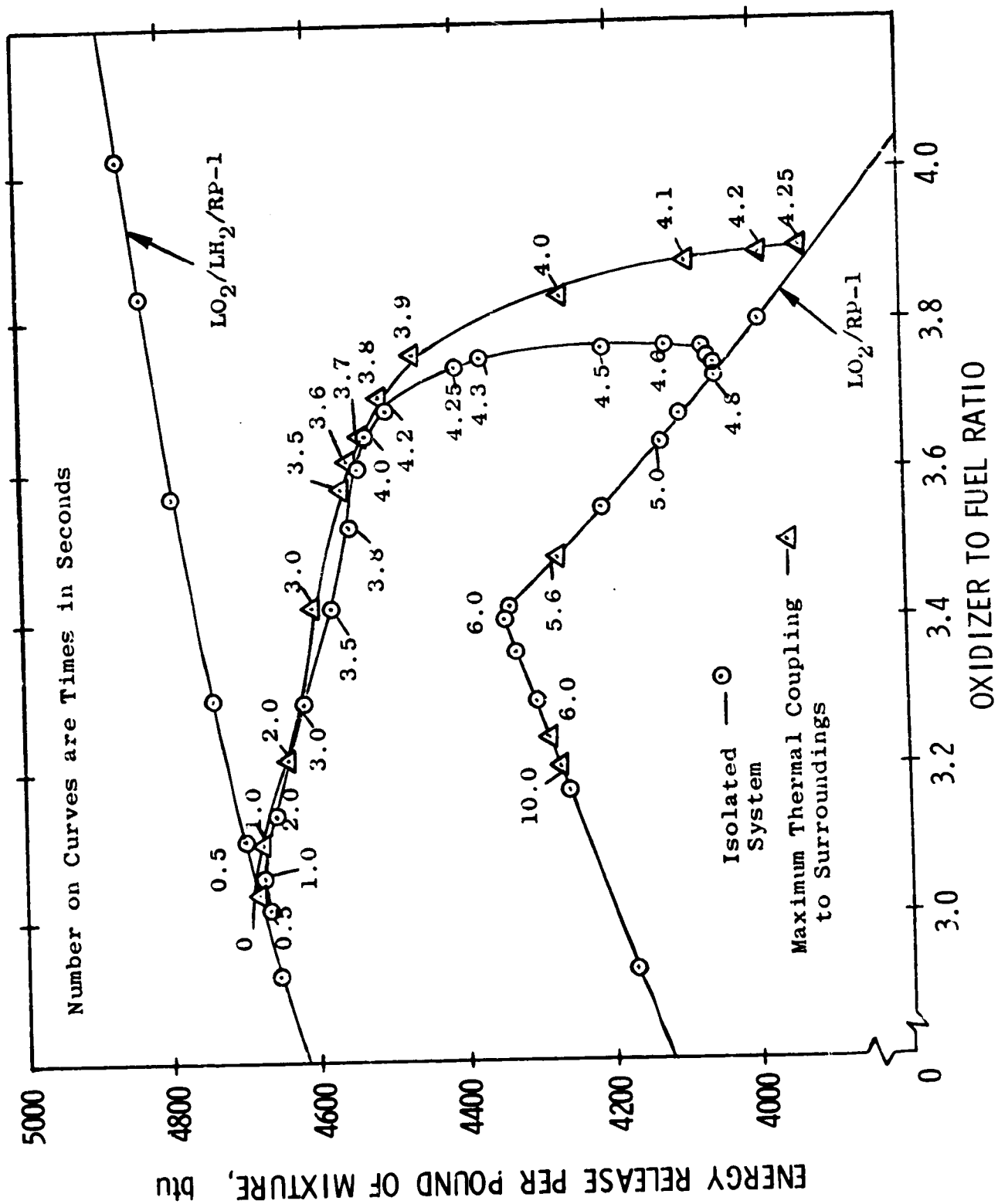


FIGURE 3. MAXIMUM ENERGY RELEASE FOR A THREE COMPONENT LIQUID PROPELLANT MIXTURE (REF. 27)

The mixing function, expressing the fraction of mass of fuel plus oxidizer actually mixed as a function of time after spill, is the best established of Farber's sub-problems. No less than four experimental methods were used to establish this function (ref. 27). A typical mixing function is shown in Figure 4. This function peaks as mixing becomes more complete, and then decays because the mixed propellant evaporates. An optimum time for ignition (optimum in that it will produce maximum explosive yield) is therefore heavily dependent on this function.

The least well-determined of the sub-problems is the definition of expected delay times for ignition. A statement from reference 28 appears appropriate "The ignition time for prediction purposes, can be a controlled value, a known value based upon the characteristics of the propellants, a statistical value with confidence limits, or it can be a value determined by the critical mass method. . . .". In other words, the ignition time is apparently anyone's best guess. It is clear from the results of liquid propellant mixing tests that autoignition always occurs for mixing of sufficiently large quantities of propellants. Farber (refs. 27-30) has hypothesized that a source of ignition which is always present upon mixing is electrostatic build-up of voltage and subsequent electrical discharge through a gas bubble, and that a critical mass exists for a given propellant mixture and set of initial conditions which provides a short upper limit on ignition time, and therefore an upper limit on explosive yield. Recent experimental work by his group (ref. 29) is directed specifically toward measurement and verification of this hypothesis, and verification is claimed (although not conclusively proven) by work reported in reference 30.

The two prediction methods developed by Farber, et al, are termed the "Seven Chart Approach" and the "Mathematical Model". Each will give an estimate of explosive yield y , expressed as a fraction of the total heat of combustion of a stoichiometric mixture of fuel and oxidizer. In the "Seven Chart Approach", a graph such as Figure 3 is normalized by dividing by the maximum heat value reached by the mixture, and then converted to a normalized yield potential y_p versus time plot such as Figure 5. The fraction mixed x as a function of time (Figure 4) is then multiplied by y_p at approximate times to give expected yield y (see Figure 6). Finally, some estimated ignition time, with suitable confidence limits, is superimposed on Figure 6 to give the final estimate of yield y . (Note that only four charts are discussed here. The remaining three charts in the seven-chart method show intermediate steps).

The "Mathematical Model" method (ref. 28) consists of fitting to experimental data a relationship between normalized yield y and mixing function x of the form

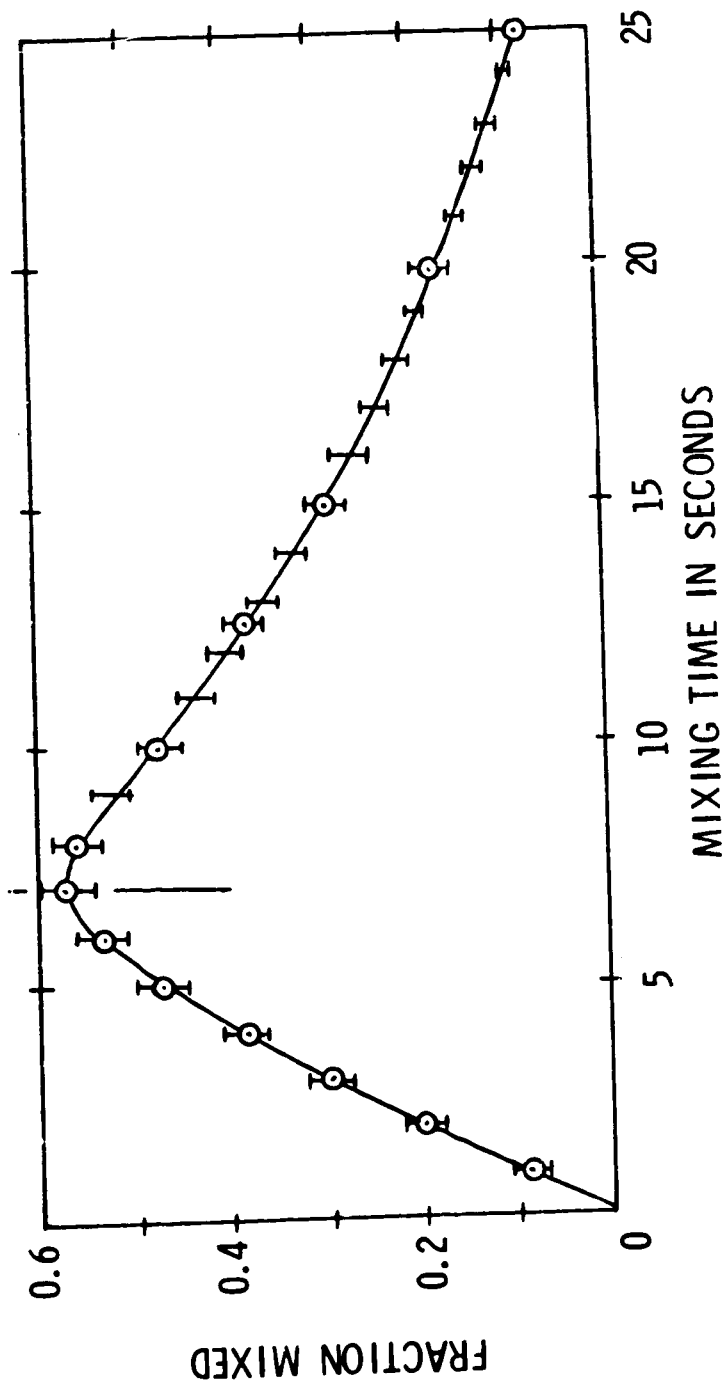


FIGURE 4. MIXING FUNCTION OR SPILL FUNCTION FOR THREE COMPONENT LIQUID PROPELLANT SPILL TESTS (REF. 27)

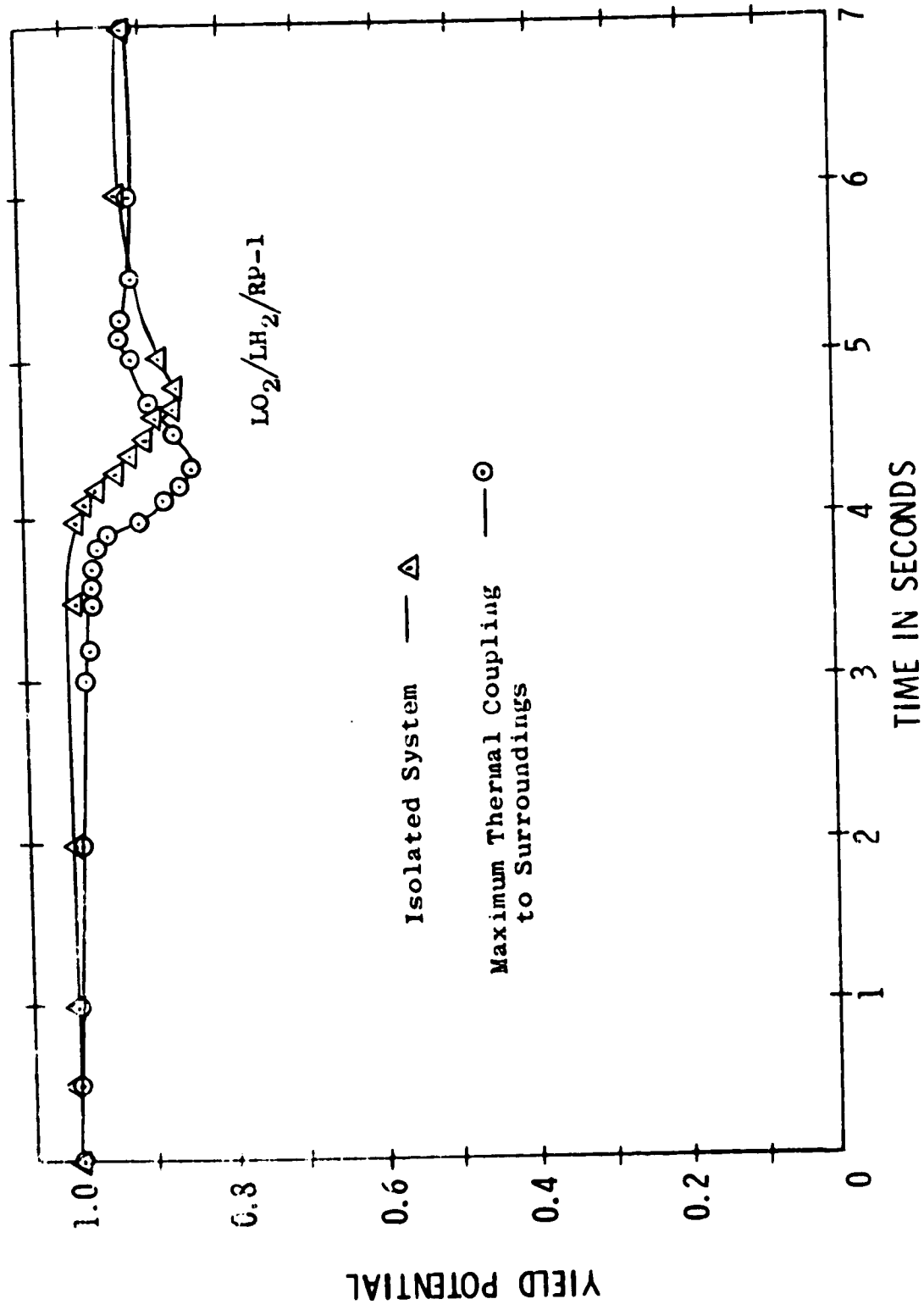


FIGURE 5. YIELD POTENTIAL AS TIME FUNCTION

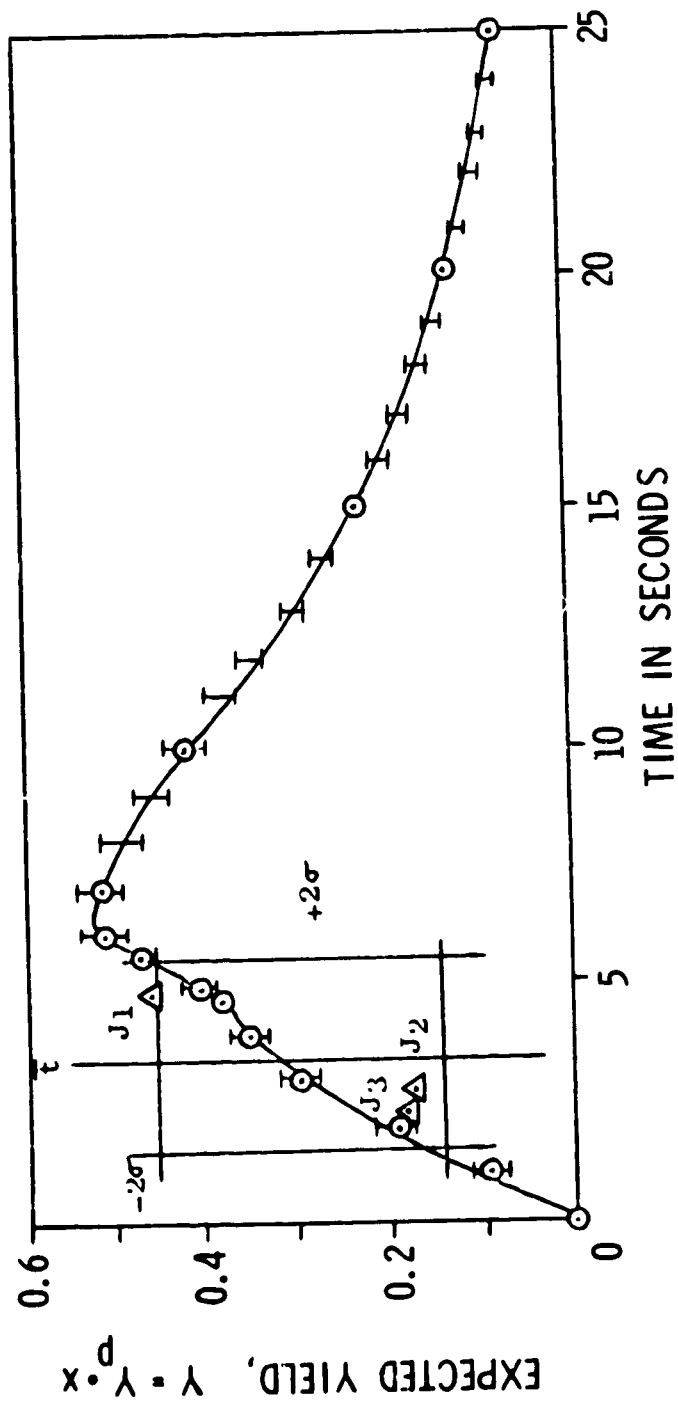


FIGURE 6. ACTUAL YIELD FOR RANDOM IGNITION AND DETONATION (REF. 27)

$$y = \frac{b}{b+c} x^d \quad (2)$$

where b , c , and d are parameters to be adjusted. An auxiliary function is also introduced which inserts a fourth parameter, a . Using the physically realistic limits of zero yield for zero spill, and a maximum for y when $x = 1$ which is defined by the fraction of mixed propellants which represent stoichiometry ($y \leq 1$), fixes the parameters b and c . Farber originally used data from reference 24 to estimate the parameter d , and has not changed this parameter since. So, essentially only the parameter a remains to be varied, and Farber claims that the parameter a represents a "scaling parameter" related to total mass of propellants. With parameters chosen from fitting data of reference 24, Farber claims (ref. 28) prediction of upper bounds on explosive yield which cover all available data through 1969 (see Figure 7).

After review of the work of Farber, Deese and co-workers, we feel that their efforts have their strengths and weaknesses, just as does the PYRO work. The greatest strengths are the excellent physical insight into the complex processes which occur during mixing and ignition of liquid propellants, and the division of the complex overall problem into sub-problems which can be studied separately. Farber and co-workers were also apparently the first to realize that explosive yields for large quantities of propellants were always limited by early autoignition. The primary weaknesses lie in lack of experimental verification of the physical processes, sometimes doubtful claims of usefulness or applicability of limited test techniques or data*, and reiteration of the same material in succeeding reports. The two methods for prediction of blast yield are well described and understandable, but both give an estimate of explosive source energy without consideration of the nature of the blast waves generated by liquid propellant explosions which were evident in Project PYRO. It is also not clear how the critical mixing function such as Figure 4 is obtained for various types of full-scale accidents or tests, or how it is scaled from laboratory experiments.

D. Estimation of Blast Wave Properties

We present here methods of estimating blast yields and blast wave properties for liquid propellant explosions, based primarily on PYRO results and on the work of Farber and Deese. Although our prediction methods retain many of the features of the previous work, they also differ somewhat where we feel changes are appropriate. Furthermore, factors which appear to have

In particular, response times, time resolution and identification of physical phenomena from thermocouple grid measurements claimed in reference 27 seem doubtful.

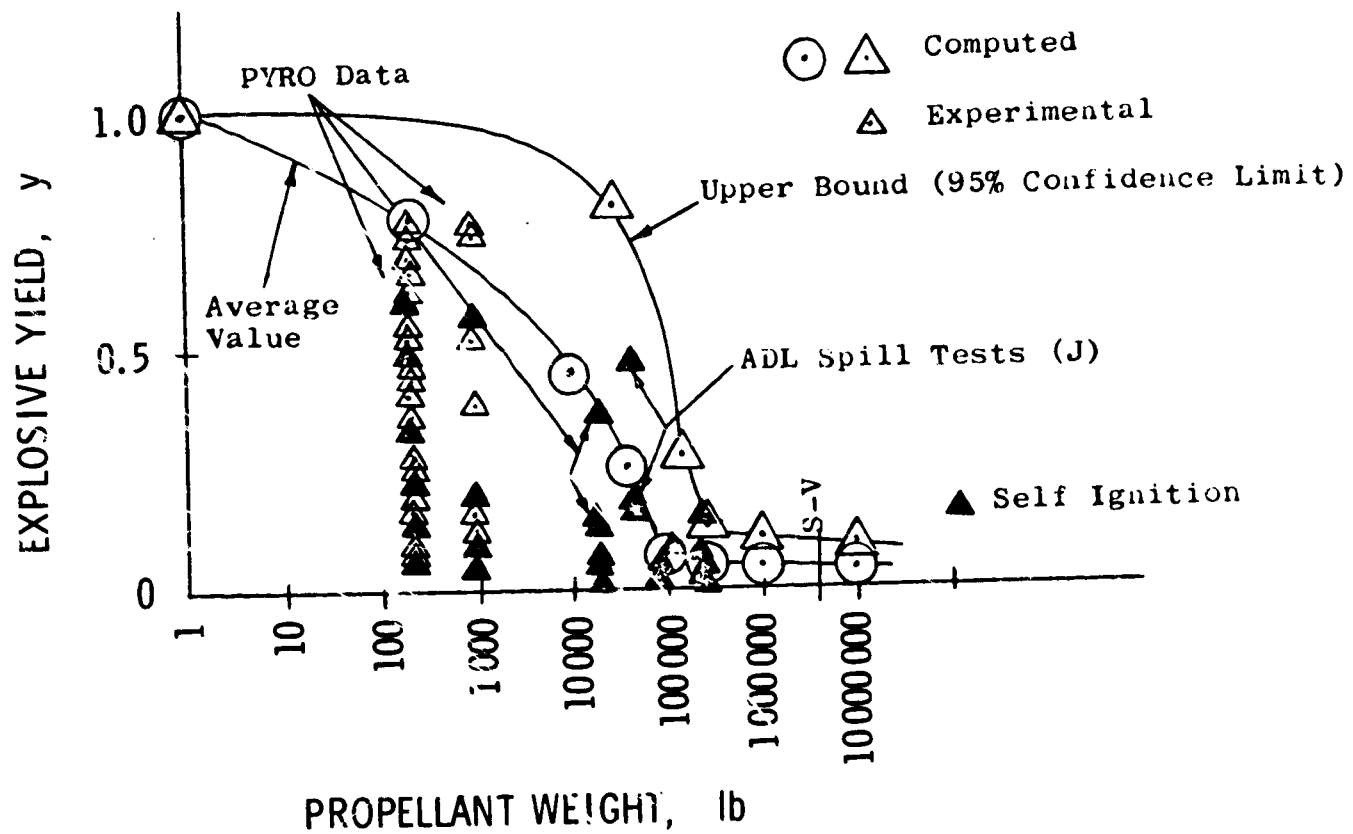


FIGURE 7. ESTIMATED EXPLOSIVE YIELD AS A FUNCTION OF PROPELLANT WEIGHT (REF. 27)

secondary effect on blast yield, such as L/D ratio of tankage, are ignored. The concept of "TNT equivalency" is used only to estimate energy of a liquid propellant explosion, and not to predict detailed blast wave characteristics. Blast is strongly dependent on type of propellant, type of simulated accident, impact velocity, and ignition time, so these factors must be accounted for in estimating blast wave characteristics and yield.

Throughout the PYRO work, blast yield is expressed as percent yield, based on an average of pressures and impulses measured at the farthest distance from the source when compared to standard reference curves (ref. 2) for TNT surface bursts (terminal yield). Hopkinson's blast scaling is used when comparing blast data for tests with the same propellants and failure conditions, but different mass of propellant. So, the blast parameters P (peak side-on overpressure) and $I/W^{1/3}$ (scaled impulse) are plotted as functions of $R/W^{1/3}$, (scaled distance) after being normalized by the fractional yield. This procedure is equivalent to determining an effective weight of propellant for blast from:

$$W = W_T \times \frac{Y}{100} \quad (3)$$

where W_T is total weight of propellant, Y is terminal blast yield in percent, and W is effective weight of propellant. Because the data are normalized by comparing to TNT blast data, the effective blast energy E can be obtained by multiplying W by the specific detonation energy of TNT, 1.4×10^6 ft lb/lb_m. We will use smoothed curves through the scaled PYRO blast data, and Equation (3), to obtain blast wave properties for any particular combination of propellants and simulated accident. We will consider each propellant combination separately.

1. Hypergolic Propellant - The hypergolic propellant in widest use, and used in the PYRO tests, is a fuel of 50% $N_2 H_4$ -50% UDMH and an oxidizer of $N_2 O_4$ in a mass ratio of 1/2. Hypergolic materials, by definition, ignite spontaneously on contact, so it is not possible to obtain appreciable mixing before ignition unless the fuel and oxidizer are thrown violently together. Ignition time is therefore not an important determinant of blast yield for hypergolics, but impact velocity and degree of confinement after impact are important factors. Project PYRO results and resulting prediction methods which are given in references 15-17 concentrate on these factors and can be used directly to obtain estimates of blast yield. The only modification which we propose is to use smoothed curves from PYRO results for peak overpressures and impulses, rather than multiplying factors.

The procedure is then as follows:

- (1) Consider failure mode, or impact velocity and type of surface impacted.
- (2) Obtain terminal yield Y in % from Table III or Figure 8 (from reference 16).
- (3) Calculate W from Equation (2) knowing total weight of propellant and Y .
- (4) At distances R of interest, compute Hopkinson-scaled distance $R/W^{1/3}$.
- (5) From appropriate smooth curves in Figures 9 and 10, read peak overpressure P and scaled impulse $I/W^{1/3}$. Multiply scaled impulse by $W^{1/3}$ to obtain I .

TABLE IV - ESTIMATE OF TERMINAL YIELD (REF. 16)

FAILURE MODE	TERMINAL YIELD RANGE (%)	ESTIMATED UPPER LIMIT
Diaphragm rupture (CBM)	0.01 - 0.8	1.5
Spill (CBGS)	0.02 - 0.3	0.5
Small explosive donor	0.8 - 1.2	2
Large explosive donor	3.4 - 3.7	5
Command destruct	0.3 - 0.35	0.5
310-ft drop (CBGS)	~1.5	3

Note that the blast yields are very low (a fraction of one percent to a few percent) for all but high velocity impacts, which is not surprising in view of the small amount of mixing which is possible before ignition. Possible error in estimation of yield is also substantial, as can be seen from the ranges of yields in Table IV and data scatter in Figures 8, 9 and 10.

2. Liquid Oxygen-Hydrocarbon Propellant - The second propellant combination which we will consider uses Kerosene (RP-1) as a fuel, and liquid oxygen (LO_2) as the oxidizer in stoichiometric mass ratio of 1/2.25. Because this liquid propellant is not hypergolic, considerable mixing can occur in

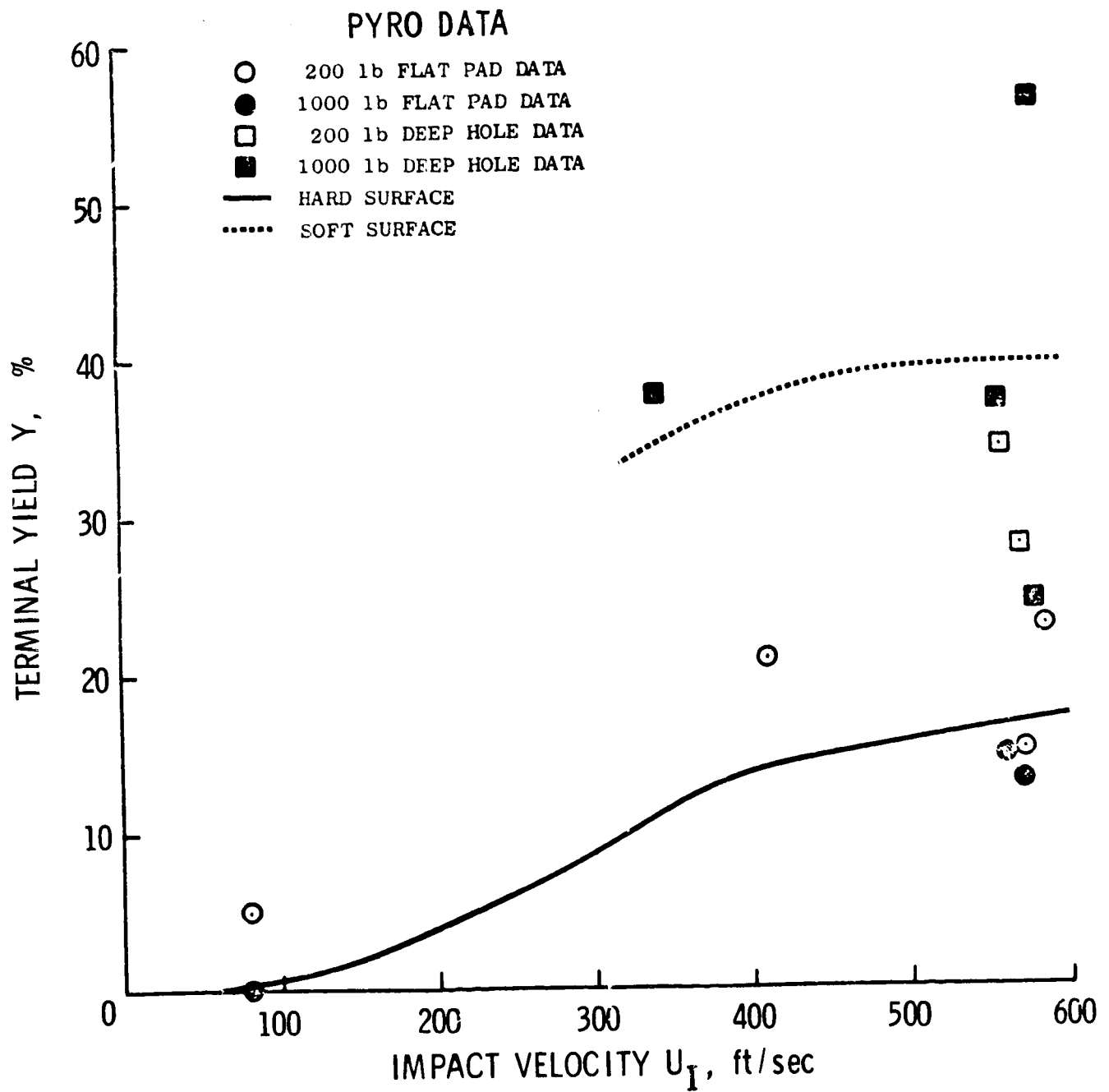


FIGURE 8. TERMINAL YIELD VS IMPACT VELOCITY FOR HYPERGOLIC HIGH-VELOCITY IMPACT (REF. 16)

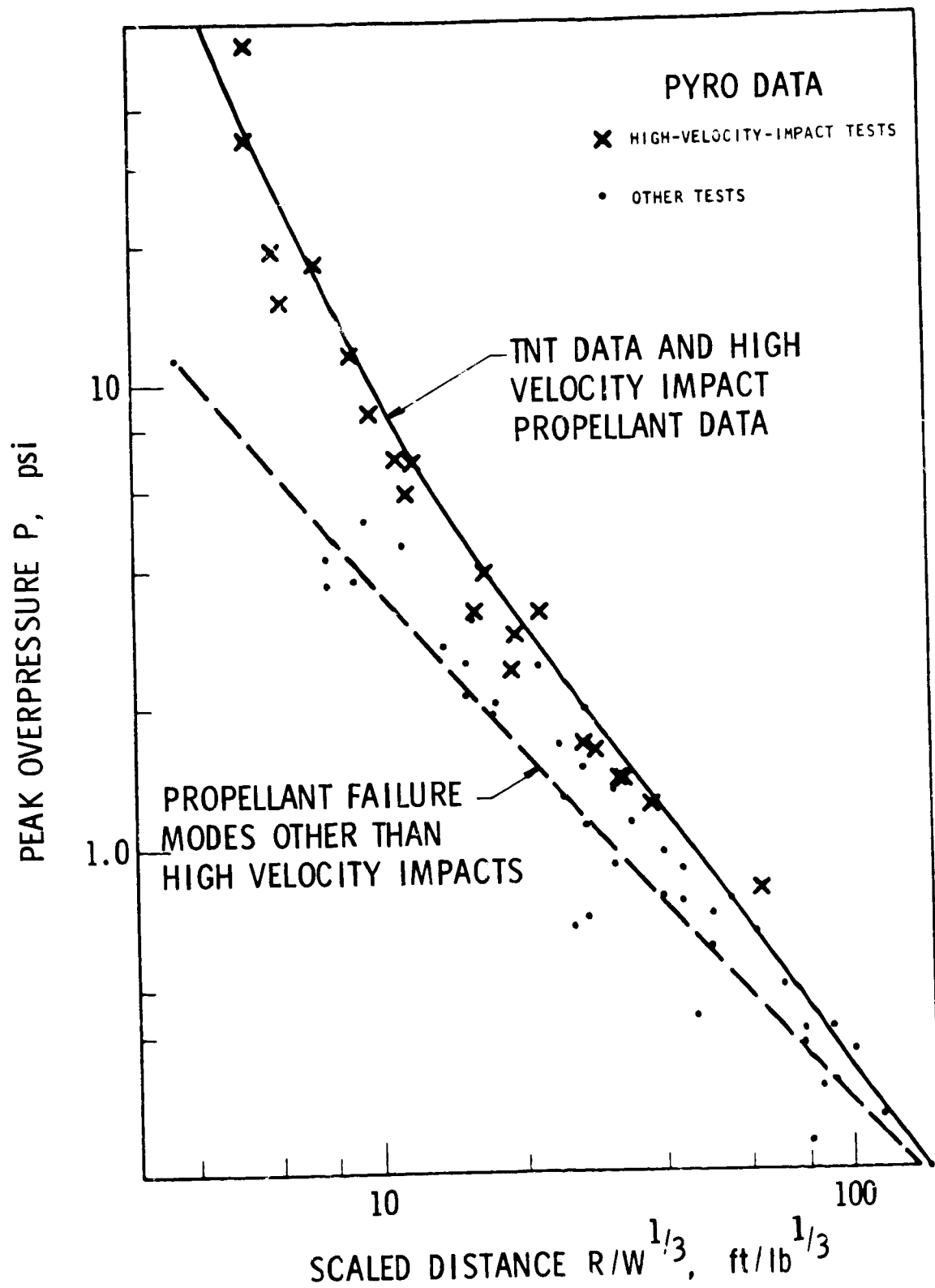


FIGURE 9. PRESSURE VS SCALED DISTANCE FOR HYPERGOLIC TESTS

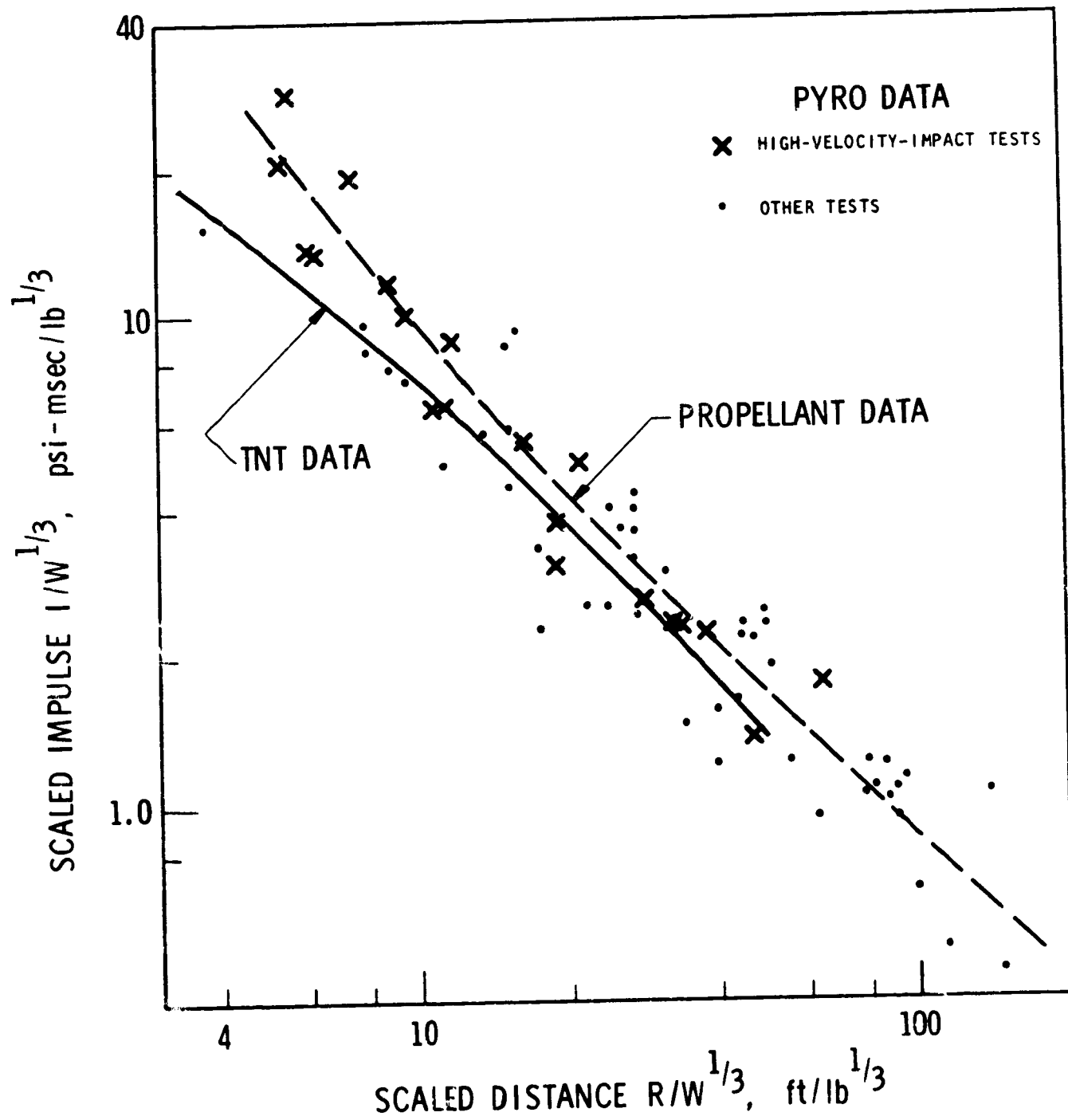


FIGURE 10. SCALED POSITIVE IMPULSE VS SCALED DISTANCE FOR HYPERGOLIC TESTS

various types of real or simulated accidents, and time of ignition after onset of mixing is an important determinant of blast yield. Other important parameters have been shown by the PYRO and other results to be the mode of failure or simulated accident, impact velocity, and propellant mass or weight. Less important parameters appear to be geometry of tankage expressed as a length-to-diameter (L/D) ratio, propellant orientation, and area of rupture of interior bulkhead for CBM case. The estimation methods which we give here are based largely on the PYRO test results, but also include conclusions and/or physical reasoning of our own and of Farber and other investigators.

For the case of mixing and an explosion within the missile tankage (CBM), time for ignition and mass of propellant are the principal determinants of blast wave properties. The scaling of ignition time assumed for PYRO is not proven by the PYRO test results (see Appendix A), so we simply plot a smooth curve through PYRO results for blast yield Y as a function of time t in Figure 11. We also use Farber's physical reasoning in plotting this curve, i. e., for zero time for mixing, yield must be zero, and for long enough time, yield must decrease. A direct plot against ignition time is used, independent of mass of propellant, because it fits the data as well as scaled time plots and also serves to indicate that scaling of ignition time has not yet been verified experimentally. Once blast yield Y has been determined from Figure 11 for an assumed ignition time, effective weight of propellant W is then calculated from Equation (3) for known Y and W_T , and blast pressures and impulses are obtained from fits to PYRO data in Figures 12 and 13, in exactly the same manner as for the hypergolic propellants.

For simulated fall-back on the launch pad (CBGS), impact velocity as well as ignition time are important parameters in estimating blast yield. PYRO prediction methods included fits to scaled time parameters and to impact velocity to a fractional power close to one. As stated before, time scaling is not proven by the data. Also, linear dependence on impact velocity is simpler than a fractional power close to one and fits the data just as well. A suitable fit of maximum yield Y_m to impact velocity, agreeing with curve A of Figure 5-41 of reference 16, is:

$$Y_m = 5\% + \frac{2.08}{(\text{ft/sec})} U_I, \quad 0 \leq U_I \leq 80 \text{ ft/sec} \quad (4)$$

where Y_m is expressed in %, and U_I is in ft/sec. Blast data for this case from reference 16 are normalized with respect to Y_m by the factor $X \cdot 100/Y_m$, and plotted versus ignition time in Figure 14. The smooth curve through the data can then be used to predict percent yield using Y_m from Equation (4) for impact velocity U_I . Again, using Equation (3), W can be found and blast parameters determined from suitable fits to PYRO data, which are given here as Figures 15 and 16.

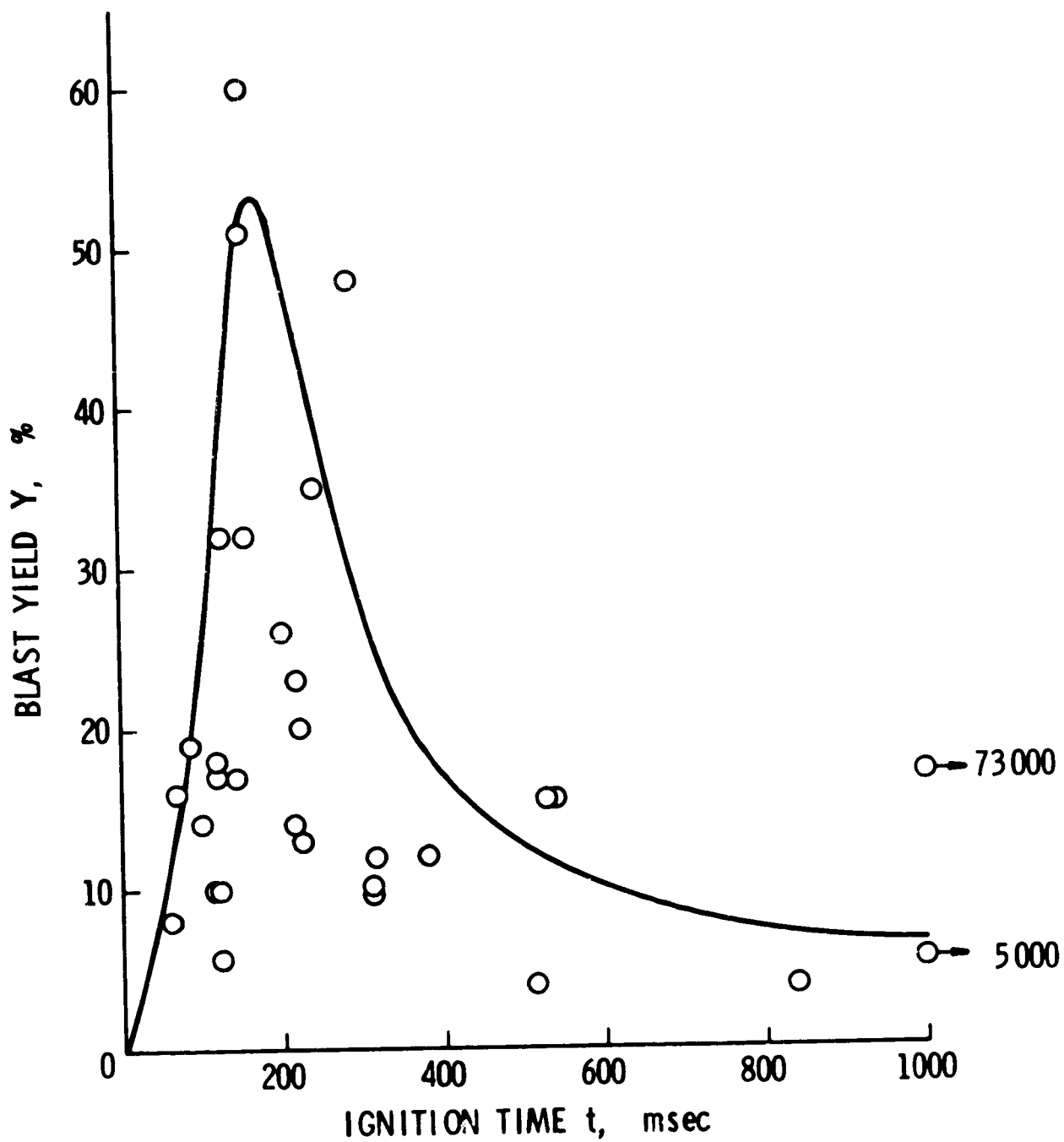


FIGURE 11. IGNITION TIME VS YIELD $LO_2/RP-1$ CBM

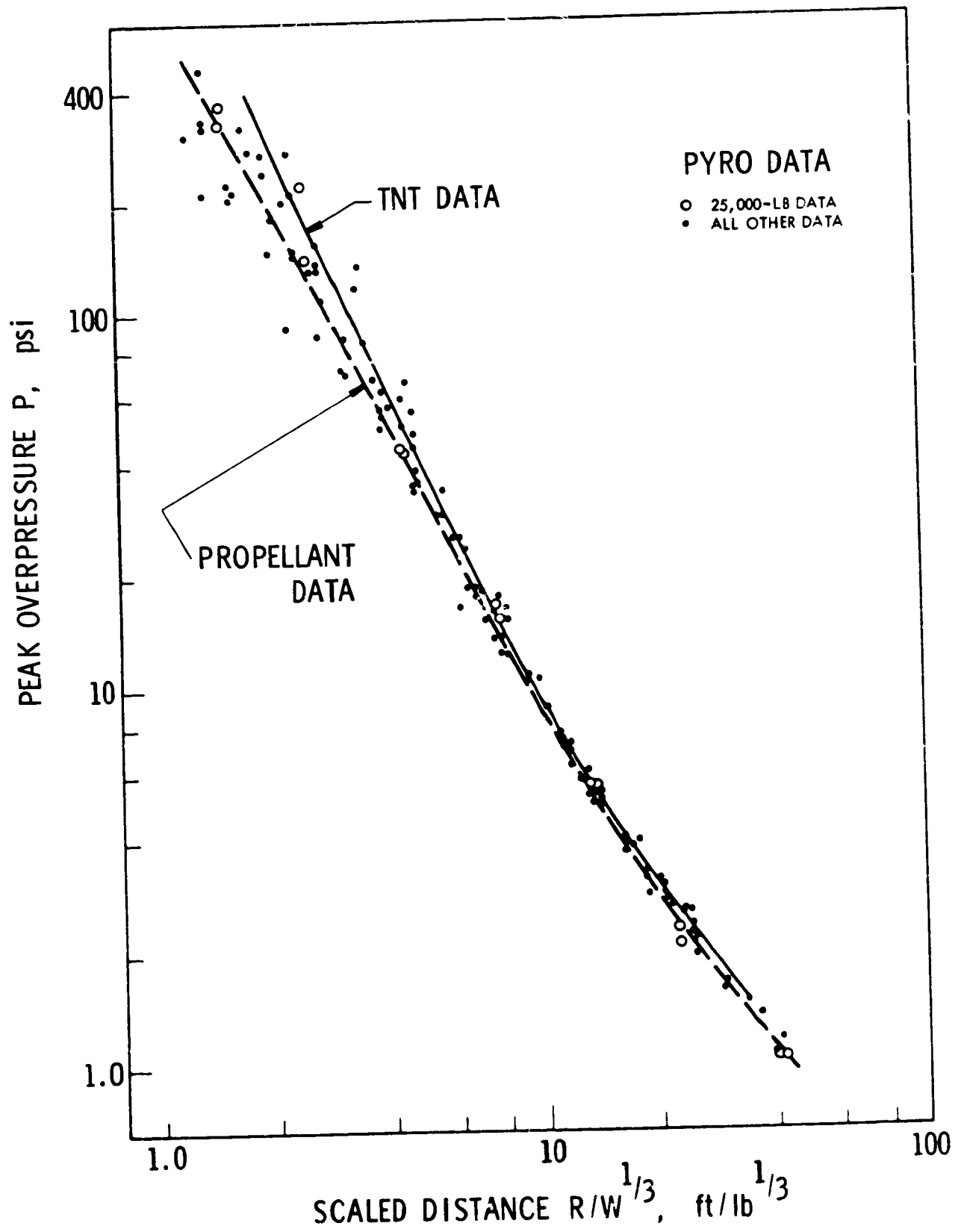


FIGURE 12. PRESSURE VS SCALED DISTANCE FOR
 $LO_2/RP-1$ CBM CASE

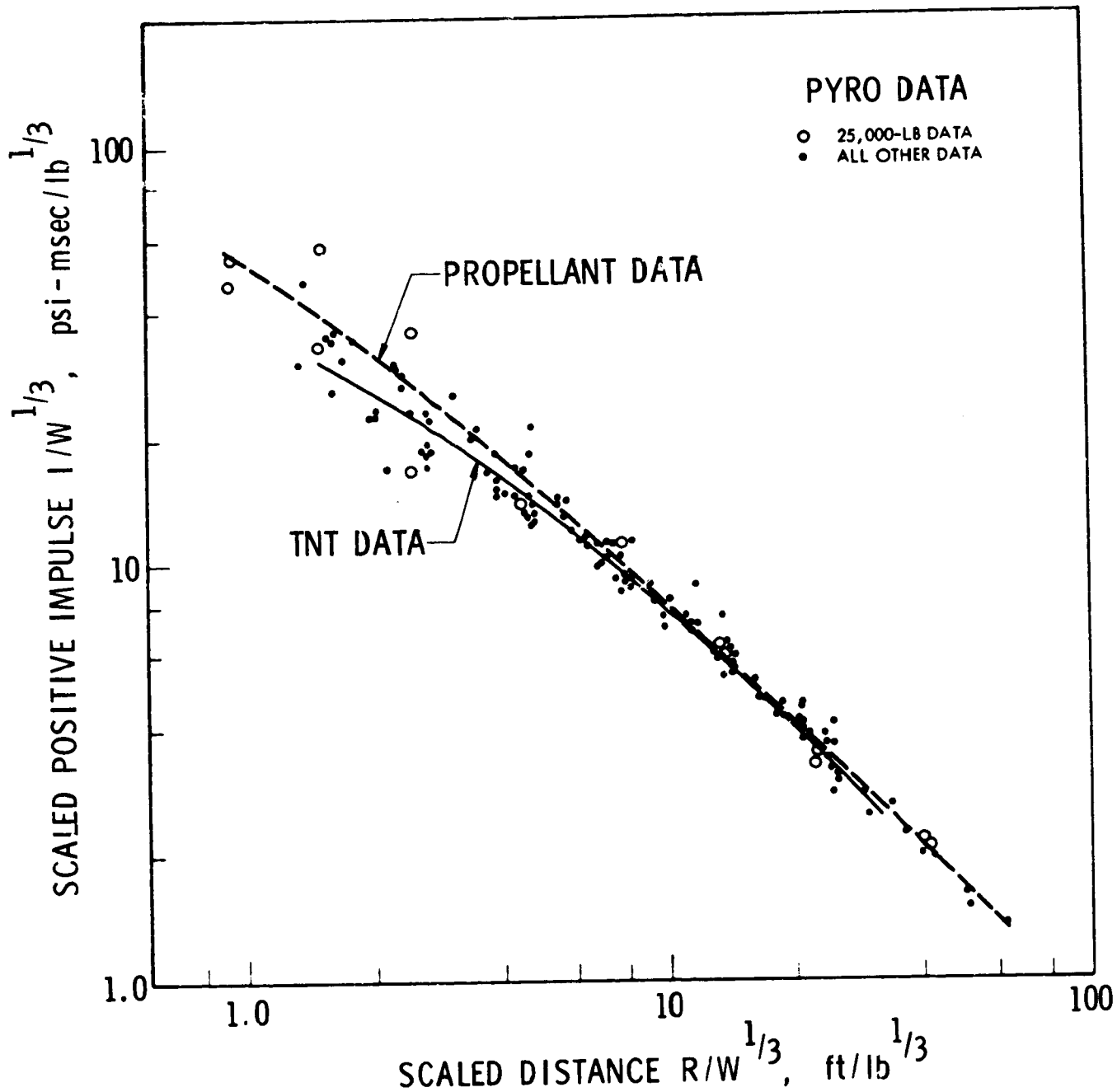


FIGURE 13. SCALED POSITIVE IMPULSE VS SCALED DISTANCE FOR $LO_2/RP-1$ CBM CASE

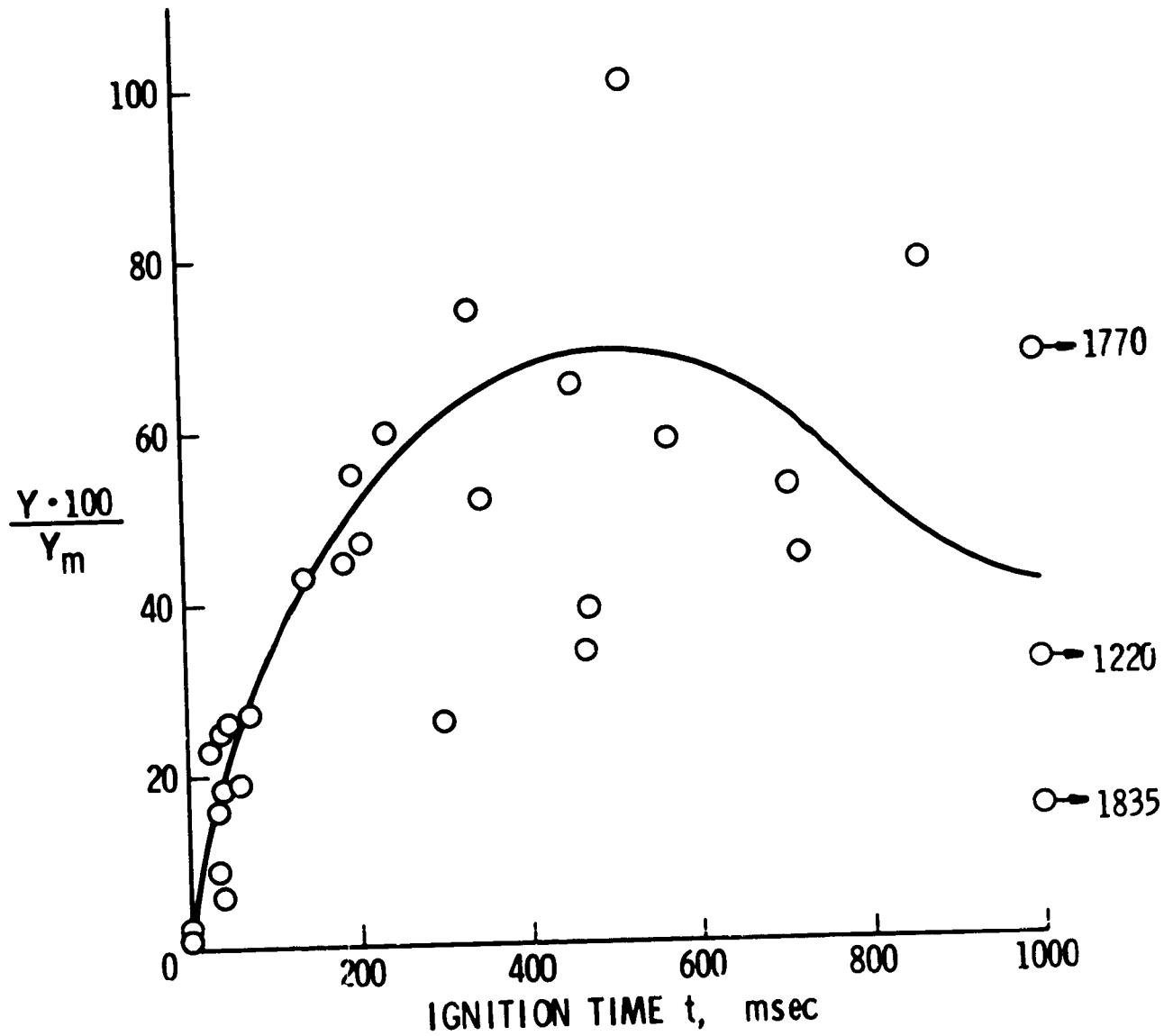


FIGURE 14. IGNITION TIME VS NORMALIZED YIELD
 $LO_2/RP-1$ CBGS

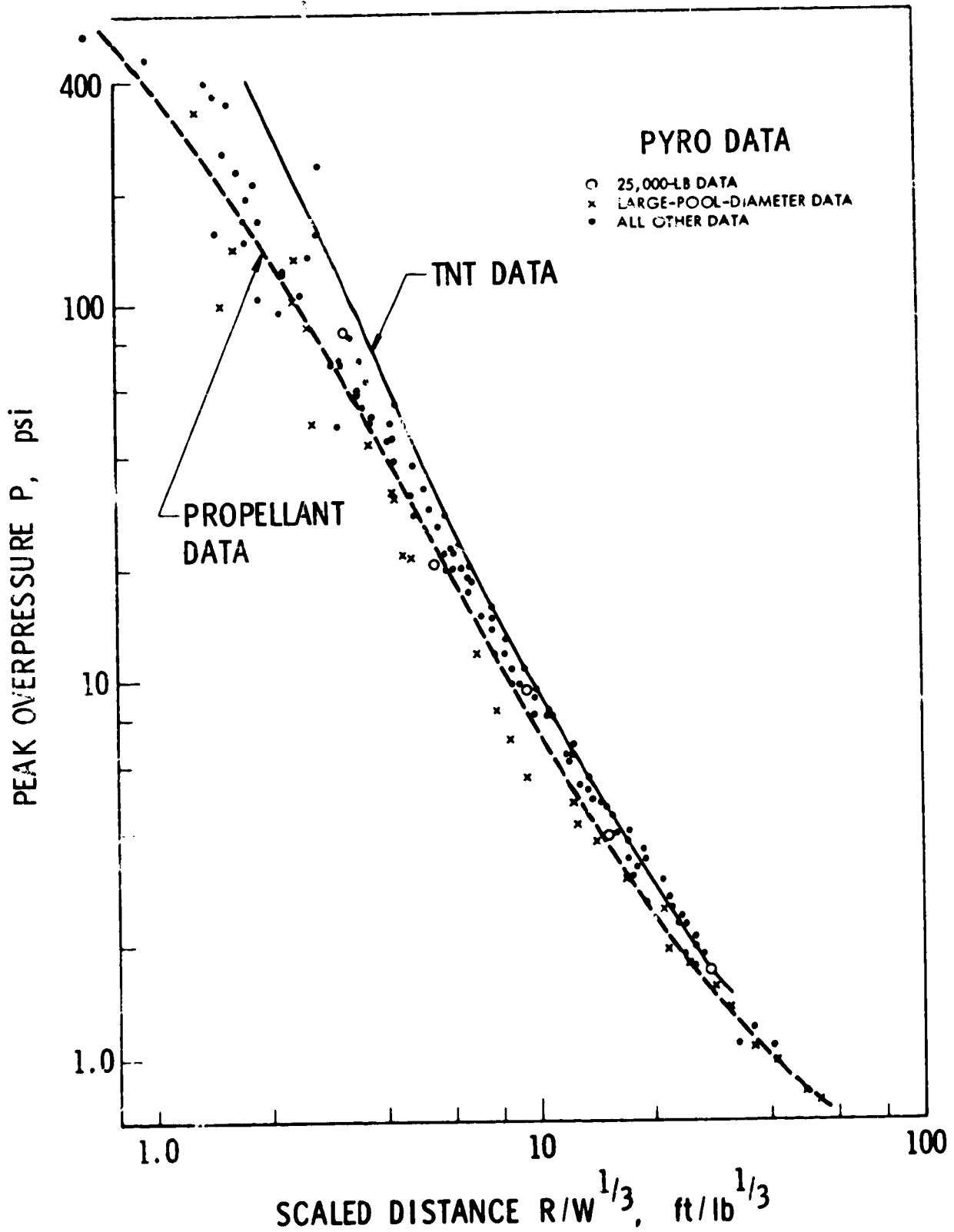


FIGURE 15. PRESSURE VS SCALED DISTANCE FOR $\text{LO}_2/\text{RP-1}$ CBGS-V CASE

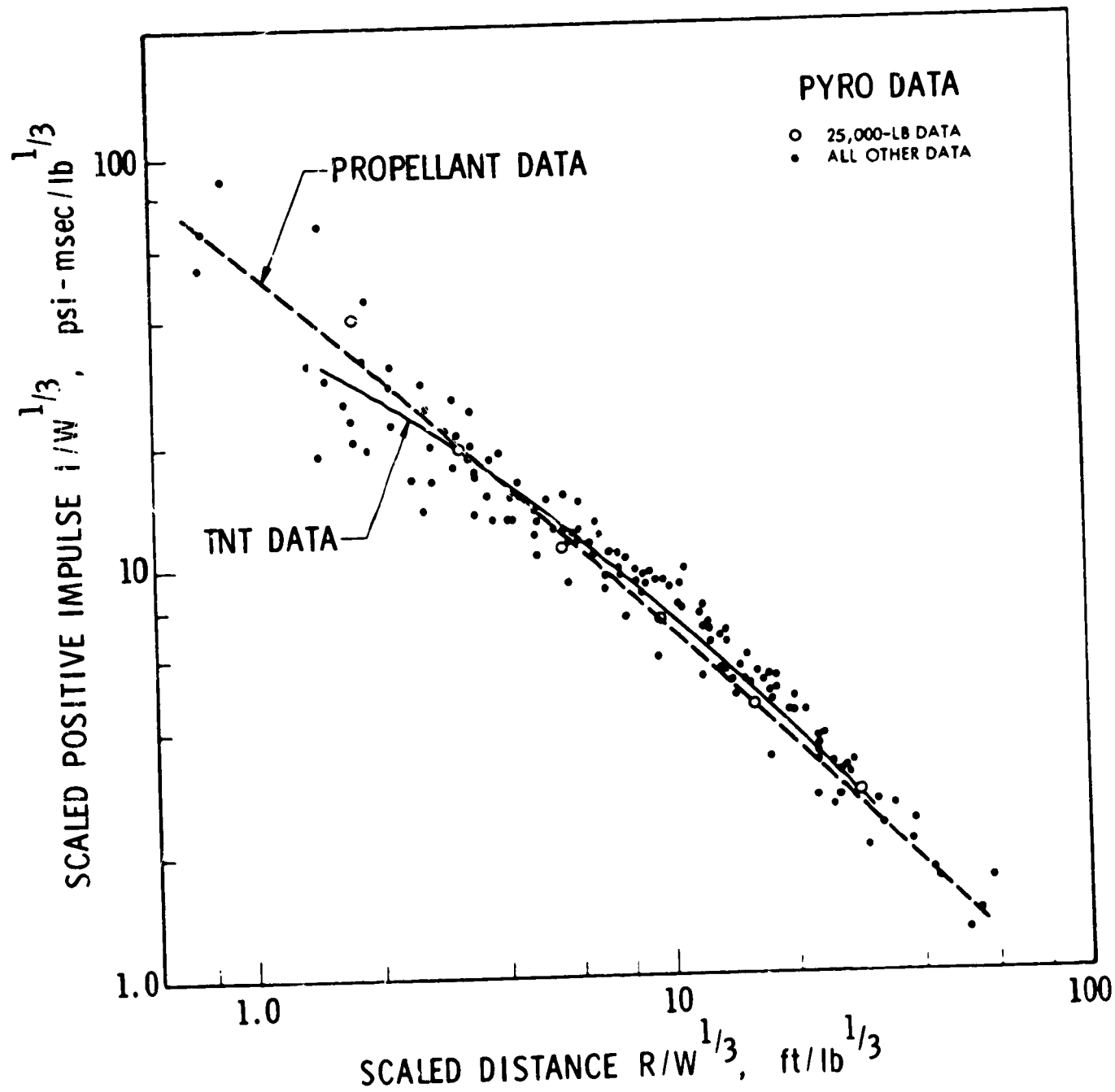


FIGURE 16. SCALED POSITIVE IMPULSE VS SCALED DISTANCE FOR $LO_2/RP-1$ CBGS-V CASE

In high velocity impacts of this propellant, the situation is somewhat simpler because there is little ignition delay and therefore only impact velocity affects yield. Prediction methods from reference 16 can then be used to estimate yield Y (see Figure 17) and blast parameters obtained from Equation (3) and Figures 15 and 16.

3. Liquid Oxygen-Liquid Hydrogen Propellant - The final propellant combination is the entirely cryogenic combination of liquid hydrogen (LH_2) fuel and liquid oxygen (LO_2) oxidizer in stoichiometric ratio by mass of 1/5.

The rationale for predicting blast parameters for this propellant combination is identical to that for $LO_2/RP-1$. For the CBM case, Figure 18 gives a plot of ignition time versus yield. After determining W from this plot and Equation (3), one can enter Figures 19 and 20 to obtain blast wave properties.

For the CBGS case, a linear fit of maximum yield versus impact velocity gives

$$Y_m = 10\% + \frac{1.35}{(\text{ft/sec})} U_I, \quad 0 \leq U_I \leq 80 \text{ ft/sec} \quad (5)$$

Using this equation to normalize ignition time versus yield, we obtain Figure 21. From the curve in Figure 21, we can find Y for a given ignition time, and then obtain W from W_T and Equation (2). Finally, blast pressure and impulse are obtained from Figures 22 and 23.

For high-velocity impact of this propellant, the blast yield is also dependent only on the impact velocity, and the prediction methods of reference 16 can be used directly. The curve in Figure 24 gives the yield Y , and Equation (3) and Figures 22 and 23 will give predictions of blast wave properties.

4. Limit to Yield for Large Mass of Propellant - Any method of predicting blast yield must, it seems clear, provide an upper limit on yield with increasing mass of propellant. All tests to date with large amounts of propellant have shown autoignition sources which prevent mixing of even a large portion of the propellant prior to ignition. The simplest way to incorporate a limit is to use the limit curve of Figure 7 generated by Farber. The curve labeled "average value" should probably be used for our purposes. Explosive yield y in Figure 7 is only approximately related to Y in all of the preceding discussion, because Farber bases his yield on actual energy of combustion of the propellant rather than TNT equivalence. But, considering the multitude of other errors in these methods, we can ignore the difference and simply assume that $y = Y/100$. (6)

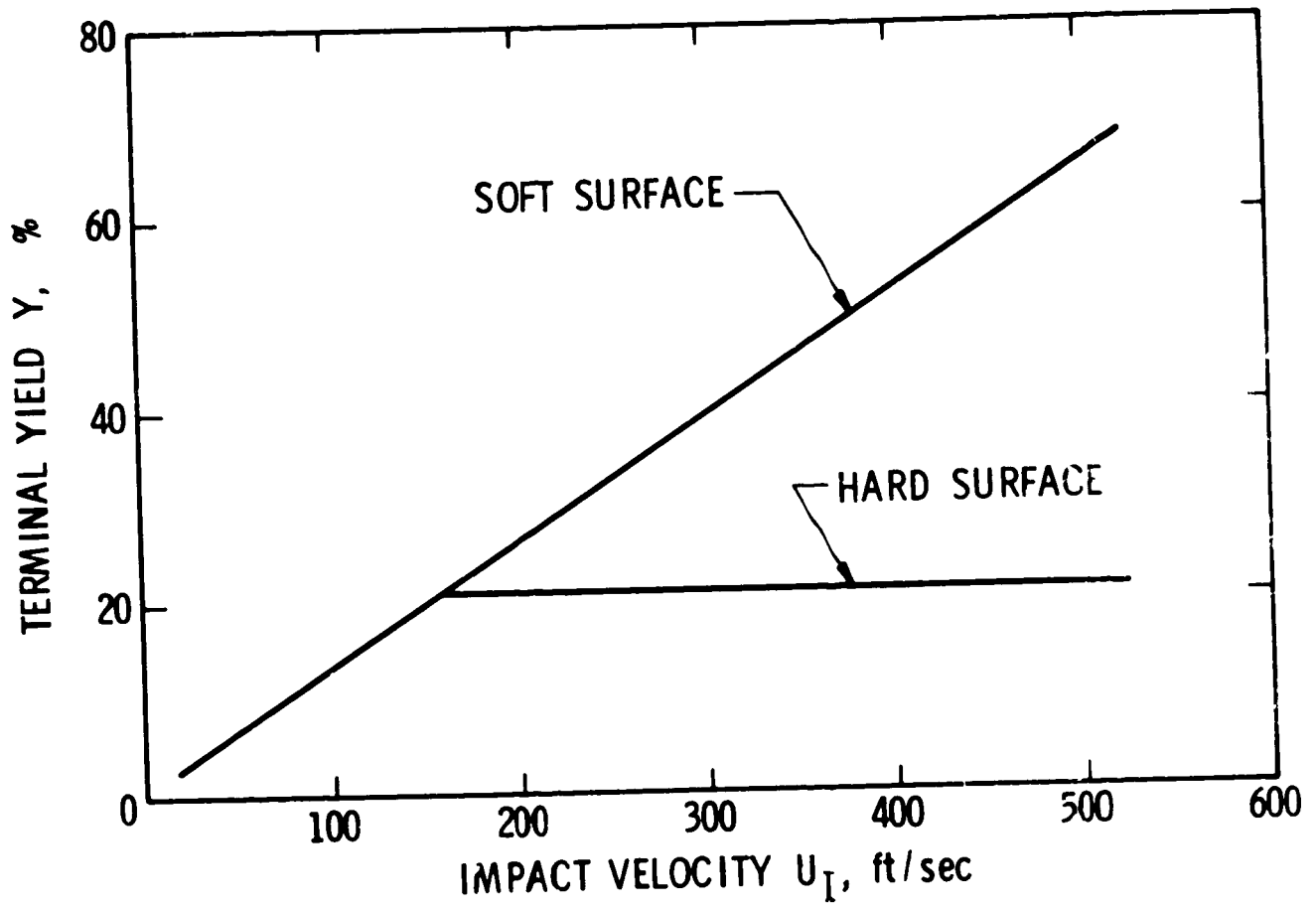


FIGURE 17. TERMINAL YIELD VS IMPACT VELOCITY FOR $LO_2/RP-1$ (REF. 16)

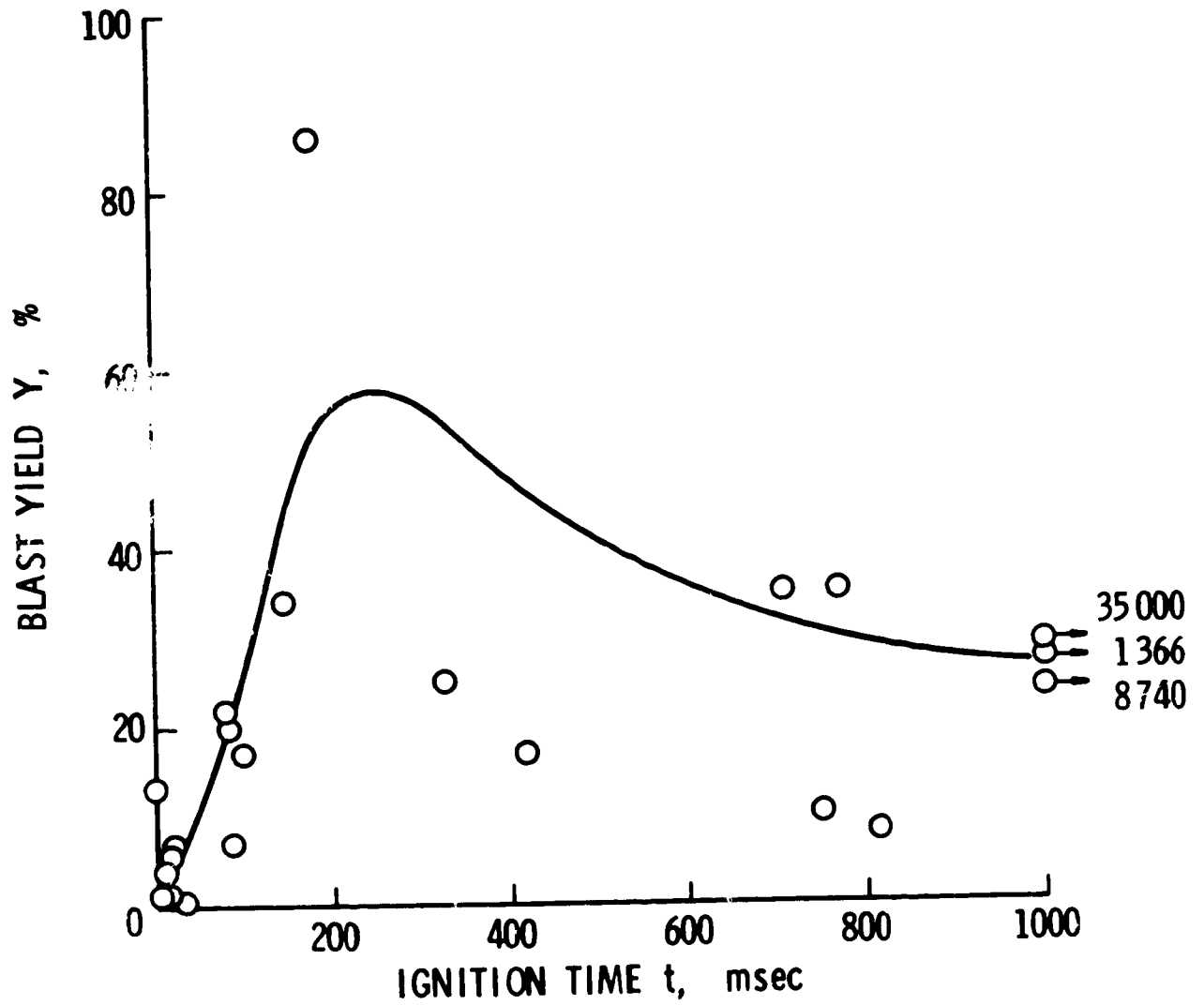


FIGURE 18. IGNITION TIME VS YIELD LO_2/LH_2 CBM

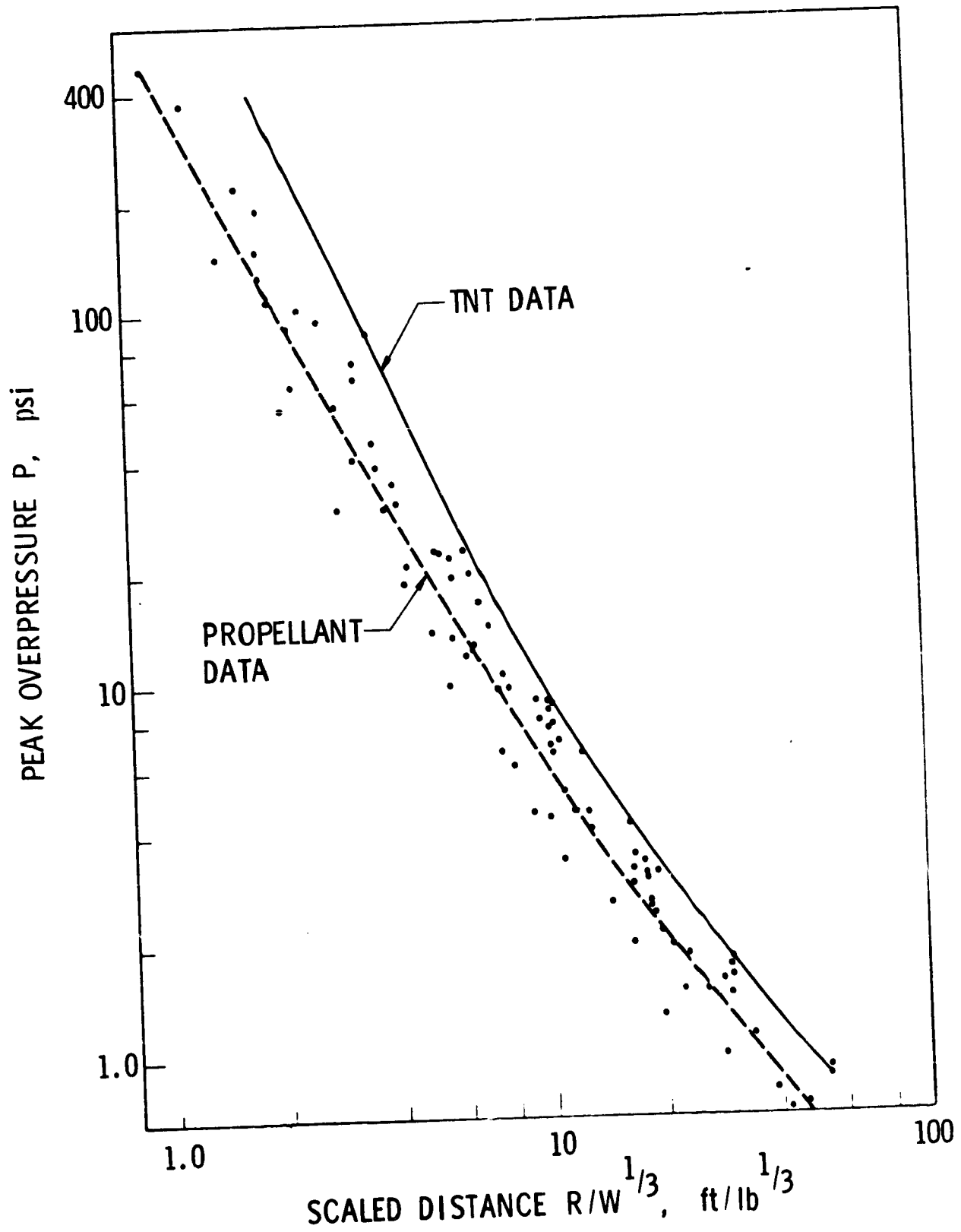


FIGURE 19. PRESSURE VS SCALED DISTANCE FOR LO_2/LH_2 CBM CASE

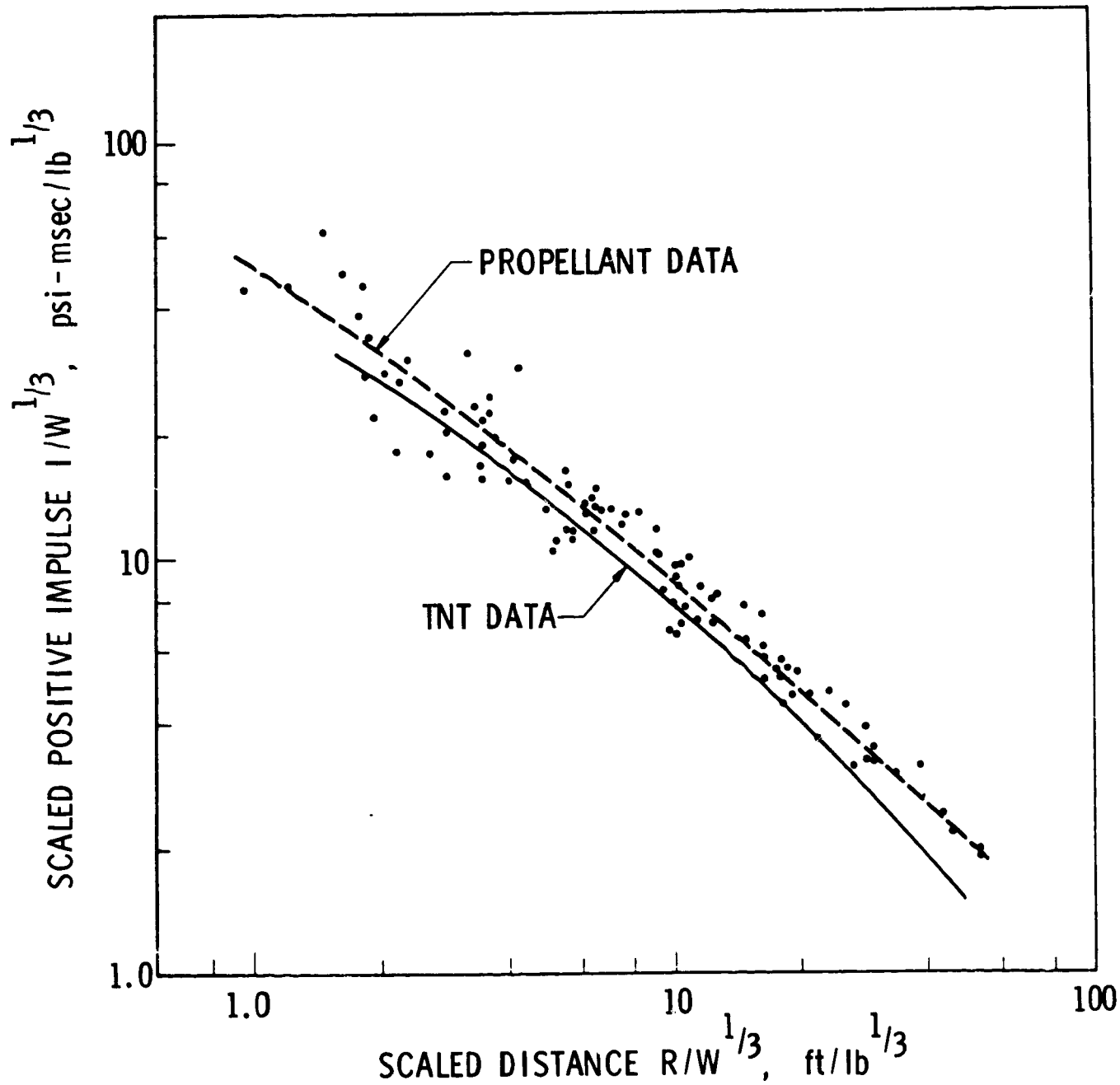


FIGURE 20. SCALED POSITIVE IMPULSE VS SCALED DISTANCE FOR LO_2/LH_2 CBM CASE

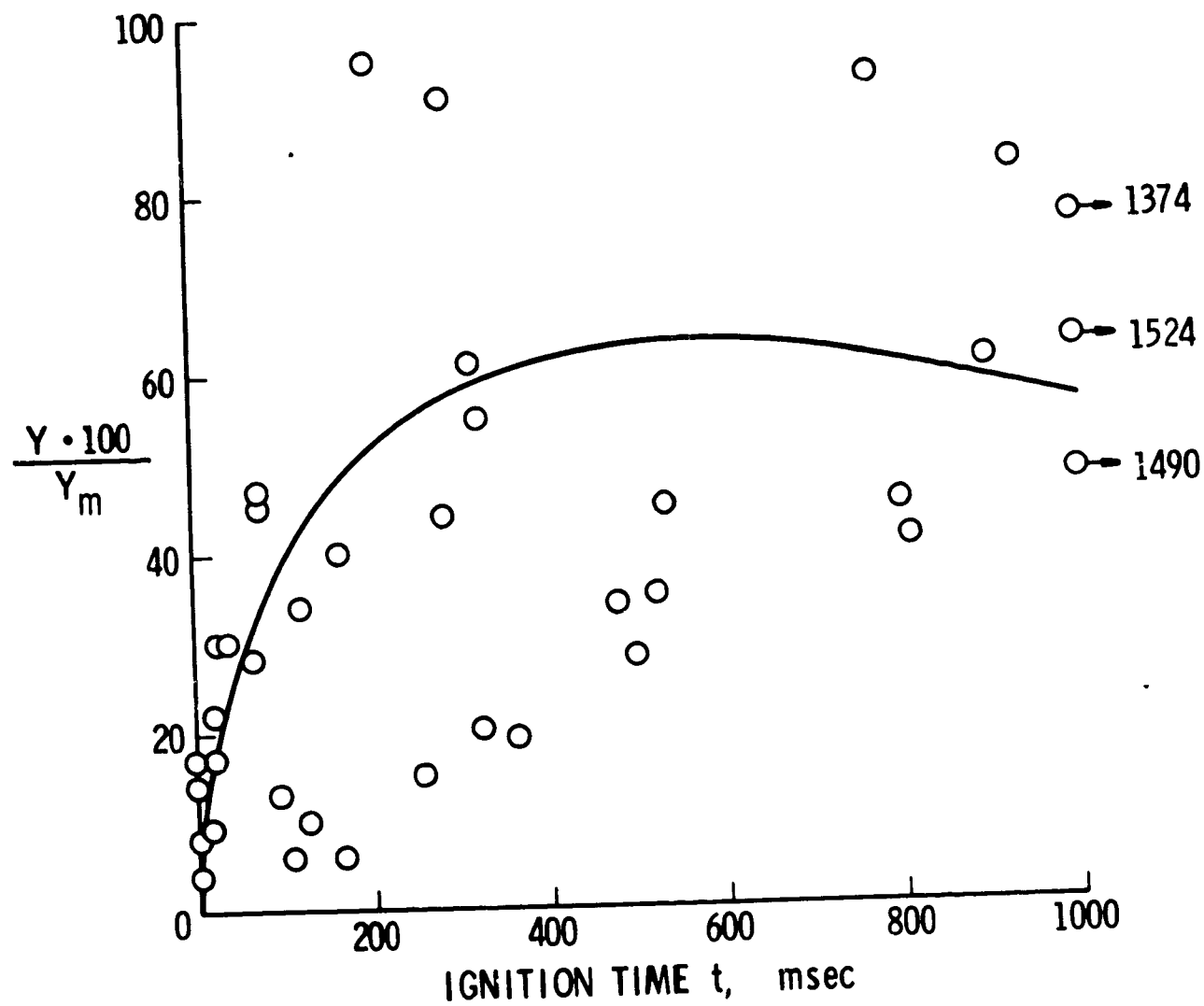


FIGURE 21. IGNITION TIME VS NORMALIZED YIELD LO_2/LH_2
CBGS

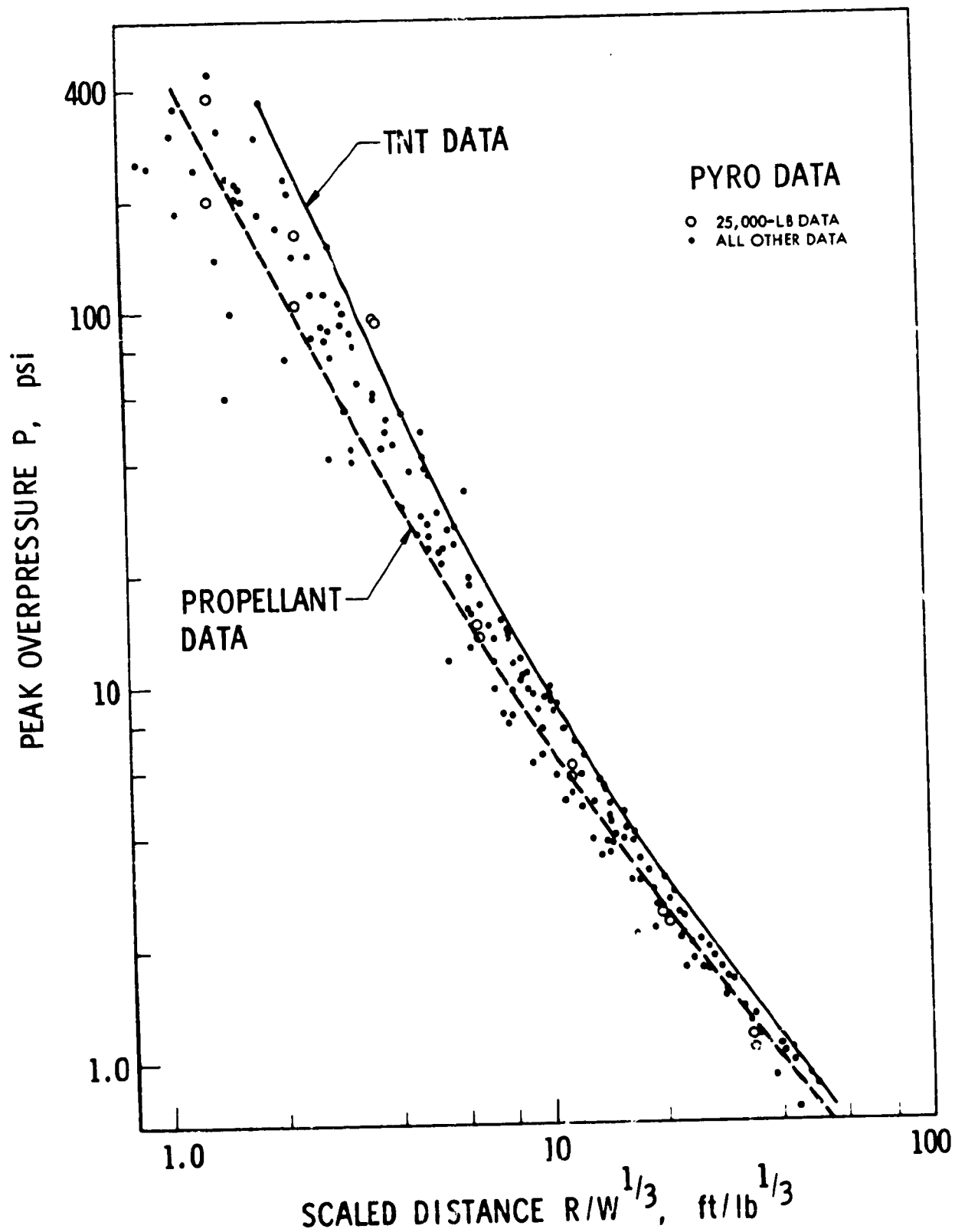


FIGURE 22. PRESSURE VS SCALED DISTANCE FOR LO_2/LH_2 CBGS-V CASE

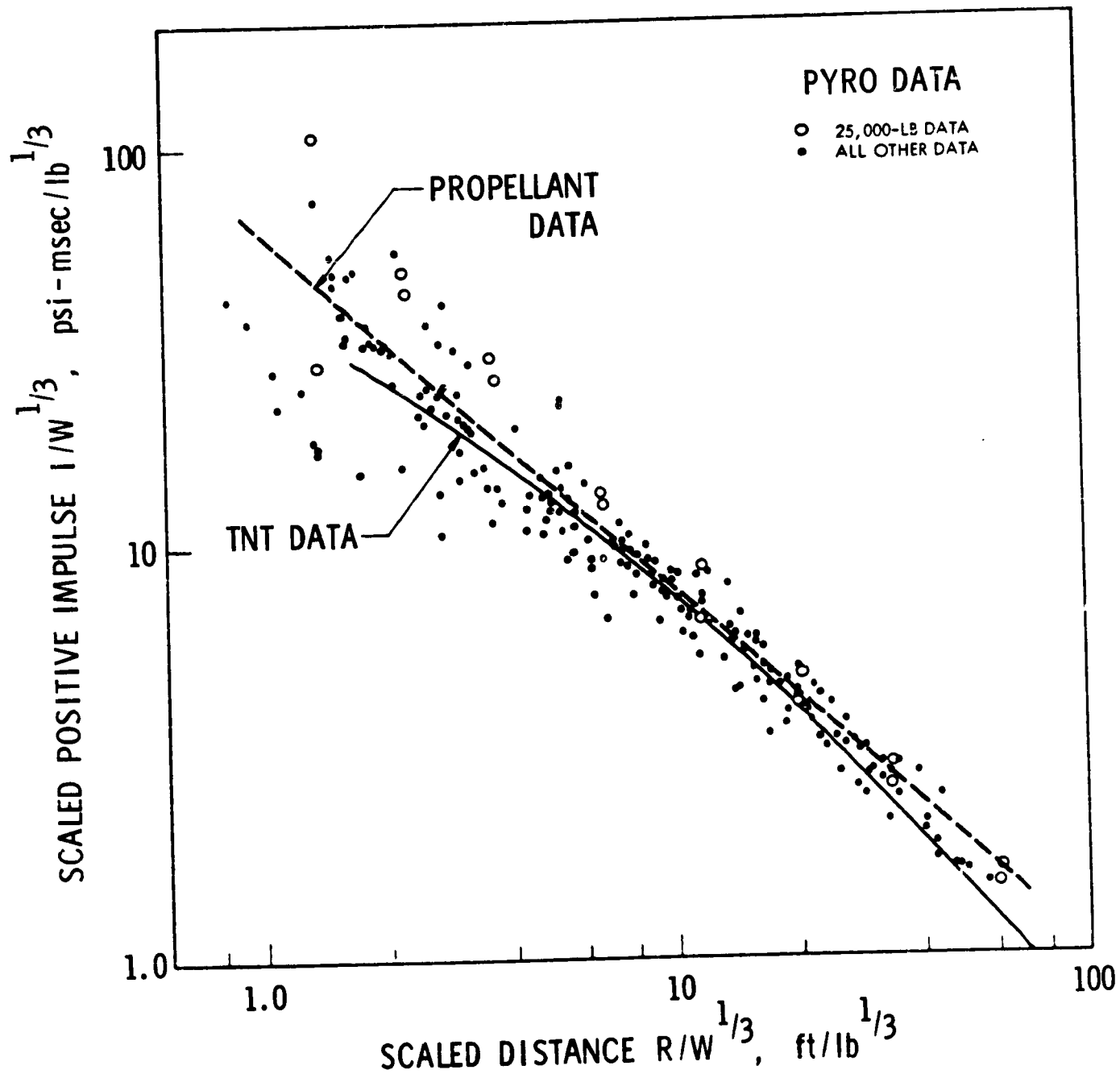


FIGURE 23. SCALED POSITIVE IMPULSE VS SCALED DISTANCE FOR LO_2/LH_2 CBGS-V CASE

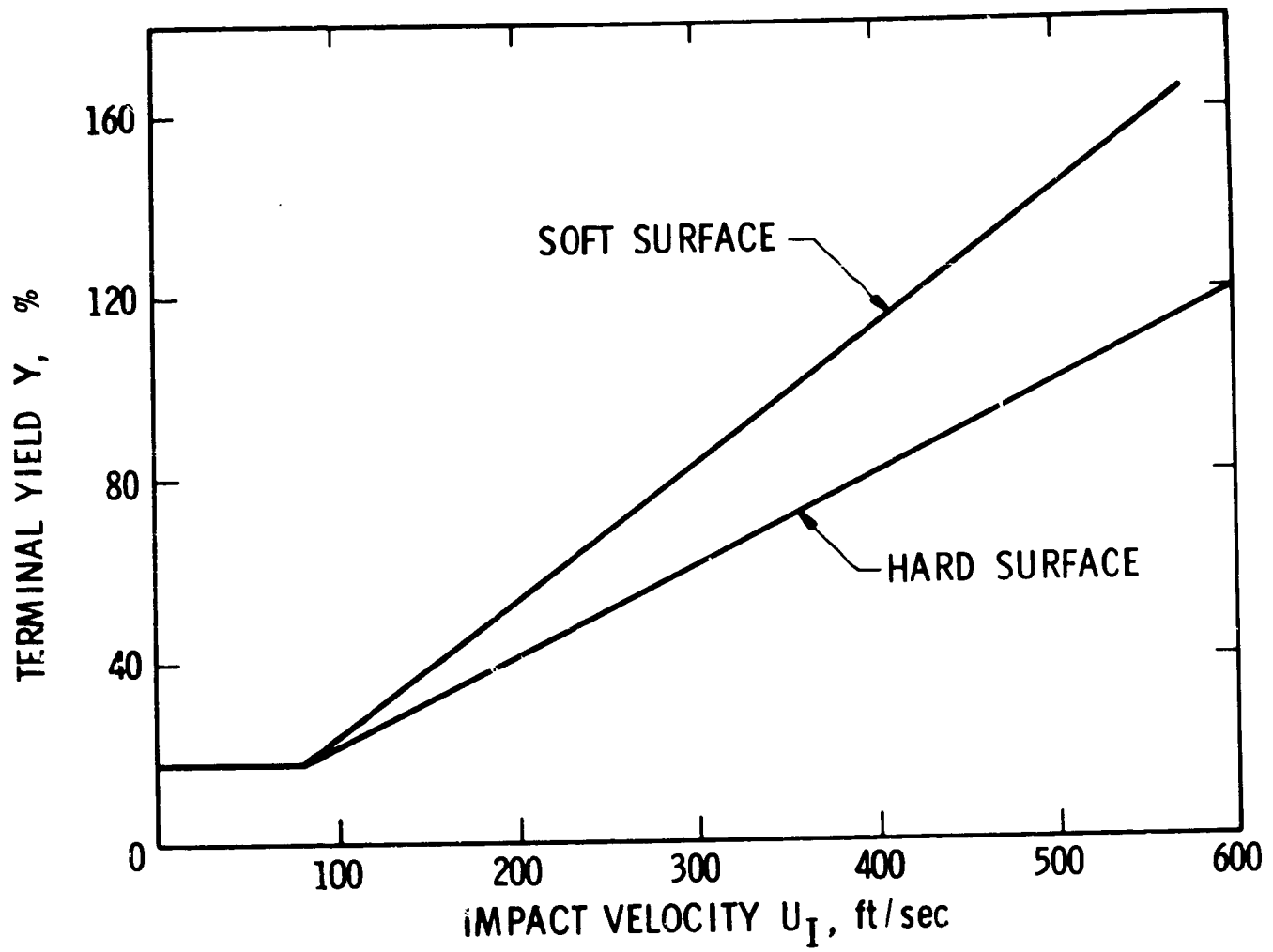


FIGURE 24. TERMINAL YIELD VS IMPACT VELOCITY FOR LO_2/LH_2 (REF. 16)

III. DETERMINATION OF FRAGMENT VELOCITY DISTRIBUTION

A. General

In our review of accident and test data for liquid propellant explosions, we found no data on the velocities of fragments produced by these explosions, outside of data available in films of Project PYRO. Only the report by Jeffers (ref. 18) contained an analysis of fragment velocities, and this analysis was based on a study of films of three of the PYRO tests.

The repository for all raw data, including films, from the extensive series of PYRO tests is the Air Force Rocket Propulsion Laboratory at Edwards Air Force Base, California. In visits to this agency, SwRI staff members viewed all of the library of PYRO films and selected for data reduction films of 94 tests in which individual fragments were visible and could be followed from frame to frame. These films were then loaned to the Institute for measurement of fragment velocities. For most of these experiments, several camera views of each test were available. Film speeds were accurately known, with timing marks at known repetition rates impressed on the edges of most films. The 94 tests for which we reduced fragment velocity data represented a spectrum of propellant types, scale of test, and type of simulated accident. In addition, reduced blast data and measured blast yields are known for each experiment and reported in references 15 and 16.

Because the PYRO films constituted our raw data for determination of fragment velocity and because reduction of these data required more detailed knowledge of test details than were available in references 15 and 16, we engaged a consultant from URS Corporation, prime contractors for PYRO. He provided us with sufficient additional information, drawings of test arrangements, etc., to enable us to obtain accurate estimates of such needed information as distance scales in the field of view of each camera and timing mark frequencies on films. He also helped us resolve unexplained discrepancies in reported PYRO test results.

Although the PYRO films provide all of our basic data on fragment velocities and can allow correlation with measured blast yields, they do not in general provide any data on fragment masses, shapes, or ranges. In only one PYRO test were these parameters measured, and this test is the only one for which any overall correlation of fragmentation effects conceivably can be made.

B. Reduction of Film Data

1. Camera Locations - Locations of the camera during PYRO tests from which fragmentation data were obtained are shown in Figure 25.

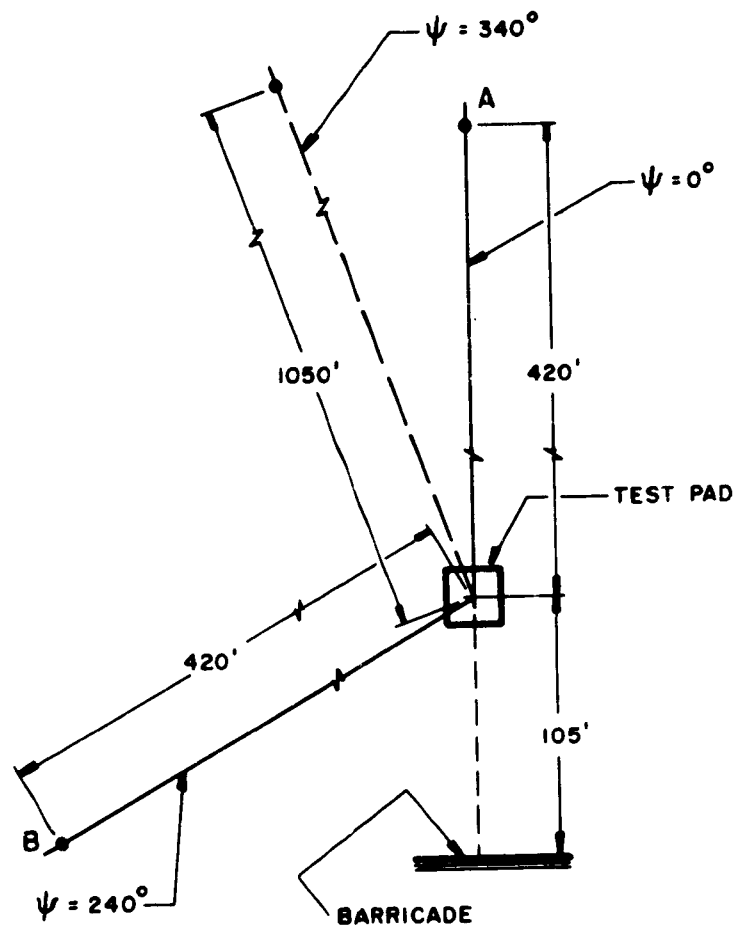


FIGURE 25. PLAN VIEW OF CAMERA LOCATIONS DURING PYRO TESTS

Cameras were located along radial lines at azimuth angles 0° , 240° and 340° and on a tower directly above the event.* A few tests were also photographed from airplanes and from the tops of nearby mountains, but these cameras were located too far away from the event to provide fragmentation data. During five tests cameras located at position B of Figure 25 were focused on the barricade located along an extension of the zero degree leg. Although fragment data were read from these films, they were not processed because the data were too few to be statistically significant.

The greatest number of films and the largest amount of data came from cameras located at the azimuth angles of 0° and 240° . These camera positions, also called positions "A" and "B", were located 420 feet from the center of the test pad. From these locations, cameras filmed the event with several different focal length lens and at indicated camera speeds ranging from 64 frames/sec to 1,000 frames/sec. Although overhead shots were available for most tests, they provided little usable data. The field of view of the cameras was small relative to the size of the fireball and the fragments were not visible in the flames. Cameras situated at azimuth position 340° were located 1,050 feet from the center of the pad and were mounted on a tower 110 feet above the ground surface. Since the elevation at the base of the tower is 36 feet above that at the test site, the cameras were actually 146 feet above the test pad. Only a few tests were photographed from this location, however, and not all of the films provided fragmentation data. Some cameras had a field of view which was so large relative to the size of the fireball that fragments could not be seen. Other cameras with longer focal length lenses provided good film data.

Generally, most data were obtained from those cameras which had a field of view slightly larger than the resulting fireball and which had the highest film speed. Because several camera views were often available from the same location (particularly for locations A and B), the view or views providing the best data were selected for reduction. For example, other factors such as field of view and quality of the film being equal, the film which had the higher framing rate was chosen for data reduction. Even at the higher framing rates, the film length was sufficient to observe the growth and start of decay of the fireball.

Most films were accompanied by data which identified the test number, camera number, camera speed, frequency of the timing mark generator, focal length of the lens, distance from the camera to the event, and the azimuth angle of the camera position. We found some of these data to be inconsistent. For example, we were informed by Project PYRO test personnel

*Obtained from drawings of field test arrangements for Project PYRO.

that cameras located 420 feet from the event were located at position "A" or position "B" (of Figure 25) on radial lines which are 120° apart. We found, however, that these positions were either labeled as 0° and 270° , respectively, or as 325° and 130° , respectively. Also, leg A was sometimes identified by an azimuth angle of 65° and the tower (located 1,050 feet from the pad) by azimuth angles of 300° and 340° (340° is correct). Consequently, we relied upon the background in the film itself to identify the leg upon which the camera was located. Except for cameras located directly above the event, (and those at distant locations which did not contribute fragmentation data), the cameras were assumed to be located at either position "A", "B", or at an azimuth angle of 340° as shown in Figure 25. This is consistent with the instructions of Project PYRO personnel.

Film data reduction was accomplished using a Vanguard Film Analyzer. Data obtained from the films included the frame number relative to the initiation of the explosion, the X and Y positions of the fragment referenced to the frame number, the spacing of the timing marks, the height to the top and bottom of the tank, the tank diameter, and, if in the field of view, the height of the tower above the test pad. The height of the tower was used for computing the scale factor. Since each test was viewed from more than one direction (from camera locations A and B) an attempt was made to identify the fragments in camera views from both locations. When available, such data (which we have labeled "Duplicate View Data") permitted a fairly accurate determination of the flight path of the fragments. If the fragments were identified only in a single view, however, (this has been labeled "Single View Data") it was not possible to determine their actual flight path. As recorded on film, the fragment position is a projection on a plane normal to the lens axis of the camera. Without additional data, such as from an additional camera view, no correction to the data to account for a flight path other than normal to the lens axis of the camera could be made. Thus, the fragment data were processed as though the fragments were traveling in a plane which was normal to the lens axis of the camera. After reducing the fragment data from the films we estimated that nearly all of the fragments sighted had a trajectory which was within ± 45 degrees of the normal to the lens axis of the camera. If this estimate is correct, computed velocities for single view data should be within +0% to -30% of the true velocity.

Since cameras at positions A and B viewed the event from approximately the same elevation as the test pad, fragment positions were recorded for a vertical plane normal to the azimuthal position of the camera. However, the camera on the tower, at azimuth 340° , was elevated above the test pad. A correction for this elevation was made so that the fragment position would be calculated for a vertical plane as for camera positions A and B. This correction is discussed in the processing for single view data.

2. Processing of Single View Data - As viewed from the camera, the fireball and fragment would appear as in Figure 26 with the positive X axis to the right and lying along ground surface and positive Y axis vertical through the center of the tank. Subscripts on the axes refer to the camera position A or B from which the data are obtained. The view shown in Figure 26 is typical of that obtained by a camera in position A. The angle between the intersection of the X-Y planes of cameras A and B is then 120° (this angle is required for processing of the duplicate view data, but not for processing the single view data). Fragment positions are measured on the film with respect to the X and Y axes. Processed data are computed with respect to the X' and Y' axes; that is, with respect to a set of axes which pass through the center of the tank.

The first items calculated from the film data are the film speed in frames per second (fps), the scale factor (SF), and the height of the event (h_e). Spacing of the timing marks (tm) are read from the film in frames per timing mark. When spacing of timing marks is multiplied by the frequency of the timing mark generator in timing marks per second, the framing rate in frames per second is obtained. To compute the scale factor a known length in the field of view is divided by its length as measured on the screen of the Vanguard Analyzer. This gives the scale factor directly if the known length is the same distance from the camera as the event; otherwise, an appropriate adjustment must be made. The height of the event (h_e) can be determined from engineering drawings if they are available, but it is also determined directly from the film data. It is computed as one-half the sum of the distances to the top and to the bottom of the tank. Even though an attempt was always made to align the X axis (Y = 0 position on the screen of the Vanguard Analyzer) with the top of the pad, this alignment was never exact. Consequently, whenever it is available, h_e obtained from the film measurement is used. Knowing the film speed, the scale factor and the height of the event, the X-Y positions of the fragment can be calculated from Equations (7) and (8).

$$X_i^j = x_i^j (SF) \quad (7)$$

$$Y_i^j = \frac{y_i^j (SF)}{\cos \theta_v \left[1 + \frac{y_i^j (SF)}{dc} \sin \theta_v \right]} - h_e \quad (8)$$

Subscript i refers to the frame number and superscript j refers to the fragment number. Lower case x and y denote the values as read from the film, and capital letters denote calculated displacements. The denominator of Equation (8) is a correction factor which adjusts for the condition that the lens optical axis may not be perpendicular to the vertical axis along which Y is

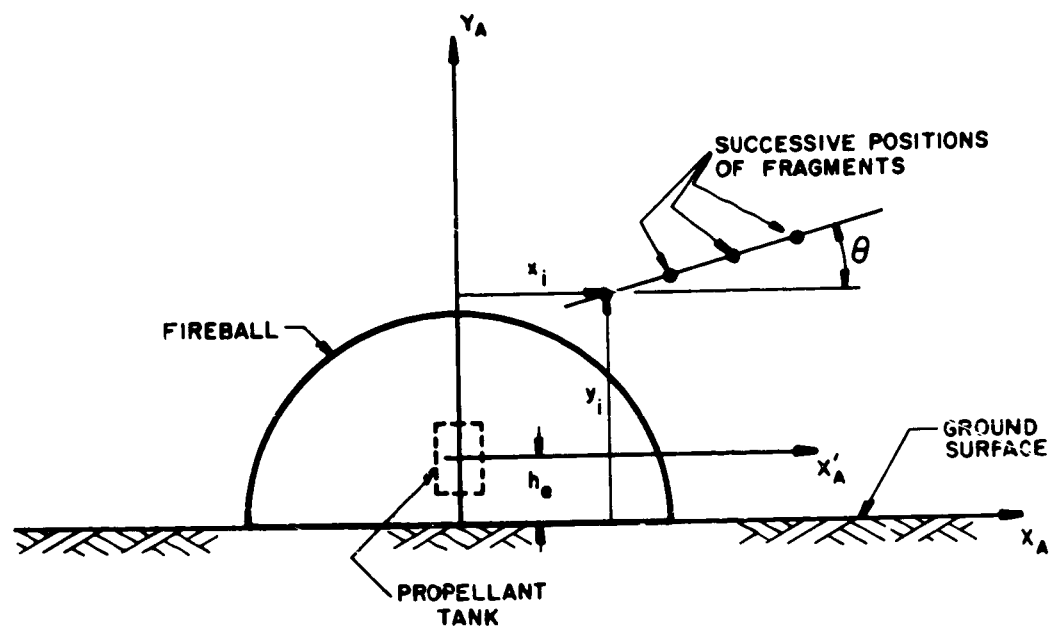


FIGURE 26. FIREBALL AND FRAGMENT AS VIEWED BY A CAMERA LOCATED AT POSITION A

to be calculated. For the camera elevated above the event as shown in Figure 27, θ_v is the positive angle between the lens axis of the camera and the horizon and d_c is the horizontal distance from the camera to the event. To obtain the vertical position of the fragment relative to the center of the tank, h_e , the distance from the X-axis ($Y = 0$) to the center of the tank is subtracted from the calculated displacements. Equation (8) is derived for the condition that the lens axis passes through the center of the tank (the assumed origin of the fragment trajectories). The error induced by neglecting the offset of the lens axis relative to the center of the tank is about 1%.

A correction similar to that in Equation (8) is needed when the fragment is not traveling in the X-Y plane, but is traveling either toward or away from the camera. The error incurred is indicated in Figure 27. It is exaggerated because the camera is shown much closer to the event relative to the height of the fragment than actually was the case when photographing the fragments. This schematic does show, however, that the calculated Y displacement is a projection of the actual displacement on a vertical plane through the center of the event. If the fragment is coming toward the camera the Y displacement calculated will be slightly greater than the actual Y displacement; whereas, when the fragment is traveling away from the camera, the calculated displacements will be slightly smaller than the actual displacements. For single view data, there is no way to correct for this error because one cannot tell which direction the fragment is actually traveling. (A similar error occurs for the horizontal displacements.) For the duplicate view data, however, it is possible to calculate the true vertical and horizontal displacements. This will be discussed under "Processing of Duplicate View Data."

Once the X and Y displacements of the fragments have been calculated for each frame number and once the times corresponding to these frame numbers have been determined by dividing the frame number (event starts in frame number one) by the framing rate, the fragment velocities can be calculated. Velocities are calculated in two ways. An average velocity is computed by assuming that the fragment has traveled in a straight line from the center of the tank to the position where it is first sighted. This velocity is given by Equation (9)

$$U_A^j = \frac{\sqrt{(X_{II}^j)^2 + (Y_{II}^j)^2}}{T_{II}^j} \quad (9)$$

where the subscript II indicates the frame number in which the fragment is first observed. In addition to this so-called average velocity, the velocity of the fragment during the period of time in which it is observed is also computed. To determine this velocity, the distance the fragment travels along

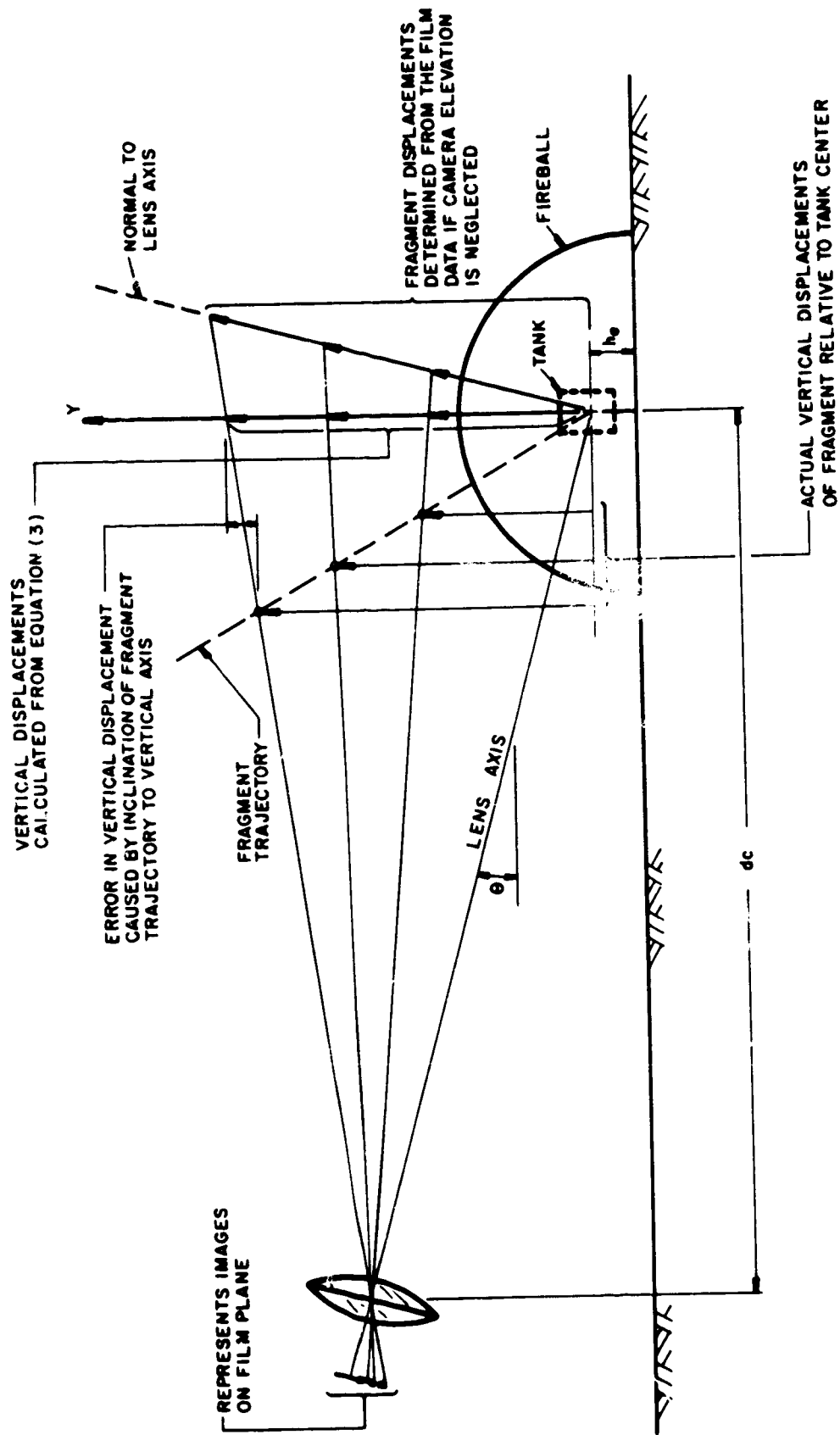


FIGURE 27. SCHEMATIC SHOWING ACTUAL AND CALCULATED FRAGMENT VERTICAL DISPLACEMENT

its trajectory after first being sighted is calculated from Equations (10) and (11)

$$\Delta S_i^j = \sqrt{(X_i^j - X_{i-1}^j)^2 + (Y_i^j - Y_{i-1}^j)^2} \quad (10)$$

$$S_i^j = S_{i-1}^j + \Delta S_i^j \quad (11)$$

where the distance S is set to 0 at the time of sighting. Velocity of the fragment, U_i , is then determined from the slope of a straight line fit to the computed distance-time data points S_i and T_i , where T_i is adjusted to 0 at the time of sighting as was S_i . The subscript i on the velocity is used to denote an instantaneous velocity. While it is true that this velocity is actually an average over the time of sighting, the elapsed time is short compared to the elapsed time between the explosion and the sighting of the fragment for which U_A was determined and the velocity of the fragment varies only slightly during the time of sighting. Also, the position of the fragment which corresponds to U_i is computed for the center of range over which the fragment is tracked (as discussed below) and U_i should be very close to the instantaneous velocity at this position.

In addition to the fragment velocities, the position of the fragment relative to the center of the event and its direction of travel are computed. Fragment coordinates are given as a radius \bar{R} , height \bar{Z} , and an azimuth angle Ψ . Since the computed velocity, U_i , is taken to be the instantaneous velocity of the fragment at the center of its range of travel while in view, the cylindrical coordinates are computed for this position also. The expressions for determining these coordinates are

$$\bar{R}^j = \frac{1}{2} (X_{IF}^j + X_{II}^j) \quad (12)$$

$$\bar{Z}^j = \frac{1}{2} (Y_{IF}^j + Y_{II}^j) \quad (13)$$

$$\Psi^j = - \frac{X_{IF}^j}{|X_{IF}^j|} (90) + \Psi_c \quad (14)$$

$$\text{IF } \Psi^j < 0.0 \quad \text{set } \Psi^j = 360 + \Psi^j \quad (15)$$

where the subscript IF denotes the final frame in which the position of the fragment was recorded. Notice that \bar{R} and \bar{Z} are simply the center position of the range of the X and Y coordinates, respectively. The azimuth

position is determined from the azimuth angle, ψ_c , of the camera viewing the fragment and the sign of the X displacement. This is based on the assumption that the fragment is traveling in the X-Y plane which is normal to the line of sight of the camera. (For fragments which are photographed, and properly identified from two different camera positions, the azimuth angle of the line of flight can be determined more exactly.) The last parameter computed for the fragment is the elevation angle of its flight path above the horizon. This angle, θ , as shown in Figure 26, is determined from the slope of a straight line fit to the X-Y data for each fragment.

3. Processing of Duplicate View Data - After the single view data for each fragment had been processed, data for those fragments which could be identified in more than one camera view, that is, in views from camera positions A and B of Figure 25, were combined to more accurately determine a true trajectory of the fragments. Fragments were difficult to identify in more than one view, however, and thus the duplicate view data are very limited. In addition, we have often found when processing the data that what appeared to be the same fragment in two separate views, apparently was not. One criterion for determining whether or not the fragment is the same in two views are the Y displacements. They should be approximately the same when viewed from the two camera positions. As noted in Figure 27, there will be some differences depending on whether the fragment is traveling toward or away from the camera; however, these differences should be small because the cameras are located 420 feet from the event and it is unusual to follow a fragment for a distance of more than 60 feet above the ground. Thus, the cameras are viewing the fragment at an angle of less than 10° above the horizon. Although no hard and fast rule was established, when the Y displacements of the two fragments differed by more than about 15%, it was assumed that two different fragments rather than the same fragment had been observed.

In duplicate view data, the same fragment is observed from cameras situated 120° apart. Thus, errors introduced by the fragment traveling toward or away from the camera tend to cancel out when averaging the Y displacements computed from the two different camera views. Consequently, the vertical displacements, δ , are calculated as the average of the vertical displacements from the single view data. This is shown in Equation (16)

$$\delta_j^i = \frac{1}{2} \left(Y_i^j + Y_i^{\text{DUP}} \right) \quad (16)$$

where the superscript DUP is the number of the fragment which provides the additional camera view of fragment "j".

Calculating the horizontal position of the fragment is more complicated. Figure 28 shows the geometry in plan view. The X displacements of the fragment, computed from the two separate camera views, are indicated by X_A

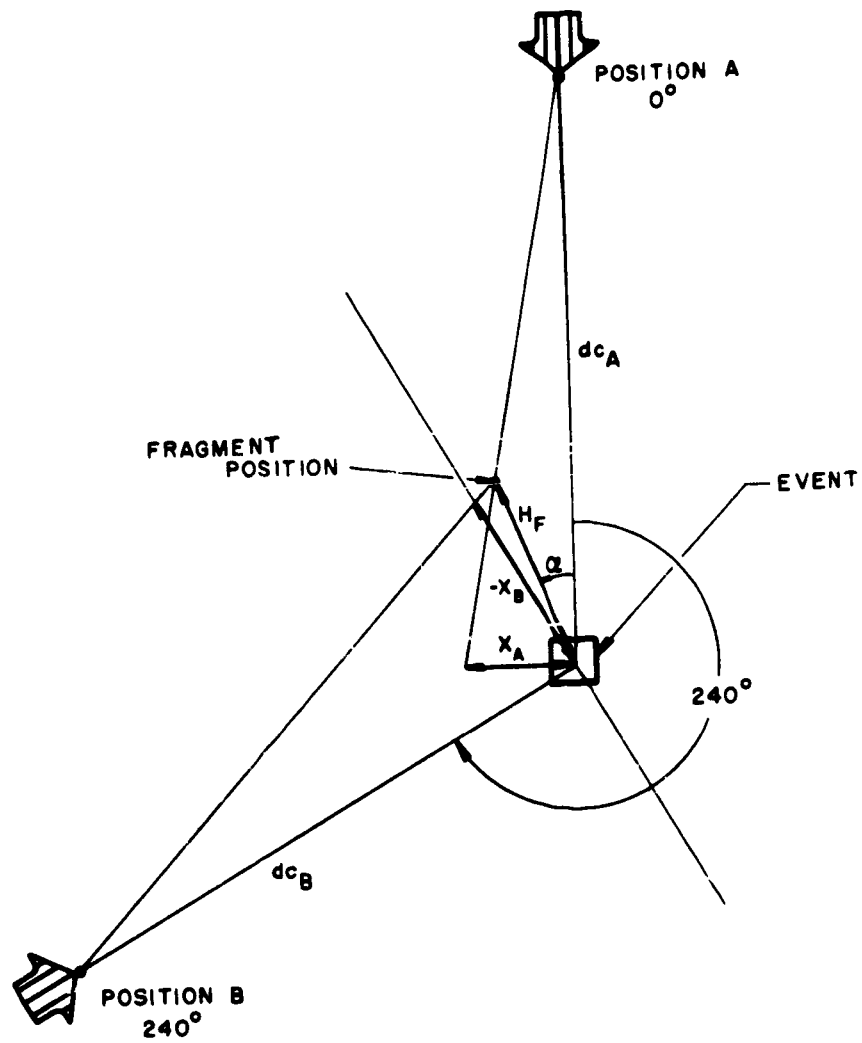


FIGURE 28. GEOMETRY FOR FRAGMENT POSITION FOR
DUPLICATE VIEWS

and X_B . These are projections of the fragment horizontal displacement upon the X-Y planes for each camera position. The true horizontal displacement of the fragment, H_F , relative to the center of the event is desired. Using simple geometrical relationships, two expressions for H_F were obtained and are given by Equations (17) and (18)

$$H_F = \frac{X_A \, dc_A}{X_A \cos \alpha + dc_A \sin \alpha} \quad \text{for } X_A \neq 0 \quad (17)$$

$$H_F = \frac{-X_B \, dc_B}{X_B \cos(60^\circ + \alpha) + dc_B \sin(60^\circ + \alpha)} \quad \text{for } X_B \neq 0 \quad (18)$$

As indicated, Equation (17) cannot be used for $X_A = 0$ and Equation (18) cannot be used for $X_B = 0$. In practice, Equation (17) was used whenever the absolute value of X_A was greater than X_B , and Equation (18) was used when the reverse was true. Subscript i and superscript j have been dropped from the equations for simplicity. The angle, α , is found by equating Equations (17) to (18), and is given by Equation (19).

$$\alpha = \tan^{-1} \frac{X_A X_B \cos 60^\circ + X_A X_B \, dc_B / dc_A + X_A \, dc_B \sin 60^\circ}{X_A X_B \sin 60^\circ - X_B \, dc_B - X_A \, dc_B \cos 60^\circ} \quad (19)$$

Equations (17), (18), and (19) hold for fragment positions in all quadrants.

The same procedures were used in calculating the average velocity, U_A , and the velocity of the fragment after acquisition, U_i , as were used for the single view data. Quantities U and H were simply substituted for X and Y. Also, with the exception of the azimuth angle, the cylindrical coordinates of the fragment and the elevation angle θ were computed as for the single view data. The azimuth position of the fragment is simply 360° minus the angle α .

4. Computer Program for Data Processing - A computer program was written to process the data as it was received in punched card form from the Vanguard Analyzer. Although the details of the program will not be presented here, it solves the equations given in the preceding sections and prints the results in a usable form. The program also creates a tape file for subsequent statistical analysis of the results.

A summary of camera data and number of fragments whose trajectories were measured is given in Appendix A. The tests are grouped by type, as defined in the PYRO reports (refs. 15 through 17), and are identified by the PYRO test numbers. Numbers of fragments whose velocities and trajectories

were measured range from a minimum of 2 per test to a maximum of 36 per test. The maximum number of fragments identified in duplicate views was 3 per test.

5. Summary of Fragment Velocity Measurements and Calculations -

The fragment velocity data derived from the PYRO films are available on punched cards and in computer printouts. The key designator for all data is the PYRO test number; for each such test having readable fragment velocity data, all of the quantities defined by the equations in Section 4 are calculated and printed for each fragment traced. The printouts are quite voluminous and so are not included in this report.

The data for each test were further reduced using standard statistical procedures and a "anned" computer program available to us through our CDC library of programs. We chose the six output variables U_A , U_i , θ , ψ , \bar{R} , and H_F for statistical treatment, and computed the mean, standard deviation, standard error of the mean, maximum, minimum, and range for each variable. Again, the computer printout sheets are too detailed for inclusion in the report, but are available for study.

A summary of results is given in Table V. Each test is identified by the PYRO test number, and the tests are grouped by propellant and type of simulated accident. Test conditions given are total weight of propellant, tank L/D ratio, and impact or drop velocity. Ignition time and measured blast yield from reference 16 are listed.* Fragmentation data are given in the last four columns, indicating number of camera views from which data were taken, number of fragments observed, mean value of fragment velocity, U_i , and standard deviation of this same parameter σ_u . These mean velocities and standard deviations were determined from the single view data only. The number of fragments which were identified in more than one camera view and processed as duplicate view data was too small for statistical analysis. Because the data represent a wide spectrum of test conditions, propellant types, and propellant weights, they should allow correlation with methods of prediction of initial velocity such as those presented later in this section, and should also lend themselves to various types of statistical analysis. A limitation to the data which may render statistical studies difficult is that relatively few fragments could be observed in any one test. Some grouping between tests with different propellants, different blast yields, etc., may be possible. To aid in rational choice of ways to group the test results, we conducted several limited model studies. These are included in this report as Appendix C.

* Blast yield in percent is defined in Section II.

TABLE V
SUMMARY OF FRAGMENT VELOCITY MEASUREMENTS

Test No.	Prop. Wt. (lbs)	Impact Or Drop Velocity (ft/sec)	Ignition Time (msec)	Yield (%)	Tank L/D	No. Of Camera Views	No. Of Fragments Observed	Mean Velocity \bar{V} (fps)	Standard Deviation σ_v (fps)
GROUP 2: HYPERGOLIC (AFRPL) TESTS									
30	200	---	---	4.00	1.93	1	7	34.6	14.0
31	200	---	---	.20	2.00	1	4	77.5	26.5
32	200	---	---	.08	2.00	1	6	131.9	97.8
33	200	---	---	8.80	---	1	7	44.8	12.8
35	200	---	---	.15	2.00	1	3	199.9	142.1
36	200	---	---	.30	1.93	1	2	34.3	25.6
39	200	---	---	---	1.93	2	12	403.0	390.0
258	1000	77	---	.30	2.00	2	7	76.0	35.9
GROUP 3: LO ₂ /RP-1 CONFINEMENT-BY-THE-MISSILE TESTS									
48	200	---	310	9.8	5.58	2	12	300	263
49	200	---	316	12	5.58	2	16	394	305
58	200	---	200	27	2.14	2	14	434	192
87A	200	---	70	16	2.14	2	15	698	374
88	200	---	60	4	5.58	2	13	291	111
95A	200	---	120	17	2.14	2	13	660	459
192	1000	---	216	14	2.07	2	14	484	246
193	1000	---	222	20	2.07	2	18	621	312
209	1000	---	121	10	2.07	3	15	898	637
237	200	---	127	32	2.14	2	5	608	287

Test No.	Prop. Wt. (lbs)	Impact Or Drop Velocity (ft/sec)	Ignition Time (msec)	Yield (%)	Tank L/D	No. Of Camera Views	No. Of Fragments Observed	Mean Velocity V_I (fps)	Standard Deviation σ_V (fps)

GROUP 3 (Cont'd) -

270A	1000	---	225	13	2.07	4	32	515	289
275	25000	---	515	4	2.14	4	20	265	202
278	25000	---	530	13	2.14	3	16	607	451
282	25000	---	540	13	2.14	3	13	976	615
301	94000	---	840	4	---	2	9	962	143

GROUP 4: LO₂/RP-1 CONFINEMENT-BY-THE GROUND-SURFACE VERTICAL TESTS

107	200	78	42	29	2.14	2	21	273	121
109	200	78	40	10	5.51	2	11	461	238
190	1000	78	570	96	2.04	2	10	343	168
191	1000	44	-0-	13	2.04	2	24	473	317
202	200	23	870	42	2.14	2	10	109	50
205	200	78	40	41	2.14	2	23	419	284
206	200	78	350	85	2.14	2	4	90	58
219	1000	44	1835	14	2.04	2	16	187	98
220	1000	44	525	96	2.04	1	8	427	213
249	200	44	710	50	2.14	2	6	280	169
284	25000	44	-0-	2	2.16	2	16	766	297

GROUP 5: LO₂/RP-1 CONFINEMENT-BY-THE GROUND-SURFACE HORIZONTAL TESTS

121	200	23*	---	30	2.14	2	8	139	199
122	200	23	---	28	2.14	2	10	90	110
125	200	78	---	52	2.14	2	7	239	256
140	200	78	---	12	2.14	2	15	166	123
162	200	78	---	24	2.14	2	10	267	257
179	200	78	---	12	2.14	2	8	225	154

* Velocity for LO₂: Velocity for RP-1 is 12 ft/sec.

Test No.	Prop. Wt. (lbs)	Impact Or Drop Velocity (ft/sec)	Ignition Time (msec)	Yield (%)	Tank L/D	No. Of Camera Views	No. Of Fragments Observed	Mean Velocity \bar{V}_I (fps)	Standard Deviation σ_v (fps)
GROUP 7: LO ₂ /LH ₂ CONFINEMENT-BY-THE MISSILE TESTS									
50	200	---	180	86	2.12	2	5	382.	457
51	200	---	80	22	2.12	2	9	115	60
52	200	---	83	7	5.80	2	17	205	424
53	200	---	1	4	2.12	2	29	319	122
54	200	---	17	6	5.80	2	26	214	168
55	200	---	1	1	5.80	2	18	279	200
56	200	---	144	10	---	2	15	208	122
57	200	---	12	1	5.80	2	27	230	237
90	200	---	35	29	2.12	1	7	116	56
91	200	---	0	13	2.12	2	12	1083	857
93	200	---	147	34	2.12	1	4	701	569
94	200	---	329	25	5.80	2	11	207	203
118	200	---	82	20	2.12	2	8	547	179
172	133	---	770	35	---	2	6	74	62
199	200	---	816	8	2.12	2	11	451	377
200	200	---	417	17	2.12	2	26	492	224
210	1000	---	20	7	2.04	2	13	541	277
212	1000	---	1366	27	2.08	2	8	664	302
213	1000	---	708	35	2.08	2	13	831	281
265	1000	---	750	10	2.08	3	28	466	241
279	25000	---	33	.2	2.16	4	16	175	90

GROUP 8: LO₂/LH₂ CONFINEMENT BY-THE-GROUND-SURFACE VERTICAL TESTS

103A	200	23	208	39	5.43	2	8	423	404
106A	200	23	325	22	5.43	2	12	267	135
114	200	78	74	54	2.02	2	17	388	352
115	200	78	93	15	5.43	2	14	157	74

Test No.	Prop. Wt. (lbs)	Impact Or Drop Velocity (ft/sec)	Ignition Time (msec)	Yield (%)	Tank L/D	No. Of Camera Views	No. Of Fragments Observed	Mean Velocity \bar{V}_I (fps)	Standard Deviation σ_v (fps)
GROUP 8 (Cont'd) -									
152	200	23	480	14	2.02	2	14	193	102
160	200	78	67	32	5.43	2	18	281	236
184	200	23	810	17	2.02	2	16	180	111
195	200	78	292	104	2.02	2	12	309	237
197	200	44	500	19	2.02	2	18	197	102
201	200	23	1524	26	2.02	2	6	166	83
204	200	44	317	42	2.02	2	17	310	201
211	1000	44	-0-	12	1.92	2	17	747	463
217	1000	44	1490	33	1.92	2	7	89	82
226	200	78	283	51	2.02	1	5	249	77
230	200	44	24	21	2.02	2	21	434	313
266	1000	44	-0-	14	1.92	3	19	482	241
288C	25000	44	365	13	2.10	2	20	698	300
289A	25000	44	166	4	2.10	3	40	1176	667
290	25000	44	105	4	2.10	3	32	878	693
291B	1000	44	---	1.2	1.92	3	14	247	88
293	1000	44	---	3.9	1.92	3	26	464	226
GROUP 9: LO ₂ /LH ₂ CONFINEMENT-BY-THE-GROUND SURFACE HORIZONTAL TESTS									
131	200	23**	---	6	2.02	2	23	295	286.
133A	200	23	---	6	2.02	2	15	282	206.
186	200	23	---	9	2.02	2	11	255	194
196	200	78**	---	17	2.02	2	13	386	296
228	200	78	---	34	2.02	2	12	360	314

** Velocity of LO₂; Velocity of LH₂, 12 ft/sec

Test No.	Prop. Wt. (lbs)	Impact Or Drop Velocity (ft/sec)	Ignition Time (msec)	Yield (%)	Tank L/D	No. Of Camera Views	No. Of Fragments Observed	Mean Velocity \bar{V}_I (fps)	Standard Deviation σ_v (fps)

GROUP 10: LO₂/LH₂ AND LO₂/RP-1 COMBINED SPECIAL TESTS
(SCALED TWO-STAGE VEHICLE)

169	200	23*	318	15	2.12	2	7	259	181
173	200	23	56	15	2.12	2	16	207	138
233	200	23	2182	109	2.02	2	14	254	234

GROUP 11: LO₂/RP-1 COMBINED SPECIAL TESTS
(SCALED TWO-STAGE VEHICLE)

294	1200	---	-0-	5.6	3.33	4	28	348	221
295	1200	44	544	70	3.33	2	8	459	388

SATURN IV BLAST

62	91000	---	183	6	---	3	36	741	469
----	-------	-----	-----	---	-----	---	----	-----	-----

* Velocity of LO₂; Velocity of LH₂ is Zero

C. Methods of Predicting Velocity

1. Explosions Within Missile Tanks

a. A Deterministic Method

(1) Choice of Parameters and Idealization of the Problem

In this section, we discuss a method for predicting maximum velocities for fragments generated by explosions within missile tankage (CBM case). A method for predicting ranges is discussed in Section IV. In order to predict maximum fragment velocities, the problem must be "idealized" in a number of ways, and the parameters must be chosen such that the theory may be applicable to a spectrum of missile explosions involving different liquid fuels and oxidizers, volume of fuel oxidizer mixtures, tank wall specific mass, and tank geometries. To idealize the problem we consider only a spherical volume V_{00} of radius R_0 in which we have a stoichiometric mixture of that amount of fuel and oxidizer which is mixed at time of detonation. Furthermore, upon detonation, all of this volume of fuel and oxidizer is assumed to be converted instantly to explosive products and energy, forming a "hot gas" which can be characterized by some ratio of specific heats, μ , initial pressure, P_{00} , and initial sound velocity a_{00} . All of the fuel or oxidizer external to this spherical volume is considered to add mass to the container wall only and takes no part in the chemical reaction of the explosive process. The container is spherically coincident to the sphere in which the explosion takes place, and the non-reacting fuel (or oxidizer) moves initially with the fragments of this container wall as if they were an integral part of the fragments (i. e., they just add mass to these fragments). Compression of the liquid fuel and oxidizer, and shock transmission effects in these liquids are ignored.

All fragments are assumed of equal size and have circular projections. If we pick a parameter, n , for the number of such fragments into which the containing sphere fractures, we can later solve the problem for various n , thus effectively varying the fragment size. It is further assumed that the sum of the concave inner surface areas of all the fragments is equal to the surface area of the original sphere of explosion.

$$A_i = 4\pi R^2/n \quad (20)$$

where R is the initial radius of the sphere of explosion [$R = r_i(\tau)$ for $\tau = 0$], and A_i is the fragment surface area. Although these are gross idealizations of the fragmentation picture, they make the problem amenable to solution and allow some estimate to be made of how sensitive the solution is to fragment size and number.

If the stoichiometric mixture of fuel and oxidizer occupies a volume V_0 and has a mass M_0 , then, at the time $\tau = 0$ the instant after the explosion, we assume the gaseous products of explosion occupy the same volume and have the same mass. The sound speed in this medium at this time is then a function of κ , one of the independent parameters. One must pick κ , M_{00} , $V_0(0)$, and $P_0(0) = P_{00}$ which characterize the sphere of explosion at $\tau = 0$ (κ , M_0 , and P_{00} will depend on the type of fuel and oxidizer, and V_0 depends on the amount of fuel and oxidizer that have mixed). One must then also pick an R , n , and M_t which characterize the containing sphere (where R is the containing sphere's initial internal radius, equal to the external radius of the sphere of explosion; n is the number of fragments into which the containing sphere fragments, and M_t is the total mass of the containing sphere, i. e., the mass of the non-reactants, as well as the actual fuel tank mass). With this information the maximum fragment velocity for any of the equal sized n fragments is calculated by the method to be described. This maximum velocity, U_m , may be used as the initial fragment velocity for the fragment range calculation (Section IV) in which the fragment is assumed to experience no acceleration due to the explosion after U_m is attained, but it experiences deceleration due to drag forces in the medium through which it is traveling.

(2) Equations for the Mathematical Model* - To obtain the initial velocities for the fragments from CBM explosions, an extension was made of the techniques of D. E. Taylor and C. F. Price (ref. 31) and of G. L. Grodzonski and F. A. Kukanov (ref. 32) relating to the motion of fragments from bursting gas reservoirs in a vacuum. These techniques were generalized from the case of spherical vessels which broke up into two perfectly hemispherical fragments to the case of a spherical vessel which fragments into n fragments, each of equal size and having a circular projection. For the case where the containing sphere is thin-walled, the equation of motion for the i -th fragment of mass M_i and radial displacement $r_i(\tau)$ having a projected area F and experiencing a pressure $P_i(\tau)$ at time τ , is given by:

$$M_i \frac{d^2 r_i(\tau)}{d\tau^2} = F P_i(\tau) \quad (21)$$

If A_i is the area of the curved surface of the spherical segment (for the i -th fragment), then

*The equations given in this section require a number of mathematical operations for their development. Many of these operations are omitted for brevity. All nomenclature is given in Appendix I.

$$A_i = 2\pi Rh = 4\pi R^2/n \quad (22)$$

where $R = r_i(0)$ and h is the segment height. Let the segment radius equal $d/2$, then it can be shown with the use of Equation (22) that

$$F = \frac{\pi d^2}{4} = 4\pi R^2 \left[\frac{1}{n} - \frac{1}{n^2} \right] \quad (23a)$$

or

$$F \simeq A_i \quad \text{for} \quad n^2 \gg n \quad (23b)$$

The equation of state assumed for the gaseous products of explosion is given by

$$P_o(\tau) V_o(\tau) = c(\tau) R_1 T_o(\tau) \quad (24)$$

The rate of change in the mass of the confined gaseous explosion products in the sphere as the sphere begins to fragment and gas is lost to the external sphere region is given by

$$\frac{dc(\tau)}{d\tau} = -k \rho_* a_* \Pi w \quad (25)$$

where ρ_* and a_* are the critical gas density and velocity as they escape through the cracked surface of the sphere, Π is the crack perimeter, w is the crack width, and k is a discharge coefficient. The crack area for the i -th fragment given by $(\Pi w)_i$ is equal to the difference between the area subtended by the initial solid angle, ϕ , at the distance $r_i(\tau)$ for time τ and the actual area of the fragment A_i .

$$(\Pi w)_i = \phi r_i^2(\tau) - A_i = \frac{4\pi R^2}{n} \left(\frac{r_i^2(\tau)}{R^2} - 1 \right) \quad (26)$$

Inherent in Equation (26) is the assumption that all fragments travel in a radial direction and that the symmetry of the fragment motion is such that the equations of motion are only a function of the magnitude of the radius, i. e., the motion of the i -th fragment in the radial direction describes the motion of any other fragment in the radial direction and shear forces are small compared to dynamic forces. Thus, we may set $r_i = r$ and, from Equations (25) and (26), we have

$$\frac{dc(\tau)}{d\tau} = -k \rho_* a_* \left(\frac{r(\tau)}{R} - 1 \right) 4\pi R^2 \quad (27)$$

The volume of the gaseous explosion products at any time τ after $\tau = 0$ is given by

$$V_o(\tau) = \left(\frac{4}{3}\right) \pi r^3(\tau) \quad (28)$$

It has been assumed that the confined gas immediately adjacent to the fragments is accelerated to the velocity of the fragments but that this constitutes a negligible fraction of the gas, the great bulk of which is unaccelerated. Thus, from one-dimensional flow equations

$$P_i(\tau) = P_o(\tau) \left[1 - \left(\frac{\kappa - 1}{2(a_o(\tau))^2} \right) \left(\frac{dr(\tau)}{d\tau} \right)^2 \right]^{\kappa/(\kappa-1)} \quad (29a)$$

$$\rho_* = \rho_o(\tau) \left(\frac{2}{\kappa+1} \right)^{1/(\kappa-1)} \quad (29b)$$

$$a_* = a_o(\tau) \left(\frac{2}{\kappa+1} \right)^{1/2} \quad (29c)$$

Equations (29) can be non-dimensionalized by setting

$$r(\tau) = Xg(\xi), \quad \tau = \theta \xi, \quad P_o(\tau) = P_{oo} P_*(\xi) \quad (30)$$

For a confined gas that behaves adiabatically we have:

$$\frac{P_o(\tau)}{P_{oo}} = \left(\frac{\rho_o(\tau)}{\rho_{oo}} \right)^\kappa = \left(\frac{T_o(\tau)}{T_{oo}} \right)^{\kappa/(\kappa-1)} = \left(\frac{a_o(\tau)}{a_{oo}} \right)^{2\kappa/(\kappa-1)} \quad (31)$$

where the double zero subscripts refer to the confined gas condition at $\tau = 0$. From Equations (20), (29), (30), and (31), one obtains:

$$\frac{M_i}{M_t} g'' = P_* \left[1 - \frac{(g')^2}{(P_*)^{(\kappa-1)/\kappa}} \right]^{\kappa/(\kappa-1)} \quad (32)$$

where primes denote derivatives with respect to ξ , M_i is the mass of the i -th fragment, and M_t is the total "shell" mass. For n fragments of equal size,

$$\frac{M_i}{M_t} = \frac{1}{n} \quad (33)$$

thus,

$$g'' = n P_* \left[1 - \frac{(g')^2}{(P_*)^{(\kappa-1)/\kappa}} \right]^{\kappa/(\kappa-1)} \quad (34)$$

where

$$X = \frac{M_t}{F} \frac{a_{oo}^2}{P_{oo}} \left(\frac{2}{\kappa-1} \right), \quad Q = \frac{M_t a_{oo}}{F P_{oo}} \left(\frac{2}{\kappa-1} \right)^{1/2} \quad (35)$$

Differentiating Equation (31) and nondimensionalizing, one obtains

$$g^3 \frac{P_*'}{P_*} = \left[-\alpha g^2 + \alpha \beta \right] P_*^{(\kappa-1)/2\kappa} - 3\kappa g^2 g' \quad (36)$$

where

$$\beta(n) = R^6 \pi^2 \left(\frac{2}{\kappa-1} \right)^{-2} \frac{P_{oo}^2}{M_t^2 a_{oo}^4} \left[\frac{1}{n} - \frac{1}{n^2} \right]^2$$

and

$$\alpha = 3\kappa \left(\frac{2}{\kappa+1} \right)^{(\kappa+1)/2(\kappa-1)} \left(\frac{2}{\kappa-1} \right)^{-1/2}$$

Equations (35) and (36) must be solved simultaneously with the initial conditions

$$r(0) = R \quad \therefore \quad g(0) = R/X$$

$$\frac{dr(0)}{d\tau} = 0 \quad \therefore \quad \frac{dg(0)}{d\xi} = 0 \quad (37)$$

$$P_o(0) = P_{oo} \quad \therefore \quad P_*(0) = 1$$

for values of ξ until the fragment acceleration is small with respect to the acceleration at $\tau = 0$. $dg/d\xi$ is a maximum as the acceleration goes to zero. $dg/d\xi$ is the normalized initial velocity for the fragments to be used in the calculation of the fragment ranges.

(3) Solution of the Equations by Numerical Techniques and Computer Program - The solution of Equations (34) and (36) may be obtained numerically for the initial conditions of Equations (37), using the Runge-Kutta method. A program which does this (in FORTRAN IV), as well as the definition of its symbols, is given in Appendix C. This program requires as input the characteristics of the gaseous explosion products at $\tau = 0$ ($A\phi$, the speed of sound; $P\phi$, the initial pressure; and $CAP1$, the ratio of specific heats), and the characteristics of the vessel (RR , the internal radius of vessel and unburned fuel; TM , the mass of the vessel and unburned fuel; and FN , the number of fragments). Also, a guess must be made on the elapsed time between detonation and zero fragment acceleration, $XMAX$.^{*} A time interval spacing, AH , must also be chosen for the calculation.

The program outputs the normalized displacement, velocity and acceleration (dynamic variables) of the fragment as a function of time; the normalized pressure within the vessel as a function of time; and the final values of time, displacement, velocity, acceleration, and pressure at $XMAX$. A sample program run is given in Appendix C.

Figure 29 shows the results for computing the maximum fragment velocity as a function of number of fragments when all other parameters are held constant. The figure indicates that the number of fragments does not affect maximum fragment velocity except at very low n (at which point the assumption of Equation (23b) does not hold). Figure 30 shows how maximum fragment velocity varies with κ and the mass ratio M_o/M_t . The ratio of explosive products mass to shell and non-reactant fuel mass, a constant initial pressure (P_{oo}), number of fragments (n), sound velocity (a_o), and radius of explosion at $\tau = 0$ (R) are assumed in this figure.

(4) Comparison of Results from this Method with Other Sources - The results of this method are compared to the cases described by Taylor and Price (ref. 31) in which:

$$\alpha = \frac{P_o V_o}{M_t a_o^2} = 2.55, \quad 0.1436$$

* A "guess" is made of $XMAX$ because the computer has to work with some finite time. If $XMAX$ is guessed too short, then $g''(\bar{s})$ (the normalized acceleration) is not reduced close enough to zero to yield an acceptable estimate of $g'(\bar{s})$. If $XMAX$ is guessed too long then the computer can not calculate the final values of g'' and g' . In practice we watched g' for each program iteration and accepted a g' which remained constant to three significant figures between iterations as the value of g'' for g' nearly zero.

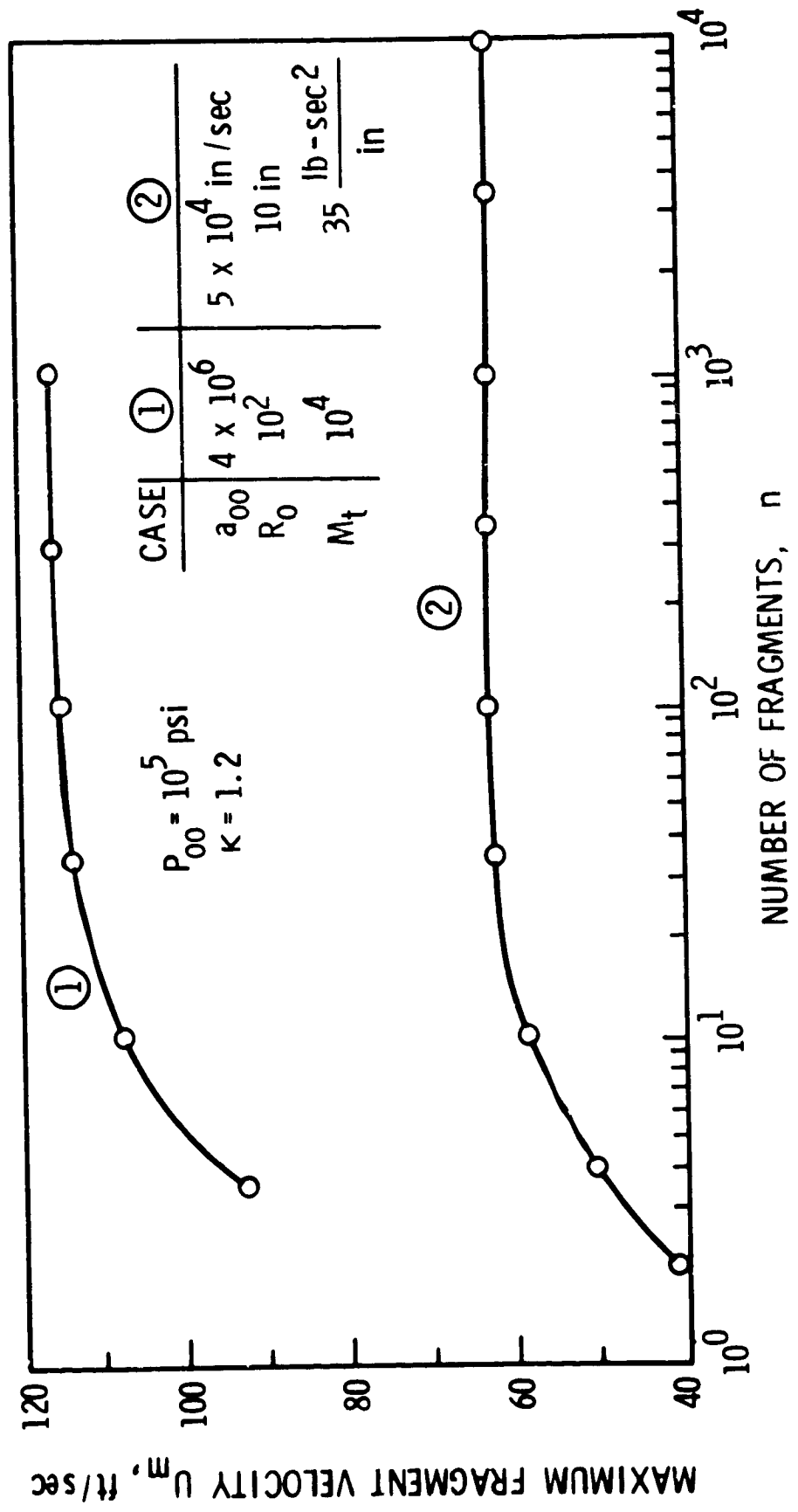


FIGURE 29. MAXIMUM FRAGMENT VELOCITY AS A FUNCTION OF NUMBER OF FRAGMENTS

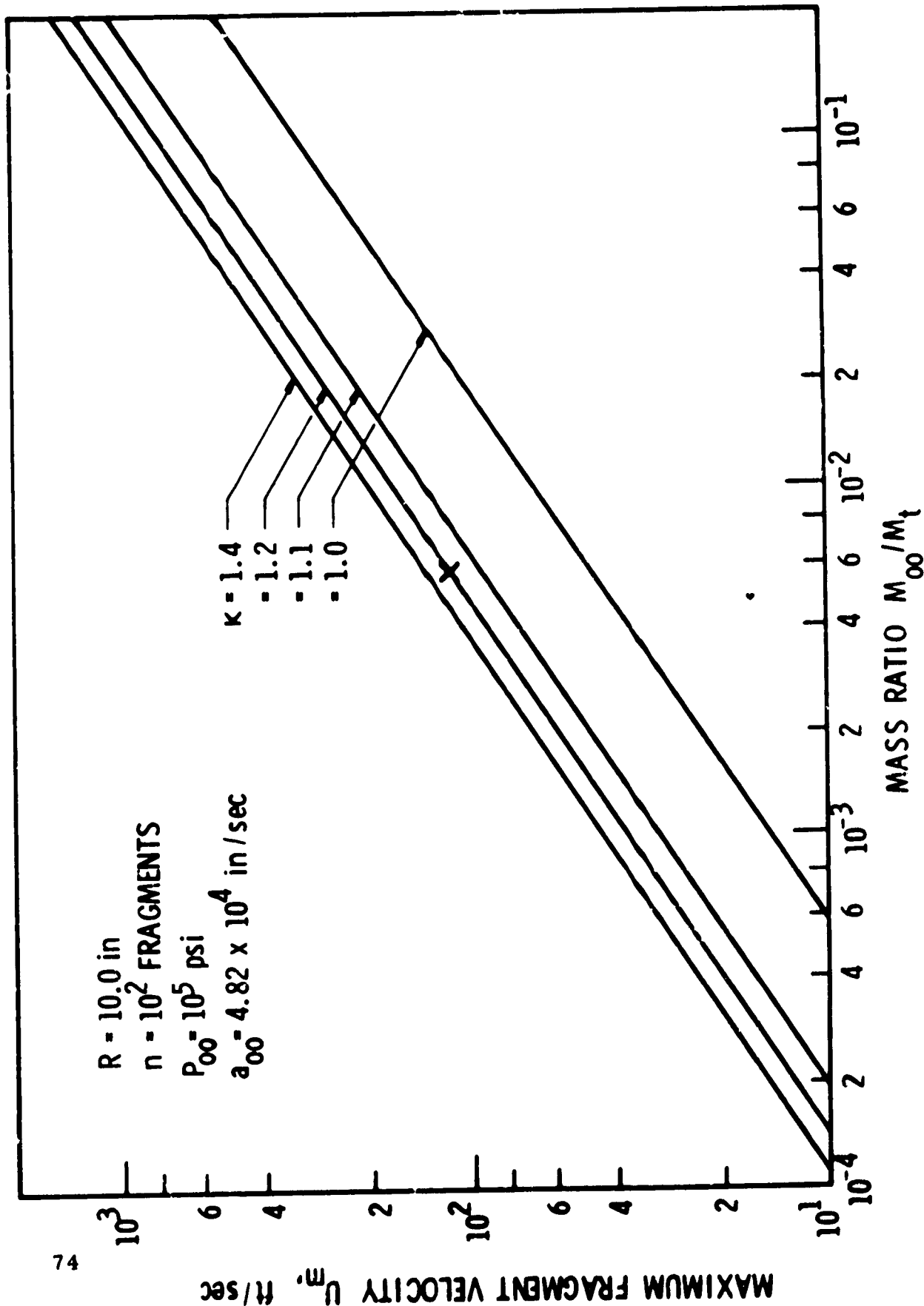


FIGURE 30. MAXIMUM FRAGMENT VELOCITY VS MASS RATIO

in Figure 31. Generally it can be seen that our results predict somewhat lower fragment velocities than they do. Some discrepancy is to be expected because our assumptions on geometry were not as precise as theirs. This is especially true where we assumed that the surface area of a spherical volume could be divided into n equal circular areas; they assumed only two hemispherical fragments whose projected areas were well defined. Nonetheless, the agreement is relatively good, especially for the greater α .

Table VI gives a comparison between fragment velocities measured in experimental work relating to hazards from bursting high pressure tanks (ref. 33) and the predicted velocities using our deterministic method. The experimental values of Pittman (ref. 33) were obtained by pressurizing spherical metal tanks with N_2 until they burst. Fragment velocities were measured by use of a breakwire system. In this system, a time interval counter was initiated by the tank rupture (start pulse) and was stopped when the first fragment reached the breakwire 1 foot away. Thus, the measured values actually are the mean fragment velocity for the first foot of travel (a stroboscopic photographic technique was also used to measure fragment velocities in some cases). Where the experimental values were not precisely determined in tests D and E, limits were assigned to the fragment velocity on the basis of the data obtained. Input data to our program was based on the tank geometry and burst pressure, described in the report, and the properties of N_2 . In general, our values agreed well with the measured values.

We believe on the basis of these comparisons with independent data that our method has proven to be sufficiently accurate in predicting fragment velocities to be useful. An effort to predict data reduced from PYRO films using this method is described later in this section.

TABLE VI. COMPARISON OF PREDICTED FRAGMENT VELOCITIES WITH PITTMAN'S DATA (ref. 33)

Test	P_0 (psi)	Rad. (in.)	Mass (lb-sec ² /in.)	Measured U_f (ft/sec)	Predicted U_f (ft/sec)
C	8×10^3	9.2	1.63×10^{-2}	1.2×10^3	1.201×10^3
D	8×10^3	27.0	4.45×10^{-1}	$< 1.3 \times 10^3$	1.61×10^3
E	8.13×10^3	27.0	4.43×10^{-1}	$> 1.17 \times 10^3$	1.60×10^3

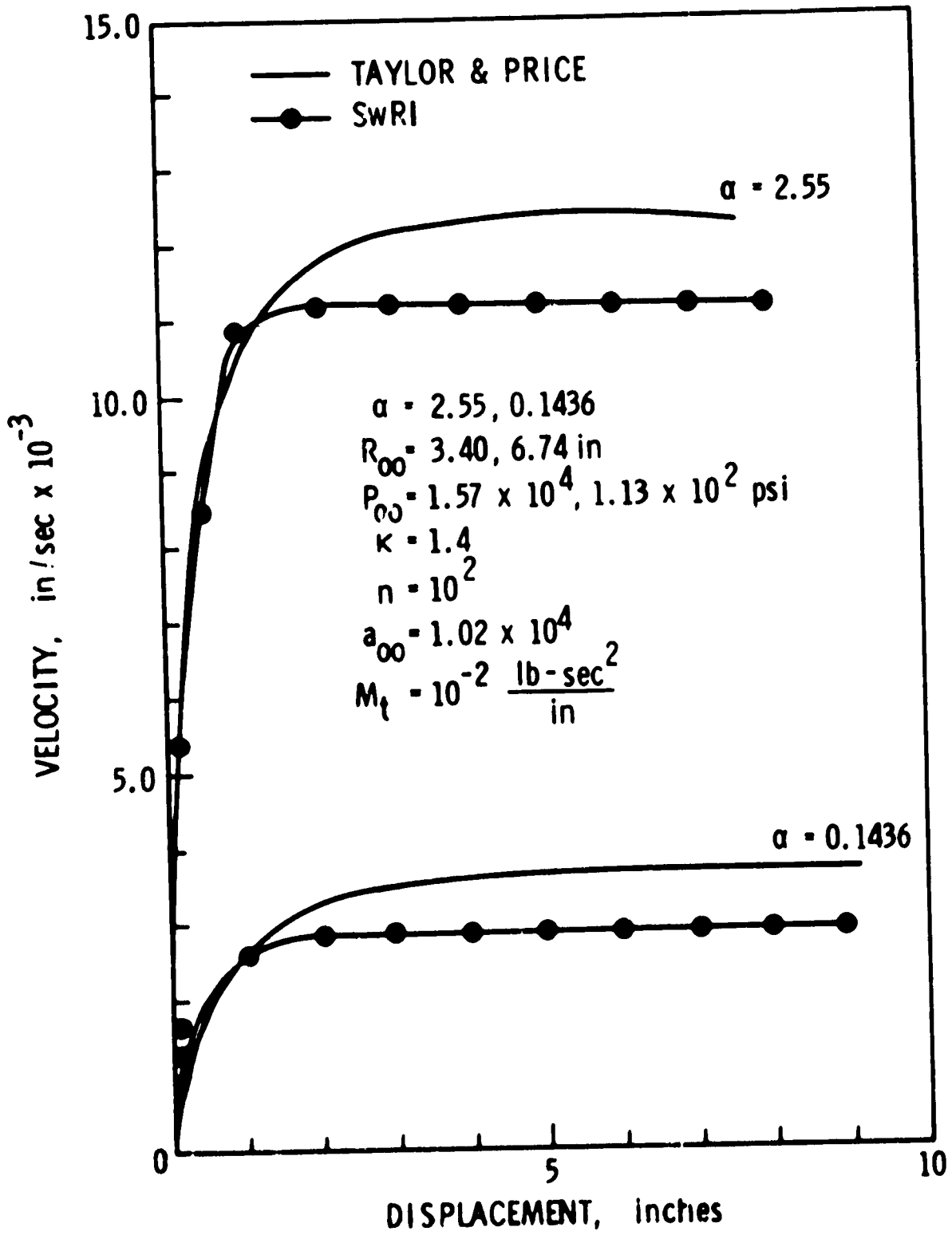


FIGURE 31. COMPARISON OF TAYLOR-PRICE TO SwRI SOLUTIONS FOR ADIABATIC CASE

2. Appurtenances Subjected to Propellant Blasts

a. General - The situation considered here is shown in Figure 32. A propellant explosion occurs after some accident which ruptures the tankage and causes propellants and oxidizers to spill, mix and ignite on the launch pad. We wish to establish a method of predicting velocities to which nearby objects (which we will call appurtenances) are accelerated by the passage of the blast wave. These objects can be parts of the launch tower, storage tanks, vehicles, and objects in or attached to the upper stages of the launch vehicle itself.

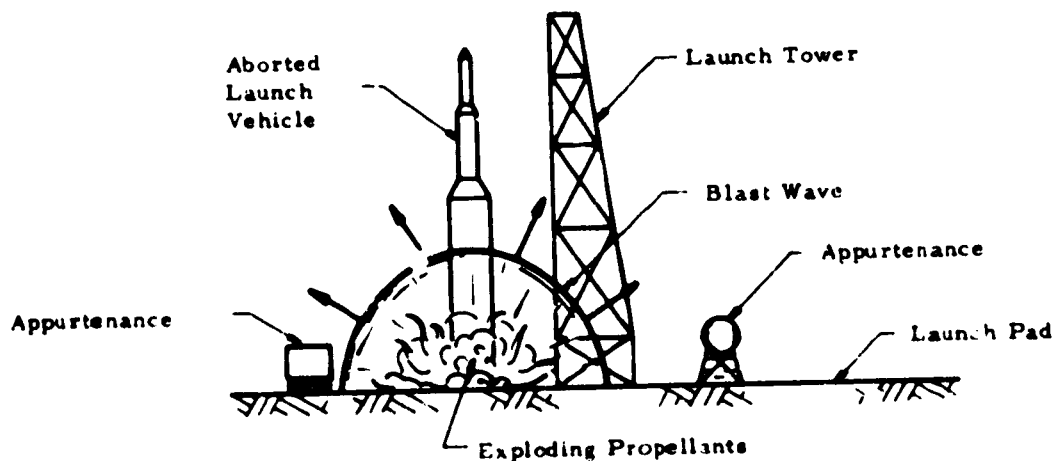


FIGURE 32. SCHEMATIC FOR ACCELERATION OF APPURTENANCES BY PROPELLANT BLAST

b. Blast from Propellant Explosions - It is clear from the results of Project PYRO and other studies that the characteristics of blast waves produced by liquid propellant explosions differ significantly from the characteristics of blast waves produced by TNT or other conventional solid explosives. These differences are discussed elsewhere (see Section 11), but some will be reiterated here because they affect estimation of velocities of appurtenances.

The first characteristic of blast from propellant explosions which differs from that of TNT is that the blast wave is relatively weaker at all distances because the propellant and oxidizer are almost never intimately mixed before being ignited. Thus, the full explosive potential of the propellant-

oxidizer computed on the basis of energy of combustion is never realized. This difference is expressed, when comparing with blast waves from TNT explosions, as a percentage or fraction of "TNT yield", where the percentage must be multiplied by the total weight of propellant plus oxidizer, and then expresses the weight of TNT which will produce the same blast properties far enough from the explosion source.

The second characteristic of the blast from propellant explosions which differs from the blast from TNT explosions is that measured parameters such as peak overpressure and positive phase impulse vary with range in a different manner. Compared to TNT blasts, equal energy propellant explosions generate blast waves with relatively low overpressures and relatively high impulses (longer durations) at close-in distances, with gradual change to nearly identical pressures and impulses with increasing range. Below about 10 psi overpressure, blast characteristics from the two types of sources appear to be essentially identical. The term "terminal yield" has been introduced to designate blast yield calculated from measured blast parameters in the low-pressure regime. The basis for estimating the terminal yield is usually a source of compiled blast data for hemispherical TNT charges detonated on the ground (see ref. 2).

A third facet of difference between TNT explosions and liquid propellant explosions can seriously affect our ability to predict fragment velocities of appurtenances. For TNT explosions, there are available both a quantity of measurements of time histories of dynamic pressures, and also proven computer programs which can predict time histories of this and other physical properties of blast waves. For liquid propellant explosions, the only complete body of data available is for time histories of overpressure, from Project PYRO (refs. 15 through 17). Methods are presented in Section II for estimation of certain blast wave properties for several propellant combinations in test configurations which simulate accidental spill and subsequent ignition (identified in Section II as CBGS - Confined By the Ground Surface). The parameters which can be estimated, given type of propellant, total weight of propellant W_t , impact velocity U_i , time of ignition t , and distance R from the center of the explosion to an appurtenance, are the side-on peak overpressure P and the side-on impulse I . As we see later, these values must be used together with other data to estimate the pressures exerted on a body as the blast wave diffracts around it.

c. Interaction of Blast Waves with Appurtenances - To be able to predict velocities to which appurtenances are accelerated by propellant blasts, we must know something about the physics of interaction of blast waves with solid objects. Some of this knowledge is briefly reviewed here. Figure 33 shows schematically, in three stages, the interaction of a blast wave with an irregular object. As the wave strikes the object, a portion is reflected from the front face, and the remainder diffracts around the object. In the

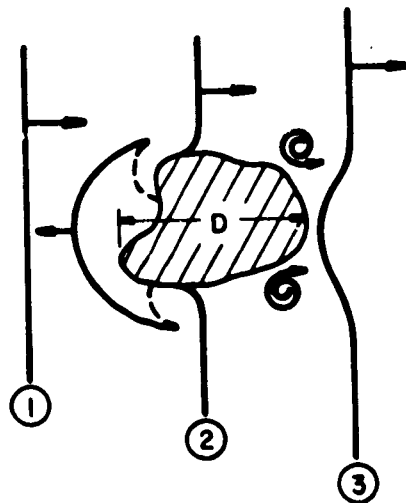


FIGURE 33. INTERACTION OF BLAST WAVE WITH IRREGULAR OBJECT.

diffraction process, the incident wave front closes in behind the object, greatly weakened locally, and a pair of trailing vortices is formed. Rarefaction waves sweep across the front face, attenuating the initial reflected blast pressure. After passage of the front, the body is immersed in a time-varying flow field. Maximum pressure on the front face during this "drag" phase of loading is the stagnation pressure.

We are interested in the net transverse pressure on the object as a function of time. This loading, somewhat idealized, is shown in Figure 34. (Details on calculation are given in *The Effects of Nuclear Weapons*, ref. 34.) At time of arrival t_a , the net transverse pressure rises linearly from zero to maximum of P_R in time $(T_1 - t_a)$ (for a flat-faced object, this time is zero). Pressure then falls linearly to drag pressure in time $(T_2 - T_1)$, and then decays more slowly to zero in time $(T_3 - T_2)$. The time history of drag pressure is a modified exponential, with maximum given by

$$C_D Q = C_D \cdot \frac{1}{2} \rho_s u_s^2 \quad (38)$$

where C_D is the steady-state drag coefficient for the object, Q is peak dynamic pressure, and ρ_s and u_s are peak density and particle velocity respectively for the blast wave. The characteristics of the diffraction phase of the loading can be determined easily if the peak side-on overpressure P_s or the shock velocity U are known, together with the shape and some characteristic dimension, D of the object. The peak amplitude of the drag phase, $C_D Q$, can also be determined explicitly from P_s or u_s . But, the time

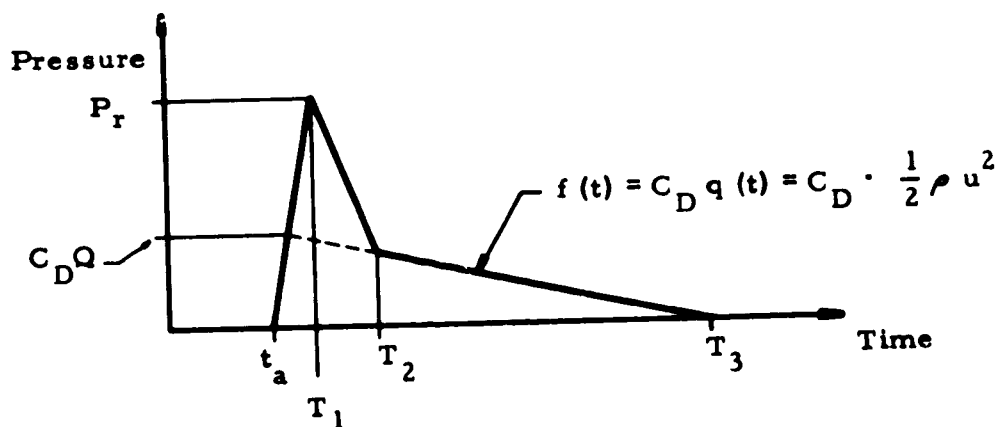


FIGURE 34. TIME HISTORY OF NET TRANSVERSE PRESSURE ON OBJECT DURING PASSAGE OF A BLAST WAVE

history of the ensuing drag loading, $C_D q(t)$, is quite difficult to predict accurately for propellant blasts.

d. Method of Estimating Net Transverse Pressure - The method we present here utilizes the fits of Section II to PYRO data for side-on blast parameters, an assumed time history of drag pressure known to be reasonably accurate for TNT and nuclear blasts, estimates of diffraction times based on shock tube experiments, drag coefficients from wind tunnel data, and reflected and stagnation blast front properties based on equations which are well known in blast physics.

Side-on overpressure is often expressed as a function of time by the modified Friedlander equation (see Chapter 1 of ref. 1).

$$p(t) = P(1 - t/T)e^{-bt/T} \quad (39)$$

where T is the duration of the positive phase of the blast wave. Integrating this equation gives the impulse

$$I = \int_0^T p(t) dt = \frac{PT}{b} \left[1 - \frac{(1 - e^{-b})}{b} \right] \quad (40)$$

The dimensionless parameter b is called the time constant, is a function of shock strength, and is reported in Chapter 6 of ref. 1. It is plotted graphically in Figure 35 for a range of shock strengths \bar{P} , where

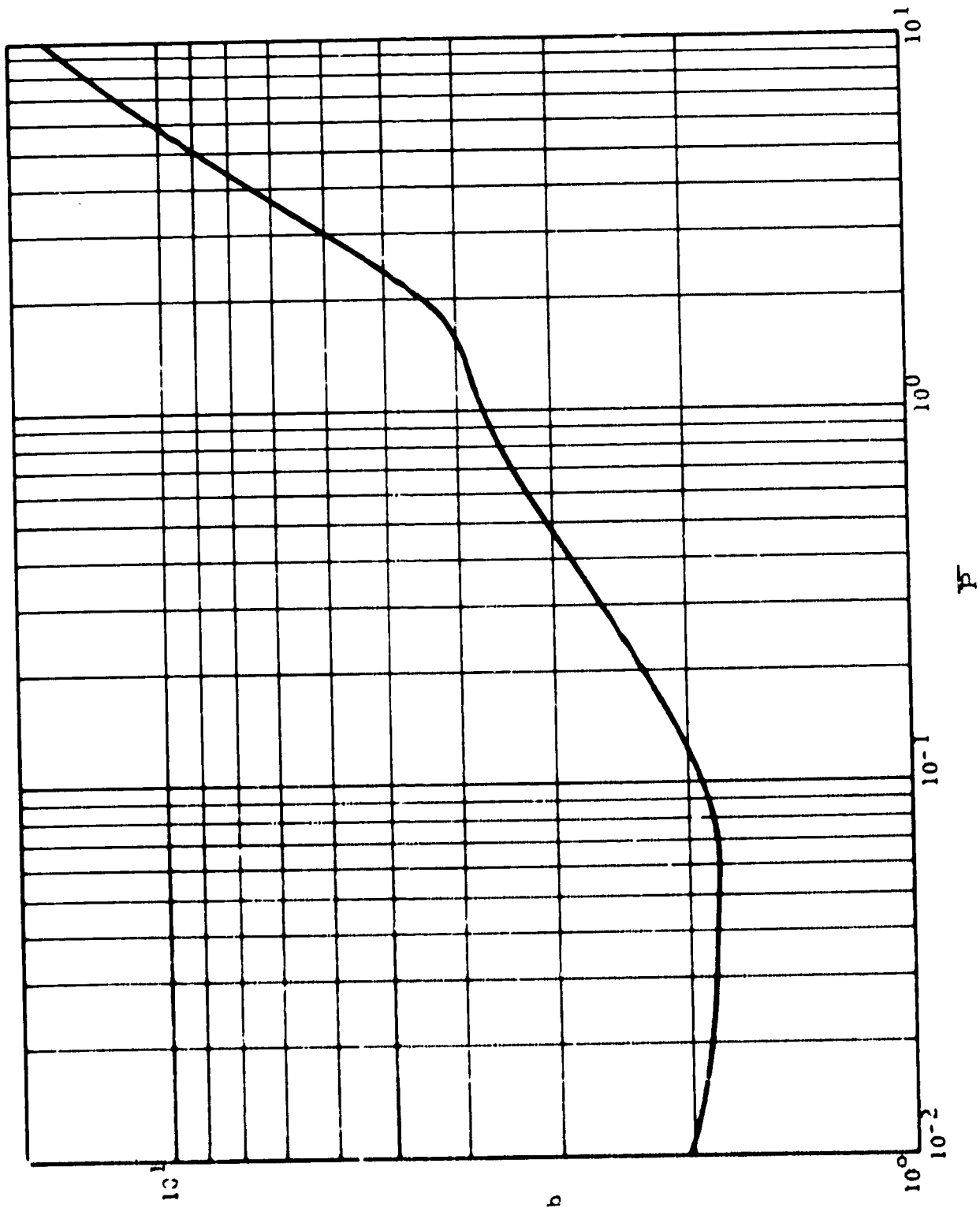


FIGURE 35. BLAST WAVE TIME CONSTANT b VS. DIMENSIONLESS OVERPRESSURE P

$$\bar{P} = P/p_0 \quad (41)$$

and p_0 is ambient air pressure. The peak reflected overpressure P_r and peak dynamic pressure Q are unique functions of P for a given ambient pressure p_0 . For shocks of intermediate to weak strengths, $\bar{P} \leq 3.5$, these functions are (see ref. 1, Chapter 6):

$$\bar{P}_r = 2\bar{P} + \frac{3\bar{P}^2}{4} \quad (42)$$

and

$$\bar{Q} = \frac{5}{2} \frac{\bar{P}^2}{7 + \bar{P}} \quad (43)$$

where

$$\bar{P}_r = P_r/p_0, \quad \bar{Q} = Q/p_0 \quad (44)$$

For the time history of drag pressure, a good fit to experimental data for TNT is a slightly modified form of that employed by Glasstone (ref. 34),

$$q(t) = Q (1 - t/T)^2 e^{-bt/T} \quad (45)$$

The procedure for determining the transverse loading blast parameters in Figure 34 which are independent of object size and shape is then as follows:

- (1) Obtain P and I from curves in Section II
- (2) Calculate \bar{P}
- (3) Read b from Figure 35
- (4) Solve Equation (40) for T , knowing P , I , and b
- (5) Substitute \bar{P} in Equations (42) and (43) to obtain \bar{P}_r and \bar{Q}
- (6) Obtain P_r and Q from Equation (44)
- (7) Substitute in Equation (45) for $q(t)$, realizing that $T = T_3 - t_a$ in Figure 34.

The remaining quantities needed to define the time history of transverse pressure are dependent on the size and shape of the object. They are only well defined for objects of regular shape, such as right circular cylinders, flat rectangular strips, etc. Methods for estimating $(T_1 - t_a)$ and $(T_2 - T_1)$ are given by Glasstone (ref. 34) for several such objects, and will not be repeated here. One does need to know, however, the shock front velocity U .

This is a unique function of the shock strength \bar{P} , and is given by (see Chapter 6 of ref. 1)

$$\bar{U}^2 = 1 + \frac{6\bar{P}}{7} \quad (46)$$

Drag coefficients C_D are available from Hoerner (ref. 35) for a variety of bodies over a wide range of flow velocities. Estimates for the subsonic flow range which applies over the shock strengths of interest to us are given in Table VII. Melding these quantities, dependent on the size and shape of the body, to the previous ones which are derivable from side-on blast wave properties permits an estimate of the entire time history of transverse pressure, at least for bodies of regular geometry.

e. Method of Predicting Appurtenance Velocity - Once the time history of net transverse pressure loading is known, the prediction of appurtenance velocity can be made quite easily. The basic assumptions are that the appurtenance behaves as a rigid body, that none of the energy in the blast wave is absorbed in breaking the appurtenance loose from its moorings or deforming elastically or plastically, and that gravity effects can be ignored during this acceleration phase of the motion. The equation of motion of the object is then

$$A p(t) = M \ddot{x} \quad (47)$$

where A is the area of the object presented to the blast front, $p(t)$ is the net transverse pressure according to Figure 34, M is the total mass of the object, and x is displacement of the object (dots denote derivatives with respect to time). The object is assumed to be at rest initially, so that




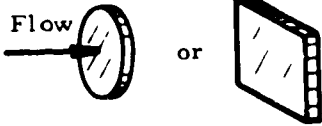
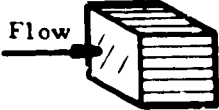
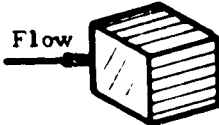
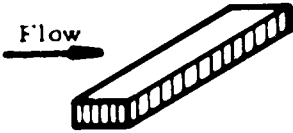
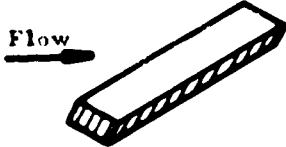

$$x(0) = 0, \quad \dot{x}(0) = 0 \quad (48)$$

Equation (47) can be integrated directly. With use of the initial conditions (48), this operation yields, for appurtenance velocity,

$$\dot{x}(t) = \frac{A}{M} \int_0^{(T_3-t_a)} p(t) dt = \frac{A}{M} I_d \quad (49)$$

where I_d is total drag and diffraction impulse. The integrations in Equation (49) can be performed explicitly if the pressure time history is described by suitable mathematical functions, or performed graphically or numerically if $p(t)$ cannot be easily written in function form. In either case, Equation (49) yields the desired result—a predicted velocity for the object.

TABLE VII
 DRAG COEFFICIENTS, C_D , OF VARIOUS SHAPES
 (Source: ref. 35)

SHAPE	SKETCH	C_D
Right Circular Cylinder (long rod), side-on		1.20
Sphere		0.47
Rod, end-on		0.82
Disc, face-on		1.17
Cube, face-on		1.05
Cube, edge-on		0.80
Long Rectangular Member, face-on		2.05
Long Rectangular Member, edge-on		1.55
Narrow Strip, face-on		1.98

D. Correlation of Velocity Prediction Methods With Data

1. Prediction of PYRO Data by a Deterministic Method for CBM - A deterministic method of predicting initial fragment velocities was described in Section III. C. It was found that initial fragment velocities could be obtained by this method when some of the geometric characteristics of the exploding vessel were known and when certain properties of the explosive products formed upon detonation within the vessel were known. The data from the Project PYRO tests were not really sufficient to properly quantify the required independent variables for this method, because exact quantities of propellant which mixed and exploded were not known. It was felt, however, that certain reasonable values could be assumed for the unknown variables (along with the measured values for other variables), and a feel for the applicability of this method could be obtained. Accordingly, results for initial fragment velocities were obtained from the computer program given in Appendix C when values for the independent variables to be described were used in it. These results were compared to PYRO data for mean initial fragment velocities obtained from analysis of films of PYRO tests. The data from the PYRO tests were limited to those cases which best approximated the constraints of the deterministic method. The correlation between the data and the theoretical values was good enough for "reasonable" values of the independent variables, that it may be concluded that a deterministic method of fragment velocity prediction may be useful if sufficient knowledge is obtained of the explosive product parameters in future testing.

a. PYRO Data - The test numbers for PYRO tests considered in this correlation are given in Table VIII. Since our deterministic method is based on a spherically symmetric containment vessel, it was reasonable to take the cylindrical test geometry of the PYRO tests which most closely approximated spherical symmetry, i. e., L/D ratio closest to 1.0. Thus, only tests with L/D = 1.8 (the smallest L/D ratio) were considered. Furthermore, only confined-by-the-missile (CBM) cases were considered since confinement-by-the-ground-surface (CBGS) cases do not represent internal explosions. To assure that well-confined explosions were being considered, only $D_0/D_t = 0.45$ cases were allowed. Finally, to simplify the assumptions made about the reactants and explosive products, it was decided to take the LH_2/LO_2 cases only.

Data for tests which meet these criteria are plotted in Figures 36 and 37 for the 200-lb and 1,000-lb tests, respectively. In these plots, the measured initial velocity is plotted versus a measured yield. The measured initial velocity was obtained from measurements taken from films of the PYRO tests (see Section II. A). The measured yield, Y_M , is a quantity obtained in the following manner. Measured blast overpressures obtained along blast lines about the center of explosion for the various tests produced the PYRO

TABLE VIII - FRAGMENT VELOCITY PREDICTIONS COMPARED
WITH MEASUREMENTS

PYRO Test No.	Total Prop. Wt. W _t lbs.	Measured Yield Y _M %	Reactants Weight W _r lbs	Reactants Energy E ft-lbs X 10 ⁻⁵	Mass Of Non-Reac- tants M _v = M _v + M _r - M _f lb-sec ² /in.	Radius Of Reactants R _o in.	Calc. Max. Frag. Velocity U _f ft/sec	Measured Mean Velocity U _f ft/sec
053	200	1.08	2.08	3.35	.633	8.0	358	362
091	200	7.83	15.63	25.2	.564	15.5	975	1500
118	200	5.41	10.82	17.4	.589	13.7	790	710
199	200	2.16	4.32	6.95	.623	10.2	543	660
200	200	4.59	9.18	14.8	.597	13.0	786	880
210	1000	1.89	18.9	30.4	2.49	16.12	540	650
212	1000	7.29	72.9	117.	2.21	25.35	1020	790
213	1000	9.46	94.60	150.8	2.11	27.15	1110	990
265	1000	2.70	27.0	43.5	2.45	17.85	636	690

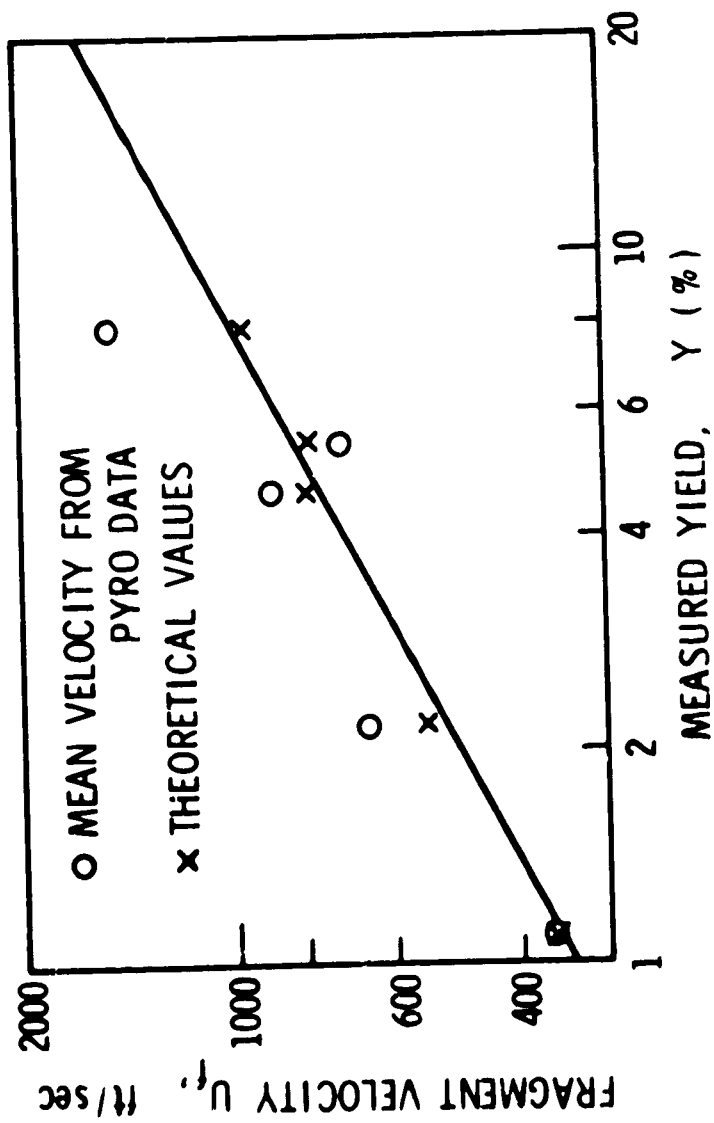


FIGURE 36. FRAGMENT VELOCITY: CORRELATION OF DATA FROM PYRO LH_2/LO_2 TESTS WITH THEORETICAL VALUES, $W_t = 200$ LBS

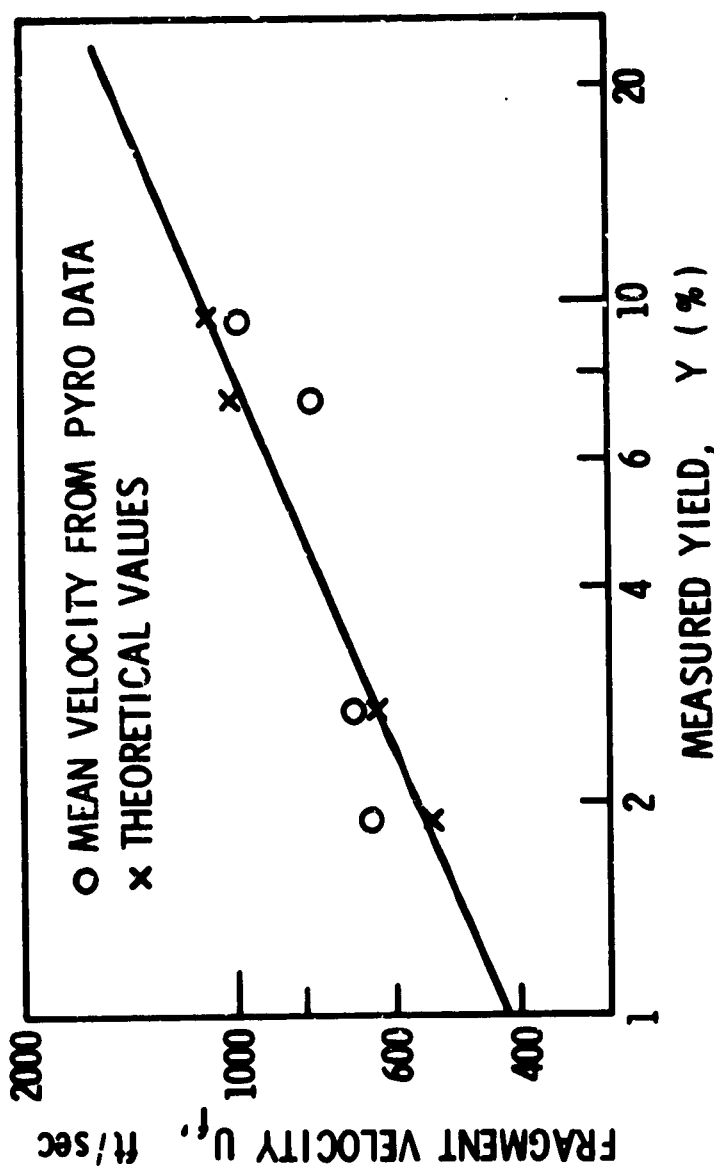


FIGURE 37. FRAGMENT VELOCITY: CORRELATION OF DATA FROM
 PYRO LH₂/LO TESTS WITH THEORETICAL VALUES,
 $W_t = 1000 \text{ LBS}^2$

CP

"yield" values, Y . This yield value is the percentage of the total propellant weight, W_t , such that

$$Y \cdot W_t = W_{TNT} \quad (50)$$

where W_{TNT} is the weight of TNT which would produce an equivalent series of blast overpressure measurements in air to those of a given test. The weight of propellant which would produce the same blast effect as TNT is

$$W_R = W_{TNT} \frac{H_{TNT}}{H_R} \quad (51)$$

where W_R is the weight of the reactants (or propellant) estimated to be involved in the explosion from the blast measurements, and H_{TNT} and H_R are the heats of explosion per unit mass for TNT and the reactants, respectively. For an LH_2/LO_2 explosion in which fuel and oxidizer are mixed stoichiometrically, Equation (51) becomes

$$W_R = \frac{W_{TNT}}{3.7} \quad (52)$$

Measured yield, Y_M , is the ratio of the weight of the reactants estimated to be involved in the explosion from the external blast measurements to the total known weight of propellant. Thus, from Equations (50) and (52),

$$Y_M = \frac{W_R}{W_t} = \frac{Y}{3.7} \quad (53)$$

Values for Y_M and W_R appear in Table VIII along with measured initial velocity.

Since measurements during the PYRO tests were all made external to the confinement vessel, it is not possible to estimate from them how much of the true blast yield was absorbed as kinetic energy of flying fragments. Thus, neither the PYRO yield value, Y , or the measured yield value, Y_M , can be used to determine the actual quantity of propellant involved in the explosion, and W_R is really only the quantity estimated by ignoring the effects of the confinement of the detonation. This is an important point, as will be seen in the ensuing discussion, because our deterministic method requires knowledge of the actual quantity of propellant involved and the characteristics of the resulting explosive products, and to obtain this information one is required to measure parameters internal to the confinement vessel, which was not done in the course of PYRO testing.

b. Data Predicted by Deterministic Method - in order to predict initial fragment velocities with our deterministic method, it is necessary to have values for the following parameters related to the confinement vessel, explosion products, and propellant ullage:

- (1) The number of fragments, n , the vessel breaks up into;
- (2) The peak overpressure, P_0 , attained in the volume occupied by the explosive products immediately after detonation;
- (3) The ratio of specific heats, κ , which describes the region of the explosive products immediately after detonation;
- (4) The speed of sound, a_0 , in the region of the explosive products immediately after detonation;
- (5) The radius, R_0 , of the region of explosive products immediately after detonation;
- (6) The mass, M , of all the propellant not involved in the explosion process plus the mass of the confinement vessel.

Physically, the explosion process is thought of as one in which a volume of the fuel and oxidizer mix stoichiometrically and then form a gas in the course of explosion whose volume and physical characteristics are described by parameters 2 through 5 above at the instant immediately after the explosion has occurred. All the rest of the propellant is thought of as inert and merely augmenting the mass of the confinement vessel.

As was seen earlier in this section, Figure 29, our deterministic method predicts that initial fragment velocities are insensitive to the number of fragments, n , when n is on the order of 10^2 or more. It is relatively insensitive down to $n = 2$. We picked $n = 10^2$ as a reasonable number of fragments for the PYRO tests investigated here. Also in this same section, Figure 30 indicates that above $\kappa = 1.2$, the initial fragment velocities are relatively independent of the value of κ . The parameter κ ranges between 1.1 and 1.4 for most gases and tends to be lower for the same gas at high temperatures ($\kappa = 1.3$ for oxygen and hydrogen at $2,000^\circ\text{C}$, for instance, while $\kappa = 1.4$ for these gases at 15°C). We picked $\kappa = 1.2$ for our explosive products "gas", although a choice of a larger κ would have changed the results very little.

Using the value for reactant weight, W_R , described under the previous heading, we were able to calculate the energy of explosion for each test as estimated from the external measurements. This was simply

$$E = W_R \cdot H_R \quad (54)$$

Based on the calculated density of a mixture of LH_2/LO_2 mixed stoichiometrically, we obtained a volume of reactants related to W_R for each test from

$$V_R = \frac{W_R}{\rho}, \quad \text{where} \quad \rho = \frac{V_H \rho_H + V_{OX} \rho_{OX}}{V_H + V_{OX}} \quad (55)$$

and

$$8 V_H \rho_H = V_{OX} \rho_{OX}$$

where ρ and V are density and volume, respectively, and the subscripts H and OX refer to LH_2 and LO_2 , respectively. It should be stressed at this point that E and V_R refer to some weight W_R of reactants that was thought to be involved in the explosion process from external measurements. Obviously, this E is less than the actual energy of explosion, since it represents only the shock energy imparted to the air about the confinement vessel and does not account for kinetic energy imparted to the fragments, energy lost as heat and light to the air, energy lost through fragment heating, etc. The calculated volume of the reactants associated with energy of explosion E is also lower than the actual volume for the above reasons. Nonetheless, assuming these values for E and V_R are reasonable approximations for the real situation, for the stoichiometric mixture of LH_2/LO_2 one may obtain the peak pressure, P_o , from:

$$E = \frac{P_{oo} V_R}{\kappa - 1} \left[\frac{P_o}{P_{oo}} \cdot \left(\frac{P_o}{P_{oo}} \right)^{1/\kappa} \right] \quad (56)$$

where P_{oo} is the ambient pressure (taken as 14.7 psi). This was done for our values of E , V_R , and κ using the Newton-Raphson iteration technique for root finding. The program used (in the FORTRAN IV language) appears in Appendix D. The results predicted peak pressures of nearly 10^4 psi within the explosive products. Since E and V_R are both proportional to W_R , this result is independent of the weight of the reactants, and the same value ($P_o = 10^4$ psi) was used for predicting fragment velocities from all PYRO tests considered.

Picking a value for velocity of sound, a_o , was complicated by the fact that this is a quantity that cannot be inferred from external measurements at all. It is an intrinsic property of the explosive products, a function of thermodynamic parameters such as temperature, density, and pressure, as well as the microscopic state of the "gas" at the instant of explosion. Since we had assumed gas-like properties for the explosion products, however, and since sound velocity would certainly be in the range 10^3 to 10^5 in./sec for gases under most conceivable conditions, we calculated fragment velocity,

U_f , as a function of a_0 and R_0 for fixed n , M , P_0 , and κ to obtain an estimate of the sensitivity of U_f to a_0 and R_0 , relatively. This plot, appearing in Figure 14, shows that over the orders of magnitude chosen for a_0 , U_f is relatively insensitive to a_0 and relatively sensitive to R_0 . Accordingly, we chose $a_0 = 10^4$ in./sec as a constant value for all tests. This value is a reasonable one for gases whose sound velocities vary in the range 1.0 to 5.0×10^4 in./sec for the most part under normal conditions. Furthermore, our results would not be as sensitive to error in this parameter as they would be to error in R_0 . If one assumes that the density of the explosive products gas is equal to the density of the LH_2/LO_2 mixture detonated as reactants (i. e., see Equation (55)) which formed it (certainly an extreme and unlikely case), nonetheless a_0 for a given R_0 calculated from

$$a_0 = \sqrt{\frac{\kappa P_0}{\rho}} \quad (57)$$

gives a fragment velocity very close to the same one obtained using $a_0 = 10^4$ in./sec (as seen from Figure 38).

The mass, M , required by our deterministic method is obtained from

$$M = M_t + M_{ta} - M_R \quad (58)$$

where subscripts t , ta , and R refer to the total propellant weight, the tank, and the reactants, respectively. Again, since M_R must be the mass of the actual quantity of reactants involved in the explosion process, it could only be estimated from the external PYRO measurements, that other internal measurements would be required to ascertain this quantity for each test. From the yield values it is apparent, however, that M_R was probably small relative to M_t and M_{ta} . We estimated M_R based on twice the calculated value W_R . This produced corrections in M on the order of less than 10%. Values obtained for M are given in Table VIII.

As was shown in Figure 38, the fragment velocities obtained from our deterministic method are most sensitive to values of R_0 chosen to describe the radius of explosive products at the instant immediately after detonation. Since W_R is obviously lower than the actual weight of reactants involved in the explosion process, at least a lower limit could be obtained for R_0 based on

$$\left(\frac{4}{3}\right) \pi R_0^3 = V_R = W_R / \rho \quad (59)$$

from Equation (55). We assigned an upper limit on R_0 based on the maximum radius a sphere would have which had the same volume as the confinement

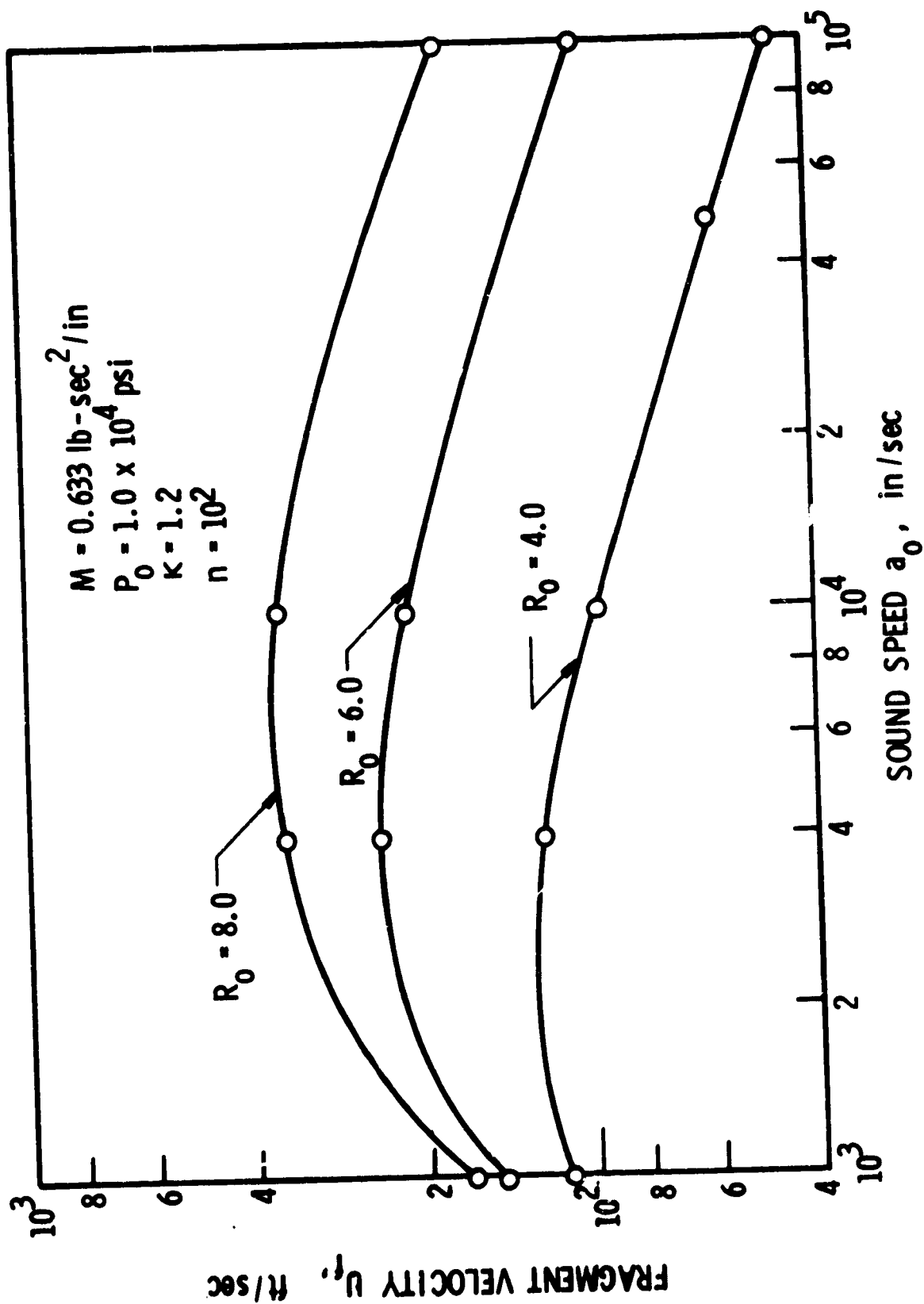


FIGURE 38. FRAGMENT VELOCITY AS A FUNCTION OF SOUND SPEED IN THE EXPLOSIVE PRODUCTS

vessel tank whose dimensions were obtained for the 200 and 1,000-lb tank tests. Thus, R_0 could be larger than the radius of the tank since the latter was a cylinder, but was of the same order of magnitude.

Within these brackets, an R_0 was chosen to give a reasonable value for initial fragment velocities for one PYRO test for each of the tank sizes. P_0 was then varied as the cube root of the measured yield for the other tests and a corresponding U_f was calculated by the deterministic method. Values for R_0 are given in Table VIII. Figures 36 and 37 show the comparison of the measured and calculated fragment velocities for the 200-lb and 1,000-lb tests.

c. Conclusions - Initial fragment velocities obtained by our deterministic method predict measured fragment velocities from Project PYRO tests relatively well when reasonable values are chosen for the unmeasured parameters. It should be noted that the values for R_0 in Table VIII are all within a reasonable range relative to tank geometry. Our results indicate that a thorough knowledge of the internal parameters on just one test for a given tank geometry could probably allow reasonable predictions for initial fragment velocity, using this method, for all tests of that geometry based on external measurements alone (i. e., internal measurements would only have to be made once). Finally, the great difficulty in any deterministic approach for predicting fragment velocities for liquid rocket explosions (CBM) in general, is in obtaining data on how much of the reactants are actually going to be involved in the explosion. It seems that fragment velocity will be relatively independent of the number of fragments and even of the thermodynamic properties of the explosion products gas (except the peak pressure generated) but it is very sensitive to the quantity of reactants involved in the explosion process.

2. Correlation of Velocity for Fragments from CBGS Tests with Predictions - The method given earlier in this section can, in theory, be used to predict velocities to which parts of the missile and appurtenances are accelerated by explosions during CBGS tests of PYRO. In practice, the method can only be applied to a limited number of the CBGS tests for which we measured fragment velocities. To use the prediction method:

- (1) We must know blast yield Y and total weight of propellant W_T .
- (2) We must know the distance R of the fragment or appurtenance from the center of the explosion.
- (3) We must know the geometry and mass of the fragment.
- (4) Blast wave properties at the initial location of the fragment must lie within the range of the PYRO data.

We obviously satisfy the first requirement, but we can only estimate the second two. Also, the parts of the tankage which we believe constitute most of the visible fragments are located so close to the source that the blast is much stronger than for any of the PYRO blast data. Accordingly, only a rough "spot check" can be made to determine if the prediction method seems reasonable.

The test chosen for prediction was Test 293, a LO₂/LH₂ CBGS test with 1,000 lb of propellant impacting at 44 ft/sec. The measured blast yield was 3.9%. Twenty-six fragments were observed, with a mean velocity of 464 ft/sec ± 226 ft/sec (Table V). From descriptions of the test apparatus and method in reference 16, the dimensions, material, and skin thickness of the tankage are known, as well as the rest position after drop impact. We believe that the majority of the observed fragments were relatively large pieces of the tank skins, made of 0.060-inch thick aluminum alloy. The lower part of the tank was about 3 ft above the center of the explosion,* but the middle of the tank was about 10 ft from the center of the explosion. So, approximate values for input parameters are as follows:

Blast

R = 10 ft
 W_T = 1,000 lb
 P₀ = 14.7 psi
 a₀ = 1,088 ft/sec

Fragment

Shape - circular disc of 12-inch diameter
 Thickness - h = 0.060 in.
 Density - ρ = 2.59 × 10⁻⁴ lb sec²/in.⁴

From Equation (3), Section II, the equivalent weight of propellant for blast is

$$W = W_T \times \frac{Y}{100} = 1,000 \times \frac{3.9}{100} = 39 \text{ lb}$$

Scaled distance is

$$R/W^{1/3} = 10/39^{1/3} = 2.94 \text{ ft/lb}^{1/3}$$

*In the PYRO CBGS tests, the tank assembly was arrested by stops at the bottom of its fall after striking cutter blades which ruptured the tank bottoms.

From Figures 22 and 23 in Section II, the blast pressure and scaled impulse are:

$$P = 80 \text{ psi}; \quad I/W^{1/3} = 30 \text{ psi-msec/lb}^{1/3}$$

$$I = 30 \times 3.4 = 102 \text{ psi-msec}$$

Dimensionless overpressure is

$$\bar{P} = P/P_0 = 80/14.7 = 5.45$$

From Figure 35, the time constant b can now be determined. It is

$$b = 10$$

From Equations (40), (41), and (44), we can calculate dimensionless reflected pressure \bar{P}_R , drag pressure \bar{Q} , and shock velocity, \bar{U} . Multiplying by P_0 or a_0 , the corresponding dimensional quantities are:

$$P_R = 490 \text{ psi}$$

$$Q = 72 \text{ psi}$$

$$U = 3.15 \times 10^4 \text{ in./sec}$$

Solving Equation (40) for duration T , we have

$$T = Ib / \left\{ P \left[1 - \frac{(1-e^{-b})}{b} \right] \right\} = 102 \times 10 / \left\{ 80 \left[1 - \frac{(1-e^{-10})}{10} \right] \right\} = 14.2 \text{ msec}$$

To complete the description of the transverse pressure loading, we must know the drag coefficient C_D and two characteristic times for the diffraction phase of the loading. The drag coefficient for a flat disc is, from Table VII, $C_D = 1.17$. The rise-time ($T_1 - T_a$) is zero,* and

$$(T_2 - T_1) = \left(\frac{D}{2} \right) \frac{1}{U} \tag{60}$$

where D is diameter of the disc.

$$(T_2 - T_1) = \left(\frac{12}{2} \right) \left(\frac{1}{3.15 \times 10^4} \right) \approx 0.2 \text{ msec}$$

*See Glasstone, ref. 34.

All of the parameters needed to define the time history in Figure 34 are now known. After numerical integration, we get for the integral in Equation (47),

$$I_d = 139 \text{ psi-msec}$$

Finally, predicted velocity is

$$U_i = \frac{A}{M} I_d = \frac{I_d}{\rho h} = \frac{139 \times 10^{-3}}{2.59 \times 10^{-4} \times 6 \times 10^{-2} \times 12}$$

$$U_i = 745 \text{ ft/sec}$$

Comparing this to the measured mean value,

$$\bar{U}_i = 464 \pm 226 \text{ ft/sec}$$

we see that the predicted value is of the correct order of magnitude, but too high. The blast parameters, and consequent predicted velocities, are, however, very strong functions of the assumed standoff distance R , particularly at small standoffs. We could quite easily have predicted velocities very much higher and very much lower than the measured values by simply choosing a range of values for R covering the extremes of distances of the tank from the blast source. All that we can conclude is that the prediction method yields velocities which appear to be of the same magnitude as the measured velocities.

E. Frequency Distribution of Initial Velocity

Since the number of fragments which could be traced in each selected film from Project PYRO were relatively small, a logical grouping of the data was considered in order to determine the initial velocity frequency distributions.

Since the data on fragment distance versus yield (%) in Section IV showed good correlation, a desirable grouping appeared to be over a medium yield (%) range within a configuration and propellant type. The groupings are shown in Table IX and are:

- (1) CBM, LO_2/LH_2 , Yield from 10 to 29%, group sample size 108.

- (2) CBM, LO₂/RP-1, Yield from 9.8 to 20%, group sample size 131.
- (3) CBGS(Vertical), LO₂/LH₂, Yield from 12 to 22%, group sample size 15.
- (4) CBGS(Vertical), LO₂/RP-1, Yield from 10 to 30%, group sample size 72.

The data for U_A^* were ordered, and 10th through 90th percentiles (in 10% steps) were determined.

The percentiles were plotted on normal and log normal probability paper. The log normal plots were the best fits. These plots are shown in Figures 39 through 42. The parameters for the log normal distribution can be estimated, according to Hahn (ref. 36) as follows:

The mean, $\hat{\mu}$, can be estimated as the logarithm (to the base e) of the 50th percentile. The standard deviation, $\hat{\sigma}$, can be estimated as two-fifths of the difference between the logarithms of the 90th and 10th percentiles. The estimated means and standard deviations are shown in Table X. Goodness of fit statistics were calculated using the "W" test as described by Hahn and Shapiro (ref. 36). The method and calculations are described in Appendix F and discussed in more detail in Section IV. The calculated values of the "W" statistics for the four log normal distributions are:

- (1) CBM LO₂/LH₂ - .925
- (2) CBM LO₂/RP-1 - .947
- (3) CBGS LO₂/LH₂ - .973
- (4) CBGS LO₂/RP-1 - .989

Referring to Figure 48, Section IV, the approximate probabilities for obtaining values as low as the calculated values of "W", given that the stated distributions are the correct ones, are:

- (1) .415
- (2) .610
- (3) .915
- (4) .990

* U_A is defined in Equation (5), and is taken to be an approximation of the initial velocity.

TABLE IX. GROUPING OF TESTS BY PROPELLANT AND CONFIGURATION

Propellant	Configuration	PYRO Test No.	Yield, Y (%)	Weight, W (lb)	Sample Size
LO ₂ /LH ₂	CBM	051	22.0	200	9
		090	29.0	200	7
		091	13.0	200	12
		094	25.0	200	11
		118	20.0	200	8
		200	17.0	200	26
		212	27.0	1,000	8
		265	10.0	1,000	27
LO ₂ /RP-1	CBM	48	9.8	200	12
		87A	16.0	200	15
		192	14.0	1,000	14
		193	20.0	1,000	14
		209	10.0	1,000	15
		270A	13.0	1,000	32
		278	13.0	25,000	16
		282	13.0	25,000	13
LO ₂ /LH ₂	CBGS (Vertical)	106A	22.0	200	12
		115	15.0	200	14
		152	14.0	200	14
		184	17.0	200	16
		197	19.0	200	18
		211	12.0	1,000	17
		230	21.0	200	21
		266	14.0	1,000	19
		288C	13.0	25,000	20
LO ₂ /RP-1	CBGS (Vertical)	107	29.0	200	21
		109	10.0	200	11
		191	13.0	1,000	24
		219	14.0	1,000	16

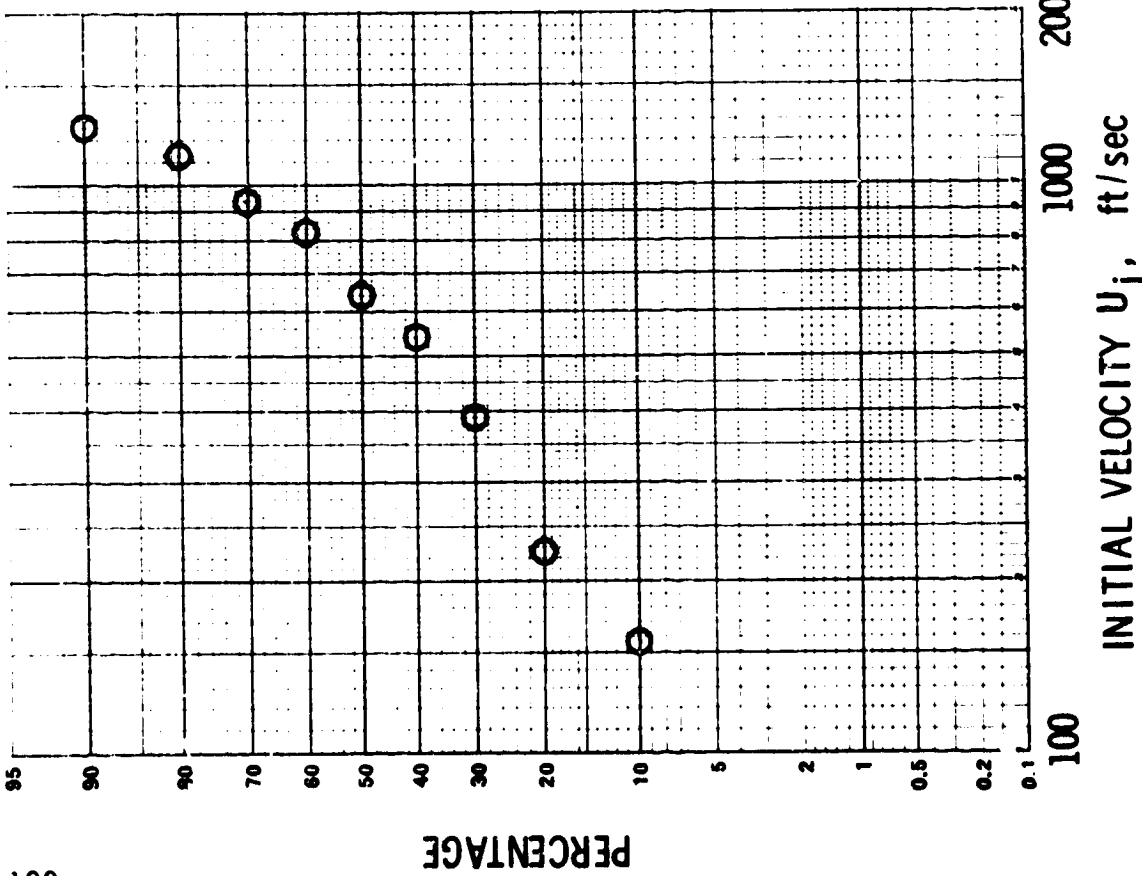


FIGURE 39. INITIAL VELOCITY DISTRIBUTION, CBM, LO₂/LH₂, LOG NORMAL PLOTS

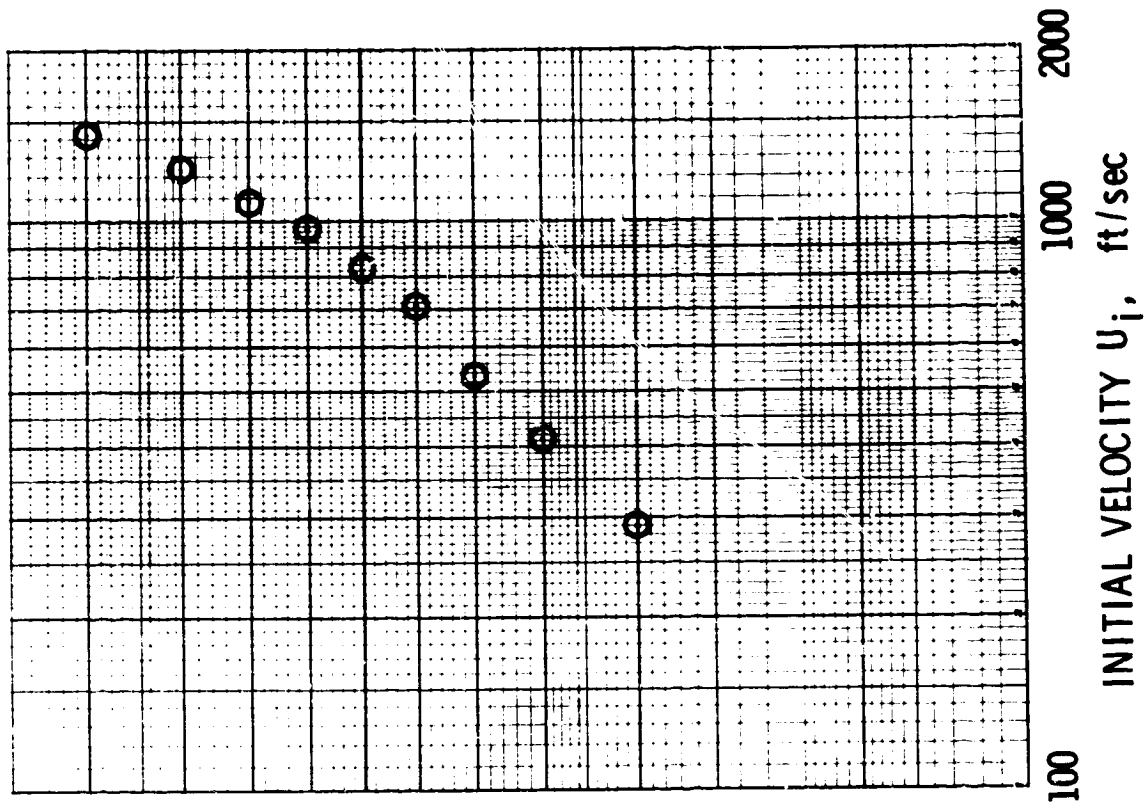


FIGURE 40. INITIAL VELOCITY DISTRIBUTION, CBM, LO₂/RP-1, LOG NORMAL PLOTS

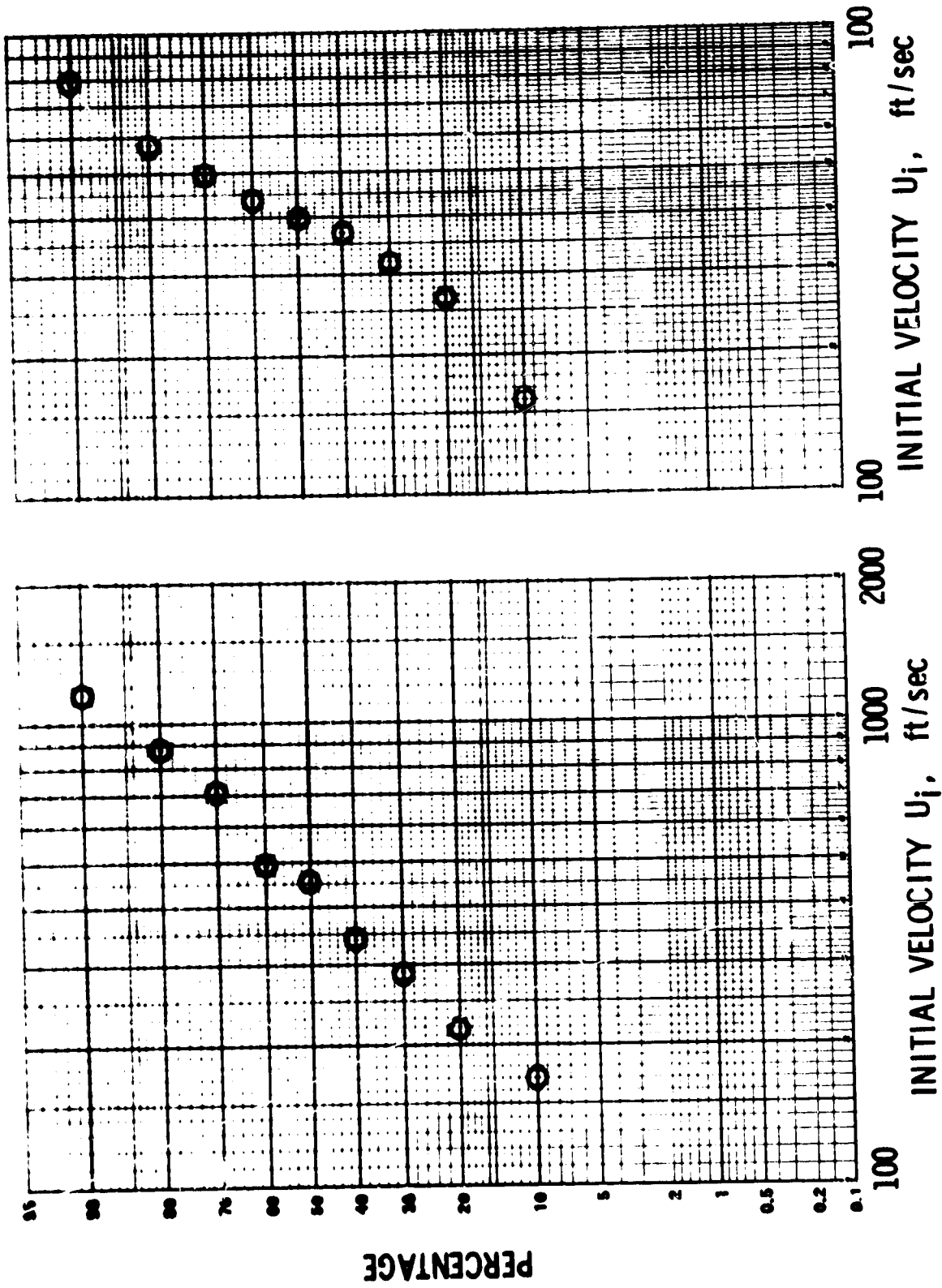


FIGURE 41. INITIAL VELOCITY DISTRIBUTION, CBGS, LO_2/LH_2 , LOG NORMAL PLOTS

FIGURE 42. INITIAL VELOCITY DISTRIBUTION, CBGS, $LO_2/RP-1$, LOG NORMAL PLOTS

TABLE X. PERCENTILES, MEANS AND STANDARD DEVIATIONS
FOR GROUPED VELOCITY DATA (fps)

Percentiles	CBM LO ₂ /LH ₂	CBM LO ₂ /RP-1	CBGS LO ₂ /LH ₂	CBGS LO ₂ /RP-1
10	105.8	290.0	170.0	160.1
20	228.6	414.3	219.2	262.3
30	393.3	536.8	289.3	316.8
40	541.8	714.2	345.1	364.9
50	642.0	822.8	459.4	388.3
60	821.4	973.3	594.3	431.2
70	915.0	1096.3	728.8	498.5
80	1102.7	1216.8	897.7	573.4
90	1249.3	1405.6	1169.9	790.5
Estimated Mean*	6.464	6.713	6.129	5.962
Estimated Standard Deviation*	.9875	.6313	.7715	.6387
* Log Normal Distribution, to base e. To convert to fps, take anti-logarithm				

Since a probability as low as .10 is considered insufficient evidence to reject the chosen distributions, the fits are assumed adequate. The derivation of data for Figure 48 in Section IV is given in Appendix G.

The normal and log normal density function equations are given in Equations (62) and (63) in Section IV.

IV. DETERMINATION OF FRAGMENT SIZE AND RANGE

A. Retrieval of Data from Accidents and Tests

All of the accident and test data which were retrieved were reviewed for pertinent information on fragment size, distance, and distribution.

The criteria for each fragment were that the range, weight and maximum projected area be specified. The nature of the test or accident, blast yield, type of propellants, etc., were also of interest.

From approximately 168 reports and memos reviewed, only eight events, listed in Table XI yielded sufficient information to meet the above-listed criteria. There were many other reports which had partial information, such as distance listed for fragments over 5 pounds, with fragments under 5 pounds listed in number per square yard.

The eight events listed in Table XI can be classified in three groups as follows:

- (1) Events 1 and 2 were Saturn IV confined by missile (CBM), LO_2/LH_2 explosions.
- (2) Events 3, 4, and 5 were spill tests using three tanks, on 120° radials with $\text{LO}_2/\text{LH}_2/\text{RP-1}$, and mixing on the ground (CBGS).
- (3) Events 6, 7, and 8 were mixing tests using two tanks with LO_2/LH_2 and pouring the contents of one tank into the other.

Event 1 was Project PYRO test number 62, a Saturn IV vehicle with 91,000 pounds of LO_2/LH_2 propellant, with self ignition, and a 5% yield. Complete details of the test can be found in Reference 16.

Event 2 was also a Saturn IV vehicle, with 101,198 pounds of LO_2/LH_2 aboard. The yield was estimated to be 1.1%. Complete details of the malfunction can be found in Reference 38.

Events 3, 4, and 5 are described fully in Reference 24. The tests were conducted using 1/25 scale quantities of the propellants for the Saturn C-2 vehicle (i. e., 7880 lb of RP-1; 32,928 lb of LO_2 ; 3032 lb of LH_2). The individual parts of the propellant were placed in spill tanks placed on 120° radials from some central location. The spill tanks were tipped toward this central location so that all three parts combined. They were then detonated from the central location by a small charge of C-4.

TABLE XI - CHART OF EVENTS

Event No.	Ref. No.	Test or Accident Type	Propellant Type	Total Propellant Weight (lb)	Yield Y, Percent
1	16	PYRO Test #62 (SATURN IV)	LO ₂ /LH ₂	91,000	5.0
2	38	S-IV	LO ₂ /LH ₂	101,198	1.1
3	24	J2 Spill Test	LO ₂ /LH ₂ /RP-1	1,754	23.0
4	24	J3 Spill Test	LO ₂ /LH ₂ /RP-1	1,754	24.4
5	24	J1 Spill Test	LO ₂ /LH ₂ /RP-1	1,754	62.6
6	39	Mixing Test	LO ₂ /LH ₂	240	86.0
7*	---	Mixing Test	LO ₂ /LH ₂	240	70.0
8*	---	Mixing Test	LO ₂ /LH ₂	240	73.0

* Data from these tests were furnished by the NASA test director, Mr. J. H. Deese. There is no formal reference.

The method for event 6 is described in reference 39. Events 7 and 8 were similar. These were autoignition mixing tests using 240 pounds of LO_2/LH_2 , pouring one tank into the other. Photographs of each fragment, along with fragment maps and fragment weights were supplied by the NASA Test Director, Mr. J. H. Deese.

B. Data Reduction

The data from each of the events were reduced by careful analysis of each fragment to assure that size (maximum projected area), weight, and distance were specified. In some cases, it was possible to fill in missing items by estimating weight and/or size from information supplied by descriptions or photographs. Because of the paucity of fragment data, considerable effort was expended to extract as much fragment data as possible, without undue loss in accuracy of the parameters. Distances for each fragment were determined from fragment maps.

For each event, data including event code, fragment number, distance (R) in feet, weight (W) in pounds, width in inches, length in inches, maximum projected area (A) in square inches, area divided by weight (A/W), and drag coefficient (CD) were entered on key punch sheets. The drag coefficient was estimated from photographs and descriptions, and subsequent comparison with Table VII. Cards were keypunched and used in the analyses which are described in the following sections. A listing of all fragment data by event is available if desired.

C. Statistical Studies

1. Computer Routines - Using the Biomedical Computer Programs (Ref. 40), with a CDC 6500 computer, the data from each event was subjected to the following routines:

- (1) Means and variances were calculated for R, W, A, A/W, CD, Log R, Log W, Log A and Log A/W.
- (2) Histograms were constructed for the parameters listed in (1) above.
- (3) Correlation plots were made for R versus W, R versus A, R versus A/W, R versus Log W, and R versus (A/W) CD.

2. Preliminary Analysis - The output from the correlation routine was studied to determine if there were discernable patterns of correlation between parameters within an event. While there was some general pattern in some cases, as a whole, the scatter was so great as to discourage further inquiry along these lines. This result could be explained by not considering

(because of a lack of knowledge) the flight angle and initial location of the fragments.

The histograms were studied to relate the parameters R, W, A, and A/W to probability frequency distributions. Since the sample size varied from 31 to 1056, the histograms varied in information content in about the same ratio. However, the form of some of the histograms suggested that a normal probability density function would supply an adequate fit, and others offered the possibility of a fit by a log normal distribution.

The normal distribution can be written as:

$$f(x) = (1/\sqrt{2\pi}\sigma) \exp \left[-(x-\mu)^2/2\sigma^2 \right], \quad -\infty < x < \infty,$$
$$-\infty < \mu, \sigma < \infty,$$
(61)

where σ is the standard deviation and μ is the mean.

The log normal distribution can be written (ref. 36):

$$f(y) = (1/\sqrt{2\pi}\sigma y) \exp \left[(\ln y - \mu)^2/2\sigma^2 \right], \quad 0 < y < \infty,$$
$$-\infty > \mu < \infty, \sigma > 0,$$
(62)

where σ is the standard deviation, μ is the geometric mean, and x is $\ln y$.

The Weibull distribution was also considered, but later results showed that better fits were obtained by the normal and log normal distributions.

Table XII presents the mean, standard deviation, standard error of the mean, sample size (number of fragments), maximum, minimum and range (maximum value minus the minimum value) for R, W, A, A/W, $\text{Log}_{10} W$, and $\text{Log}_{10} A$.

3. Probability Density Functions - The data for each parameter of interest within an event was sorted in ascending order and the value for the parameter for the 10th to the 90th percentiles in 10% steps was identified. Table XIII is a listing of these values. The use of order statistics tends to equalize the effects of varying sample size from event to event.

A plot on normal and log normal probability paper was then made for each parameter for each event. Figure 43 is a plot of distance for event 3 on normal probability paper. Figure 44 is a plot of the same data on log normal probability paper. Since the points on the normal probability paper lie closer to a straight line than those on the log normal paper, the normal

TABLE XII - CALCULATED STATISTICS FOR PARAMETERS OF EIGHT EVENTS

Event	Var	Mean	S.D.	S.E. of Mean	Sample Size	Maximum	Minimum	Range
1	R	447.4282	193.9981	10.5056	341	1027.0000	105.0000	922.0000
	W	6.7962	5.8208	.3152	341	36.0000	1.0000	35.0000
	A	576.8806	754.2380	40.8443	341	8064.0000	12.0000	8052.0000
	A/W	86.9405	60.6467	3.2842	341	524.0000	3.7000	520.3000
	CD	1.7669	.3855	.0209	341	2.0000	.9000	1.1000
	Log ₁₀ W	.6976	.3484	.0189	341	1.5563	0.0000	1.5563
	Log ₁₀ A	2.5377	.4507	.0244	341	3.9066	1.0792	2.8274
2	R	337.1053	203.1829	32.9606	38	1100.0000	50.0000	1050.0000
	W	24.8421	28.4802	4.6201	38	110.0000	1.0000	109.0000
	A	1129.1711	1839.8043	298.4557	38	9360.0000	2.4000	9357.6000
	A/W	54.8526	46.1599	7.4881	38	184.0000	.3000	183.7000
	CD	1.5789	.4503	.0731	38	2.0000	1.0000	1.0000
	Log ₁₀ W	1.1423	.4970	.0806	38	2.0414	0.0000	2.0414
	Log ₁₀ A	2.4764	.8554	.1388	38	3.9713	.3802	3.5911
3	R	829.6571	556.7326	54.3315	105	2200.0000	50.0000	2150.0000
	W	72.8381	92.4500	9.0222	105	536.5000	2.2000	534.3000
	A	1034.2390	2089.7322	203.9370	105	13824.0000	7.1000	13816.9000
	A/W	22.7210	57.5698	5.6182	105	356.9000	.4000	356.5000
	CD	1.9448	.2085	.0203	105	2.0000	1.0000	1.0000
	Log ₁₀ W	1.5891	.5118	.0500	105	2.7294	.3424	2.3871
	Log ₁₀ A	2.5203	.6448	.0629	105	4.1406	.8513	3.2894
4	R	739.6395	341.6650	36.8427	86	1655.0000	64.0000	1591.0000
	W	102.1744	169.0271	18.2267	86	1224.0000	5.0000	1219.0000
	A	1973.3023	4756.2041	512.8747	86	34560.0000	72.0000	34488.0000
	A/W	16.2012	10.8261	1.1674	86	28.8000	2.6000	26.2000
	CD	1.9930	.0369	.0040	86	2.0000	1.8000	.2000
	Log ₁₀ W	1.7540	.4507	.0486	86	3.0878	.6990	2.3888
	Log ₁₀ A	2.8246	.6001	.0647	86	4.5386	1.8573	2.6812

<u>Event</u>	<u>Var</u>	<u>Mean</u>	<u>S. D.</u>	<u>S. E. of Mean</u>	<u>Sample Size</u>	<u>Maximum</u>	<u>Minimum</u>	<u>Range</u>
5	R	985.9677	574.3974	103.1648	31	2280.0000	115.0000	2165.0000
	W	70.5161	50.6852	9.1033	31	210.0000	10.0000	200.0000
	A	489.4839	599.3872	107.6531	31	2880.0000	54.0000	2826.0000
	A/W	8.8258	9.0274	1.6214	31	28.8000	1.0000	27.8000
	CD	1.8516	.1998	.0359	31	2.0000	1.2060	.8000
	Log 10 W	1.7089	.3847	.0691	31	2.3222	1.0000	1.3222
	Log 10 A	2.4676	.4379	.0787	31	3.4594	1.7324	1.7270
	R	157.7708	88.1819	2.7136	1056	485.0000	4.0000	481.0000
	W	.5717	2.7653	.0851	1056	48.0000	.0010	47.9990
	A	24.5509	141.1202	4.3427	1056	2862.8000	.1000	2862.7000
6	A/W	171.3169	1493.0327	45.9449	1056	41142.8570	.0830	41142.7740
	CD	1.3703	.3902	.0120	1056	2.2000	.5000	1.7000
	Log 10 W	-1.2874	.8424	.0259	1056	1.6812	-3.0000	4.6812
	Log 10 A	.5220	.7195	.0221	1056	3.4568	-1.0000	4.4568
	R	152.1062	85.8493	4.7621	325	435.0000	5.0000	430.0000
	W	1.1725	5.2164	.2894	325	57.6250	.0020	57.6230
	A	43.3142	212.4915	11.7869	325	2592.0000	.2000	2591.8000
	A/W	83.7016	233.3535	12.9441	325	4000.0000	.3080	3999.6920
	CD	1.6929	.3970	.0220	325	2.0000	1.0000	1.0000
	Log 10 W	-.8078	.7047	.0391	325	1.7606	-2.6990	4.4596
Log 10 A	.8361	.6999	.0388	325	3.4136	-.6990	4.1126	
8	R	152.1901	79.4361	5.0040	252	342.5000	4.5000	338.0000
	W	2.0779	9.8528	.6207	252	107.5000	.0030	107.4970
	A	47.0048	160.4646	10.1083	252	1824.0000	.1000	1823.9000
	A/W	99.4114	122.6657	7.7272	252	960.0000	.4690	959.5310
	CD	1.6540	.3479	.0219	252	2.0000	.9000	1.1000
	Log 10 W	-.7704	.8158	.0514	252	2.0314	-2.5229	4.5543
	Log 10 A	.9933	.7240	.0456	252	3.2610	-1.0000	4.2610

TABLE XIII - PERCENTILES FOR PLOTTING PARAMETERS
OF EVENTS 1 THROUGH 8

Event	Percent	Distance (R) (ft)	Weight (W) (lb)	Area (A) (in ²)	Area/Weight (A/W) (in ² /lb)
1	10	222	2.0	96.0	26.0
	20	287	2.0	145.0	44.0
	30	331	3.0	209.0	55.5
	40	372	4.0	280.0	67.2
	50	408	5.0	360.0	76.0
	60	449	7.0	440.0	88.0
	70	521	8.0	578.0	100.0
	80	608	9.0	768.0	120.0
	90	722	16.0	1296.0	144.0
2	10	60	2.5	8.0	1.2
	20	130	5.0	34.0	6.1
	30	225	8.0	140.0	19.3
	40	300	10.0	220.0	33.6
	50	325	14.0	330.0	43.2
	60	350	21.0	528.0	55.9
	70	375	26.0	1062.0	72.0
	80	450	40.0	1566.0	90.0
	90	550	90.0	3600.0	113.1
3	10	138	8.0	44.0	2.2
	20	198	11.0	144.0	3.8
	30	375	20.0	192.0	3.9
	40	695	26.0	216.0	4.4
	50	825	42.0	288.0	5.6
	60	990	61.0	360.0	14.1
	70	1050	90.0	480.0	24.0
	80	1523	108.0	864.0	28.1
	90	1650	141.0	3456.0	28.8
4	10	242	13.0	120.0	3.3
	20	466	26.0	180.0	3.8
	30	510	35.0	216.0	4.4
	40	608	41.0	360.0	7.5
	50	708	52.0	576.0	14.0
	60	823	76.0	864.0	26.2
	70	912	95.0	1152.0	27.9
	80	1003	125.0	2304.0	28.1
	90	1110	185.0	4320.0	28.3

Event	Percent	Distance (R) (ft)	Weight (W) (lb)	Area (A) (in ²)	Area/Weight (A/W) (in ² /lb)
5	10	210	15.0	72.0	2.1
	20	300	18.0	144.0	3.5
	30	680	20.0	192.0	3.6
	40	825	48.0	240.0	3.7
	50	925	55.0	288.0	3.8
	60	1035	65.0	360.0	4.0
	70	1120	97.0	432.0	7.2
	80	1220	110.0	576.0	13.4
	90	1730	125.0	1296.0	27.0
6	10	45.0	.005	0.4	14.286
	20	82.0	.010	0.5	27.996
	30	106.0	.018	1.3	54.762
	40	127.0	.028	2.0	70.000
	50	148.0	.044	2.7	80.176
	60	169.0	.069	4.1	88.888
	70	192.0	.108	6.3	100.000
	80	233.0	.210	12.0	119.469
	90	281.0	.627	24.0	160.894
7	10	50	.025	1.0	10.000
	20	80	.051	2.0	20.000
	30	103	.090	3.0	30.000
	40	125	.100	4.0	45.557
	50	141	.100	6.0	57.600
	60	162	.135	8.0	69.767
	70	185	.209	14.0	80.000
	80	238	.400	24.0	93.023
	90	293	1.833	60.0	127.660
8	10	35	.022	1.5	10.000
	20	67	.039	2.5	28.000
	30	108	.064	3.8	44.280
	40	142	.100	5.5	61.303
	50	162	.113	8.0	78.571
	60	180	.193	14.0	96.154
	70	196	.380	22.8	103.131
	80	213	.721	40.0	125.000
	90	248	2.009	90.0	166.667

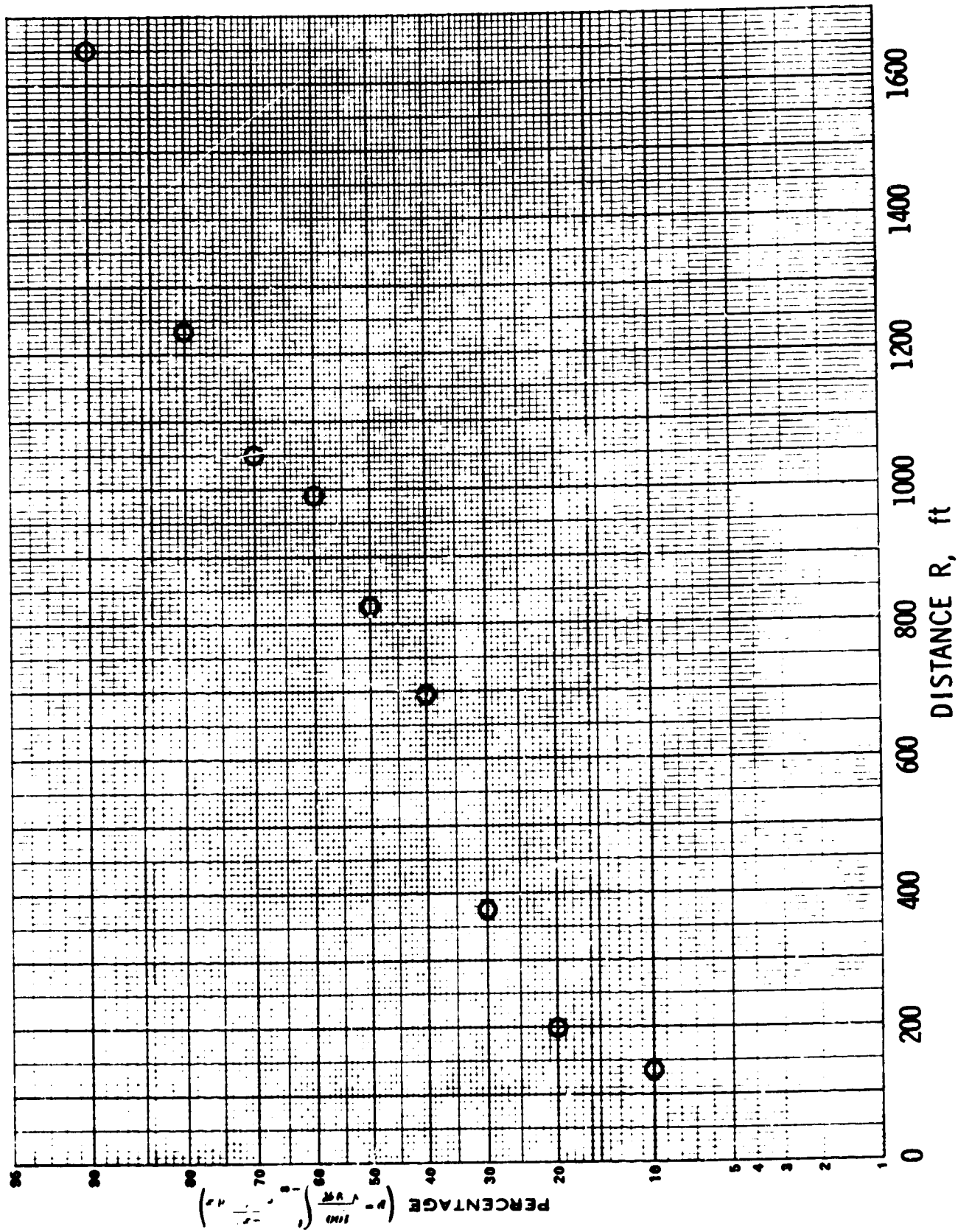


FIGURE 43 . EVENT 3 PROBABILITY DISTRIBUTION (NORMAL). DISTANCE R

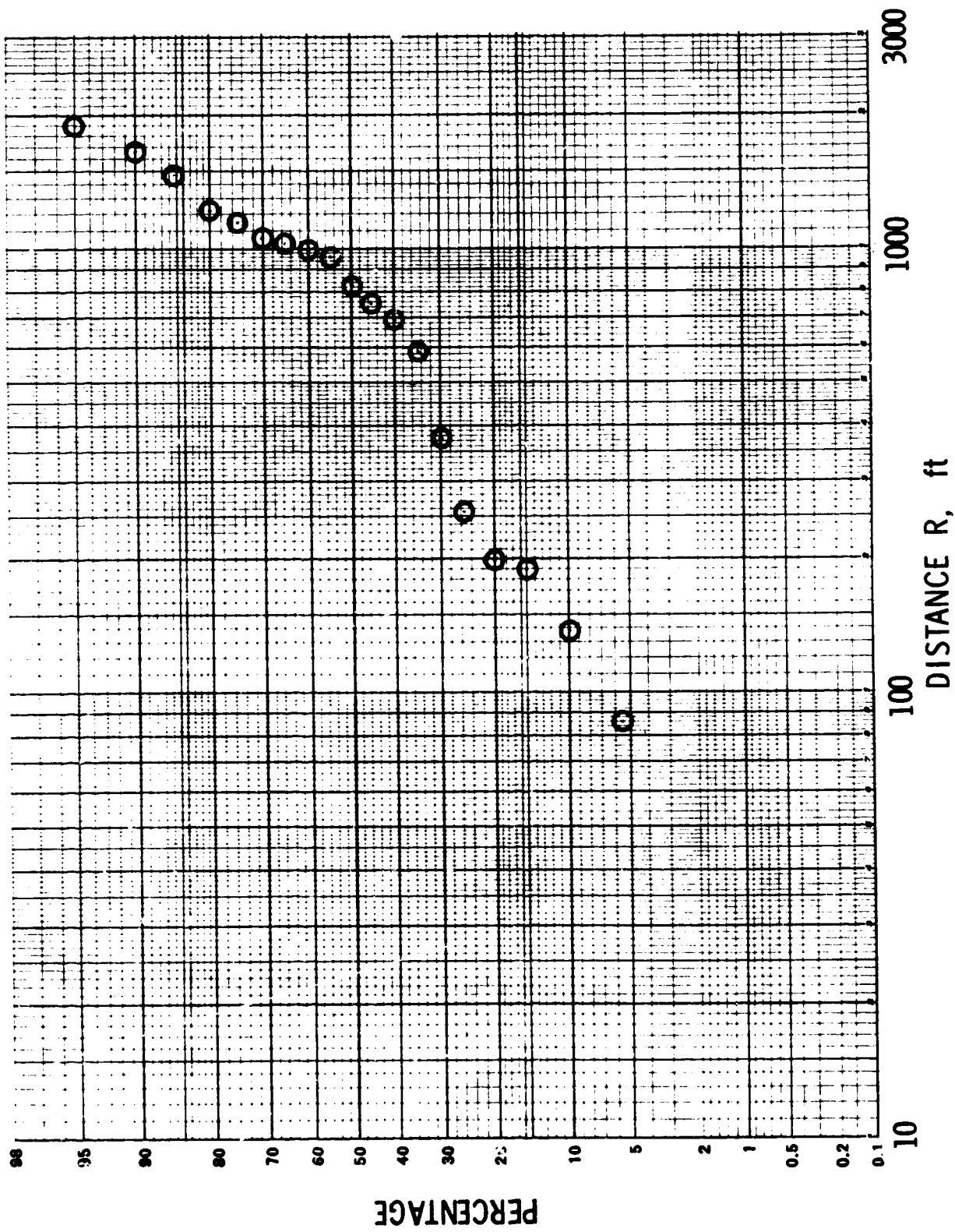


FIGURE 44. EVENT 3 PROBABILITY DISTRIBUTION (LOG NORMAL), DISTANCE R

distribution appears to be a better fit. Figures 45, 46 and 47 are examples of the other plots. From the plots over all 8 events, it appeared that the normal distributions adequately fitted the distance (R), and A/W and that log normal distributions best fitted the weight (W) and area (A). A complete summary of the fragment data is given in Table XIV, giving the estimated standard deviation (S), and mean (M) for the respective distributions for each parameter in each event.

A "W" statistic for goodness of fit for each parameter was calculated using the methods outlined by Hahn and Shapiro (Ref. 36).

The approximate probability of obtaining the calculated test statistic, given that the chosen distribution is correct, was then determined, and is shown in Table XV. Figure 48 is a plot of Table XV, and can be used to determine the approximate probability of obtaining a value as low as the calculated value of "W", given that the selected distribution is the correct one. The values in Table XVI were calculated using the method and formula outlined by Hahn and Shapiro (Ref. 36).

Table XVI is a summary of the "W" test on normality for R, W, A, and A/W for the eight events. The method, and sample calculations for the W statistic and the probability of obtaining the calculated value of W are given in Appendices E and F.

Referring to Table XVI, we see that there are 32 distributions, one each for R, W, A, and A/W for each of the eight events. The probability of obtaining the calculated value of "W" is greater than 50 percent for all except the A/W distributions for events 3, 4, and 5, indicating adequate fits for all except these three distributions, as it is customary to consider values exceeding 2 to 10% as adequate grounds for not rejecting the hypothesis that the data belong to the chosen distribution. It is interesting to note that each of the parameters is distributed in the same family (i. e., normal or log normal) across all eight events. That is, distance (R) has a normal distribution function in each of the eight events, indicating a repeatable pattern.

The estimate for the means and standard deviations for each of the distributions is given in Table XIV.

D. Methods of Prediction of Range Versus Fragment and Blast Yield Parameters

1. Determination of Mean Range of Fragments Versus Blast Yield by Regression Analysis - The mean distance R versus the yield Y in percent and equivalent pounds of TNT, W_{TNT} for the 8 events was plotted on log-1 σ paper and is shown in Figures 49 and 50, respectively. As can be seen, when events 6, 7 and 8 which are the mixing tests are excluded, there is more

TABLE XIV - SUMMARY OF FRAGMENT DATA

Event No.	No. of Fragment	Yield, Y		Range, R (1) in Feet		Weight, W, lbs			Area, A, IN ²			Area/Weight			
		%	lbs TNT	Dist	M	S	Dist	M	S	Dist	M	S	Dist	M	S
1	341	5.0	4.55x10 ²	N	447	194	L	4.98	2.23	L	344.9	2.8	N	86.9	60.6
2	38	1.1	1.08x10 ³	N	377	203	L	26.49	3.14	L	299.5	7.16	N	54.9	46.2
3	105	23.0	4.03x10 ²	N	630	557	L	38.82	3.25	L	331.5	4.4	N	22.7	57.6
4	86	24.4	4.28x10 ²	N	740	342	L	56.35	2.82	L	667.7	3.98	N	16.2	10.8
5	31	62.6	1.097x10 ³	N	986	574	L	51.16	2.42	L	293.5	2.75	N	8.8	9.0
6	1056	86.0	2.06x10 ²	N	158	88	L	0.05	6.95	L	3.3	5.2	N	171.3	149.3
7	325	70.0	1.67x10 ²	N	152	86	L	0.16	5.04	L	6.9	5.0	N	83.7	233.4
8	252	73.0	1.75x10 ²	N	152	79	L	0.17	6.54	L	9.8	5.3	N	99.4	122.7

(1) Dist. is the type of frequency distribution,
 N is normal, and
 L is log normal

TABLE XV - APPROXIMATE PERCENTAGE POINTS OF
"W" TEST FOR NORMALITY (n = 9)

<u>"W"</u>	<u>Percentage</u>
.764	1.0
.791	2.0
.829	5.0
.859	10.0
.921	38.2
.935	50.0
.945	64.3
.969	87.1
.978	94.8
.988	99.0

TABLE XVI - SUMMARY OF "W" TEST ON NORMALITY FOR R, W, A, (A/W)

Event No.	Distance (R)		Weight (W)		Area (A)		Area/Weight (A/W)	
	Dist	"W" ^{**} P ^{**}	Dist	"W"	Dist	"W"	Dist	"W"
1	N*	.969 .871	LN**	.954	LN	.994	N	.987
2	N	.982 .968	LN	.998	LN	.966	N	.959
3	N	.942 .574	LN	.949	LN	.966	N	.799
4	N	.981 .966	LN	.989	LN	.967	N	.791
5	N	.967 .850	LN	.921	LN	.994	N	.672
6	N	.988 .990	LN	.992	LN	.945	N	.983
7	N	.969 .871	LN	.936	LN	.989	N	.972
8	N	.989 .995	LN	.975	LN	.978	N	.983

* N is normal distribution

** LN is Log Normal distribution

* "W" is calculated statistic

* P is approximate probability of obtaining a value as low as the calculated value of W, given that the chosen distribution is the correct one.

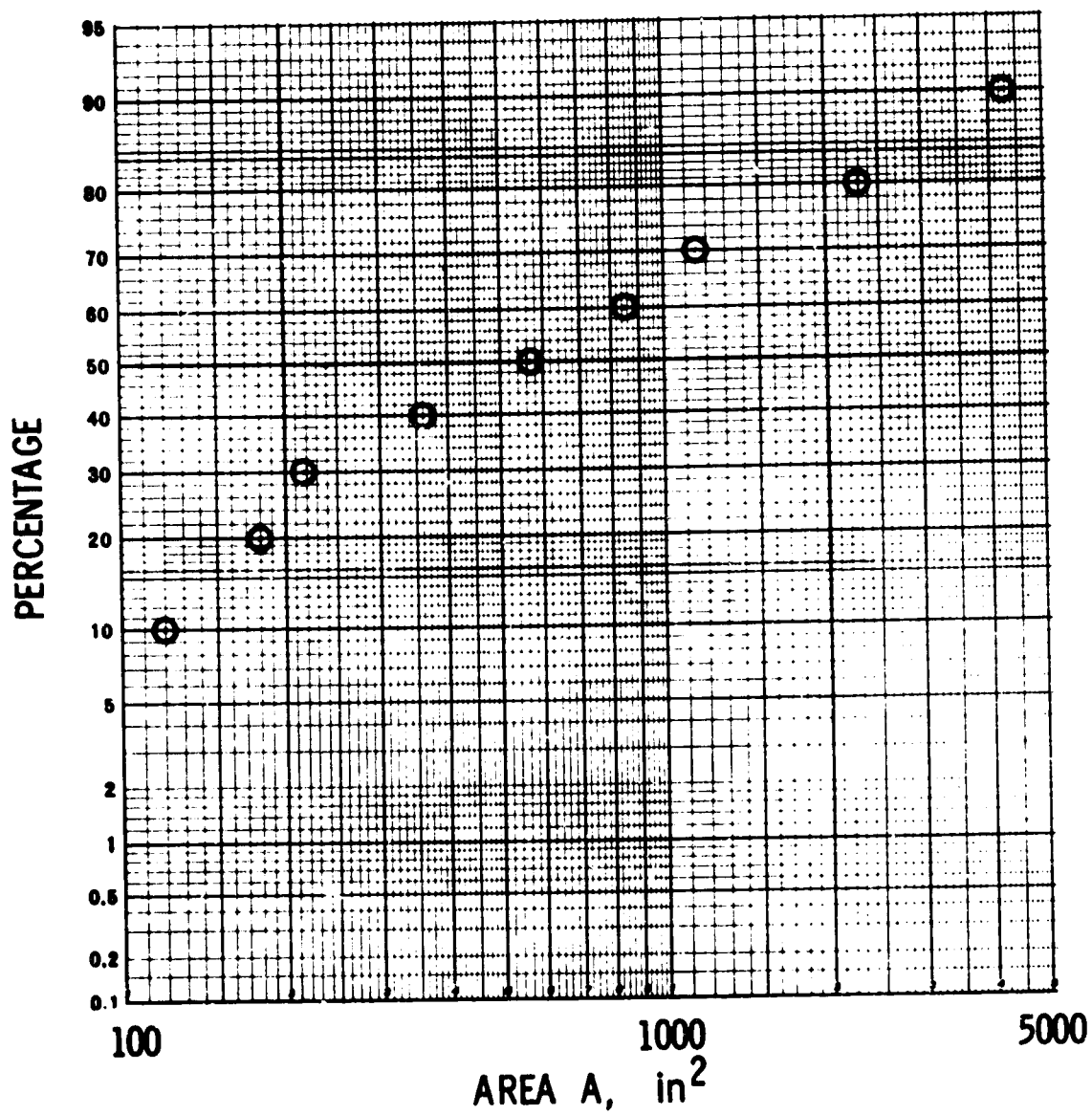


FIGURE 45. EVENT 4 PROBABILITY DISTRIBUTION (LOG NORMAL), PROJECTED AREA A

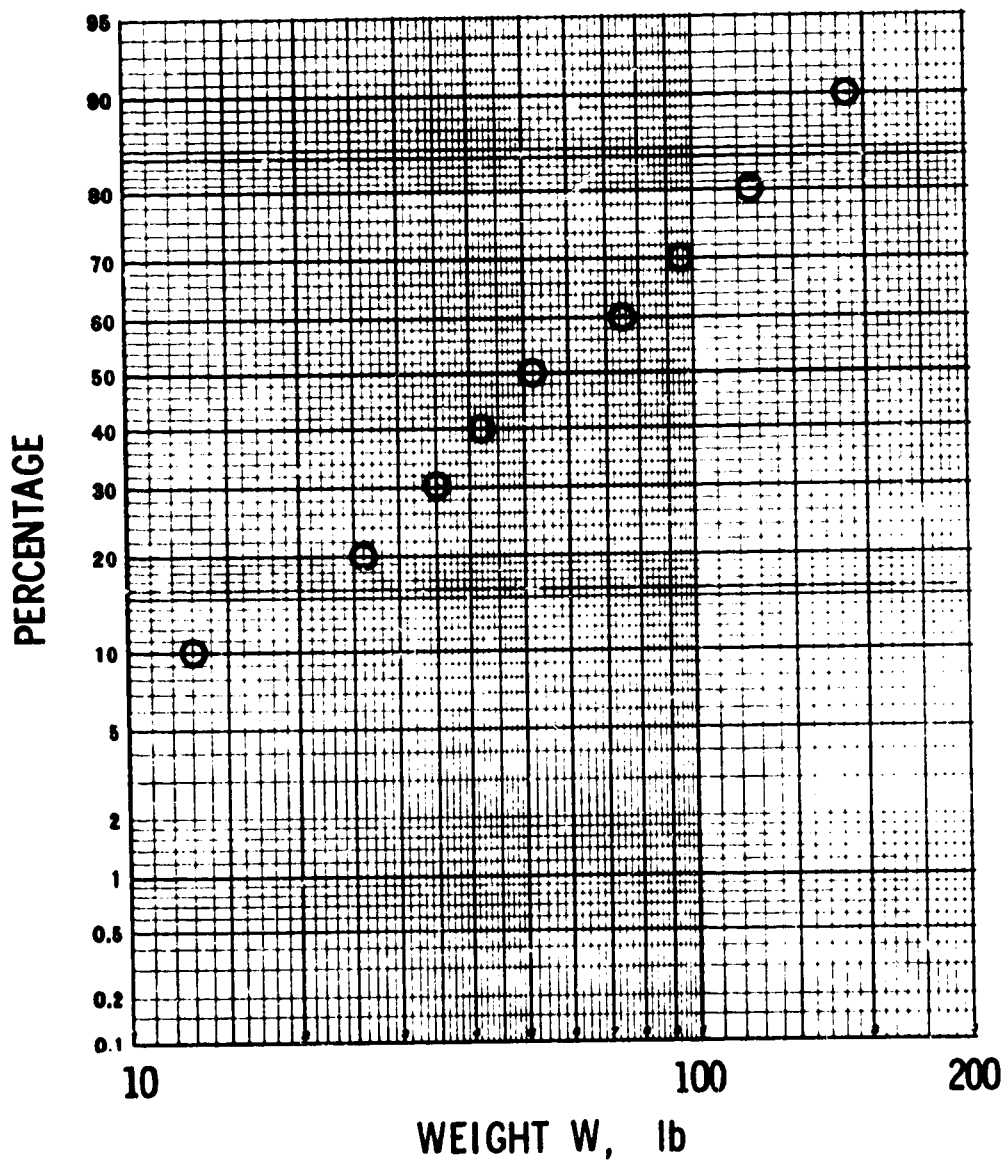


FIGURE 46. EVENT 4 PROBABILITY DISTRIBUTION
(LOG NORMAL), WEIGHT W

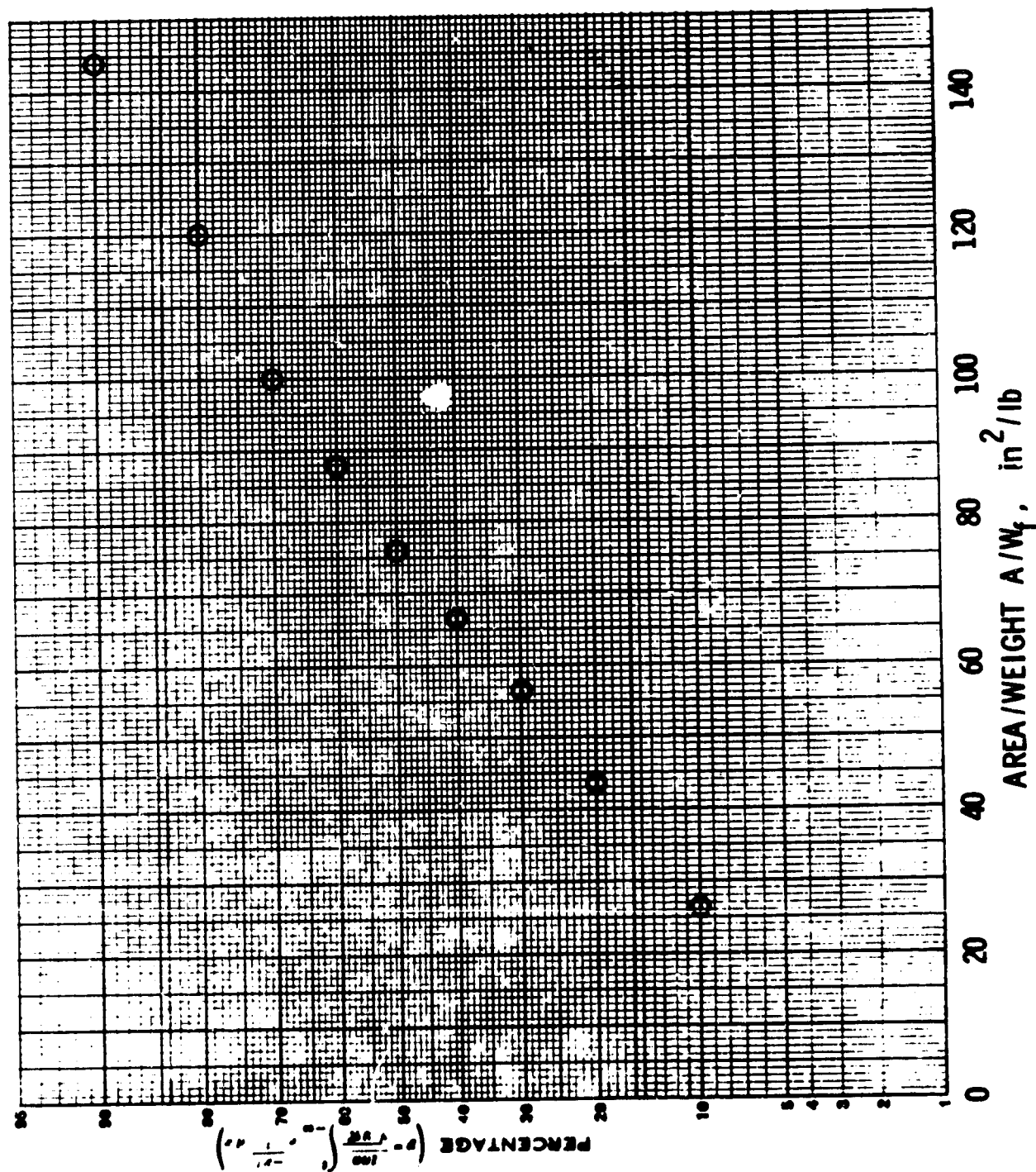


FIGURE 47 . EVENT 1 PROBABILITY DISTRIBUTION (NORMAL);
AREA/WEIGHT A/W

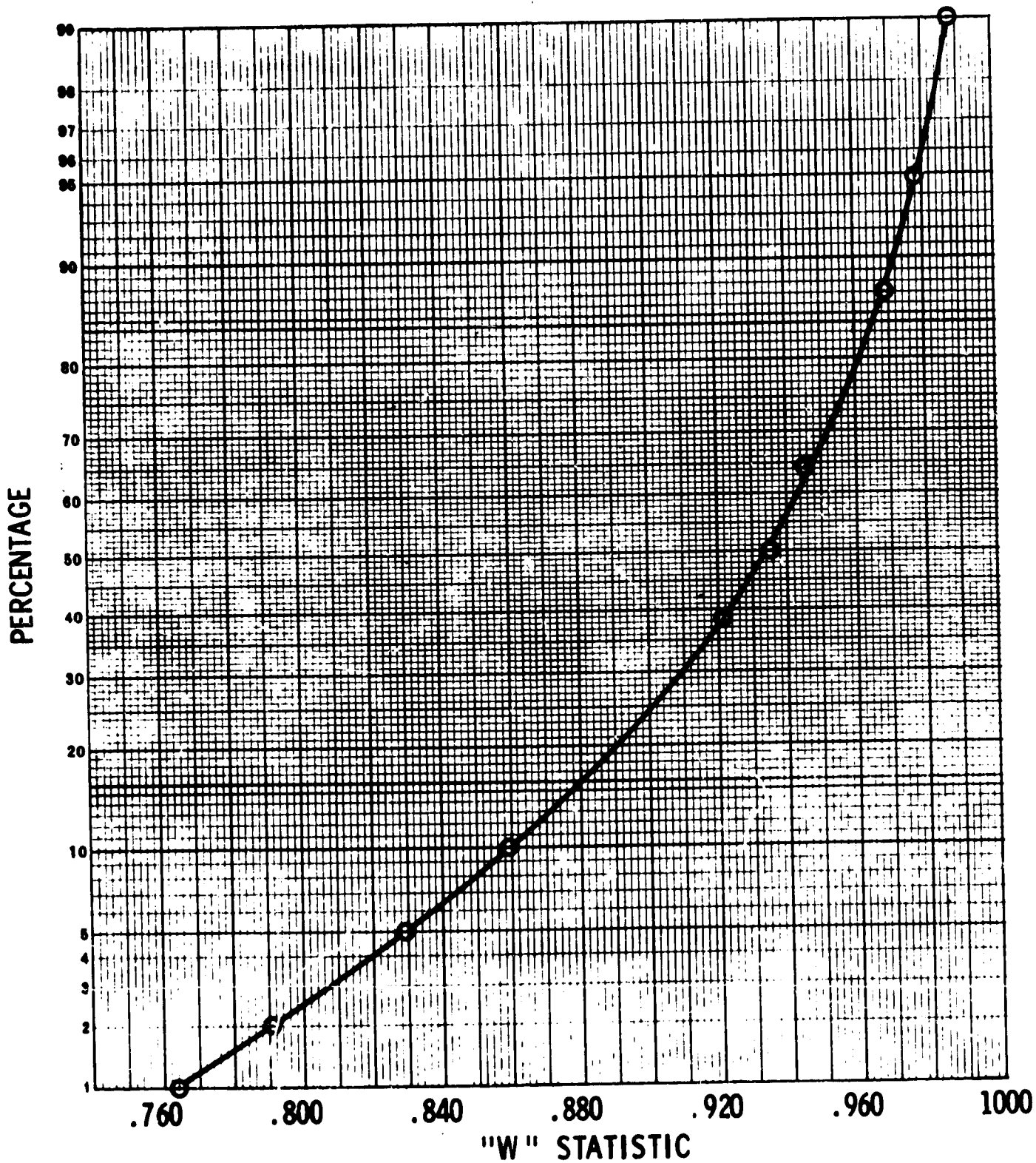


FIGURE 48 . APPROXIMATE PROBABILITY PERCENTAGE POINTS OF 'W' TEST FOR NORMALITY (n = 9)

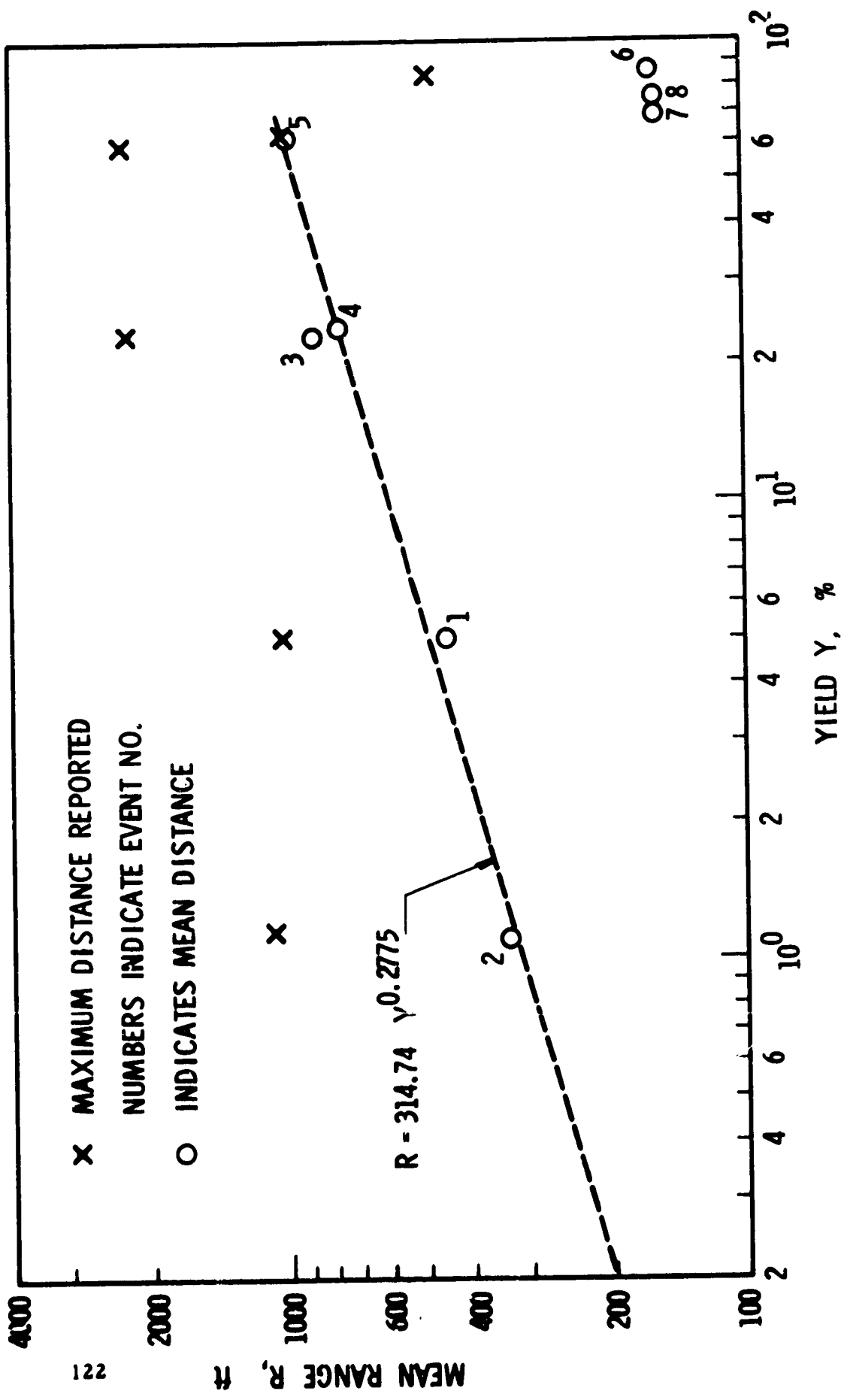


FIGURE 49 . MEAN DISTANCE VS. YIELD

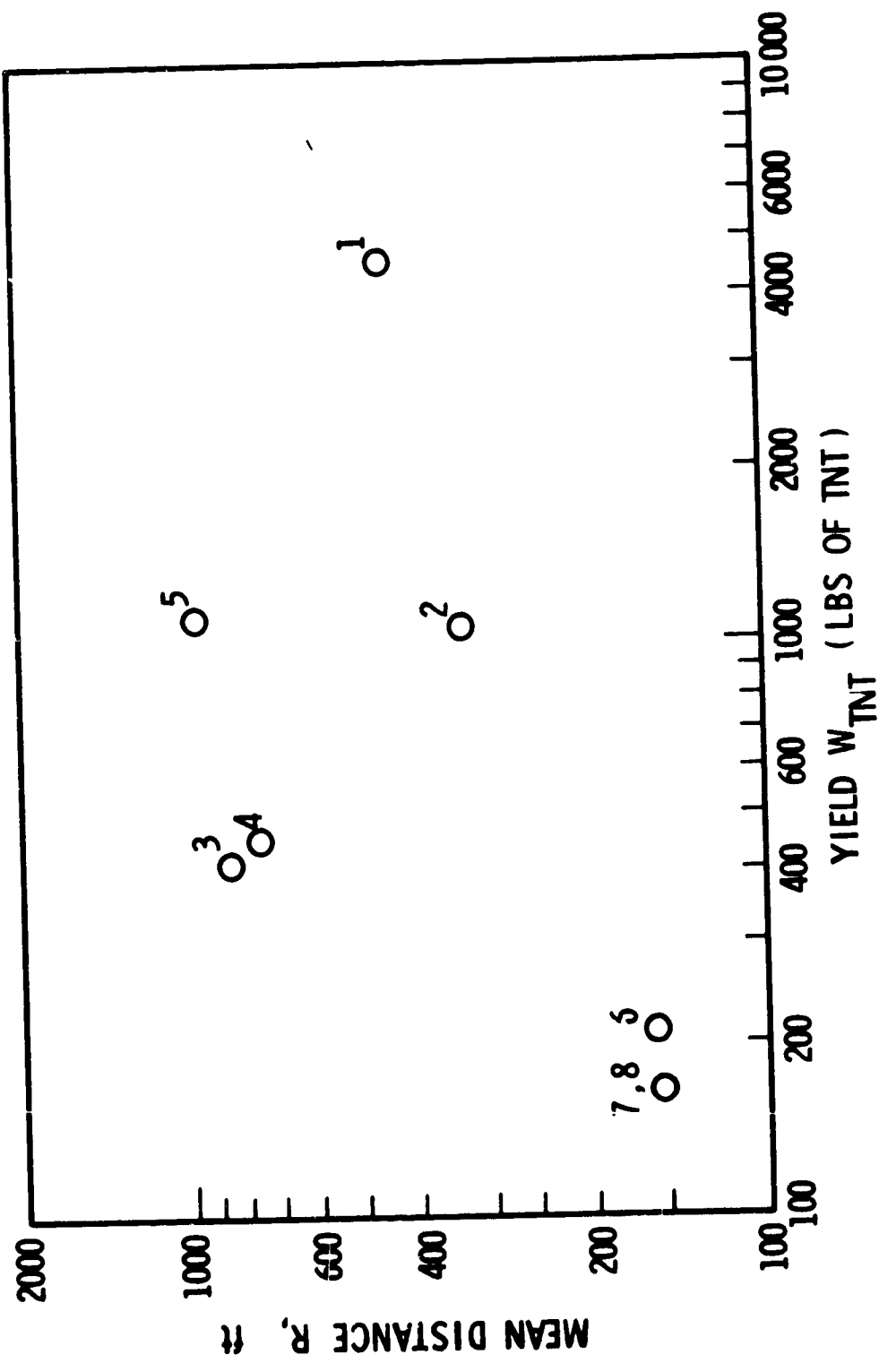


FIGURE 50. MEAN DISTANCE VS. YIELD IN LBS OF TNT

scatter on the TNT chart than on the percent yield chart. A regression equation was derived to describe a linear fit to the points. Events 6, 7 and 8 were excluded on the basis that the propellants were mixed differently than in events 1 through 5. The equation is:

$$\hat{R} = 314.74 Y^{0.2775} \quad (63)$$

This equation should be limited to the range of weights and configurations of events 1 through 5.

The line is drawn on Figure 49, and the predicted versus observed values of the mean distance for the 5 events can be read from the chart. On Figure 49, the maximum observed distance is also shown for each event.

In Figure 51, the upper dashed line shows the estimated distance which should contain at least 95% of the fragments. Table XVII shows the upper 95% confidence limit (CL) on the estimate of the mean (M), the upper 90% confidence limit on the estimate of the standard deviation, and the various quantities necessary to calculate these confidence limits.

The confidence limit on the mean was calculated using the following formula:

$$CL = M + \frac{S}{\sqrt{n}} t_{n; 95},$$

n is the number of fragments and $t_{n; 95}$ is the value of the t distribution with n degrees of freedom at the 95th percentile.

The confidence interval for the standard deviation was calculated using the following formula:

$$CL = \left[\frac{\sum X_i^2 - (\sum X_i)^2 / n}{\chi^2_{(n-1); 90}} \right]^{1/2} \quad (64)$$

Where X_i is the distance of the ith fragment, n is the number of fragments, and $\chi^2_{(n-1); 90}$ is the value of a chi square distribution with n-1 degrees of freedom at the 90th percentile.

Then, using the new upper confidence level values of M and S, the range \hat{R}_{95} in which 95% of the fragments should fall was calculated as follows:

$$\hat{R}_{95} = M + S t_{n; 95}$$

The interval from the mean (M) to \hat{R}_{95} is indicated for each event on Figure 51

TABLE XVII - CONFIDENCE LIMITS ON MEAN, STANDARD DEVIATION,
AND DISTANCE CONTAINING 95% OF FRAGMENTS

Event No.	Sample Size	Yield		Normal Distribution						Distance (R)			Max Dist
		%	TNT	M	S	S. E.	95% CL		90% CL S	95% CL Dist			
							M	M					
1	341	5	4.55×10^2	447	194	10.5	464	204.5	784.4	1027			
2	38	1.1	1.08×10^3	377	203	32.96	433	240	838.6	1100			
3	105	23	4.03×10^2	830	557	54.33	647	611	1662	2200			
4	86	24.4	4.28×10^2	740	342	36.84	801	380	1433	1655			
5	31	62.6	1.097×10^2	986	574	103.16	1161	693	2162	2280			
6	1056	86	2.06×10^2	158	88	2.714	162	90.56	311	485			
7	325	70	1.673×10^2	152	86	4.762	160	90.7	310	435			
8	252	73	1.753×10^2	152	79	5.004	158	84.1	308	342			

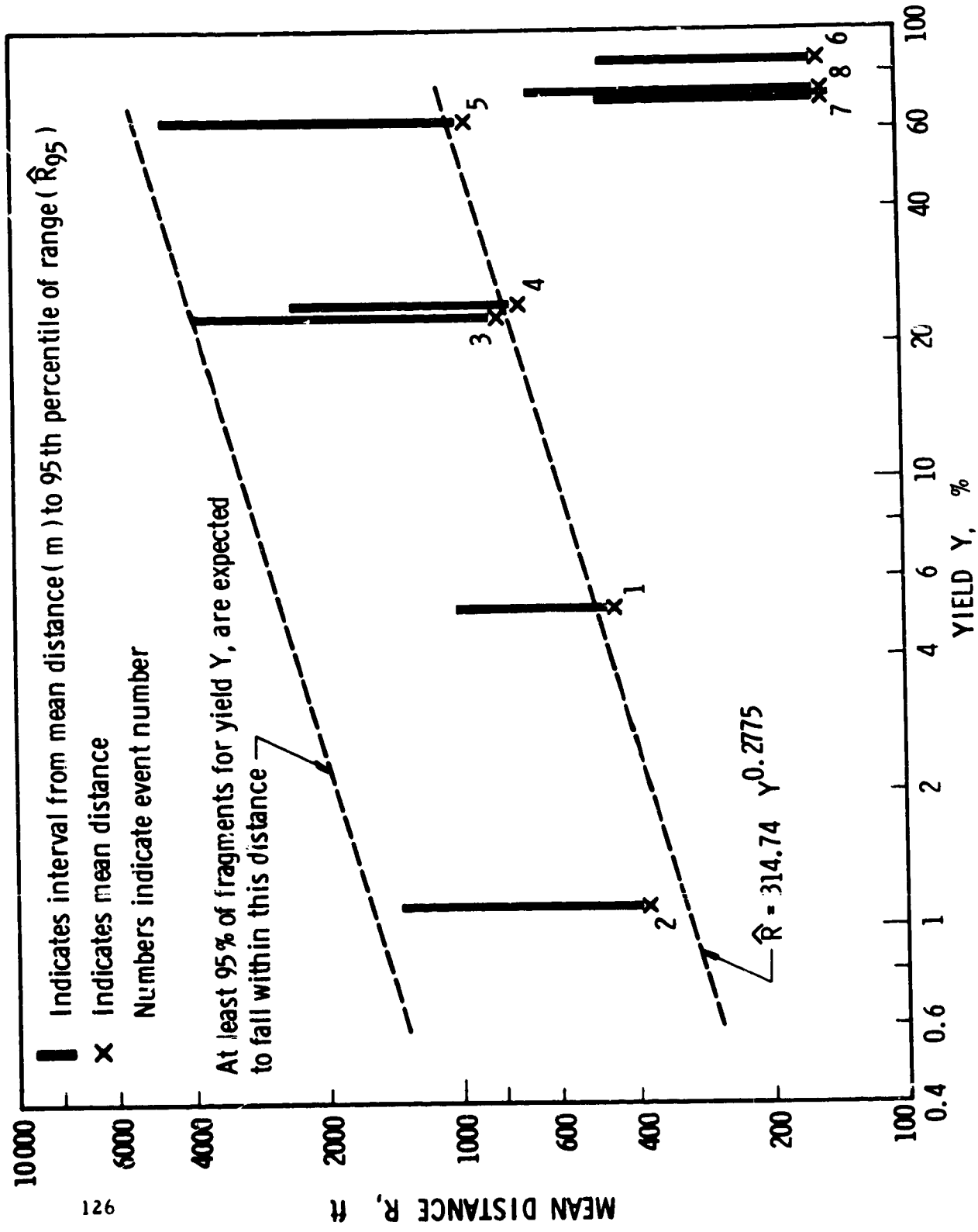


FIGURE 51. MEAN DISTANCE VS. YIELD WITH ESTIMATED RANGE CONTAINING 95% OF THE FRAGMENTS (R_{95})

by a bar.

A line was then drawn parallel to the regression line, and just touching the longest bar. Thus, the distances read from this line could be expected to encompass at least 95% of the fragments resulting from a given yield.

2. Determination of Mean Range of Fragments by Use of Ballistic Equations - The range of a fragment produced by a missile explosion may be determined from ballistics equations if sufficient information is available about the initial fragment velocity and fragment characteristics. Specifically, it is necessary to know the following parameters:

- (1) The fragment mass, M
- (2) The initial fragment velocity, U_f
- (3) The initial elevation of fragment trajectory, θ
- (4) The fragment cross-sectional area, A
- (5) The drag coefficient for the fragment, C_D
- (6) The density of air, ρ_{air}

Having given these parameters, the range of the fragment may be obtained from the equations of motion solved for the total time of flight of the fragment. This method is described and the following equations completely derived by J. J. Oslake, et al, (Ref. 41) for the case of a missile exploding on the launch pad with the assumption that air density remains constant along the trajectory of the fragments produced. Only drag and gravitational forces are assumed to act on the fragments where

$$F_d = - (1/2) \rho U_z^2 A C_D, \quad F_g = - M g \quad (65)$$

are the vertical component of the drag force and the gravitational forces, respectively. ($\rho = \rho_{\text{air}}$ and U_z = vertical velocity of the fragment.) The equation of motion for vertical acceleration may be integrated to obtain t as a function of U_z , which gives

$$t_r = \frac{1}{\sqrt{cg}} \tan^{-1} (U_{z0} \sqrt{c/g}) \quad (66)$$

for the case in which $U_z = 0$ (i. e., t_r is the time of rise for the fragment). In Eq. (66) U_{z0} is the initial vertical fragment velocity and

$$c = \left(\frac{1}{2}\right) \frac{\rho_{\text{air}} A C_D}{M} \quad (67)$$

The equation of motion for the fall of the fragment may be similarly integrated to obtain

$$t_f = \frac{1}{2\sqrt{cg}} \ln \left[(2 e^{2CZ_M} - 1) + \left[(2 e^{2CZ_M} - 1)^2 - 1 \right]^{1/2} \right] \quad (68)$$

where

$$Z_M = \frac{1}{c} \ln \left[\frac{1}{\cos(\sqrt{cg} t_r)} \right] \quad (69)$$

The total time of flight of the fragment is

$$\tau = t_r + t_f \quad (70)$$

where t_r and t_f are functions of initial conditions only. Finally, the equations of motion for radial acceleration of the fragment may be integrated to obtain the range R in terms of τ :

$$R = \frac{1}{c} \ln(1 + c U_{Ro} \tau) \quad (71)$$

The range may be determined from our initial parameters, since c is a function of M , A , C , ρ_{air} (Eq. (67)); U_{Ro} is the radial component of the given initial velocity, U_f :

$$\left. \begin{aligned} V_{Ro} &= U_f \cos \theta \\ V_{Zo} &= U_f \sin \theta \end{aligned} \right\} \quad (72)$$

and thus is a function of U_f and θ ; and τ is a function of initial conditions U_f , θ , c and g .

A computer program in FORTRAN IV which computes fragment range as a function of the independent parameters mentioned above is given in Appendix H. This program was checked against the results of J. J. Oslake, et al (Ref. 41); the check appears in Appendix H. The symbols used in the program as well as the input and output parameters are also discussed there.

This method of range prediction requires considerable information about the fragments emanating from the missile explosion. In general, the

initial fragment velocity, U_f , may be determined by one of the methods described in Section III. B. Fragment mass, cross-sectional area, and drag coefficients must be determined empirically. Drag coefficients for fragments at various velocities are described by L. D. Heppner and J. E. Steedman (ref. 42). Coefficients for regular shaped projectiles (spheres and cylinders) are described by E. Richards (ref. 43). A correlation between range predicted by this method and that determined statistically for a "mean" (or average) fragment from the PYRO test data, event 062, is given in Section IV. E.

E. Correlation

1. Standard Statistical Tests

a. Standard Deviation Versus Mean Distance - Figure 52 is a plot of the standard deviation of the distance versus the mean distance R for each of the eight events. As one might expect, the standard deviation increases as mean distance increases.

b. Results of Scaling A/W Parameter - From Appendix B, formula B 13 is:

$$G_7' = A_f / W_f^{2/3} \quad (73)$$

where A_f is the fragment cross-sectional area (in^2), and W_f (lb) is the fragment weight.

Figure 53 is a plot of the geometric means of A/W versus geometric mean distance R (ft) for the eight events. Figure 54 is a plot of the geometric means of $A/W^{2/3}$ versus geometric mean distance.

The points, excluding events 3, 4 and 5 have been fitted to a line with a regression analysis which resulted in the prediction equation:

$$\hat{R} = 9.864 (A/W^{2/3})^{0.78} \quad (74)$$

where \hat{R} is the mean range (ft), A is the area of the fragment (in^2), and W is the weight of the fragment (lb).

The exclusion of events 3, 4 and 5 can be justified on the basis that A/W for these three events were noticeably low in probability of belonging to the log normal family of distributions, while A/W for the other events showed a high probability of belonging to the log normal family.

Comparing the points in Figure 52 with those in Figure 54, it is obvious that, in this case, scaling of the A/W parameter improved the correlation

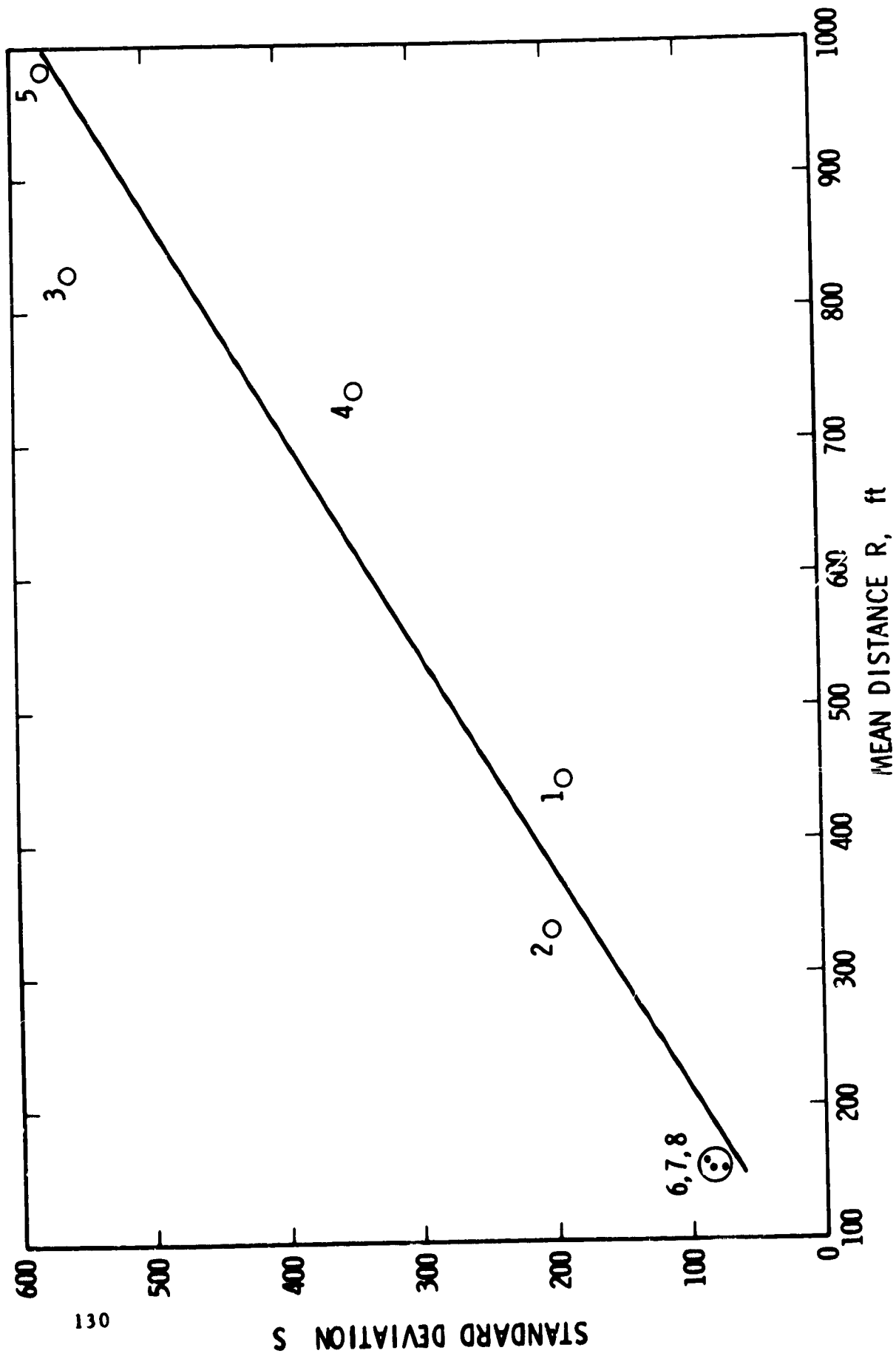


FIGURE 52 . STANDARD DEVIATION S VS. MEAN DISTANCE R

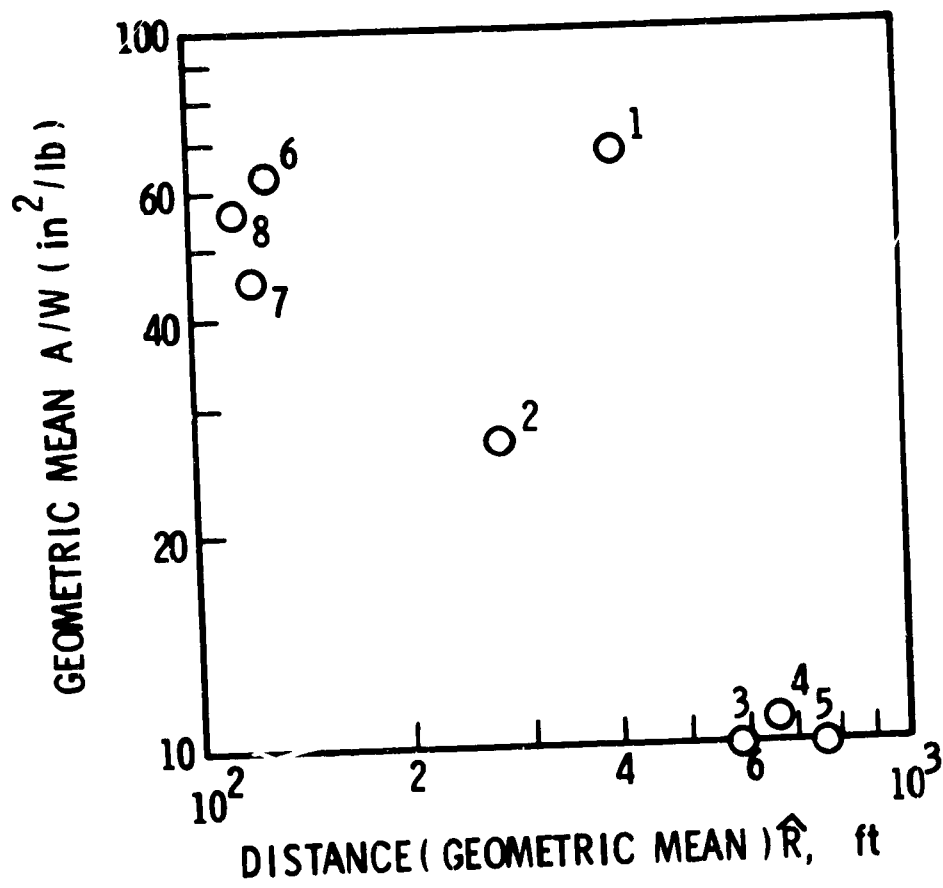


FIGURE 53. GEOMETRIC MEAN $\frac{A}{W}$ VS. GEOMETRIC MEAN DISTANCE

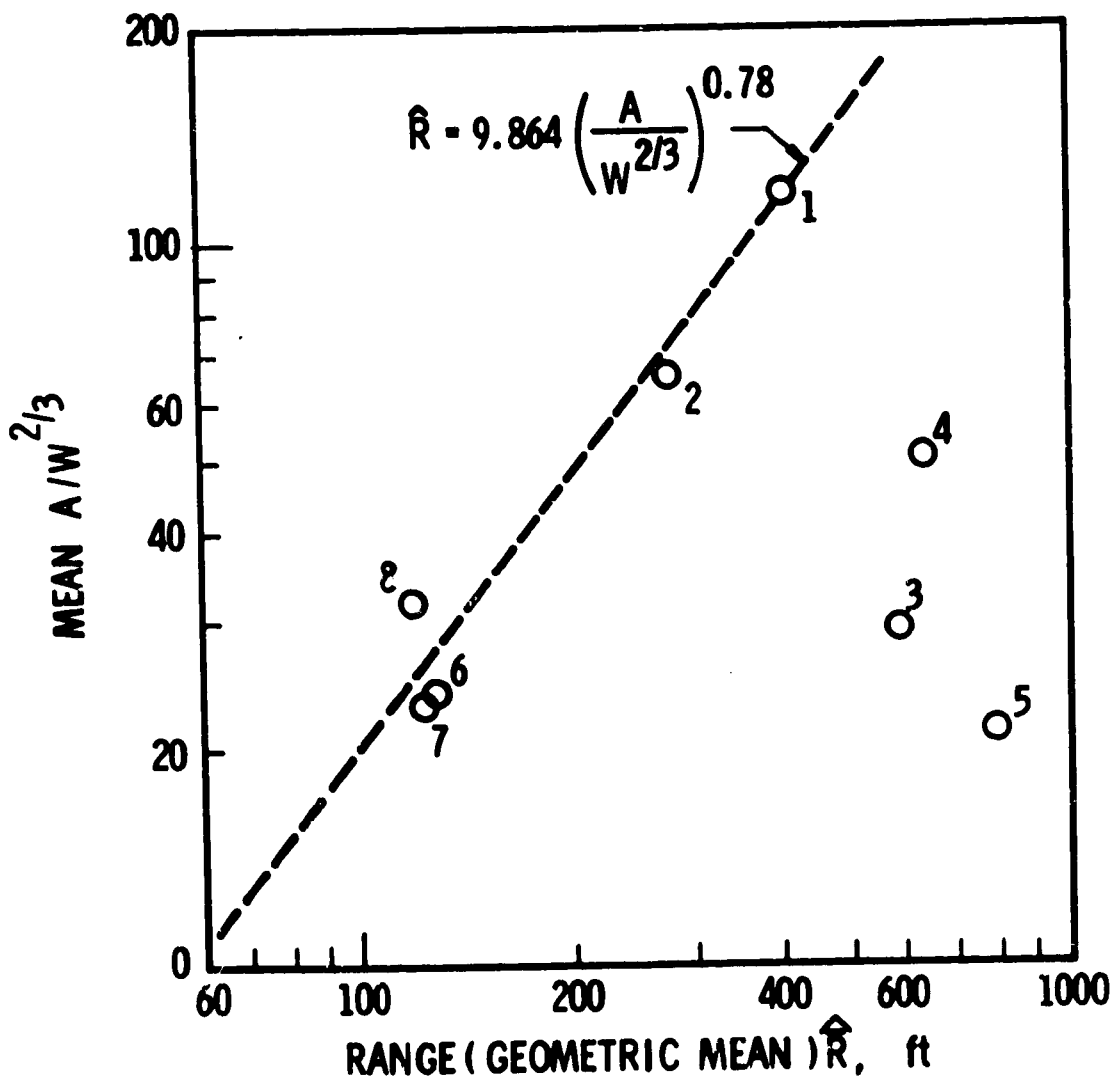


FIGURE 54 . REGRESSION OF GEOMETRIC MEAN $\frac{A}{W^{2/3}}$ VS. GEOMETRIC MEAN RANGE, \hat{R}

of the scaled parameter with distance. In fact, the correlation coefficient, τ , is .97, showing a high degree of correlation between R and $A/W^{2/3}$.

2. Correlation of Statistically Determined Mean Range of Fragment to the Range Determined by Ballistic Equations for a "Mean" Fragment - The approach to the fragment range prediction problem which we originally anticipated was to substitute data obtained from statistical analysis of test events into the ballistic equations described in Section IV.C.2. This would have permitted range predictions on the basis of observations of the initial fragment velocities and fragment physical characteristics alone.

Unfortunately, we were only able to find one test which had sufficient data to check this method. This was the full-scale test of a Saturn IV fuel tank described in the Project PYRO Report, (ref. 16). For this test, both films of the explosions and a post-explosion fragment survey were available. It is identified as Event 1 in Table XII. The data provided were sufficient to calculate the characteristics of a "mean" fragment or a fragment whose properties were considered to be those described by the arithmetic mean of all the fragments observed. From our statistical analysis, the properties of this fragment were:

- (1) The mean weight, $\bar{W} = 6.797$ lb
- (2) The initial mean velocity, $\bar{U}_f = 741$ ft/sec
- (3) The mean elevation angle, $\bar{\theta} = 12.77^\circ$
- (4) The mean cross-sectional area, $\bar{A} = 4.0$ ft²
- (5) The mean range, $\bar{R} = 447.4$ ft

Values for C_D (the fragment drag coefficient) were obtained from references 42 and 43. $C_D = 0.404$ if the fragment is modeled as a sphere while $C_D = 0.75$ if the fragment is modeled as irregular in the sense described by Heppner and Steedman in their study of fragment simulating projectiles, (ref. 42).

Table XVIII shows the results of range predictions using the various C_D and the data from the Saturn IV test in program (TEMP) (see Appendix H).

TABLE XVIII - PREDICTED VS. MEASURED FRAGMENT RANGES

C_D	Predicted \hat{R} for Mean Fragment, ft	Measured \hat{R} , ft
.404	579	447.4
.750	353	447.4

It can be seen from these results that reasonably accurate range values may be obtained if an appropriate C_D is chosen.

This range prediction method could be more useful if the fragments were broken down into classes of narrow mass ranges whose mean velocity, elevation angle, etc., were obtained from empirical considerations. Then a predicted range mapping could be made, as a function of yield, with the use of these ballistic equations. To do a complete empirical study, however, would probably require arena tests using models of the actual missile tanks.

V. EFFECTS OF FRAGMENTS

A. Introduction

It is desirable to have the capability to predict the probable damage levels to humans, structures, vehicles, etc. at various ranges from an exploding missile. Damage can be produced due to the blast wave emanating from the rupture of the missile or the interaction of the blast wave with objects surrounding the missile.

Damage caused by blast waves has been extensively studied and is a result of the peak overpressure or impulse of the blast wave depending on the nature of the "target". Ref. 34 gives examples of this kind of data for damage to humans as a function of peak overpressure. Since peak overpressure is a function of range and yield, damage levels can be associated with these parameters.

In order to predict damage as a result of fragmentation, it is necessary to know the value of the terminal ballistic parameters of the fragments (i. e., velocity, range, mass, cross-sectional area, etc.). Insofar as the value of these parameters can be determined from the characteristics of the missile explosion, damage levels can be predicted as a function of yield.

In Sections II and IV of this report, we have tried to investigate methods of determining fragment initial velocity and range by statistical and deterministic methods. By and large, however, the empirical data are not sufficient to cover the fragment damage problem on the basis of existing missile explosion data. A great deal of work has been done, however, on the problem of fragment damage from bomb explosions. We feel that much of this work is applicable to the exploding missile problem, even though the initial fragment velocities for the exploding missile would be primarily subsonic, whereas those for exploding bombs are usually supersonic.

A considerable amount of investigation has been made of what the terminal ballistics characteristics of a fragment must be in order to cause damage to various "targets". Equations for penetration of wood, steel, etc., of various thicknesses (as well as human simulators) have been developed from empirical data which may be used to predict damage levels as a function of fragment mass, velocity, and area. The probability of damage to these targets at any range would be a function of the probability of arrival of a fragment meeting the minimum specifications for the damage equations. The probable fragment damage for a given range as a result of a missile explosion is thus predictable when these two parts of the problem are solved:

- (1) The probability of arrival at any given range of a fragment of specified mass and cross-sectional area, velocity, etc.

- (2) The probability of penetration or damage to a specific "target" struck by a fragment of the specified mass, cross-sectional area, velocity, etc.

B. The Probability of Arrival of a Fragment of Specified Characteristics Versus Range

1. Fragment Characteristics - It is necessary to characterize the fragments in various ways such that trajectory analysis will allow a mapping of fragments from a unit solid angle about the explosion to a unit area on the ground surface at some range, R, from the explosion center. Specifically, it is necessary to know the fragment mass distribution; cross-sectional area or projected area distribution, and the drag coefficient for the fragments.

Many of these characterizations are obtained from empirically derived equations for bomb studies. One accepted equation in bomb studies relating fragment mass and area is:

$$M = k A^{3/2} \quad (75)$$

where M is a fragment mass, A is its cross-sectional area and k is some constant (ref. 44). For a mild steel fragment of "flattened" shape $k = 1.45$, for instance (where A is taken as the mean projected area of the fragment) (ref. 45). The distribution of fragment masses may be given by:

$$N(M) = N_0 \exp \left\{ - (M/\mu)^\gamma \right\} \quad (76)$$

where N is the number of fragments with masses greater than M, and μ equals 1, 1/2, or 1/6 the average fragment mass depending on whether γ equals 1, 1/2 or 1/3, respectively (ref. 46). Equation (76) actually thus defines three different mass distribution laws which are applicable for various types of explosions (for a thick walled shell in a three-dimensional breakup, μ equals the average fragment mass and $\gamma = 1$, for instance).

Appropriate values for the drag coefficient must be chosen in order to calculate the aerodynamic coefficient in the drag force equation, c, [see Section III.B-1, Equation (67)]. Some values for C_D were given in Section IV-C. For bomb tests, the values $C_D = .48, .60$ for sub- and supersonic fragment velocities seem to be common (Refs. 46 - 48) giving:

$$\begin{aligned} F_d &= .0031 m^{-1/3} U^2 \text{ subsonic} \\ F_d &= .0039 m^{-1/3} U^2 \text{ supersonic} \end{aligned} \quad (77)$$

for the drag forces (mass in engineering units and velocity in ft/sec.)

Empirical equations such as those obtained from bomb studies should be developed for missile explosions where the fragments are larger and have lower initial velocities. Until such equations are developed, some good predictions can probably be made using the equations relating to subsonic velocities for bomb fragments of relatively large mass.

2. Trajectory Analysis - A trajectory analysis may be carried out on fragments of known characteristics as was demonstrated in Section IV-C. These techniques result in a range calculation but not a terminal velocity calculation. Solution of the equations of motion for a fragment traveling at the speed U along its trajectory:

$$\left. \begin{aligned} \ddot{\bar{X}} + \beta V \dot{\bar{X}} + g \sin \alpha &= 0 \\ \ddot{\bar{Y}} + \beta V \dot{\bar{Y}} + g \cos \alpha &= 0 \end{aligned} \right\} \quad (78)$$

where β is the aerodynamic coefficient with the same definition as c in Equation (65). Sections II-B, \bar{X} and \bar{Y} are local coordinates of the fragment at time t measured in a coordinate system moving with the fragment, and α is the elevation angle of the fragment relative to the trajectory in the \bar{X} , \bar{Y} coordinate system) will yield the terminal velocity and range. These equations are solved by Feinstein and Nazooka (ref. 48) using a technique in which gravitational effects are a perturbation on the drag equations.

$$\ddot{\bar{X}}_0 + \beta \frac{\dot{\bar{X}}^2}{\bar{X}} = 0 \quad (79)$$

For trajectories in which the fragments had an initial elevation angle less than that required for maximum range (low register trajectory)

$$X = (\bar{X}_0 + \bar{X}_p) \cos \alpha_0 - \bar{Y} \sin \alpha_0 \quad (80)$$

where

$$\begin{aligned} \bar{X}_0 &= \ln(1+u)/\beta \\ \bar{X}_p &= -(g/2)t^2 \sin \alpha (1+u/3)/(1+u) \\ u &= \beta V_0 t \\ \bar{Y} &= (g/2)t^2 \cos \alpha [u(1+u/2) - \log(1+u)] / u^2 \end{aligned} \quad (81)$$

t is the time of flight obtained from the equation

$$Y = \bar{X}_0 + \bar{X}_p \sin \alpha_0 + \bar{Y} \cos \alpha_0 = 0 \quad (82)$$

and $\alpha = \alpha_0$ is the initial elevation angle. Solutions for other trajectories are obtained numerically for time interval steps t in which displacements occur.

$$\begin{aligned}\Delta X &= \bar{X} \cos \alpha - \bar{Y} \sin \alpha \\ \Delta Y &= \bar{X} \sin \alpha + \bar{Y} \cos \alpha\end{aligned}\tag{83}$$

Terminal velocity can be obtained by straightforward differentiation of Equations (78) and (79) with respect to time, t , but Feinstein omitted this step.

3. Mapping From Explosion Center to the Ground Plane - Feinstein uses Eqs. (80) through (83) to map the number density of fragments from bombs, n_i , in a mass interval i from those passing through an area element $R_0^2 \cos \alpha_0 \Delta \phi \Delta \alpha_0$ on a hemisphere immediately surrounding the bomb, to those landing in an area on the ground plane at range R , $R \Delta \phi \Delta R$. For n_i^0 density of fragments at the elemental area at the hemisphere and n_i density of fragments at the elemental area at the ground plane

$$n_i = n_i^0 \frac{R_0^2 \cos \alpha_0}{R \left| \frac{dR}{d\alpha_0} \right|}\tag{84}$$

The trajectory equations and initial conditions on the fragments yield the value for $R + dR/d\alpha_0$. n_i^0 , R_0 , and α_0 are related by fragment arena data.

In a simpler view, n_i^0 could be obtained from Eq. (77) and the explosion could be assumed to have spherical symmetry. As in Feinstein's calculation, Eq. (75) would be assumed to hold. Values for C_D would be chosen appropriate to the type of fragments expected from missile explosions and the number of fragments in a mass interval classification as a function of range would be calculated using Equation (84) and trajectory equations. Finally, the probability of impact on a target of area A_i of a fragment in mass interval i may be obtained from Poisson statistical equations, and the probability of damage for a given "target" would be assessed on the basis of vulnerability criteria and the flux of fragments as a function of range meeting those criteria.

Feinstein has actually solved the problem of hazards to humans as a result of several types of bomb explosions using his technique. His results (for the assumption that fragments of 58 ft-lb or greater of energy are hazardous to humans) are given in the form of probability of injury contours. We suggest that this technique or a simplified version of it coupled with more complete data on missile explosions could be used to produce similar results for the missile explosion problem.

C. Vulnerability Criteria

1. Structures - When a fragment emanating from an explosion arrives at the "target", the degree of damage it will produce is generally a function of its terminal velocity, mass, cross-sectional area, and the characteristics of the target. The relationships between these quantities and some measure of damage level for structures are empirical equations which are unrelated to the source of the fragment. Thus equations of this type which have been extensively developed for prediction of damage from bomb fragments would be applicable to the exploding missile problem.

An accepted form for vulnerability equations is:

$$U = k \frac{e^{\alpha} A^{\beta}}{M^{\gamma}} \quad (85)$$

where U is the fragment velocity. A is the presentation area of the fragment, M is the fragment mass, and e is the thickness of the target material. This equation of the "de Marre type" predicts the terminal velocity of a fragment required to penetrate the distance e into a structure where the constants α , β , γ , and k are a function of the material from which the structure and fragment are made. These constants are obtained empirically for various materials, and example values for the constants can be seen in Table XIX.

Some fragments from missile explosions are sufficiently large that penetration of a structure is not likely to be the primary damage mode. For such fragments the kinetic energy of the fragment may be of most interest in relating to probable structural damage. In some cases, the mass of the fragment would be sufficient to crush a structure were it to land on top of it. Clearly the damage potential of fragments from missile explosions is related to the types of structures which are in danger of damage and the materials and techniques used in their construction. To classify and investigate all such structures is beyond the scope of this report.

2. Personnel - The simplest criterion for fragment damage to personnel is the so-called "kinetic energy criterion" which is attributed to Crazz' "Lehrbuch der Ballistik". This criterion states that a fragment having 58 ft-lb of kinetic energy is capable of producing a human casualty. This criterion was widely used during World War II to predict casualty levels and was used by Feinstein (ref. 44) in 1972 to obtain probability of casualty contours from the equations described in Section V-B. Like most empirical values its justification is that it seems to give correct results more often than not.

TABLE XIX - CONSTANTS FOR VULNERABILITY EQUATIONS

Target Material	Fragment Material	α	β	γ	k
Yellow Pine	9/32"-9/16" steel spheres	3/4	3/4	3/4	66.6
Flywood	9/32"-9/16" steel spheres	3/4	3/4	3/4	82.3
Steel	Steel	3/4	3/8	1/2	272 X 10 ²

where A is in inches squared

e is in inches

M is in lb

U is in ft/sec

Other empirical values for the characteristics of fragments which will produce an incapacitating wound have been obtained from

$$M_1 U_1^\alpha = M_2 U_2^\alpha \quad (86)$$

where M is the mass of one of two fragments, i , and U_i is its velocity. This equation attests that having determined the mass and velocity of one fragment capable of incapacitating personnel all other fragments satisfying Eq. (86) also would be potentially incapacitating. The value for α is variously given as 2.5, 3.0, etc.

A "standard" assessment for fragments capable of producing casualties which has been widely used, is the wood penetration test. In this test, pine wood panels of thicknesses ranging from 1/2 to 1 inch are present in the range of fragments from an explosion. Where the panels are perforated, it is assumed a casualty would have occurred, otherwise not.

At this time, it would seem that acceptance of an empirical "standard" such as the kinetic energy criterion of 58 ft-lb would be the best idea in investigating potential fragment damage to personnel as a result of a missile explosion. Acceptance of this value would allow the use of bomb fragment data which was based on that value. Ultimately, it would seem reasonable to try and obtain data on the probability of injury as a function of kinetic energy of the fragments, and extend existing bomb fragment data to the case of more massive fragments of the type which may be encountered in missile explosions.

VI. DISCUSSION OF RESULTS

A major part of the work consisted of efforts to retrieve data relevant to the basic problem of fragmentation of liquid propellant vessels by literature search and visits to various government and private agencies. We believe that we were successful in assembling the majority of such data which are still available in the literature and in the files and archives of NASA and Department of Defense agencies, and in entering the data in the ASRDI data bank. The primary sources of data were the Project PYRO experiments (refs. 15-17), recent experiments conducted at NASA-Kennedy Space Center (ref. 39), and several accident reports (refs. 24 and 38). These sources, however, yielded only partial information with one exception. They gave either data on initial fragment velocities together with measured blast yield, or data on final locations, masses, and shapes of fragments. The only exception was PYRO Test #62, which gave both types of data.

The following observations are appropriate in order to place the results obtained from fragment velocities measured from PYRO films into the proper perspective.

- (1) Velocities were measured for many different combinations of tank size (and total propellant weight), tank height to diameter ratio, propellant types and test type, that is, confined by missile or confined by ground surface.
- (2) Velocities were measured at different positions in space depending on where they were first sighted. The instantaneous velocity of the fragment immediately after sighting was determined, and an average velocity of the fragment was determined by assuming that it traveled in a straight line from the center of the tank to a point at which the fragment was first sighted. No attempt was made to estimate the initial velocity of the fragment at the tank wall from the velocities calculated at a later time.
- (3) Velocities determined from data obtained from a single camera view are only approximate because the fragments often had components of velocities directed toward or away from the cameras which could not be detected. The necessary assumption that such fragments travelled normal to the camera lens axis introduced possible errors of +0% to -30%, i.e., velocities were generally underestimated. Likewise the coordinates of the fragment in terms of the radial position, height, and azimuth angle could not be determined accurately.

- (4) For fragments which could be observed from two different camera locations (spaced 120° apart), their true trajectory and thus their true velocity could be obtained. Unfortunately, fragments were difficult to identify in more than one camera view and so true velocities were obtained for only a few fragments.
- (5) It was not possible to relate on a one-to-one basis fragment velocity and heading with fragment size, shape or final range.

In spite of these limitations to the fragment velocity data, we feel that the data we obtained were very useful, and reasonable correlations with predicted values of velocity have been obtained. Nevertheless, we feel that the velocity data warrant additional study directed perhaps toward predicting the initial fragment velocities and those we had measured. We also feel that controlled experiments should be performed which would permit correlation between measured fragment velocities and the resulting missile masses. Techniques could be employed to allow initial velocities to be correlated with the final fragment size, weight, and position. An overhead camera located above the event with a wide field of view should facilitate velocity measurements and tracking during such a test. Tag markings would also facilitate fragment identification.

The fragment initial velocities, as estimated by the calculated parameter U_f (see Section III) for the four pooled groups (CBM- LO_2/LH_2 , CBM- $\text{LO}_2/\text{RP-1}$, CBGS- LO_2/LH_2 , CBGS- $\text{LO}_2/\text{RP-1}$) were fitted by log normal distributions. The means and standard deviations of these distributions are given in Table VIII.

The goodness of fit test, using the "W" statistic (ref. 36) showed probabilities from .415 to .99 of obtaining the calculated values of W, giving us no cause to reject assumed distributions. Thus, the log normal distributions appear to be an adequate fit for the fragment initial velocity distributions.

These probability density functions can be used to represent fragment initial velocity densities for the subject propellant combinations within the two configurations, CBM and CBGS.

Complete details of all data sources and analyses are given in the main body of the report.

In Section II, we reviewed data pertinent to blast yield for propellant explosions, and also presented methods for estimation of blast yield and the free-field blast wave properties for various types of explosions and propellants. These methods relied heavily on the extensive series of test results from Project PYRO (refs. 15-17), but also incorporated much of the physical

insight apparent in the work of Farber and co-workers (refs. 27-30). The methods allow estimation of blast wave peak overpressure and impulse, given propellant type, total propellant weight, type of accident, mixing time, and distance from the center of the explosion. Predictions are limited, however, to the range of scaled distances of the PYRO tests. A major difference in our prediction methods and those of reference 17 is in choice and scaling of ignition time. We believe that the scaling for this time assumed in references 15 and 17 is not verified by the test results, and discuss this point at some length in Appendix A, together with a dimensional analysis of ignition time scaling.

Density functions for fragment distance R, weight W, area A, and area/weight A/W, were estimated for each of eight events. A complete listing of the form and estimated parameters is given in Table XIV. Goodness of fit tests using the "W" statistic supported the selected density functions, in all but 3 cases out of the 32. These three cases were A/W distributions for events 3, 4, and 5.

The form of the density functions was constant for each parameter. That is, for all eight events, R and A/W followed normal density functions, and W and A followed log normal distributions.

Distance \hat{R} versus percent yield Y for events 1 through 5 shows a very good correlation in Figure 48. A prediction equation was derived, and is:

$$\hat{R} = 314.74 Y^{0.2775} \quad (63)$$

Confidence intervals were calculated for the means and variances for R for each of the eight events, and are shown in Table XVIII. In addition the 95th percentile was calculated for R for each of the first five events, and is shown on Figure 51.

Using Equation C13 from Appendix C, dimensional analysis for fragment trajectories, a new parameter G_7^1 was calculated:

$$G_7^1 = A_f / W_f^{2/3} \quad (73)$$

Plotting the geometric mean distance R of events 1, 2, 6, 7 and 8 versus G_7^1 (Figure 54 demonstrated a good correlation between these two variables), the scaling of W by taking the 2/3 root brought the distance R into a good linear correlation (on log-log paper) with G_7^1 . A second prediction equation,

$$\hat{R} = 9.864 (A/W^{2/3})^{0.78} \quad (74)$$

results in a correlation of 0.97. Thus, within the limits of the accuracy

allowed by the fragment data available from these 5 events, the prediction equation could be used to predict mean distance \hat{R} for a fragment of given maximum projected area A , and weight W .

Data sources and analysis are given in the body of the report. The damage potential from fragments as a function of range, for exploding missiles, can be as important a consideration as the damage potential due to the blast wave. To obtain useful data such as probability of damage as a function of range for various missile types and "targets" of interest, some criterion for damage to the particular target must be accepted and the probability of arrival at any given range of a fragment meeting that criterion must be calculated. The former can perhaps be accepted from bomb fragment damage studies, although fragments from liquid propellant explosions are larger and slower. The latter must be obtained from empirical equations developed to define the distribution of fragment characteristics at the instant the missile explosion occurs and from suitable solutions of the trajectory equations. Using these techniques, a "mapping" of the fragments from missile to target and probability of damage to a specific target as a function of range may be calculated. We suggest an expanded data base relating to distribution of fragment characteristics from missile explosions. The supplementation of bomb fragment data to cover larger and more massive fragments will probably be necessary before accurate damage probability maps can be made.

VII. CONCLUSIONS

This report presents the results of an extensive study of fragmentation effects of liquid propellant rockets or vessels which explode after accidental mixing of the propellants. The work was entirely investigative and analytic, and included no experiments.

Some specific conclusions are as follows:

- (1) Accident reports and results of tests simulating accidental explosions provided a significant source of data on fragmentation effects of exploding liquid propellant vessels.
- (2) Data on initial fragment velocities, masses and shapes of fragments, and ranges of fragments showed wide statistical variations. When the data were fitted to statistical distribution functions, however, good statistical fits were obtained for these parameters or combinations of these parameters. In some instances, the combinations of parameters were chosen by dimensional analysis.
- (3) Methods were developed or adopted for prediction of blast wave properties, initial velocities of fragments, and fragment range. These methods were compared with data and appeared to give reasonably good correlation.
- (4) Some approximate methods for estimating damage to various "targets" by impacting fragments are presented. These could not, however, be correlated with data obtained during the data retrieval part of our work because no data were available on terminal (or impact) velocities of fragments from bursting propellant vessels.
- (5) The analyses and empirical fits to data included in this report do allow prediction of blast yield and subsequent fragmentation patterns and velocities for the common propellant combinations over a wide spectrum of type of accident, weight of propellant, and time of ignition.

We believe that the work reported here constitutes the first relatively comprehensive study of fragmentation effects from exploding liquid propellant vessels. As noted above, predictions can be made of some of these effects using results from this report. But, there are limitations imposed by limitations in the fragmentation data - which has, after all, been retrieved from sources in which study of fragmentation effects was secondary or even entirely incidental. There seems to be little doubt that one could better test the

prediction methods presented here if he were able to design and conduct experiments with the specific purpose of observing and measuring fragmentation effects.

VIII. RECOMMENDATIONS

The results of this study can, we believe, form the basis for development of relatively simple methods of assessing hazards to people and damage to facilities from the impact of fragment from liquid propellant explosions. But, the study does not in itself generate such methods because its primary aim was the collection and analysis of fragmentation data from past tests and accidents. We have pointed out previously that none of the data collected came from experiments designed to obtain initial or terminal fragment effects. There is also an almost complete lack of terminal ballistics effects data or methods for assessing hazards of the relatively large, odd-shaped, low-velocity fragments which predominate in liquid propellant explosions. The authors therefore feel that, although simplified methods for overall estimation of fragment hazards can be generated, some additional experimental work would be very desirable to validate these methods.

We recommend the following studies:

- (1) Using the initial velocity prediction methods developed here, the statistical fits to data on fragment mass and shape, and exercising the trajectory equations of Section IV, expected variations in impact velocities for a spectrum of fragments could be computed for a number of hypothetical explosions. These impact conditions could then be overlaid on expected densities of human observers or bystanders and on nearby structures to estimate fragment hits. Using the very much oversimplified assumption that a fragment hit on a person is a kill, or that a fragment hit on a structure causes some specified dollar damage, each "scenario" could then be assessed for fragment kills and property damage. In this way, a simplified damage assessment model could be generated, based on the work in this report. It is recommended that this be done, but that the user be strongly cautioned that the model could be considerably refined and improved, if better data were available in certain areas.
- (2) A careful set of small-scale experiments be designed to obtain more accurate initial velocity data for tests simulating several types of accidents. Vessels or nearby objects should be carefully designed to produce fragments of known geometry and size, and their motions followed with at least two high-speed cameras. Such data should serve to improve the data presented in this report, with much more "two-view" data yielding accurate trajectories.

- (3) As a part of the initial velocity experiments, accurate missile maps should be made to determine fragment impact locations. The pre-formed fragments should be carefully marked so that impact locations of many of the fragments could be correlated with initial velocities and launch angles.
- (4) Studies of the terminal ballistics effects of impacts of relatively large, slow fragments of irregular shape would be very desirable for animals (to make estimates for humans), and for a variety of structures. Cost might be prohibitive. Some analytic studies could well provide partial answers, however.

The order in which the above recommendations are listed is also our suggested order of priority. The first study is purely analytical, but yields an approximate hazards assessment method. The other three are primarily experimental, and serve to generate data which should refine the method.

APPENDIX A

MODEL ANALYSIS FOR MIXING OF LIQUID ROCKET PROPELLANTS

In the Project PYRO studies, a basic assumption was that, for any particular type of simulated accident, the time of ignition to produce maximum blast yield could be scaled as

$$\bar{t} = t/W^{1/3} \quad (A1)$$

where \bar{t} is scaled time, t is time of ignition delay after missile failure, and W is total weight of propellant in the missile. It is not clear that this is the proper scaling, and no model analysis is presented in the PYRO final reports to justify such scaling. There are instead statements that the experimental data appear to agree with this scaling, but the inherent scatter in blast yields makes this conclusion doubtful. We thought that a model analysis should be conducted to ascertain, if possible, how ignition times for maximum yield should scale.

From both the Project PYRO work and Dr. Farber's work, it seems clear that intimate mixing of fuel and oxidizer is needed to maximize the blast yield for a given type of accident. The time for ignition must be great enough to allow as much mixing as possible, but not so great that all of the most volatile liquid can have evaporated. The physics of the processes which occur on mixing of LH_2 and LO_2 , RP-1 and LO_2 , and $LH_2/$ RP-1/ LO_2 have been studied most exhaustively by Farber and his associates. They have, however, considered the dynamics of impact or other accident leading to the mixing in only a cursory manner. To conduct a model analysis, we should be able to list the physical parameters affecting this problem, and their dimensions, which is the prerequisite to conduct of the analysis.

A number of the physical processes which occur are a function of the particular propellant combinations, and conditions just prior to an accident, rather than the details of the accident. These processes should be governed by parameters which will be common to all possible types of accidents, and will thus be considered first. Those propellants and oxidizers which are cryogenic will be essentially at their boiling temperatures, while fuel such as RP-1 will be at or near the temperature of the ambient air. Once the propellants start to mix, violent boiling of the colder liquids will occur, while the warmer ones will be chilled and perhaps frozen. The processes will involve conductive heat transfer, convective heat transfer, and eventually radiative transfer to the ambient atmosphere. Gravity is perhaps important in convective processes and in rate of upward migration of bubbles formed during boiling. Latent heats of fusion and boiling are obviously important, as are temperature differences

and gradients. Parameters affecting these processes, and their dimensions in a M, L, T, θ (mass, length, time, temperature) system are listed in Table 1.

To complete the list of parameters for model analyses, we must consider specific types of accidents, and also add other parameters known to affect the blast yield. Consider first the case identified by PYRO as CBM (confinement-by-the-missile). This case is shown schematically in Figure A1.

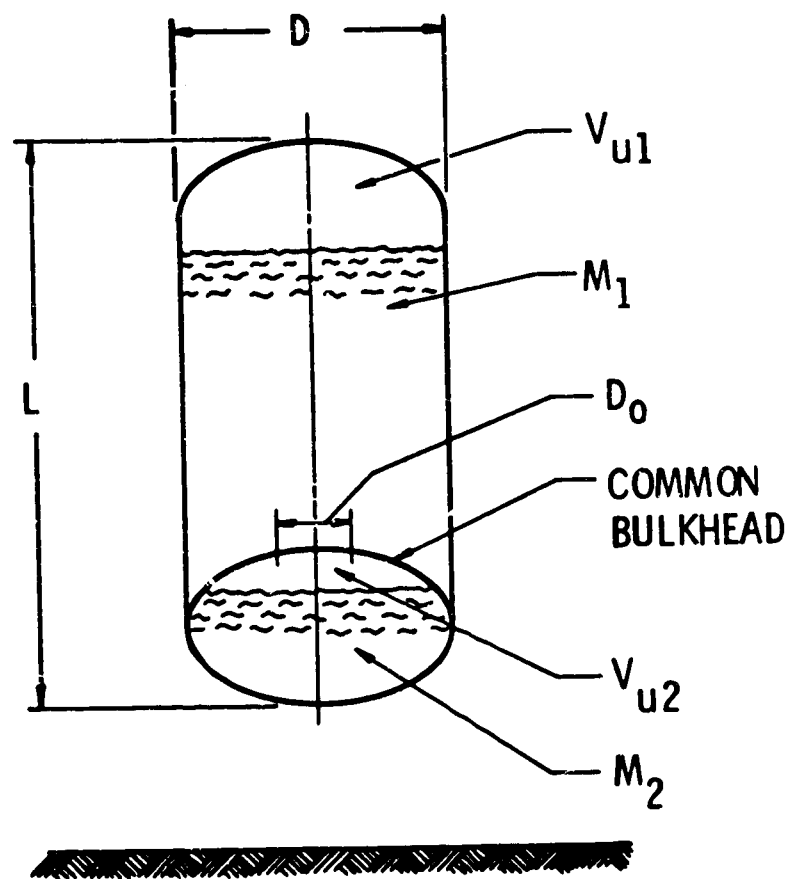


FIGURE A1.
SCHEMATIC OF CBM CASE

A rupture is assumed to occur in the common bulkhead, idealized as a circular opening of diameter D_0 . Oxidizer then spills through this opening under the effects of gravity, and mixes with the fuel. Geometry of the tankage, ruptured area, distance for oxidizer to fall, static head to force oxidizer

through the opening, etc., all seem important. These can be characterized by the tank dimensions shown, ullage volumes, initial masses of fluids, gravity, and a generic length l indicating location within the tankage. (Velocities of impact of fluids are important, but these are fixed once the other parameters described above are determined.) The specific heat of combustion (or explosion) for propellants mixed in stoichiometric ratios, together with fraction mixed at time of ignition, should determine total energy driving the blast wave. Adding these parameters to Table A1, we have in Table A2 the total list of 20 parameters for this type of accident. These parameters will yield $20 - 4 = 16$ dimensionless groups, when the methods of dimensional analysis are applied. One such set is given in Table A3.

The model law in Table A3 can be used to express any one of the dimensionless groups (π terms) as a function of the remaining ones. Because we are interested in time scaling, which is contained in π_{11} , we would probably express π_{11} as a function of π_1 through π_{10} , and π_{12} through π_{16} . The law can also be used to fix interrelations between scale factors for physical quantities. In its present form, Table A3 is too general to provide much guidance. It states that all of the dimensionless groups must be maintained constant between model and prototype tests for accurate scaling. Let us consider, however, the practical limitations of testing and the effects of these limitations.

Two of the physical parameters in Table A2 are constants of nature for testing on earth, and cannot be altered. Scale factors for these quantities*, the Stefan-Boltzmann constant σ and earth's gravity g , are therefore unity, i. e.,

$$\lambda_{\sigma} = \lambda_g = 1 \quad (A2)$$

Also, we wish to employ the same propellants under the same initial temperatures and atmospheric conditions (or, at least, this is what was done in Project PYRO). This renders a number of other scale factors unity, namely:

$$\lambda_{H_{fi}} = \lambda_{H_{bi}} = \lambda_{H_e} = \lambda_{v_i} = \lambda_{K_i} = \lambda_{(\rho c_p)_i} = \lambda_{\theta_i} = \lambda_{\theta_a} = 1 \quad (A3)$$

These limitations cause several π terms to be identically satisfied, namely, π_1 and π_{12} . Furthermore, by making the model geometrically similar to the prototype in all respects, a number of other π terms will be satisfied.

* A scale factor λ is defined as the ratio of a quantity in the model to the corresponding quantity in the prototype.

TABLE A1 - PARAMETERS AFFECTING HEAT TRANSFER OF MIXING LIQUID PROPELLANTS

Parameter	Symbol	Dimensions
Ambient Air Temperature	θ_a	θ
Initial Temps. of Liquids*	θ_i	θ
Temp. in Mixture	θ_m	θ
Heats of Fusion*	H_{fi}	$L^2 T^{-2}$
Heats of Boiling*	H_{bi}	$L^2 T^{-2}$
Masses*	M_i	M
Thermal Conductivities*	K_i	$MLT^{-3} \theta^{-1}$
Kinematic Viscosities*	ν_i	$L^2 T^{-1}$
Volumetric Heat Capacities*	$(\rho c_p)_i$	$ML^{-1} T^{-2} \theta^{-1}$
Time	t	T
Gravity	g	LT^{-2}
Convective Heat Transfer Coefficient	h	$MT^{-3} \theta^{-1}$
Stefan-Boltzmann Constant	σ	$MT^3 \theta^{-4}$

* Subscript i denotes a number of similar properties.

TABLE A2 - PARAMETERS FOR PROPELLANT MIXING FOR
CBM ACCIDENT

Parameter	Symbol	Dimensions
Ambient Air Temperature	θ_a	θ
Initial Temps. of Liquids	θ_i	θ
Temp. in Mixture	θ_m	θ
Heats of Fusion	H_{fi}	$L^2 T^{-2}$
Heats of Boiling	H_{bi}	$L^2 T^{-2}$
Heat of Explosion	H_e	$L^2 T^{-2}$
Masses	M_i	M
Thermal Conductivities	K_i	$MLT^{-3} \theta^{-1}$
Kinematic Viscosities	ν_i	$L^2 T^{-1}$
Volumetric Heat Capacities	$(\rho c_p)_i$	$ML^{-1} T^{-2} \theta^{-1}$
Time	t	T
Gravity	g	LT^{-2}
Convective Heat Transfer Coefficient	h	$MT^{-3} \theta^{-1}$
Stefan-Boltzmann Constant	σ	$MT^{-3} \theta^{-4}$
Tank Diameter	D	L
Tank Length	L	L
Opening Diameter	D_o	L
Generic Length	l	L
Ullage Volumes	V_{ui}	L^3
Total Mass of Propellant	M_t	M

TABLE A3 - DIMENSIONLESS GROUPS FOR PROPELLANT MIXING FOR CBM ACCIDENT

Term No.	Group	Description
π_1	θ_i / θ_a	Temperature Ratios
π_2	θ_m / θ_a	
π_3	H_{fi} / gL	
π_4	H_{bi} / gL	
π_5	H_e / gL	
π_6	D / L	Length Ratios
π_7	D_o / L	
π_8	l / L	
π_9	V_{ui} / L^3	Volume Ratios
π_{10}	M_i / M_t	Mass Ratios
π_{11}	$tg^{1/2} / L^{1/2}$	Scaled Tim
π_{12}	$(\rho c_p)_i v_i / K_i$	Prandtl No.
π_{13}	hL / K_i	Nusselt No.
π_{14}	$v_i / L^{3/2} g^{1/2}$	Pseudo Reynolds No.
π_{15}	$\sigma_a^3 g^3 / K_i L^2$	Ratio of Radiation to Conduction
π_{16}	$K_i L^{1/2} \theta_a / M_t g^{3/2}$	Ratio of Conduction to Inertia

These are π_6 , π_7 , π_8 , π_9 and π_{10} . Employing these restrictions, the remaining π terms require the following interrelations between scale factors.

$$\pi_2 \longrightarrow \lambda_{\theta_m} = 1$$

$$\pi_3, \pi_4, \pi_5 \longrightarrow 1 = \lambda_L$$

$$\pi_{11} \longrightarrow \lambda_t = \lambda_L^{1/2}$$

$$\pi_{13} \longrightarrow \lambda_h \lambda_L = 1$$

$$\pi_{14} \longrightarrow \lambda_L^{3/2} = 1$$

$$\pi_{15} \longrightarrow \lambda_L^2 = 1$$

$$\pi_{16} \longrightarrow \lambda_L^{1/2} = \lambda_L^3$$

(A4)

A quick examination will show that these interrelations can only be satisfied if all scale factors, including the length scale factor λ_L , are unity. That is, no sub-scale model is possible which correctly scales all of the phenomena which were initially assumed to be important! This impasse is not unusual in attempting to model complex phenomena. One must now consider those effects which will hopefully be of minor importance, and let them deliberately go out of scale.

For the problem we are considering, radiation heat transfer to the outside atmosphere can perhaps be safely neglected, because the mixture is confined within the tank up to the time of interest. So, let us ignore term π_{15} . For the mixing fluids, conduction and convection are probably the primary modes of heat transfer, so we wish to retain π_{13} , Nusselt No., because this term is a ratio of these two effects. Inertia effects are undoubtedly important and should be retained. Gravity is triply important because it affects mixing impact conditions, convection, and bubble migration. Whether viscosity is important is not certain. We will assume that it is not, and ignore π_{14} . Heats of fusion, boiling and explosion appear to be important, so we should retain π_3 , π_4 and π_5 . This reduced form of the law can be written:

$$\left(\frac{t}{L^{1/2}} \right) = f_1 \left[\left(\frac{0}{a} \right), \left(\frac{H_i}{gL} \right), \text{geom. similarity, } \left(\frac{hL}{k_i} \right), \right. \\ \left. \left(\frac{k_i L^{1/2} 0}{M_t g^{3/2}} \right) \right] \quad (A5)$$

But, we still have problems! The second term in the bracket in Eq. (A5) requires that $\lambda_L = 1$, which negates sub-scale testing. If we relax this requirement, the last term in the bracket makes

$$\lambda_L^{1/2} = \lambda_{M_t} \quad (A6)$$

But, $\lambda_{M_t} = \lambda_L^3$ if identical materials are used, and (A6) is only satisfied if $\lambda_L = 1$. To obtain any model law which does allow small-scale testing, we must throw out all effects except inertia, heat conduction, and heat convection. This very much reduced law is

$$\left(\frac{t}{L^{1/2}} \right) = f_2 \left[\text{geom. similarity, } \left(\frac{0}{a} \right), \left(\frac{hL}{k_i} \right) \right] \quad (A7)$$

It says that, if geometric similarity is maintained, a model will have similar temperature distributions during the mixing process at similar locations and similar scaled times, provided the film coefficient h scales inversely as the length scale factor. Recalling that $\lambda_g = 1$ and $\lambda_L = \lambda_{M_t}^{1/3}$, the dimensionless time parameter $(t g^{1/2} / L^{1/2})$ requires that time scales as

$$\bar{t} = (t / M_t^{1/6}) \quad (A8)$$

where \bar{t} is not dimensionless, but uniquely determines the dimensionless time parameter mentioned before.

This conclusion regarding time scaling is, of course, dependent on the series of assumptions used to re-visit the basic model law. One critical assumption was that gravity effects were important and must not be allowed to go out of scale. Although the physics of the mixing process seem to be strongly dependent on gravity, let us examine the consequences of letting gravity go out of scale. We will make the same assumptions as before regarding use of the same fluids at the same initial temperatures, and assume geometric similarity. Let us also modify the π terms somewhat by combining and substitution. We can, for example, square π_1 and multiply it by π_3 through

π_5 to give new terms which can be substituted. In a similar manner, g can be eliminated from all terms but π_{11} . The resulting modified terms are:

$$\begin{aligned}
 \pi_3' &= H_{fi} t^2 / L^2 \\
 \pi_4' &= H_{bi} t^2 / L^2 \\
 \pi_5' &= H_e t^2 / L^2 \\
 \pi_{14}' &= \nu_i t / L^2 \\
 \pi_{15}' &= \sigma_0 L / k_i t^6 \\
 \pi_{16}' &= k_i \theta_a t^3 / M_t L
 \end{aligned}
 \tag{A9}$$

These terms dictate the following interrelations between scale factors

$$\left. \begin{aligned}
 \pi_3', \pi_4', \pi_5' \lambda_t &= \lambda_L \\
 \pi_{14}' \lambda_t &= \lambda_L^2 \\
 \pi_{15}' \lambda_L &= \lambda_t^6 \\
 \pi_{16}' \lambda_t^3 &= \lambda_{M_t} \lambda_L
 \end{aligned} \right\}
 \tag{A10}$$

As before, only the assumption that all scale factors are unity will satisfy all of these terms. But, heats of fusion, boiling and explosion will be properly scaled by choosing $\lambda_t = \lambda_L$. So, by letting gravity, viscosity, radiation, and ratio of conduction to inertia go out of scale, we can generate another restricted scaling law.

$$(H_i t^2 / L^2) = f_3 \left[\text{geom. similarity, } (\theta_m / \theta_a), \left(\frac{hL}{k_i} \right) \right]
 \tag{A11}$$

Time scaling related to total mass of propellants scales in this law as

$$\bar{t} = (t / M_t)^{1/3}
 \tag{A12}$$

This can be seen to be the scaling for time to produce maximum yield which was assumed in Project PYRO.

Which time scaling is correct, Eq. (A8) or Eq. (A12)? If all phenomena are to be properly scaled, neither is strictly correct. If gravity effects are truly important, Eq. (A8) is more nearly correct. If scaling of heats of fusion, boiling, etc. is more important than scaling gravity effects, then Eq. (A12) is more nearly correct. To test either hypothesis, sufficient test data must exist to fit data scaled in either manner over a relatively large range of total propellant weights for any given combination of fuel and oxidizer. Even then, it may be difficult to determine which scaling law to use because the propellant mass is raised to a small fractional power ($1/3$ or $1/6$) in either case, and the dependence of the scaled time on propellant mass is therefore quite weak.

We reviewed the PYRO test results to ascertain whether those data substantiated correlation of a specific law for scaling of ignition time with blast yield.

The PYRO tests indicated that, for hypergolic propellants, ignition time is unimportant because ignition occurs immediately on contact of the fuel and oxidizer. Blast yield did depend on impact velocity for high velocity impact tests of hypergolics.

For non-hypergolic propellants, one would expect the blast yield to be a function of type of simulated accident, type of propellant, impact velocity, etc., in addition to time of ignition. Blast yield is expressed in the PYRO reports as a percent of an equivalent weight of TNT, based on the measured terminal yield from each experiment. This procedure essentially normalizes the results for all tests with respect to mass of propellant so that data on yields versus ignition times or scaled ignition times can be easily compared. We will make such comparisons for the propellant combinations $LO_2/RP-1$ and LO_2/LH_2 , and for the CBM and CBGS type of test.

In Figure A2, we see blast yields Y plotted as a function of ignition time t for all $LO_2/RP-1$ CBM tests*. Different symbols are used for different masses of propellant. It is immediately evident that the data scatter is large, but the data do indicate an increase in yield up to 150-200 msec, and then a substantial decrease for longer ignition times. The data are plotted as a function of time, rather than time scaled by division by either $M_t^{1/3}$ or $M_t^{1/6}$. Replotting the data with time scaled in either of these manners

* For physical reasons, finite blast yield at zero ignition time is paradoxical. If propellants are not given time to mix, no explosion should be possible. Data points for zero ignition time probably represent a small, but non-zero, ignition time.

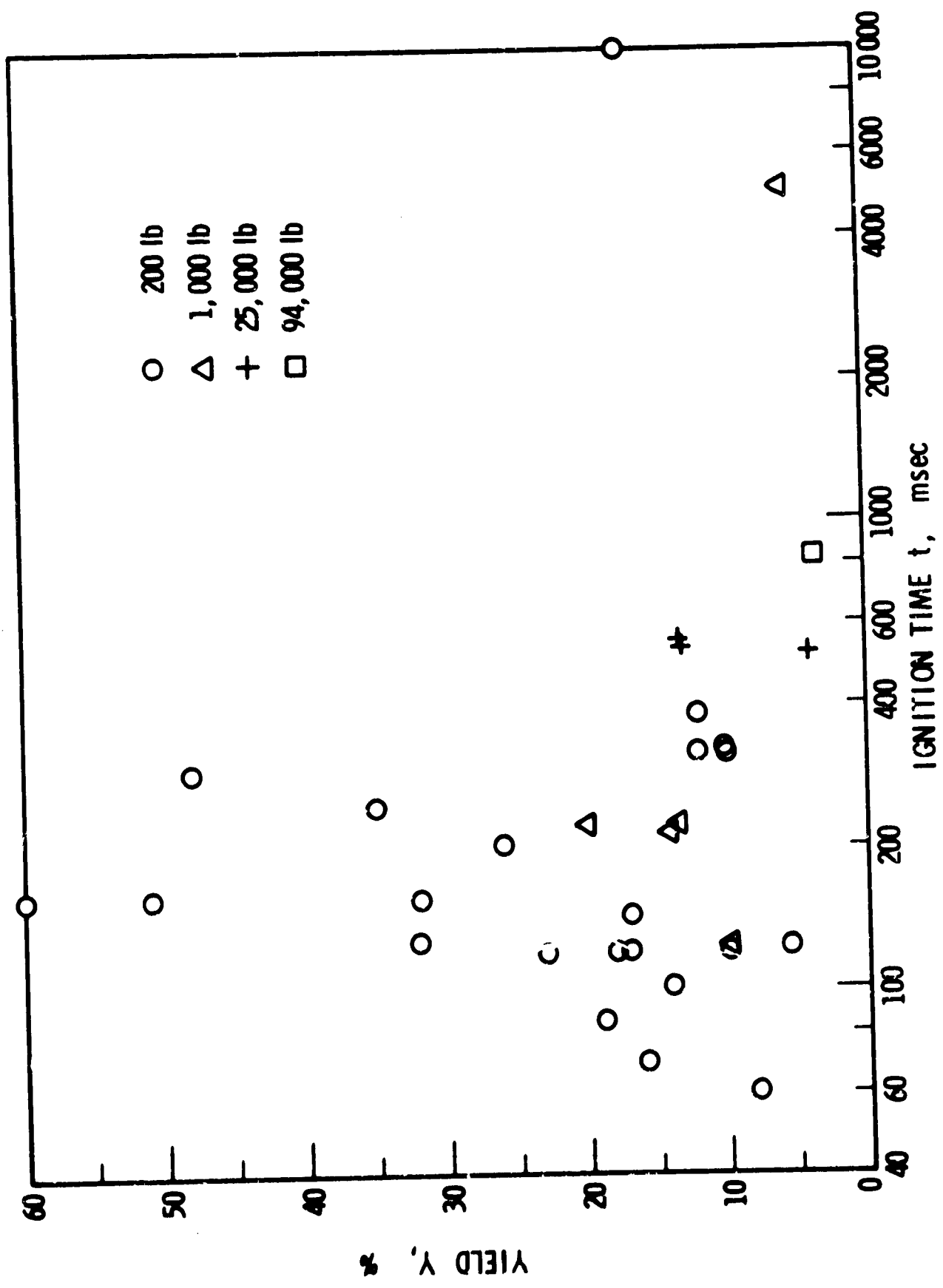


FIGURE A2. YIELD VS. IGNITION TIME LO₂/RP-1 CBM TESTS

produces no less data scatter than is already present. Figure A3 shows a similar plot for LO_2/LH_2 CBM tests. Again, the scatter is considerable, but a trend to increasing yield with increasing time is evident, with no apparent decrease at long times. One isolated data point with a high yield may indicate peaking at near 200 msec, but this is inconclusive. Again, replotting on scaled time based doesn't improve the scatter.

Data for all $\text{LO}_2/\text{RP-1}$ CBGS tests are plotted in Figure A4. It is evident that impact velocity for this propellant and type of test does have a significant effect on blast yield, and that yield increases for a maximum and then decreases. The same trends are evident in the data for LO_2/LH_2 CBGS tests plotted in Figure A5. Some type of normalization of yield versus impact velocity would undoubtedly reduce the scatter evident in these two figures, but the spread would still be great. As for the CBM tests, there is no evidence that scaling ignition time would decrease the data scatter.

We draw different conclusions from this study of the PYRO blast data than do the authors of that study. They concluded that, for all but the $\text{LO}_2/\text{RP-1}$ CBM tests, explosive yields scaled as a function $\bar{t} = (t/M_t^{1/3})$. We conclude, on the other hand, that the data do not verify any particular scaling for ignition time. The blast yield is certainly a function of ignition time and that function can perhaps be estimated from the PYRO data for specific propellants and types of test. Direct plots of yield versus ignition time appear to be as valid as plots versus $(t/M_t^{1/3})$, $(t/M_t^{1/6})$, or perhaps any other scaling involving a small fractional power of M_t .

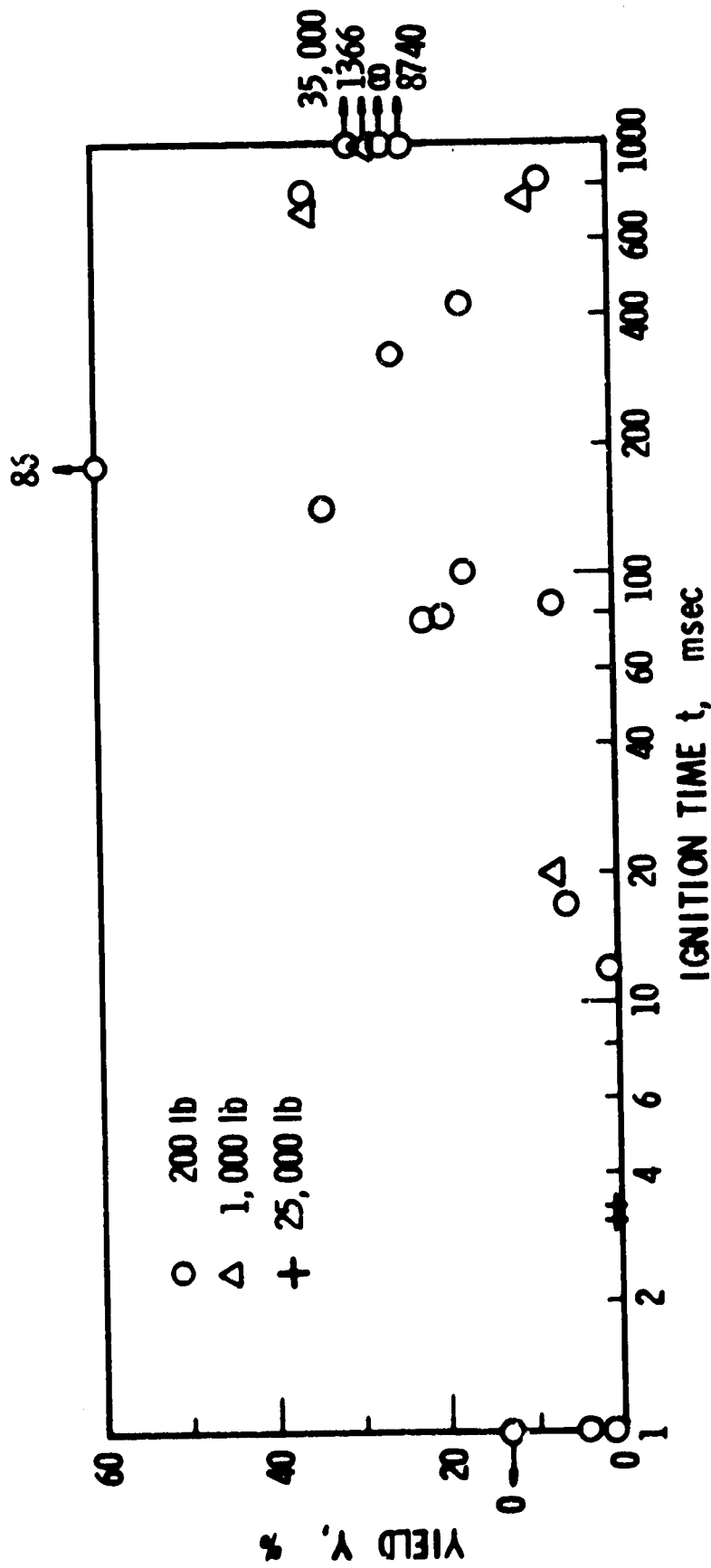


FIGURE A3. YIELD VS. IGNITION TIME LO₂/LH₂ CBM TESTS

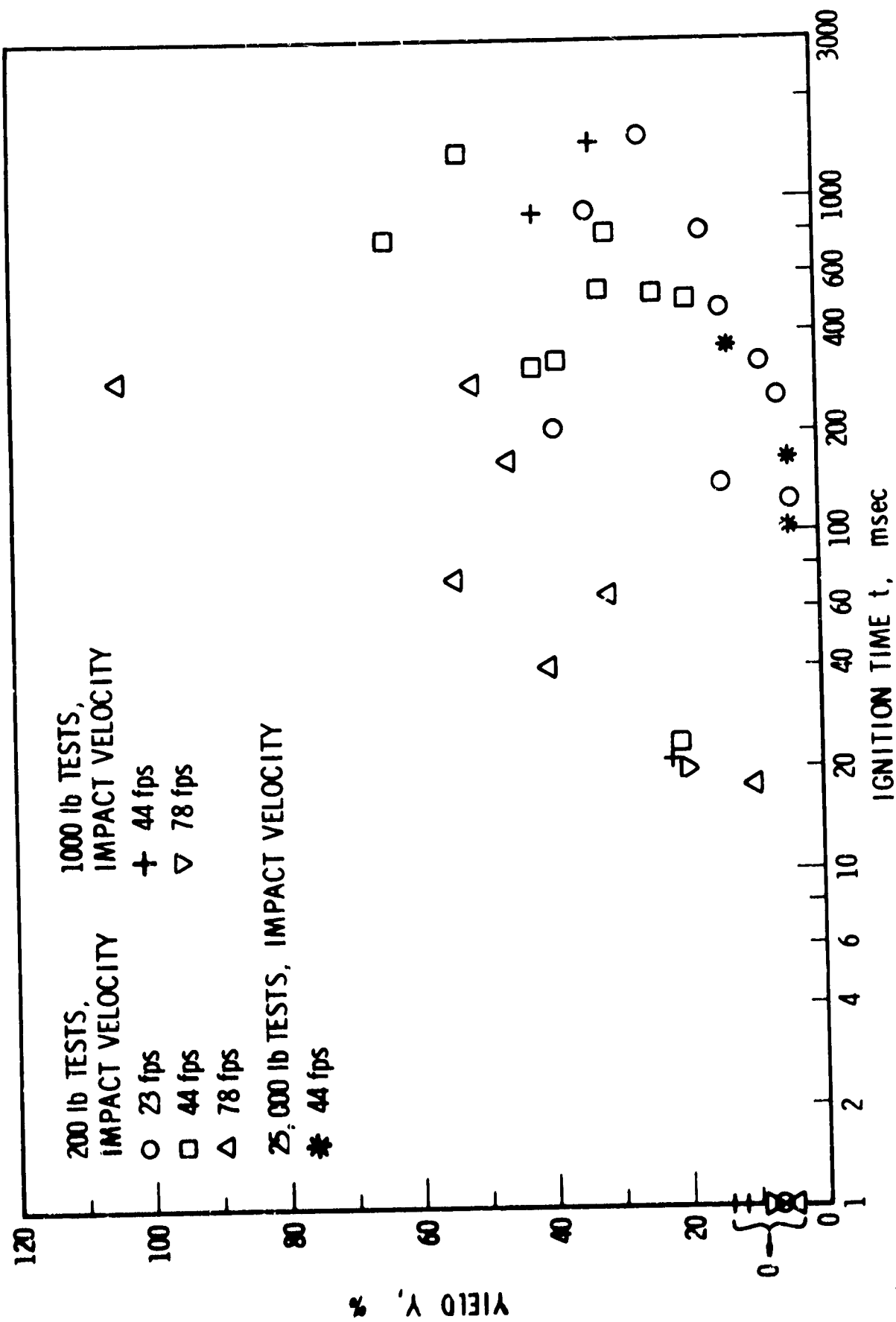


FIGURE A4. YIELD VS. IGNITION TIME LO_2/LH_2 CBGS TESTS

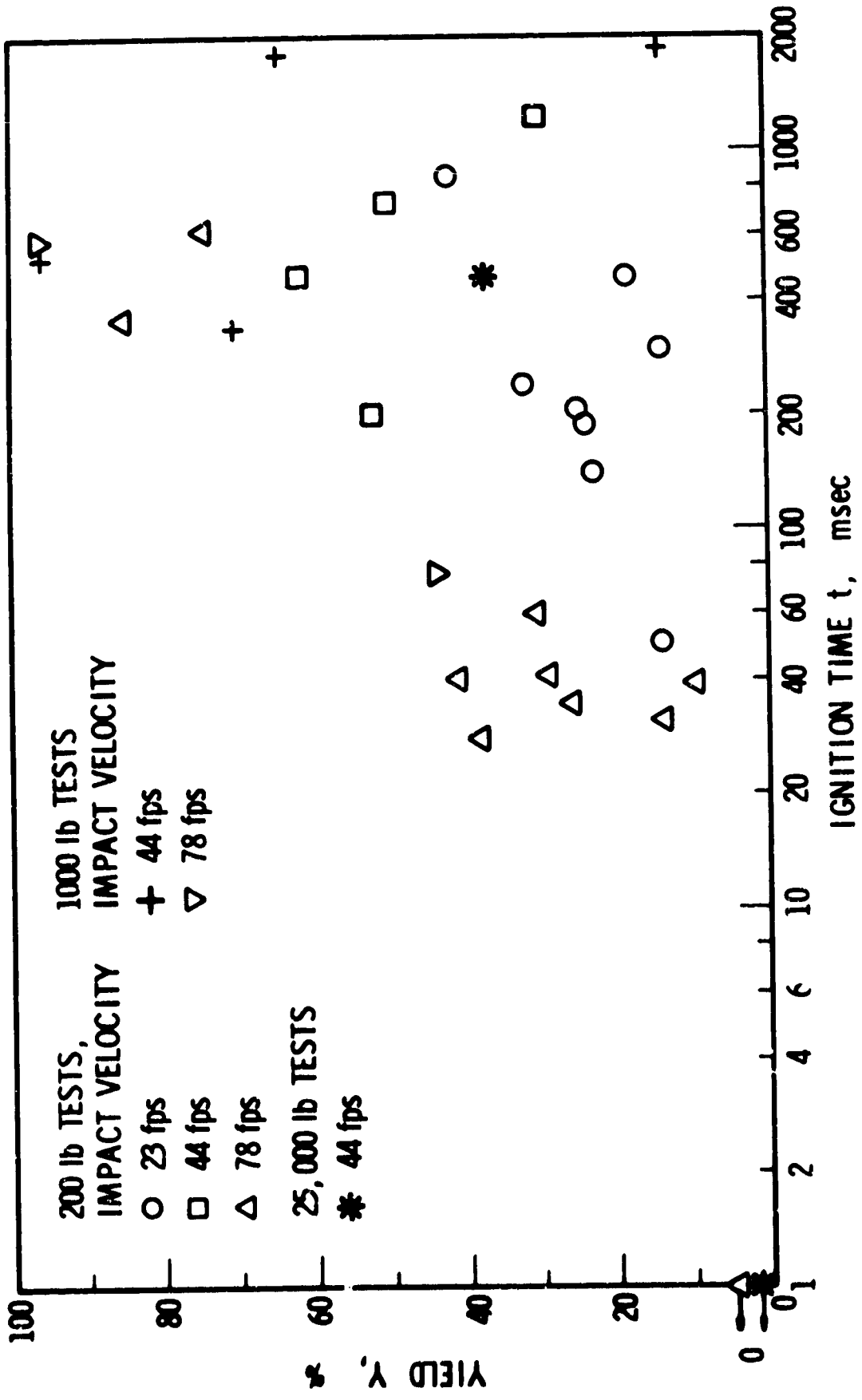


FIGURE A5. YIELD VS. IGNITION TIME LO₂/RP-1 CRGS TESTS

APPENDIX B

SUMMARY OF DATA OBTAINED FROM FILMS READ

PYRO TEST NO.	DISTANCE T. CAMERA (FT)	BEARING		FREQUENCY OF TIMING MARKS (TM/SEC)	FILM SPEED		NO. OF FRAGMENTS RECORDED	NO. OF DUPLICATE FRAGMENTS
		GIVEN	ASSUMED (DEG)		GIVEN	CALCULATED (PPS)		

GROUP 1: HYPERGOLIC HIGH-VELOCITY-IMPACT TESTS

No Tests Read in This Group

GROUP 2: HYPERGOLIC (AFRPL) TESTS

30	420	65	0	100	1000	Not Read ²	7	0
31	420	65	0	10	64	82	4	0
32	420	65	0	120	1000	1228	6	0
33	420	65	0	10	64	46	7	0
35	420	65	0	120	1000	Not Read	3	0
36	420	65	0	60	64	NR	2	0
39 ³	420	270	240	120	1000	1423	7	0
	420	0	0	120	1000	951	5	0
	420	270	240	120	1000	990	2	0
258	420	0	0	120	400	390	5	0

GROUP 3: LO₂/RP-1 CONFINEMENT-BY-THE-MISSILE TESTS

48 ³	420	0	0	120	1000	1329	7	0
	420	270	240	120	1000	1370	5	0
49	420	0	0	120	1000	997	8	2
	420	270	240	120	1000	1178	8	0
58	420	0	0	120	1000	NR	10	0

PYRO TEST NO.	DISTANCE TO CAMERA (FT)	BEARING		FREQUENCY OF TIMING MARKS (TM/SEC)	FILM SPEED		NO. OF FRAGMENTS RECORDED	NO. OF DUPLICATE FRAGMENTS
		GIVEN	ASSUMED (DEG)		GIVEN	CALCULATED (PPS)		
Group 3 (Cont'd) -								
	420	270	240	120	1000	NR	4	2
87A	420	0	0	120	1000	964	7	0
	420	270	240	120	1000	NR	8	0
	420	0	0	120	1000	991	6	0
88	420	270	240	120	1000	867	7	0
	420	0	0	120	1000	1104	5	0
95A	420	270	240	120	1000	1100	8	0
	420	270	240	120	1000	809	6	1
192	420	0	0	120	400	400	8	0
	420	270	240	120	1000	NR	6	1
193	420	270	240	120	400	NR	12	0
	420	0	0	120	400	NR	2	0
209	420	270	240	120	1000	728	6	0
	420	270	240	120	1000	762	7	0
	420	0	0	120	400	397	4	0
237	420	270	240	120	1000	897	1	0
	420	0	0	120	400	395	2	0
270A	420	270	240	120	1000	983	7	0
	420	270	240	120	1000	1097	12	0
	420	0	0	120	400	403	11	0
	1000	300	340	120	1000 ⁷	403	3	0
275	420	130	240	60	1000	671	5	3
	420	325	0	60	1000	683	9	1
	420	325	0	60	400	200	3	0
	1000	340	340	10	64	44	3	0
278	420	325	0	120	1000	NR	3	0
	420	325	0	120	1000	1107	2	0

Group 3 (Cont'd) -

PYRO TEST NO.	DISTANCE TO CAMERA (FT)	BEARING		FREQUENCY OF TIMING MARKS (TM/SEC)	FILM SPEED		NO. OF FRAGMENTS RECORDED	NO. OF DUPLICATE FRAGMENTS
		GIVEN	ASSUMED (DEG)		GIVEN	CALCULATED (PPS)		
Group 3 (Cont'd) -								
	420	325	0	120	400	397	11	0
282	420	325	0	120	1000	1417	3	0
	420	325	0	120	400	403	8	0
	1000	340	340	60	400	393	2	0
301	420	0	0	120	1000	994	4	0
	420	0	0	120	1000	386	5	0
	---	---	---	---	400	NR	4	0

GROUP 4: LO₂/RP-1 CONFINEMENT-BY-THE-GROUND SURFACE VERTICAL TESTS

107	420	0	0	120	400	NR	9	0
	420	270	240	120	1000	1678	12	0
109	420	270	240	120	1000	1545	6	0
	420	0	0	120	400	NR	5	0
190	420	270	240	120	1000	1063	5	0
	420	0	0	120	400	406	5	0
191 ³	420	270	240	120	1000	990	8	0
	420	0	0	120	400	399	16	0
202	420	270	240	120	1000	1048	4	0
	420	0	0	120	400	398	6	0
205	420	270	240	120	1000	1177	10	0
	420	0	0	120	400	398	13	0
206	420	270	240	120	1000	987	1	0
	420	0	0	120	64	72	3	0
219	420	270	240	120	1000	1050	4	0
	420	0	0	120	400	401	12	0
220	420	0	0	120	400	396	8	0
249	420	0	0	120	1000	993	2	0

PYRO TEST NO.	DISTANCE TO CAMERA (FT)	BEARING		FREQUENCY OF TIMING MARKS (TM/SEC)	FILM SPEED		NO. OF FRAGMENTS RECORDED	NO. OF DUPLICATE FRAGMENTS
		GIVEN	ASSUMED (DEG)		GIVEN	CALCU- LATED (PPS)		
Group 4 (Cont'd)								
	420	0	0	120	400	395	4	0
284	---	---	240	120	1000	1109	6	0
	---	---	0	120	1000	1195	10	0
	---	---	---	120	400	405	11	0
	---	---	---	120	400	399	6	1
GROUP 5: LO ₂ /RP-1 CONFINEMENT-BY-THE-GROUND-SURFACE HORIZONTAL TESTS								
121	---	---	240	---	1000	1014	6	0
	---	---	0	---	1000	975	2	0
122	---	---	240	---	1000	947	4	0
	---	---	0	---	1000	899	6	0
125	---	---	240	---	1000	1350	3	0
	---	---	240	---	---	64	4	0
	---	---	240	---	1000	1200	6	1
140	420	270	240	120	400	402	9	0
	420	0	0	120	400	393	5	0
162 ³	420	0	0	---	1000	1154	5	0
	420	270	240	---	400	399	4	0
179	---	---	240	---	1000	1216	4	0
	---	---	---	---	---	---	---	---

GROUP 6: LO₂/RP-1 HIGH-VELOCITY-IMPACT TESTS

No Tests Read in This Group

PYRO TEST NO.	DISTANCE TO CAMERA (FT)	BEARING		FREQUENCY OF TIMING MARKS (TM/SEC)	FILM SPEED		NO. OF FRAGMENTS RECORDED	NO. OF DUPLICATE FRAGMENTS
		GIVEN	ASSUMED (DEG)		GIVEN	CALCULATED (PPS)		
50	420	0	0	120	1000	1157	2	0
	420	270	240	120	1000	1107	3	0
51	420	0	0	120	1000	1090	4	0
	420	270	240	120	1000	1200	5	0
52	420	0	0	120	1000	1066	5	0
	420	270	240	120	1000	1048	12	0
53	420	270	240	120	1000	1196	16	0
	420	0	0	120	1000	1185	13	0
54	420	0	0	120	1000	1156	17	0
	420	270	240	120	1000	1269	9	0
55	420	0	0	120	1000	1076	9	0
	420	---	240	120	---	1162	9	0
56 ³	420	0	0	120	1000	1200	10	0
	420	270	240	120	1000	1282	5	0
57	420	0	0	120	1000	1192	16	0
	420	270	240	120	1000	1237	11	0
90	420	0	0	120	64	NR	7	0
91	420	0	0	120	1000	960	6	0
	420	270	240	120	1000	NR	6	0
93	420	0	0	120	1000	1029	4	0
94	420	0	0	120	1000	1082	5	0
118	---	---	240	120	1000	971	6	1
	---	---	0	120	1000	862	3	0
172	---	---	240	120	1000	679	5	0
	---	---	240	120	1000	888	2	0
	---	---	0	120	64	70	4	0
	---	---	---	100	1000	985	2	0

GROUP 7: LO₂/LH₂ CONFINEMENT-BY-THE-MISSILE TESTS

PYRO TEST NO.	DISTANCE TO CAMERA (FT.)	BEARING		FREQUENCY OF TIMING MARKS (TM/SEC)	FILM SPEED		NO. OF FRAGMENTS RECORDED	NO. OF DUPLICATE FRAGMENTS
		GIVEN	ASSUMED (DEG)		GIVEN	CALCU- LATED (PPS)		
Group 7 (Cont'd) -								
199	420	270	240	120	1000	949	6	0
	420	0	0	120	400	399	5	0
200	420	270	240	120	1000	895	11	0
	420	0	0	120	400	398	15	0
210	420	270	240	120	1000	NR	9	0
	420	0	0	120	400	NR	4	0
212	420	270	240	120	1000	NR	1	0
	420	0	0	120	400	NR	7	0
213	420	270	240	120	1000	730	4	0
	420	0	0	120	400	392	9	0
265	420	270	240	120	1000	993	1	0
	420	0	0	120	400	394	13	0
	1000	300	340	120	400	375	14	2
279	420	130	240	120	4000	2497	4	0
	420	325	0	120	1000	1127	5	0
	1000	340	340	120 ⁵	400	184	3	0
	1000	340	340	10	64	NR	4	0

GROUP 8: LO₂/LH₂ CONFINEMENT BY-THE-GROUND-SURFACE VERTICAL TESTS

103A	420	270	240	120	1000	1432	6	0
	420	0	0	120	64	NR	2	0
106A ³	420	0	0	120	400	NR	6	0
	420	270	240	120	1000	1494	6	0
114	---	---	240	---	---	1359	7	0
	---	---	0	---	---	400	10	0
115	---	---	240	---	---	1225	4	0
	---	---	0	---	---	324	10	0

PYRO TEST NO.	DISTANCE		BEARING		FREQUENCY OF TIMING MARKS (TM/SEC)	FILM SPEED		NO. OF FRAGMENTS RECORDED	NO. OF DUPLICATE FRAGMENTS
	TO CAMERA (FT)	GIVEN	GIVEN	DEG)		GIVEN	CALCU- LATED (PPS)		
Group 8 (cont'd) -									
152	420	0	270	0	120	400	393	7	0
	420	270	0	240	120	1000	1046	7	0
160	420	0	0	0	120	400	399	9	0
	420	270	0	240	120	1000	1170	9	1
184	---	270	0	240	120	1000	928	8	0
	---	0	0	0	120	400	399	8	0
195	420	270	0	240	120	1000	1109	6	0
	420	0	0	0	120	64	72	6	0
197	420	270	0	240	120	1000	1101	7	0
	420	0	0	0	120	400	393	11	0
201	420	270	0	240	120	1000	1192	3	0
	420	0	0	0	120	400	392	3	0
204	420	270	0	240	120	1000	1048	5	0
	420	0	0	0	120	400	403	12	0
211	420	270	0	240	120	1000	1091	6	0
	420	0	0	0	120	400	398	11	0
217	---	---	---	240	---	---	1071	2	0
	---	---	---	0	---	---	64	5	0
226	420	0	0	0	120	400	396	5	0
230	420	270	0	240	120	1000	1098	10	0
	420	0	0	0	120	400	396	11	0
260	420	270	0	240	120	1000	1239	5	0
	420	0	0	0	120	400	400	8	0
	1000	300	0	340	120	400	395	6	0
288C	---	---	---	0	100	1000	1221	6	0
	---	---	---	340	120 ^S	400	377	14	0
	---	---	---	---	120	400	NR	6	0
	---	---	---	---	120	400	393	4	0
289A	---	---	---	0	120	1000	1097	8	0

PYRO TEST NO.	DISTANCE		BEARING		FREQUENCY OF TIMING MARKS (TM/SEC)	FILM SPEED		NO. OF FRAGMENTS RECORDED	NO. OF DUPLICATE FRAGMENTS
	TO CAMERA (FT)		GIVEN	ASSUMED (DEG)		GIVEN (PPS)	CALCU- LATED		
Group 8 (Cont'd) -									
	---		---	240	120	1000	1217	16	0
	---		---	340	60	400	NR	16	0
	---		---		120	400	NR	23	0
	---		---		120	400	NR	12	0
	---		---	240	120	1000	1173	8	0
290	---		---	340	---	---	403(EST)	15	0
	---		---	0	---	1000	1067	9	0
	---		---		120	400	371	9	0
	---		---		120	400	391	4	0
	---		---		120	400	1207	4	0
	---		---	240	120	1000	1315	5	1
291B ³	---		---	340	120 ⁶	64	400	5	0
	---		---	340	60	400	400	10	0
	---		---	0	120	1000	1180	9	0
293 ³	---		---	240	120	1000	1181	9	0
	---		---	340	120 ⁵	400	394	7	0

GROUP 9: LO₂/LH₂ CONFINEMENT-BY-THE-GROUND-SURFACE HORIZONTAL TESTS

131	---		---	240	120	800	1010	13	0
	---		---	0	120	400	394	10	0
133	---		---	240	120	500	1091	6	0
	---		---	0	120	400	398	9	0
186	---		---	240	120	1000	1063	5	0
	---		---	0	120	400	399	6	0
196	420		---	240	120	1000	1124	4	1
	420		---	0	120	400	402	9	0
228	420		---	240	120	1000	1300	6	0
	420		---	0	120	400	396	6	0

PYRO TEST NO.	DISTANCE TO CAMERA (FT.)		BEARING		FREQUENCY OF TIMING MARKS (TM/SEC)	FILM SPEED		NO. OF FRAGMENTS RECORDED	NO. OF DUPLICATE FRAGMENTS
	GIVEN	ASSUMED (DEG)	GIVEN	CALCULATED (PPS)					
GROUP 10: LO ₂ /LH ₂ SPECIAL TESTS									
169	420	0	0	120	1000	399	4	0	
	420	270	240	120	1000	882	3	0	
173	---	---	0	120	400	399	9	0	
	---	---	240	120	1000	802	7	0	
233	420	270	240	120	1000	1332	6	0	
	420	0	0	120	400	396	8	0	
GROUP 11: LO ₂ /LH ₂ AND LO ₂ /RP-1 COMBINED SPECIAL TESTS (SCALED TWO-STAGE VEHICLE)									
294 ³	---	---	0	120	1000	1021	8	0	
	---	---	240	120	1000	1330	5	0	
	---	---	0	10	64	NR	7	0	
	---	---	340	60	400	NR	8	0	
295	---	---	0	120	1000	1078	5	0	
	---	---	0	10	64	NR	3	0	

GROUP 12: CLOSE-IN BLAST DATA

No Tests in This Group

PYRO TEST NO.	DISTANCE TO CAMERA (FT)	BEARING		FREQUENCY OF TIMING MARKS (TM/SEC)	FILM SPEED		NO. OF FRAGMENTS RECORDED	NO. OF DUPLICATE FRAGMENTS
		GIVEN	ASSUMED (DEG)		GIVEN (PPS)	CALCU- LATED		
62	1000	---	340	120	64	73	4	0
	420	270	240	120	1000	1127	6	0
	420	---	0	---	1000	1162	26	0

SATURN IV TEST

- 1 Number Assigned for Data Processing Purposes
- 2 Unable to Read Timing Marks So Given Value Was Used
- 3 Tests Were Not Identified By Groups But Were Placed in Groups Which Seemed Appropriate
- 4 Information Not Given on Film Or On Film Can
- 5 TM Frequency of 60 Was Given. But 60 Was Obviously Too Low And So 120 Was Used
- 6 TM Frequency of 10 Was Given. But 10 Was Obviously Too Low And So 120 Was Used
- 7 Timing Marks Definitely Not What Was Given

APPENDIX C

MODEL ANALYSES FOR FRAGMENT VELOCITIES, RANGE, ETC., FOR BURSTING LIQUID PROPELLANT VESSELS

In an attempt to facilitate comparisons of the data which have been unearthed during this study, let us conduct several limited model analyses relating to various aspects of the problem. To avoid too complex model laws, we will divide the problems into several subproblems.

Initial Velocities for CBM Case

Consider first the bursting and acceleration of vessel fragments by an internal explosion (CBM case). A list of physical parameters appropriate to this case and part of the problem are given in Table C1, with dimensions in a Force-Length-Time (FLT) system. The twenty-one parameters in Table C1 can be combined into eighteen dimensionless groups (Pi terms) by the methods of dimensional analysis. One such grouping is given in Table C2, based on mass of propellant, heat of explosion of propellant, and a characteristic length as repeating variables. Table C2 includes descriptions of the pi terms.

The dependent variables in Table C2 are essentially π_{13} , π_{14} , π_{16} , and π_{17} . Terms π_1 through π_5 are mass or density ratios, and terms π_6 through π_{11} require geometric similarity. Term π_{12} dictates scaling of energy release, and is equivalent to fractional blast yield y . Term π_{15} can be considered as a ratio of vessel burst pressure p_v to the pressure which would be generated by contained reaction of all of the mass of propellant. Finally, π_{18} requires identical equation of state for the reaction products of the exploding propellant.

The model law in Table C2 can be expressed in functional form as

$$\begin{aligned} & \left[(U_f/H_e^{1/2}), (pL^3/M_t H_e), (tH_e^{1/2}/L), n \right] \\ & = \left[\text{Density ratios, Geom. sim., } (E/M_t H_e), \right. \\ & \quad \left. (p_v L^3/M_t H_e), \kappa \right] \end{aligned} \tag{C1}$$

If we confine our comparisons to tests with geometrically similar tanks made of the same materials and filled with the same propellant mixtures, then the density ratio terms and terms describing geometric similarity will all be the

TABLE C1 - PHYSICAL PARAMETERS FOR VESSEL BURST
BY INTERNAL EXPLOSION

Symbol	Dimensions	Parameter
M_v	FT^2L^{-1}	Total mass of vessel
M_t	FT^2L^{-1}	Total mass of propellant
M_r	FT^2L^{-1}	Reactive mass of propellant
E	FL	Energy release during explosion (blast yield)
H_e	L^2T^{-2}	Heat of explosion of propellant mixture
D	L	Tank diameter
L	L	Tank length
D_o	L	Diameter of internal bulk-head rupture area
h_v	L	Thickness of vessel material
ρ_p	FT^2L^{-4}	Density of propellant
ρ_v	FT^2L^{-4}	Density of vessel material
n	---	Number of fragments
M_f	FT^2L^{-1}	Mass of individual fragments
A_f	L^2	Mean presented area of individual fragments
U_f	LT^{-1}	Velocity of individual fragment
V_v	L^3	Internal volume of tank
V_u	L^3	Ullage volume of tank
κ	---	Ratio of specific heats for explosion products
P	FL^{-2}	Pressure within tank during explosion
t	T	Time
P_c	FL^{-2}	Burst pressure of vessel

TABLE C2 - DIMENSIONLESS GROUPS FOR VESSEL BURST
BY INTERNAL EXPLOSION

Number	Term	Description
π_1	M_v/M_t	Mass or density ratios
π_2	M_r/M_t	
π_3	M_f/M_t	
π_4	$\rho_p L^3/M_t$	
π_5	$\rho_v L^3/M_t$	
π_6	D/L	Geometric similarity
π_7	D_o/L	
π_8	h_v/L	
π_9	A_f/L^2	
π_{10}	V_u/L^3	
π_{11}	V_v/L^3	Energy scaling
π_{12}	$E/M_t H_o$	
π_{13}	$U_f/H_o^{1/2}$	Velocity scaling
π_{14}	$p_l^3/M_t H_o$	Pressure scaling
π_{15}	$p_v L^3/M_t H_o$	
π_{16}	$t H_o^{1/2}$	Time scaling
π_{17}	n	Number of fragments
π_{18}	λ	Ratio of specific heats

same independent of scale, $\lambda_L^3 = \lambda_{M_t}$, and κ will not change. * Also, the burst pressures p_v for geometrically similar vessels of the same material are identical ($\lambda p_v = 1$). Because we are using the same propellant, $\lambda_{H_e} = 1$. Under these restricted conditions, Equation C1 reduces to**

$$\left[U_f, p, (t/L), n \right] = f(y) \quad (C2)$$

In other words, Equation (C2) says that initial fragment velocity, pressure rise within tank prior to rupture, time scaled proportional to length, and number of fragments generated should all be functions of fractional yield.

Many other interpretations can be made of this law. If we do not make the simplifying assumptions above, then we may be able to compare some test results for different propellants. Terms π_{12} and π_{13} can be combined to form:

$$\pi'_{12} = U_f^2 M_t / E \quad (C3)$$

which can replace π_{12} in Equation (C1).

This term defines an equivalent dimensional group

$$G'_{12} = U_f^2 W_t / Y \quad (C4)$$

where W_t is total weight of propellant and Y is blast yield in percent. We have recorded most of our fragmentation data in terms of these quantities, and so can plot G'_{12} , or its square root, versus Y (equivalent to π_{12}) or against π_{15} , provided we use a consistent set of units. It is quite likely that κ is only weakly dependent on type of propellant, so perhaps we can ignore it. The model law does point out that (D/L) and (D/D_0) are potentially important geometric ratios, and that mean fragment area may scale as the square of the length scale.

Initial Velocities for CEGS and HVI Cases

In this case, the propellants spill, mix on the ground, and then ignite or the missile impacts the ground at high velocity. Solid objects and nearby

*The symbol λ denotes a scale factor, and a subscript letter denotes the physical parameter being scaled.

**Note that these products are not now nondimensional, because we have deleted dimensional terms which do not change.

appurtenances are then accelerated by the resultant blast wave to some maximum velocity ("initial" velocity). The pertinent physical parameters are somewhat different than for the CBM case. Geometry of the vessel is no longer important, but gravity and impact velocity must be considered. A list is given in Table C3. Again using as repeating variables M_t , H_0 and L , we obtain a group of fifteen pi terms from the eighteen physical parameters. These are given in Table C4.

Many of the terms in Table C4 can be seen to be identical to those in Table C2. These include the mass ratios π_1 through π_3 , area ratio π_4 , volume ratio π_7 , scaling for fragment velocity π_9 , energy scaling π_{10} , pressure scaling π_{12} , time scaling π_{14} , and number of fragments π_{15} . The terms which are new are π_5 , π_6 , π_8 , π_{11} , and π_{13} , and some terms in Table C2 do not appear. This model law can be expressed as:

$$\begin{aligned} & \left[(U_{fi}/H_0^{1/2}), (pL^3/M_t H_0), (qL^3/M_t H_0), (tH_0^{1/2}/L), (A_{fi}/L^2), n \right] \\ & = f \left[\text{Density ratios, Geom. sim., } (E/M_t H_0), C_{Di}, (U_i/H_0^{1/2}), \right. \\ & \quad \left. (gL/H_0) \right] \end{aligned} \quad (C5)$$

The term π_{11} , if strictly adhered to during tests of the same propellant, would prevent comparison of tests conducted at different geometric scales, because $\lambda_g = 1$, $\lambda_{H_0} = 1$, and therefore $\lambda_L = 1$.

If we deliberately let this term go out of scale, which is equivalent to ignoring gravity effects, then almost the same model law as for the CBM case results, with the addition of a requirement of scaling of impact velocity from π_8 . If we assume that we cannot ignore effect of gravity on such physical processes as spreading and intermingling of the fuel and oxidiser after spill, initial trajectory of fragments, etc., then Equation (C5) requires a change in heat of explosion H_0 in order to change length scale. It is suggested that we simply try plotting fragment velocities from CBGS data versus blast yield for the same propellant. We know from the PYRO work that blast yield is a function of impact velocity V_i , so term π_8 may be already accommodated by measuring blast yield. An alternative might be to plot the term

$$\pi'_9 = V_{fi} / \sqrt{gL} \quad (C6)$$

versus blast yield for the same propellant. Correlation here would indicate that gravity effects were indeed important.

TABLE C3 - PHYSICAL PARAMETERS FOR FRAGMENT ACCELERATION
AFTER SPILL AND EXPLOSION

Symbol	Dimensions	Parameter
M_v	FT^2L^{-1}	Total mass of vessel
M_t	FT^2L^{-1}	Total mass of propellant
M_r	FT^2L^{-1}	Reactive mass of propellant
M_{fi}	FT^2L^{-1}	Mass of the solid body or appurtenance
E	FL	Energy release during explosion
H_e	L^2T^{-2}	Heat of explosion of propellant
V_p	L^3	Volume of propellant
U_i	LT^{-1}	Impact velocity
g	LT^{-2}	Acceleration of gravity
l_i	---	Length ratios
L	L	Characteristic length
n	---	Number of fragments
A_{fi}	L^2	Mean presented area of i^{th} solid body or appurtenance
U_{fi}	LT^{-1}	Velocity of same
C_{Di}	---	Drag coefficient of same
p	FL^{-2}	Overpressure in blast wave
q	FL^{-2}	Dynamic pressure in blast wave
t	T	Time

TABLE C4 - DIMENSIONLESS GROUPS FOR FRAGMENT
ACCELERATION AFTER SPILL

Number	Term	Description
π_1	M_v/M_t	Mass ratios
π_2	\dots/M_t	
π_3	M_{fi}/M_t	
π_4	A_{fi}/L^2	Geometry
π_5	l_i	
π_6	C_{Di}	
π_7	V_p/L^3	Volume ratio
π_8	$V_i/H_e^{1/2}$	Velocity scaling
π_9	$U_{fi}/H_e^{1/2}$	
π_{10}	$E/M_t H_e$	Energy scaling
π_{11}	gL/H_e	Gravity scaling
π_{12}	$pL^3/M_t H_e$	Pressure scaling
π_{13}	$qL^3/M_t H_e$	
π_{14}	$tH_e^{1/2}/L$	Time scaling
π_{15}	n	Number of fragments

Trajectories of Fragments in Free Flight

After the fragments have been accelerated to their maximum velocities, then the problem is one of exterior ballistics for each fragment. Most of the parameters governing the resulting trajectories differ from those in the previous problems. They are listed in Table C5, and a possible set of pi terms is given in Table C6.

The first four pi terms in Table C6 are initial conditions, π_5 and π_6 are aerodynamic coefficients, and π_4 through π_{10} specify geometric similarity. Term π_9 can also be considered as the dependent variable. Term π_{11} specifies gravity scaling, which is essential in trajectory problems and cannot be ignored. Terms π_{12} and π_{13} are wind velocity and air density scaling, respectively. The model law can be written as:

$$(R_f/L) = f \left[(U_f t/L), (\omega_f t), \theta_f, \psi_f, C_{D_f}, C_{L_f}, (A_f/L^2), (x_{if}/L), l_i, (gt^2/L), (U_w t/L), (\rho_a L^3/M_f) \right] \quad (C7)$$

From our physical knowledge of exterior ballistics and the problem of fragment scatter, we can considerably reduce this function space. Range may be dependent on azimuth angle ψ and scaled wind velocity $(U_w t/L)$, but this dependence is weak for high velocity and "chunky" fragments. Furthermore, our data from missile maps average ranges over all azimuths, so this dependence is not considered. The "lifting" characteristics of the fragments are represented by C_{L_f} and by initial spin $\omega_f t$. Again, these characteristics represent random and uncontrolled quantities which we cannot assess, so we again ignore them. A reduced form for Equation (C7) is then

$$(R_f/L) = f \left[(U_f t/L), \theta_f, C_{D_f}, (A_f/L^2), (x_{if}/L), l_i, (gt^2/L), (\rho_a L^3/M_f) \right] \quad (C8)$$

Of these remaining parameters, the first two and the fifth are scaled initial conditions. The drag coefficient is a function of (A_f/L^2) and l_i and is therefore superfluous. So, for fragments of similar geometry and same scaled initial conditions, the law further reduces to

$$(R_f/r) = f \left[(U_f t/L), (gt^2/L), (\rho_a L^3/M_f) \right] \quad (C9)$$

TABLE C5 - PHYSICAL PARAMETERS FOR
FRAGMENT TRAJECTORIES

Symbol	Dimensions	Parameter
U_f	LT^{-1}	Initial linear velocity
ω_f	T^{-1}	Initial angular velocity
C_{Df}	---	Drag coefficient
C_{Lf}	---	Lift coefficient
A_f	L^2	Mean presented area
M_f	FT^2L^{-1}	Mass of fragment
θ_f	---	Initial elevation angle
ψ_f	---	Initial azimuth angle
x_{if}	L	Initial coordinates of fragment
R_f	L	Range of fragment
g	LT^{-2}	Acceleration of gravity
ρ_a	FT^2L^{-4}	Density of air
l_i	---	Length ratios
U_w	LT^{-1}	Wind velocity
t	T	Time
L	L	A characteristic length

TABLE C6 - DIMENSIONLESS GROUPS FOR
FRAGMENT TRAJECTORIES

Number	Term	Description
π_1	$U_f t/L$	Initial Conditions
π_2	$\omega_f t$	
π_3	θ_f	
π_4	ψ_f	
π_5	C_{D_f}	Aerodynamic Coefficients
π_6	C_{L_f}	
π_7	A_f/L^2	
π_8	x_{if}/L	Geometric Similarity
π_9	R_f/L	
π_{10}	l_1	
π_{11}	gt^2/L	Gravity Scaling
π_{12}	$U_w t/L$	Velocity Scaling
π_{13}	$\rho_a L^3/M_f$	Density Scaling

Now, because $\lambda_g = 1$, π_{11} requires that

$$\lambda_t^2 = \lambda_L \quad (C10)$$

The first term in Equation (C9) then requires that

$$\lambda_{U_f} \lambda_L^{1/2} = \lambda_L,$$

or

$$\lambda_{U_f} = \lambda_L^{1/2} \quad (C11)$$

i. e., initial velocities should scale as the square root of the length scale for the same scaled range. The third term is automatically satisfied because $\lambda_{\rho_a} = 1$ and $\lambda_L^3 = \lambda_{M_f}$.

We can combine π_7 and π_{13} to form

$$\pi_7' = A_f \rho_a^{2/3} / M_f^{2/3} \quad (C12)$$

Because $\lambda_{\rho_a} = 1$, a dimensional form of this term is

$$G_7' = A_f / W_f^{2/3} \quad (C13)$$

where W_f is weight of fragment.

This may provide a rational grouping for plotting versus scaled range.

APPENDIX D

COMPUTER PROGRAM ENTITLED /W2/ IN FORTRAN IV

Function: This program computes initial fragment velocity.

Given the following input data:

A) Characteristics of some explosive fuel-oxidizer gas mixture at moment $t = 0$ of detonation.

(CAP1) Ratio of specific heats, κ

(AO) Speed of sound in medium in in./sec

(PØ) Initial pressure in psi

B) Characteristics of containing vessel

(RR) Internal radius of vessel + unburned fuel in inches

(TM) Mass of vessel + unburned fuel in lb/sec²/in.

(FN) No. of fragments

C) Calculatory requirements

(AH) Time interval of each calculation in seconds

(XMAX) Maximum time to last calculation in seconds

Variables: The definition and units of the variables in this program are given in the following table.

TABLE (D-1)

Program Variable	Variable	Definition	Units
FF	F	projected fragment area	in. ²
CAP1	κ	specific heat ratio for explosive mixture	none
AO	a_o	speed of sound in explosive products mixture	in/sec

<u>Program Variable</u>	<u>Variable</u>	<u>Definition</u>	<u>Units</u>
PO	P_{oc}	initial pressure after explosion	psi
FN	n	number of fragments	none
RR	R	radius of explosive products mixture	in.
TM	M_t	mass of shell + unexploded fuel	lb-in ² /sec
FK		coefficient	none
AH		time interval	sec
XMAX		maximum time	sec
FN1		if ≤ 1 displays T-NORM G, G', G''	none
FN2		if ≤ 1 displays normal pressure + time	none
FN3		if ≤ 1 calculates maximum range	none
G1	u_f	distance to initial velocity	in.
G2		initial fragment velocity	ft/sec
G3		initial fragment acceleration	in/sec ²
G4		final explosive product mixture pressure	psi
T1		time to initial velocity	sec
JJ		counting variables	none
PI		the constant π	none
CAP2		the quantity $(1 - \kappa)/\kappa$	none
CAP3		the quantity $-1/\kappa$	none
CAP4		the quantity $(3\kappa - 1)/2\kappa$	none
XX		displacement normalization coefficient (see Eq. -35)	in.

<u>Program Variable</u>	<u>Variable</u>	<u>Definition</u>	<u>Units</u>
THETA		time normalization coefficient (see Eq. -35)	sec
A1	α	the coefficient α (Eq. -36)	none
B1	β	the coefficient β (Eq. -36)	none
C \emptyset		normalized initial fragment displacement from center of sphere	none
X		normalized time	none
Y(2)		normalized velocity	none
Y(3)		normalized pressure	none
Y(1)		normalized fragment displacement	none
NA		number of differential equations to be solved	none
F(1), F(2), F(3)		differential equations solved (see Eqs. -34 and -36)	none
TT		normalized time	none
PS		normalized pressure	none

The subprogram entitled (RUNGE) is described in the following:

FORTRAN IV

RUNGE - KUTTA

FILE NAME: F16

SUBROUTINE NAME: RUNGE

PURPOSE: This subroutine employs the Fourth Order Runge Kutta Method to solve N simultaneous first-order ordinary differential equations by calculating successive values of Y according to the formula:

$$Y_{i+1} = Y_i + \frac{h}{6} (K_1 + 2K_2 + 2K_3 + K_4)$$

where $K_1 = f(x_i, Y_i)$

$$K_2 = f(x_i + \frac{h}{2}, y_i + \frac{hK_1}{2})$$

$$K_3 = f(x_i + \frac{h}{2}, y_i + \frac{hK_2}{2})$$

$$K_4 = f(x_i + h, y_i + hK_3)$$

METHOD:

The subroutine is called by the calling program five times in order to approximate successive Y(I)'s; the first time to initialize, the second time to calculate K₁(I), the third time to calculate K₂(I), the fourth time to calculate K₃(I) and the fifth time to calculate K₄(I). In addition, each time the subroutine is called, it calculates a new Y(I) and a new X(I) which are returned to the calling program where the functions (first-order differential equations) are evaluated with the new X(I) and Y(I). These values of the function are then returned to the subroutine where they are used as K₁(I), K₂(I), K₃(I), or K₄(I) and appropriately accumulated to obtain Y_{i+1}(I) in the 5 calls to the subroutine.

ARGUMENTS:

The subroutine RUNGE uses nine arguments: N, Y, F, X, H, M, SAVEY, PHI, K

1. The first argument, N, represents the number of simultaneous first-order ordinary differential equations to be solved.
2. The second argument, Y, is the array name which the calling program uses to transmit the initial Y(I) values for each differential equation. Upon completion of the 5 calls to RUNGE, Y(I) will contain the new approximated values for the Y_{i+1}(I)'s.

3. The third argument, F, is the array which contains the current values of the differential equations calculated by the main program, i. e., F(J) contains the value of the Jth first-order differential equation.
4. The fourth argument, X, represents the independent variable which should be initialized in the main program before calling RUNGE. RUNGE increments X by the stepsize H.
5. The fifth argument, H, represents the step size for X.
6. The sixth argument, M, indicates which of the five passes of the subroutine is to be executed. The main program must initialize this argument as 1. RUNGE then successively increments the variable by 1 up to 5.
7. The seventh argument, SAVEY, is used within RUNGE and must be dimensioned in the calling program to be of size N.
8. The eighth argument, PHI, is also used internally by RUNGE, but must be dimensioned in the calling program to be of size N.
9. The ninth argument, K, is manipulated within RUNGE. K should be tested right after the call to RUNGE, in the calling program.

When K=1, control should transfer to a set of code in the calling program which calculates new values for the first-order differential equations, F(I), with the current values of X and Y(I). Then RUNGE should be called again.

When K=2, the approximation for Y(I) is completed. Values for the $Y_{i+1}(I)$'s are stored in Y(I) at this time, and normal flow of the calling program should resume.

LIMITATIONS
AND
COMMENTS:

1. The calling program must dimension SAVEY and PHI.
2. The calling program must set M=1 before calling RUNGE.
3. The calling program must set up the N first-order differential equation values in an array F to be passed through to RUNGE when the subroutine returns with K=1.
4. The calling program must set up separate arrays if all X and Y values for the set of differential equations are to be saved, perhaps for plotting purposes.

PROGRAM /W2/ LISTING

```

DIMENSION F(3),Y(3),V1(3),V2(3),PS(50),TT(50)
300 FORMAT (2/,20H READ IN TRAJ. ANGLE)
3001 FORMAT (E10.3)
301 FORMAT (2/,35H READ IN DRAG COEF. AND AIR DENSITY)
3011 FORMAT (2E10.3)
302 FORMAT (2/,25H READ IN FRAGMENT MASS COEF.)
303 FORMAT (4/,25H CONDITIONS ON TRAJECTORY)
304 FORMAT (/,21H AMBIENT AIR DENSITY=,E10.3,17H LBS./CUBIC FT.)
305 FORMAT (/,16H AIR DRAG COEF.=,E10.3)
306 FORMAT (/21H FRAGMENT MASS COEF.=,E10.3)
307 FORMAT (/,18H TRAJECTORY ANGLE=,E10.3,8H DEGREES)
3071 FORMAT (3/,9H CHECK C=,E10.3)
308 FORMAT (3/,15H MAXIMUM RANGE=,E10.3,4H FT.)
309 FORMAT (2/,45H READ IN KAPPA, SOUND SPEED, INITIAL PRESSURE)
310 FORMAT (3E10.5)
311 FORMAT (2/,78H READ IN NO. OF FRAGMENTS, RADIUS OF EXPL.,
MASS OF SHELL-FUEL, DISCHARGE COEF.)
312 FORMAT (4E10.3)
313 FORMAT (2/,36H READ IN TIME INTERVAL, MAXIMUM TIME)
314 FORMAT (2E10.3)
315 FORMAT (3/,20H GAS CHARACTERISTICS,/,7H KAPPA=,E10.3,
15H SOUND SPEED=,E10.5,7H IN/SEC,/,10H PRESSURE ,E10.3,4H PSI,
2/,23H VESSEL CHARACTERISTICS,/,5H RADIUS=,E10.3,5H INS.,
8H MASS=,E10.3,17H LBS.-SEC.SQ./IN,/,18H NO. OF FRAGMENTS=,E10.3,2/)
316 FORMAT (2/,33H DISPLAY DYNAMIC VAR.? YES=1 NO=2)
317 FORMAT (2/,33H DISPLAY NORM. PRESS.? YES=1 NO=2)
318 FORMAT (2/,35H TAKE RANGE CALCULATION? YES=1 NO=2)
319 FORMAT (3/,11H FINAL VALUES,/,5H TIME=,E10.3,4H SEC,/,
10H DISTANCE=,E10.3,4H INS,/,10H VELOCITY=,E10.3,7H FT/SEC,/,
14H ACCELERATION=,E10.3,10H 1/SG-SEC,/,10H PRESSURE=, E10.3,
4H PSI)
320 FORMAT (3/,21H CHARACTERISTICS OF MOTION OF FRAGMENTS (NORMALIZED)
,2/,10H T=TIME,4H INS,10H,2HG,7H,14H,/)
321 FORMAT (2/,21H PRESSURE (NORMALIZED),/,4H,7H T-NORM, 1,
6HP-NORM,/)
322 FORMAT (10H INITIAL CONDITIONS,/,6H K(0)=,E10.4,7H C(0)=,E10.4,8H
V(0)=,E10.4,9H P-NORM=,E10.4,2/)
JJ=0
WRITE (1,310)
READ (0,310) CAPI,AD,PA
WRITE (1,311)
READ (0,312) FN,RR, TM,FK
WRITE (1,313)
READ (0,314) AH,XMAX
WRITE (1,316)
READ (0,3001) FN1
WRITE (1,317)
READ (0,3001) FN2
WRITE (1,318)
READ (0,3001) FN3
WRITE (1,315) CAPI,AD,PA,RR, TM,FK
PI= 3.1415926535
FF=4.0*PI*(RR**2.00)*((1/FN)-(1/FN**2.0))
XX=TM*(AH**2.0)*(2.0/(CAPI-1))/(FF*PA)
THETA=TM*AH*(2.0/(CAPI-1.0)**0.5)/(FF*PA)
CAP2=(1.00-CAPI)/CAPI
CAP3=-1.0/CAP2

```

```

CAP4=(3.0*CAP1-(1.0))/(2.0*CAP1)
AI=3.0*FK*CAP1*((2.0/(CAP1+1.0))**((CAP1+1.0)/(2.0*(CAP1-1.0))))*((2.0/
CAP1-1.0)**0.5)
BI=((RR)**2.0)*((2.0/(CAP1-1.0))**2.0)*((FF*P1)**2.0)/((TM**2.0)*(A2**4
0))
C0=RR/XX
X=0.0
Y(1)=C0
Y(2)=0.0
Y(3)=1.0
WRITE (1,322) X,Y(1),Y(2),Y(3)
NA=3
F(1)=Y(2)
F(2)=FN*Y(3)*((1.00-(Y(2)**2.0)*(Y(3)**CAP2))**CAP3)
F(3)=((Y(1)**-3.0)*(Y(3)**CAP4)*(AI*BI-AI*(Y(1)**2.0)))-3.0*CAP1*(Y(2)*Y
3)/Y(1))
IF (FN1-1.0) 200,200,30
200 WRITE (1,320)
30 CALL RUNGE (NA,X,Y,F,AH,KA,"1,W2)
IF (KA-1) 40,50,40
50 F(1)=Y(2)
F(2)=F(1)*Y(3)*((1.00-(Y(2)**2.0)*(Y(3)**CAP2))**CAP3)
F(3)=((Y(1)**-3.0)*(Y(3)**CAP4)*(AI*BI-AI*(Y(1)**2.0)))-3.0*CAP1*(Y(2)*
3)/Y(1))
G0 T0 30
40 IF (FN1-1.0)45,45,201
45 WRITE (1,312) X,Y(1),Y(2),F(2)
201 CONTINUE
JJ=JJ+1
TT(JJ)=X
PS(JJ)=Y(3)
IF (X-XMAX) 41,10,10
41 CONTINUE
G0 T0 30
10 CONTINUE
IF (FN2-1.0) 202,202,203
202 WRITE (1,321)
WRITE (1,3011) (TT(I),PS(I),I=1,JJ)
203 CONTINUE
T1=THETA*X
G1=XX*Y(1)-XX*C0
G2=XX/THETA*(Y(2))
G2=G2/12.0
G3=(XX/(THETA)**2.0)*F(2)
G4=P0*Y(3)
WRITE (1,319)T1,G1,G2,G3,G4
IF (FN3-1.0) 204,204,205
204 CONTINUE
205 CONTINUE
END

```

A SAMPLE RUN OF /W2/

FIN

READ IN KAPPA, SOUND SPEED, INITIAL PRESSURE
1.4, 13520., 8000.

READ IN NO. OF FRAGMENTS, RADIUS OF EXPLO., MASS OF SHELL-FUEL, DISCHARGE
COEFF.
10 ., 27., .445, 1.0

READ IN TIME INTERVAL, MAXIMUM TIME
5.1E-03, 4.5E-02

DISPLAY DYNAMIC VAR.? YES=1 NO=2
1

DISPLAY NORM. PRESS.? YES=1 NO=2
1

TAKE RANGE CALCULATION? YES=1 NO=2
2

GAS CHARACTERISTICS
KAPPA= .140E+01 SOUND SPEED=.13520E+04 IN/SEC
PRESSURE= .800E+04 PSI

VESSEL CHARACTERISTICS
RADIUS= .270E+02 INS. MASS= .445E+00 LBS.-SEC.SQ./IN.
NO. OF FRAGMENTS= .110E+03

INITIAL CONDITIONS
K(0)= .0000E+01 S(0)= .4817E-01 G(0)= .0000E+01 P-NORM= .1000E+01

CHARACTERISTICS OF MOTION OF FRAGMENTS (NORMALIZED)

T-INT	R	G'	S''
.000E-02	.473E-01	.392E+00	.467E+02
.100E-01	.517E-01	.543E+00	.166E+02
.150E-01	.546E-01	.600E+00	.632E+01
.20E-01	.576E-01	.633E+00	.262E+01
.250E-01	.606E-01	.632E+00	.117E+01
.300E-01	.632E-01	.636E+00	.401E+00
.350E-01	.671E-01	.637E+00	.124E+00
.400E-01	.703E-01	.638E+00	.275E-01
.450E-01	.735E-01	.638E+00	.297E-02
.500E-01	.767E-01	.638E+00	.144E-04

PRESSURE (NORMALIZED)

T-NORM P-NORM

.500E-02	.902E+00
.100E-01	.706E+00
.150E-01	.516E+00
.200E-01	.357E+00
.250E-01	.258E+00
.300E-01	.181E+00
.350E-01	.127E+00
.400E-01	.907E-01
.450E-01	.650E-01
.500E-01	.474E-01

FINAL VALUES

TIME= .927E-03 SEC

DISTANCE= .160E+02 INS

VELOCITY= .161E+04 FT/SEC

ACCELERATION= .235E+02 IN/SQ-SEC

PRESSURE= .379E+03 PSI

APPENDIX E

COMPUTER PROGRAM ENTITLED /ROOT/ IN FORTRAN IV

Function: This program computes the root to the equation

$$E = \frac{P_{oo} V}{\kappa - 1} \left[\frac{P_o}{P_{oo}} - \left(\frac{P_o}{P_{oo}} \right)^{1/\kappa} \right]$$

(see Section II. C) for the following input data:

- (EN) Energy of explosion of reactants ft-lb
 (VØ) Volume of reactants in³

Variables: The definition and units of the variables in this program are given in the following table.

Program Variable	Variable	Definition	Units
XK	κ	specific heats ratio	
P	P_{oo}	ambient pressure	psi
A, B, C		coefficients of the polynomial $A P_o - B P_o^{1/K} - C = 0$	
EN	E	Energy of explosion of reactants	ft-lb
VO	V	volume of reactants	in ³
XS		initial guess solution	
M		maximum number of iterations	
X		desired root	psi
F		value of the equation at X	
FP		value of the equation derivative at X	

The subprogram entitled /RCOTN/ is described in the following:

Newton's Root Finding

This subroutine finds a root of an arbitrary differentiable equation $F(X)=0$ using the Newton-Raphson iteration method.

CALLING SEQUENCE: CALL ROOTN(X,F,FP,XS,E,M,IFL)

Input:

- XS** = initial estimate of root
- E** = error tolerance
- M** = maximum number of iterations allowed

Output:

- X** = value of root
- F** = function value at X
- FP** = derivative of function value at X
- IFL** = error flag
 - 0 - if normal
 - 1 - if no convergence in M iterations
 - 2 - if derivative equals zero

METHOD: Given a function $f(x)$, find a root of $f(x)=0$ using an initial estimate x_s . The iteration algorithm used is Newton-Raphson:

$$x_{i+1} = x_i - \frac{f(x_i)}{f'(x_i)}$$

where $f'(x_i)$ is the derivative of $f(x)$ evaluated at x_i .

The procedure has converged if:

$$f(x_{i+1}) \leq 100E$$

and if either:

$$\left| \frac{x_{i+1} - x_i}{x_{i+1}} \right| < E \quad \text{when } |x_{i+1}| > 1$$

or:

$$|x_{i+1} - x_i| < E \quad \text{when } |x_{i+1}| \leq 1$$

where E is the user supplied error tolerance.

COMMENT: The user supplies a SUBROUTINE subprogram XNFUN(X,F,FP) which computes $f(x)$ and $f'(x)$.

Reference Hildebrand, F. B., Introduction to Numerical Analysis, McGraw-Hill
New York, 1956 pp. 447-450.

PROGRAM /ROOT/

```

COMMON /ABC/ A,B,C,D
1 FFORMAT (2/,15H READ IN ENERGY)
2 FFORMAT (E12.5)
3 FFORMAT (2/,15H READ IN VOLUME)
4 FFORMAT (2/,4H EN=,E12.5,4X,4H V0=,E12.5)
5 FFORMAT (2/,11H READ IN XS)
6 FFORMAT (2/,10H READ IN E)
7 FFORMAT (2/,10H READ IN M)
8 FFORMAT (I2)
9 FFORMAT (2/,3H X=,E12.5,4X,3H F=,E12.5,4X,4H FP=,E12.5)
10 FFORMAT (2/,11H CALC. A? ?)
11 FFORMAT (6H YES=1,4X,5H N?=?2)
12 FFORMAT (2/,4H A?=?,E12.5)
XX=1.2000
P=14.7
A=1.0/P
B= (1.0/P)**(1.0/XX)
WRITE (1,1)
READ (0,2) EN
WRITE (1,3)
READ (0,2) V0
WRITE (1,4) EN,V0
C=(EN*(XX-1.0))/(P*V0*144.)
D= (1.0/XX)*B
WRITE (1,5)
READ (0,2) XS
WRITE (1,6)
READ (0,2) E
WRITE (1,7)
READ (0,2) M
CALL SUBM (K,F,FP,XS,E,I,IFL)
WRITE (1,9) X,F,FP
WRITE (1,10)
WRITE (1,11)
READ (0,5) JJ
IF (JJ-1) 20,20,23
20 CONTINUE
A1=((K*X*(1.705E+03)/(26.5))**.5)
WRITE (1,12) A1
23 CONTINUE
24 CONTINUE SUBM (K,F,FP)
COMMON /ABC/ A,B,C,D
XX=1.2000
F= A*(1-(B*(C*(1.0/XX))))-C
FP= A-(B*(C*(1.0/XX)-1.0))
RETURN
END

```


SAMPLE RUN OF /ROOT/

READ IN ENERGY
3.35E05

READ IN VOLUME
7.82E-02

EN= .33500E+06 $\bar{V}_0 = .78200E+01$

READ IN XS
1.0E05

READ IN E
.1

READ IN M
100

X= .90533E+04 F= .12561E-03 FP= .48592E-01

APPENDIX F

CALCULATION OF "W" GOODNESS OF FIT STATISTIC FROM REFERENCE 36

Table of Coefficients (a_{n-i+1}) used in W test for normality for $n = 9$
 0.5888, 0.3244, 0.1976, 0.0947

Step 1 Rearrange observations for ordered Sample X_1, X_2, \dots, X_n from percentile values in Table V

Step 2 Compute

$$S^2 = \sum_{i=1}^n (X_i - \bar{X})^2 = \sum_{i=1}^n X_i^2 - \left(\frac{\sum X_i}{n} \right)^2$$

where \bar{X} is data mean.

Step 3 For when n is odd, set $k = (n-1)/2$ then compute

$$\begin{aligned} b &= A_n (X_n - X_1) + A_{n-1} (X_{n-1} - X_2) + \dots + A_{n-k+1} (X_{n-k+1} - X_k) \\ &= \sum_{i=1}^k A_{n-i+1} (X_{n-i+1} - X_i) \end{aligned}$$

Step 4 Compute the test statistic $W = \frac{b^2}{s^2}$

Step 5 Compare the calculated value of W with the percentiles of the distribution of the test statistic. From Table X of reference 36,

n	1%	2%	5%	10%	50%
9	0.764	0.791	0.829	0.859	0.935

This table gives the minimum values of W that we would obtain with 1, 2, 5, 10 and 50% probability as a function of n , if the data actually came from a normal distribution. Thus, small values of W indicate non-normality.

1. Calculation of W Statistic for Fragment Parameters $R, W, A, A/W$

Event 1 Distance

Normal Distribution

$$S^2 = 1,910,052 \frac{(3920)^2}{9} = 1,910,052 - 1,707,377.778 = 202,674.222$$

$$b = 0.5888 (722-222) + 0.3244 (608-287) + 0.1976 (521-331) + .0947 (449-372)$$

$$b = 443.1683$$

$$b^2 = 196398.1421$$

$$W = \frac{b^2}{S^2} = \frac{196,398.1421}{202,674.222} = .969$$

Log Normal

$$S^2 = 326.895411 - \frac{(54.14941195)^2}{9} = 326.895411 -$$

$$325.7954239 = 1.0999871$$

$$b = 1.045378098$$

$$b^2 = 1.092815368$$

$$W = \frac{b^2}{S^2} = .993$$

Event 2 Distance (Normal)

$$S^2 = 185,405.5556$$

$$b^2 = 182068.623$$

$$b = 426.695$$

$$W = .982$$

Event 3 Distance (Normal)

$$S^2 = 2,330,136.889$$

$$b^2 = 2,194,581.81$$

$$b = 1481.4121$$

$$W = .942$$

Event 4 Distance

$$S^2 = 628,382.889$$

$$b^2 = 616,345.7389$$

$$b = 785.0769$$

$$W = .981$$

Event 5 Distance

$$S^2 = 1,748,338.889$$

$$b = 1300.255$$

$$b^2 = 1,690,633.065$$

$$W = .967$$

Event 6 Distance

$$S^2 = 44172$$

$$b = 208.9122$$

$$b^2 = 43644.30731$$

$$W = .988$$

Event 7 Distance (Normal)

$$S^2 = 47,296$$

$$b = 214.0407$$

$$b^2 = 45813.42126$$

$$W = .969$$

Event 8 Distance (Normal)

$$S^2 = 38,674.8889$$

$$b = 193.7642$$

$$b^2 = 37,544.5652$$

$$W = .971$$

Event 1 Weight (Ln Normal)

$$S^2 = 4.02243396$$

$$b = 1.959105363$$

$$b^2 = 3.838093823$$

$$W = .954$$

Event 2 Weight (Ln Normal)

$$S^2 = 9.55743464$$

$$b = 3.087710481$$

$$b^2 = 9.533956014$$

$$W = .998$$

Event 3 Weight (Ln Normal)

$$S^2 = 8.308249$$

$$b = 2.808424493$$

$$b^2 = 7.887248133$$

$$W = .949$$

Event 4 Weight (Ln Normal)

$$S^2 = 5.4833992$$

$$b = 2.328636257$$

$$b^2 = 5.422546817$$

$$W = .989$$

Event 5 Weight (Ln Normal)

$$S^2 = 5.2896359$$

$$b = 2.207715255$$

$$b^2 = 4.874006647$$

$$W = .921$$

Event 6 Weight (Ln Normal)

$$S^2 = 18.40217547$$

$$b = 4.27189715$$

$$b^2 = 18.24910526$$

$$W = .992$$

Event 7 Weight (Ln Normal)

$$S^2 = 12.28668662$$

$$b = 3.391847545$$

$$b^2 = 11.50462977$$

$$W = .936$$

Event 8 Weight (Ln Normal)

$$S^2 = 16.56249558$$

$$b = 4.018598852$$

$$b^2 = 16.14913673$$

$$W = .975$$

Event 1 Area/Weight (Normal)

$$S^2 = 11,152.03556$$

$$b = 104.89576$$

$$b^2 = 11,003.12047$$

$$W = .987$$

Event 2 Area/Weight (Normal)

$$S^2 = 11639.72$$

$$b = 105.62921$$

$$b^2 = 11157.53001$$

$$W = .959$$

Event 3 Area/Weight (Normal)

$$S^2 = 1012.18$$

$$b = 28.43535$$

$$b^2 = 808.5691296$$

$$W = .799$$

Event 4 Area/Weight (Normal)

$$S^2 = 1064.262222$$

$$b = 29.01741$$

$$b^2 = 842.0100831$$

$$W = .791$$

Event 5 Area/Weight (Normal)

$$S^2 = 515.8288889$$

$$b = 18.61245$$

$$b^2 = 346.423295$$

$$W = .672$$

Event 6 Area/Weight (Normal)

$$S^2 = 16338.98741$$

$$b = 126.724354$$

$$b^2 = 16059.0619$$

$$W = .983$$

Event 7 Area/Weight (Normal)

$$S^2 = 11,373.60751$$

$$b = 105.1395562$$

$$b^2 = 11054.32628$$

$$W = .972$$

Event 8 Area/Weight (Normal)

$$S^2 = 19,558.42122$$

$$b = 138.6416769$$

$$b^2 = 19221.51457$$

$$W = .983$$

Event 1 Area (Ln Normal)

$$S^2 = 5.4012421$$

$$b = 2.317066189$$

$$b^2 = 5.368795724$$

$$W = .994$$

Event 2 Area (Ln Normal)

$$S^2 = 29.313013$$

$$b = 5.322848019$$

$$b^2 = 28.33271103$$

$$W = .966$$

Event 3 Area (Ln Normal)

$$S^2 = 11.8267759$$

$$b = 3.380014318$$

$$b^2 = 11.42449679$$

$$W = .966$$

Event 4 Area (Ln Normal)

$$S^2 = 11.6117262$$

$$b = 3.350700597$$

$$b^2 = 11.22719449$$

$$W = .967$$

Event 5 Area (Ln Normal)

$$S^2 = 5.5540099$$

$$b = 2.350202139$$

$$b^2 = 5.523450094$$

$$W = .994$$

Event 6 Area (Ln Normal)

$$S^2 = 15.45026354$$

$$b = 3.821539598$$

$$b^2 = 14.6041649$$

$$W = .945$$

Event 7 Area (Ln Normal)

$$S^2 = 13.00914442$$

$$b = 3.586886773$$

$$b^2 = 12.86575672$$

$$W = .989$$

Event 8 Area (Ln Normal)

$$S^2 = 14.3944438$$

$$b = 3.752708615$$

$$b^2 = 14.08282195$$

$$W = .978$$

2. Calculation of W Statistic for Initial Velocity Distributions

CBM LO₂-LH₂

$$S^2 = 4.1582624$$

$$b = 7.961656617$$

$$b^2 = 3.848096683$$

$$W = .925$$

CBM LO₂-RP1

$$S^2 = 2.217937$$

$$b = 1.449243666$$

$$b^2 = 2.100307203$$

$$W = .947$$

CBGS LO₂-LH₂

$$S^2 = 3.4304869$$

$$b = 1.827121225$$

$$b^2 = 3.338371974$$

$$W = .973$$

CBGS LO₂-RPI

$$S^2 = 1.707618$$

$$b = 1.299335448$$

$$b^2 = 1.688272606$$

$$W = .989$$

APPENDIX G

CALCULATION OF APPROXIMATE PROBABILITY FOR OBTAINING THE CALCULATED VALUE OF "W"

For $n = 9$, from Table XI of reference 36, $\alpha = -2.968$, $n = 1.400$, $\epsilon = 0.3900$

Approximate probability of obtaining the calculated value of W , assuming a normally distributed variable can be obtained by finding:

$$Z = Y + n \ln \left(\frac{W - \epsilon}{1 - W} \right)$$

$$Z = -2.968 + 1.400 \ln \left(\frac{W - 0.3900}{1 - W} \right)$$

For $W = .942$

$$\begin{aligned} Z &= -2.968 + 1.400 \ln \left(\frac{.552}{.058} \right) = -2.968 + 1.400 \ln 9.517241379 \\ &= -2.968 + 1.400 (2.253105036) = -2.968 + 3.15434705 = .186347 \end{aligned}$$

$$\Pr (Z \leq 0.186) = .57$$

For $W = .994$

$$Z = 3.4885$$

$$\Pr = .999$$

For $W = .969$

$$Z = 1.13$$

$$\Pr = .871$$

For $W = .954$

$$Z = .54$$

$$P = .7054$$

The following values and table result from using the above methods.

$W = .921$
 $W = .910$
 $W = .899$
 $W = .888$
 $W = .877$
 $W = .866$
 $W = .855$
 $W = .844$

$Z = -.3$
 $Z = .186$
 $Z = .268$
 $Z = 1.13$
 $Z = .540$
 $Z = 1.63$
 $Z = 2.628$
 $Z = 3.4885$

$P(Z \leq -.3) = .382$
 $P(Z \leq .186) = .574$
 $P(Z \leq .268) = .643$
 $P(Z \leq 1.13) = .871$
 $P(Z \leq .540) = .705$
 $P(Z \leq 1.63) = .948$
 $P(Z \leq 2.62) = .995$
 $P(Z \leq 3.488) = .999$

Summary of the Above Results

W	%
.764	.010
.791	.020
.829	.050
.859	.100
.921	.382
.935	.500
.945	.643
.969	.871
.978	.948
.988	.999

APPENDIX H

COMPUTER PROGRAM ENTITLED /TEMP/ IN FORTRAN IV

Function: This program computes the range of a fragment from the equations described in Section IV.D for the following input data.

S1	Initial trajectory angle of fragment	radians
S2	Fragment drag coefficient	
S3	Ambient air density	lb-ft ³
S4	Fragment mass coefficient (ratio of fragment mass to tank mass)	
TM	Tank mass	lb-sec ² /in.
FF	Projected cross-sectional area of fragment	in ²
G2	Fragment initial velocity	ft/sec

Variables: The definition and units of the variables in this program are given in the following table.

<u>Program Variable</u>	<u>Variable</u>	<u>Definition</u>	<u>Units</u>
S1	θ	Initial trajectory angle	radians
S2	C_D	Drag coefficient	
S3	ρ_{air}	Air density	lb-ft ³
S4		Mass coefficient	
TM	M	Fragment mass	lb-sec ² /in.
FF	A	Fragment cross-sectional area	in ²
G2	U_f	Initial velocity	ft/sec
PI	π	The constant π	
GR	g	Gravitational constant	in/sec ²

<u>Program Variable</u>	<u>Variable</u>	<u>Definition</u>	<u>Units</u>
S5		The quantity $2A/$	in^2
S6	c	Coefficient defined in Section IV. D.	in^{-1}
S7	V_{Ro}	Initial radial velocity	ft/sec
S8	V_{zo}	Initial vertical velocity	ft/sec
S9		The quantity $V_{zo} (c/g)^{1/2}$	in.
S10		The quantity $\tan^{-1} V_{zo} (c/g)^{1/2}$	
S11		The quantity $1/ (cg)^{1/2}$	sec
S12		The quantity $\cos \tan^{-1} V_{zo} (c/g)^{1/2}$	
S13		The quantity $2.0 \text{ LOG } (1.0/S12)$	
S14		The quantity $2.0 e^{S13} - 1.0$	
S15	τ	Time of flight of fragment	sec
S16	R	Fragment range	ft
TR	t_R	Time of rise of fragment	sec
ZM	Z_m	Maximum height reached by fragment	in.
S17		The quantity $2.0 e^{2c Z_m} - 1.0$	sec
TF	t_f	Time of fall of fragment	sec
T	τ	Time of flight of fragment	sec

Sample runs: Substitution of the following data in the program yielded the range values R (appearing in Figure (H-1) as X's). Thus, results of this program are in accord with Oslake, et al.

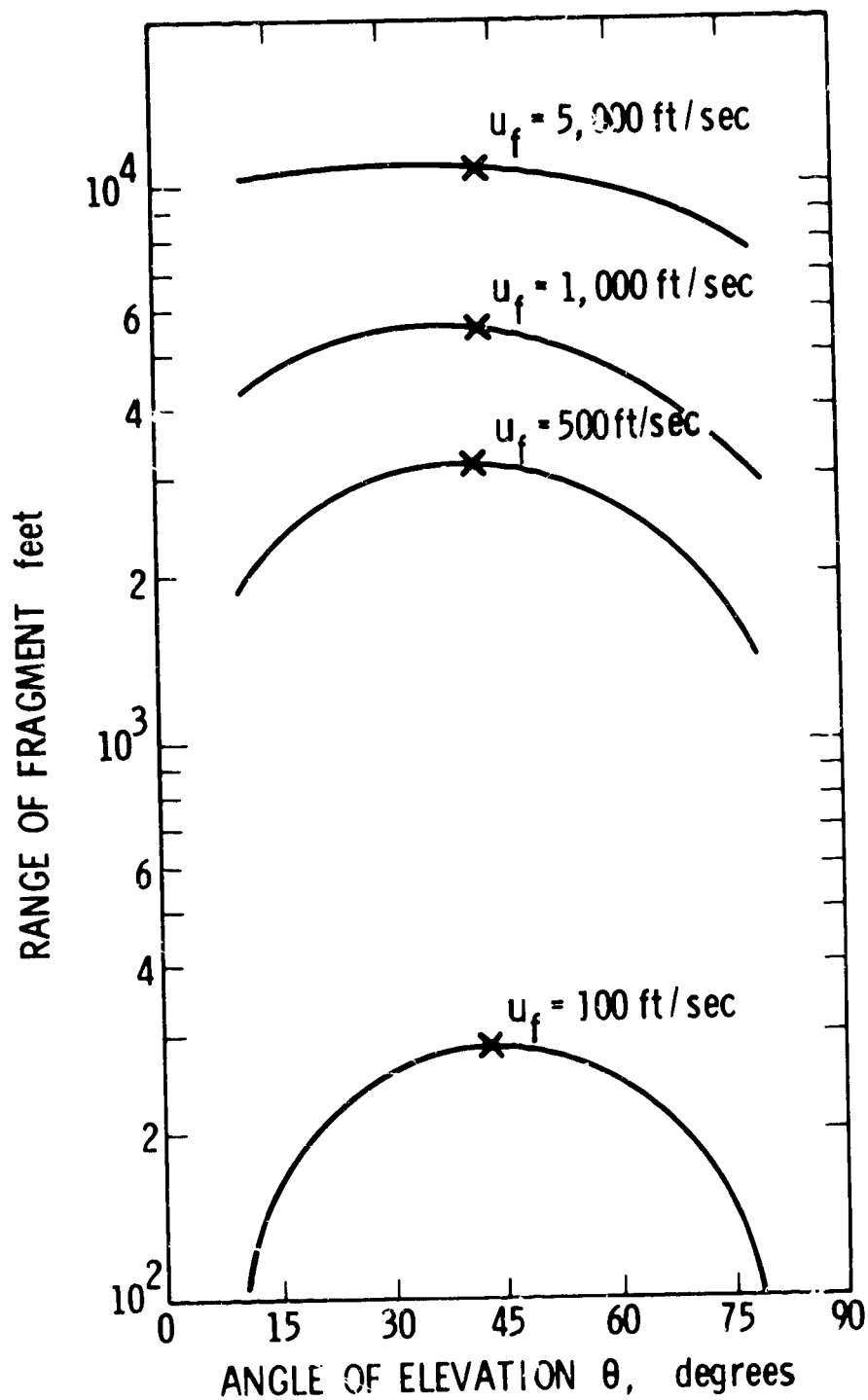


FIGURE H1. FRAGMENT RANGE VERSUS ELEVATION ANGLE FOR CONSTANT $\frac{W}{C_D A} = 100 \text{ LB/FT}^2$, AND CONSTANT u_f

TABLE H-1 - DATA FOR PROGRAM CHECK

S1 = 43.3°	G2 = 100 ft/sec	R = 2.89 x 10 ² ft
S2 = 1.2	500 ft/sec	3.19 x 10 ³ ft
S3 = 7.48 x 10 ⁻² lb/ft ³	1000 ft/sec	5.50 x 10 ³ ft
S4 = 1.0	5000 ft/sec	1.09 x 10 ⁴ ft
FF = 4.52 x 10 ³ in ²		
TM = 6.2 lb-sec ² /in.		

A sample run for the case in which a "mean" fragment from test 062 of PYRO was considered ($C_D = .750$) is given in the following.

READ IN TRAJ. ANGLE
12.77

READ IN DRAG COEF. AND AIR DENSITY
.75,7.48E-02

READ IN FRAGMENT MASS COEF.
1.0
1.0

READ IN NO. OF FRAGMENTS

FRAG. MASS
1.76E-02

FRAG. PROJ. AREA
5.77E02

INITIAL VEL.
7.41E02

AMBIENT AIR DENSITY = .748E-01 LBS./CUBIC FT.

AIR DRAG COEFF.= .750E+00
FRAGMENT MASS COEF.= .100E+01
TRAJECTORY ANGLE= .128E+02 DEGREES

CHECK C= .875E-03
722.6715304
163.7890693
2.956115468
1.244598802
.52384E+01

MAXIMUM RANGE= .353E+03 FT.
.52384E+01
STOP

SDO FORMAT (2/,20H READ IN TRAJ. ANGLE)
SDO1 FORMAT (E10.5)
SDO2 FORMAT (2/,35H READ IN DRAG COEF. AND AIR DENSITY)
SDO3 FORMAT (E10.3)
SDO4 FORMAT (2/,25H READ IN FRAGMENT MASS COEF.)
SDO5 FORMAT (4/,35H CONDITIONS ON TRAJECTORY)
SDO6 FORMAT (/,21H AMBIENT AIR DENSITY=,E10.3,17H LBS./CU FT.)
SDO7 FORMAT (/,16H AIR DRAG COEF.=,E10.3)
SDO8 FORMAT (/,21H FRAGMENT MASS COEF.=,E10.3)
SDO9 FORMAT (/,15H TRAJECTORY ANGLE=,E10.3,8H DEGREES)
SDO10 FORMAT (3/,9H CHECK C=,E10.3)
SDO11 FORMAT (3/,15H MAXIMUM RANGE=,E10.3,4H FT.)
SDO12 FORMAT (2/,25H READ IN NO. OF FRAGMENTS)
SDO13 FORMAT (2/,17H FRAG. PROJ. AREA)
SDO14 FORMAT (/,11H FRAG. MASS)
SDO15 FORMAT (/,13H INITIAL VEL.)
SDO16
PI=3.1415926535
NITE (1,300)
DUM (0,3001) S1
NITE 1821
NITE(311.0*31)/(2.0*PI)
NITE (1,301)
DUM (0,3011) S2,S3
NITE (1,302)
DUM (0,3021) S4
NITE (1,311)
DUM (0,3031) F1
NITE (1,320)

```

READ (0,3001) TM
WRITE (1,201)
READ (0,3001) FF
WRITE (1,202)
READ (0,3001) G2
WRITE (1,304) S3
WRITE (1,305) S2
WRITE (1,306) S4
WRITE (1,307) S1
S5=(2.0*(FF/PI))
S6=(0.5*(((S3/GR)*S5*S2)/(S4*(TM/FN))))/(12.0**3.0)
WRITE (1,3071) S6
S7=G2*COS((2.0*PI)*(S1/360.0))
S8= G2*SIN((2.0*PI)*(S1/360.0))
S9=(S8*((S6/GR)**0.5))*(12.0)
S10=ATAN(S9)
S11=(1.0/(S6*GR)**0.5)
S12=COS(S10)
S13=2.0*ALOG(1.0/S12)
S14=(2.0*EXP(S13))-1.0
S15=S11*(S10+(0.5*ALOG(S14+(((S14**2.0)-1.0)**0.5))))
WRITE (1,3001) S15
S16=(1.0/S6)*ALOG(1.0+(S6*S7*S15*12.0))
S16=S16/12.0
WRITE (1,303) S16
TR=S11*ATAN(S9)
S17=(1.0/S6)*ALOG(1.0/COS(TR/S11))
S17=(2.0*EXP(2.0*S6*ZM))-1.0
TF=0.5*S11*ALOG(S17+(((S17**2.0)-1.0)**0.5))
T=TF+TR
WRITE (1,3001) T
END

```


APPENDIX I

LIST OF SYMBOLS

<u>Symbol</u>	<u>Definition</u>	<u>Units*</u>
a, a _o	Sound speed	LT ⁻¹
a, b, c, d	Parameters in a math model	---
b	Time constant of blast wave	---
d, D, D _o	Diameters	L
dc _A , dc _B	Distances to cameras	L
g	Acceleration of gravity, nondimensional displacement	LT ⁻² , ---
h	Convective heat transfer coefficient, segment height	MT ⁻³ θ ⁻¹ , L
h _e	Height of explosion center	L
k	Discharge coefficient, constant in fragment drag equation	---, ML ⁻³
ℓ	Generic length	L
n, N, N _o	Numbers of fragments	---
p _o , p _{oo}	Ambient pressure	FL ⁻²
q	Drag pressure	FL ⁻²
r	Displacement of a fragment	L
t, T, T _i , τ	Times	T
u, u _s , U, U _I , U _i , U _A , U _m	Velocities	LT ⁻¹

* Units used are force (F), length (L), mass (M), time (T) and temperature (θ), rather than dimensions in any particular physical system.

** A dash in the units column indicates a dimensionless quantity.

<u>Symbol</u>	<u>Definition</u>	<u>Units*</u>
w	Crack width	L
x	Mixing function	---
x_i, y_i	Coordinates of fragments	L
y	Yield Fraction	---
A, A_i	Areas	L^2
C	Mass of explosive charge or confined gas	M
C_D	Drag coefficient	---
E	Energy of reactants	FL
F	Projected area of a fragment	L^2
G_i, G_i'	Dimensional parameters fixed by nondimensional groups	various
H_e, H_R, H_{TNT}	Heats of explosion	$L^2 T^{-2}$
H_{f_i}	Heats of fusion	$L^2 T^{-2}$
H_{b_i}	Heats of boiling	$L^2 T^{-2}$
I, I_d	Blast wave impulses	FTL^{-2}
K_i	Thermal conductivities	$MLT^{-3} \theta^{-1}$
L	Tank length	L
M, M_i, M_T	Masses	M
P, P_r, Q	Peak pressures	FL^{-2}
R	Distance from accident	L
R_1	Universal gas constant	$L^2 T^{-2} \theta^{-1}$
S_i	Displacements	L
T	Temperature	θ

<u>Symbol</u>	<u>Definition</u>	<u>Units*</u>
$V, V_o, V_{oo}, V_R,$ V_H, V_{ui}	Volumes	L^3
$W, W_r, W_m,$ W_{TNT}, W_T	Weights of propellants, explosives, reactants. Also, fragment weight	F
"W"	The "W" statistic	---
$X_A, Y_A; X_i,$ Y_i	Displacements and distances	L
Y, Y_m, Y_M	Blast yields as percents of TNT equivalent	---
$\bar{P}, \bar{P}_r, \bar{Q}$	Scaled blast pressures	---
\bar{U}	Scaled shock velocity	---
\bar{Z}	Average displacement	L
\hat{R}	Predicted mean fragment range	L
α, β, θ	Coefficients	---
α	Angle	---
β	Coefficient	---
δ_j^i	Average vertical displacement	L
θ, θ_v	Elevation angles	---
$\theta_a, \theta_i, \theta_m$	Temperatures	θ
κ	Ratio of specific heats	---
λ_i	Scale factors	---
$\mu, \hat{\mu}$	Statistical means	various
ν_i	Kinematic viscosities	$L^2 T^{-1}$

<u>Symbol</u>	<u>Definition</u>	<u>Units*</u>
ξ	Time ratio	---
π	Crack length	L
ρ, ρ_*, ρ_s	Densities	ML^{-3}
$(\rho C_p)_i$	Volumetric heat capacities	$ML^{-1} T^{-2} \theta^{-1}$
σ	Stefan-Boltzmann constant	$MT^3 \theta^{-4}$
σ_u	Standard deviation of velocity	LT^{-1}
ϕ	Solid angle	---
ψ, ψ^j	Azimuth angles	---

REFERENCES

1. Baker, Wilfred E., Explosions in Air, Univ. of Texas Press, Austin, Texas, May 1973.
2. Kingery, C. N. and B. F. Pannill, "Peak Overpressure vs. Scaled Distance for TNT Surface Burst (Hemispherical Charges)", BRL Memo Report No. 1518, Aberdeen Proving Ground, Md., April 1964. AD 443 102
3. Carter, P. B., Jr., "A Method of Evaluating Blast Parameters Resulting from Detonation of Rocket Propellants", AEDC-TDR-64-200, Arnold Engineering Dev. Center, Air Force Systems Command, Oct. 1964. AD 450140
4. Gurney, R. W., "The Initial Velocities of Fragments from Bombs, Shells, and Grenades," BRL Report 405, 1943.
5. Henry, I. G., "The Gurney Formula and Related Approximations for the High-Explosive Deployment of Fragments," Hughes Aircraft Company, Report No. PUB-189, Culver City, California, April 1967.
6. Ahlers, E. B., "Fragment Hazard Study," Minutes of the Eleventh Explosives Safety Seminar, September 1969, pp. 81-107.
7. Gwaltney, R. C., "Missile Generation and Protection in Light-Water-Cooled Power Reactor Plant," ORNL-NSIC-22, Oak Ridge National Laboratory, September 1968.
8. Gates, R. W., "Containment of Fragments from a Runaway Reactor," Stanford Research Institute, Menlo Park, California, SRIA-117 AEC Research and Development Report UC-80, Reactor Technology TID-4500 (27th Edition), February 15, 1964. Final Report prepared for U. S. Atomic Energy Commission, Contract No. AT(04-3)-115, Project Agreement No. 2.
9. Proceedings of the Second United Nations International Conference on Peaceful Uses of Atomic Energy, Vol. 11, Reactor Safety and Control, United Nations, Geneva, 1958.
10. Brittan, R. O. and J. C. Heap, "Reactor Containment," pp. 66-78 in Ref. 9.

11. Gurney, R. W., "Fragmentation of Bombs, Shells, and Grenades," BRL Report 635, March 1947.
12. Sterne, T. E., "A Note on the Initial Velocities of Fragments from Warheads," BRL Report 648, September 1947.
13. Sterne, T. E., "The Fragment Velocity of a Spherical Shell Containing an Inert Core," BRL Report 753, March 1951.
14. Thomas, L. H., "Theory of the Explosion of Cased Charges of Simple Shape," BRL Report 475, July 1944.
15. Willoughby, A. B., C. Wilton and J. Mansfield, "Liquid Propellant Explosive Hazards. Final Report-Dec. 1968. Vol. I - Technical Documentary Report," AFRPL-TR-68-92, URS-652-35, URS Research Co., Burlingame, California.
16. Willoughby, A. B., C. Wilton and J. Mansfield, "Liquid Propellant Explosion Hazards, Final Report-Dec. 1968. Vol. II - Test Data," AFRPL-TR-68-92, URS 652-35, URS Research Co., Burlingame, California.
17. Willoughby, A. B., C. Wilton and J. Mansfield, "Liquid Propellant Explosion Hazards. Final Report-Dec. 1968. Vol. III - Prediction Methods," AFRPL-TR-68-92, URS 652-35, URS Research Co., Burlingame, California.
18. Jeffers, S. L., "Fragment Velocity Measurements from Three Project Pyro Experiments," Report SC-DR-69-329, Aerospace Nuclear Safety Department 9510, Sandia Laboratories, Albuquerque, New Mexico, June 1969.
19. Hunt, D. L., F. J. Walford and F. C. Wood, "An Experimental Investigation into the Failure of a Pressure Vessel Containing High Temperature Pressurized Water," AEEW-R 97, United Kingdom Atomic Energy Authority, Reactor Group, September 1961.
20. Larson, R. J., and W. C. Olson, "Measurements of Air Blast Effects from Simulated Nuclear Reactor Core Excursions," BRL Memorandum Report No. 1102, Aberdeen Proving Ground, Md., September 1957.
21. Muzzall, C. E. (editor), "Compendium of Gas Autoclave Engineering Studies," Report Y-1478, Y-12 Engineering Division, Union Carbide Corporation, Nuclear Division, Oak Ridge, Tennessee, November 1964.

22. Baker, W. E., S. Silverman and T. D. Dunham, "Studies of Explosions in the NASA-MSC Vibration and Acoustic Test Facility (VATF)", Final Report on Contract NAS9-7749, Southwest Research Institute, March 1968.
23. Farber, E. A. and Deese, J. H., "A Systematic Approach for the Analytical Analysis and Prediction of the Yield from Liquid Propellant Explosions", Tech. Paper No. 347, Eng. Progress at the Univ. of Florida, XX, 3, Mar. 1966.
24. (Anonymous), "Summary Report on a Study of the Blast Effect of a Saturn Vehicle", Report No. C63850, Arthur D. Little, Inc., Cambridge, Mass., Feb. 1962.
25. Pesante, R. E. and Nishibazashi, M., "Evaluation of the Blast Parameters and Fireball Characteristics of Liquid Oxygen/Liquid Hydrogen Propellant", Report No. 0954-01(01)FP, Aerojet-General Corp., Downey, Calif., Apr. 1967.
26. Gayle, J. B., Blakewood, C. H., Bransford, J. W., Swindell, W. H. and High, R. W., "Preliminary Investigation of Blast Hazards of RP-1/LOX and LH₂/LOX Propellant Combinations", NASA TM X-53240, George C. Marshall Space Flight Center, Huntsville, Ala., Apr. 1965.
27. Farber, E. A., Klement, F. W. and Bonzon, C. F., "Prediction of Explosive Yield and Other Characteristics of Liquid Propellant Rocket Explosions," Final Report, October 31, 1968, Contract No. NAS 10-1255, Univ. of Florida, Gainesville, Florida.
28. Farber, E. A., "Characteristics of Liquid Rocket Propellant Explosion Phenomena. No. 448. Part VIII. Prediction of Explosive Yield and Other Characteristics of Liquid Propellant Rocket Explosions," Vol. XXIII, No. 11, Engineering Progress at the Univ. of Florida, Nov., 1969.
29. Farber, E. A., "Characteristics of Liquid Rocket Propellant Explosion Phenomena Series. Report No. IX. Critical Mass (Hypothesis and Verification) of Liquid Rocket Propellants," Univ. of Florida, Gainesville, Florida, September 1971.
30. Farber, E. A., Smith, J. H. and Watts, E. H., "Electrostatic Charge Generation and Auto-ignition Results of Liquid Rocket Propellant Experiments", Report No. X, Univ. of Florida, Gainesville, Florida, Oct. 1972.

31. Taylor, D. B. and C. F. Price, "Velocities of Fragment From Bursting Gas Reservoirs," ASME Transactions, Journal of Engineering for Industry, Nov. 1971.
32. Grodzovski, G. L., and F. A. Kukanov, "Motion of Fragments of a Vessel Bursting in a Vacuum," Soviet Engineering Journal, Mar/Apr 1965.
33. Pittman, J. F., "Blast and Fragment Hazards From Bursting High Pressure Tanks," NOLTR 72-102, May 1972.
34. Glasstone, Samuel, The Effects of Nuclear Weapons, U. S. Government Printing Office, Revised Edition, April 1962.
35. Hoerner, Sighard F., Fluid-Dynamic Drag, Published by the Author, Midland Park, New Jersey, 1958.
36. Hahn, Gerald J. and Shapiro, Samuel S., Statistical Models in Engineering, John Wiley and Sons Inc., New York, 1967.
37. Fletcher, R. F., "Liquid-Propellant Explosions", Jour. of Spacecraft and Rockets, 5, 10, pp 1227-1229, Oct. 1968.
38. (Anonymous), SIV All Systems Vehicle Malfunction 24 January 1964, Douglas Missile & Space Division, Santa Monica, California.
39. Deese, J. H., Test Conductors Damage Assessment Report on Auto-Ignition L02/LH2 Mixing Test Experimental Expersion of 2 March 1972, Systems Engineering Division, Kennedy Space Center, NASA.
40. Dixon, W. J., Biomedical Computer Programs, University of California Press, Los Angeles, California 1970.
41. Oslake, J. J., Getz, R. J., Romine, R. A. and Soofitov, K., "Explosive Hazards of Rocket Launchings," Ford Motor Co. Technical Report 4-108:98, Nov. 1960, AD253-235.
42. Heppner, L. D. and Steedman, J. E., "Drag Coefficient for Fragment Simulating Projectiles, 20 MM, Caliber .50, and Caliber .30," APG DPS-286, Aug. 1961, AD 822-489.
43. Richards, E., "Comparative Dispersion and Drag of Spheres and Light Cylinders," APG BRL TR-717, March 1950.

44. Feinstein, D. I., "Fragmentation Hazards to Unprotected Personnel" TR ITTRI-J6176 January 1972.
45. Transue, W. R. and Saramel, K. M., "Terminal Ballistics - Fragmentation Effects," TR Institute of Research Lehigh University, December 1947.
46. Thomas, J. H., "Computing Effect of Distance on Damage by Fragments" APG-BRL Report No. 468, May 1944.
47. Lewz, H., "Asymptotic Integration of Fragment Trajectories" APG-BRL Report No. 559 and Technical Note No. 496, September 1951.
48. Feinstein, D. I. and Nazooka, H. H., "Fragment Hazards From Detonation of Multiple Munitions in Open Stores," TR IITRI-J6176, August 1971.